Supplementary information on canister integrity issues

SVENSK KÄRNBRÄNSLEHANTERING

Supplementary information on canister integrity issues

Svensk Kärnbränslehantering AB

Abstract

Context

In the licensing process for a KBS-3 spent nuclear fuel repository at Forsmark the Land and Environmental Court considered, in its statement to the Swedish Government, that supplementary information regarding five issues related to the long-term behaviour of the copper canisters should be presented and evaluated. The issues are:

a) Corrosion due to reaction in oxygen-free water.

b) Pitting due to reaction with sulphide, including the influence of the sauna effect on pitting.

c) Stress corrosion cracking due to reaction with sulphide, including the influence of the sauna effect on stress corrosion cracking.

d) Hydrogen embrittlement.

e) The effect of radioactive radiation on pitting, stress corrosion cracking and hydrogen embrittlement.

At SKB, work on these issues has long been in progress. In response to the Court statement, SKB intensified its on-going work in the areas, and this report summarises and presents conclusions regarding the phenomena *per se* and their importance for post-closure safety of the final repository for spent nuclear fuel. The focus is to a large extent on new material that has not been used as bases for the statement from the Court.

Conclusion regarding canister issues

As a background for the evaluations, a description of the repository environment is provided where the unsaturated and saturated buffer phases, as well as the eroded buffer case are discussed. A number of new studies support the extended description of the unsaturated conditions.

Regarding the sauna effect, it is concluded that no significant salt accumulation as a consequence of vaporization of inflowing water from a fracture intersecting a deposition hole will occur in a KBS-3 repository. The conclusions are based on laboratory studies, model calculations and field experiments. Thus, the conclusion is that the sauna effect will not occur in a KBS-3 repository at Forsmark and the process is, therefore, not included in the further analyses in this report.

Regarding copper corrosion in pure, oxygen-free water, it is concluded that there is no reason to assume that this corrosion mode occurs to an extent that exceeds that predicted by established thermodynamic data. The conclusion is based on a thorough evaluation of available scientific evidence on the matter. It was also concluded that data used by a few researchers to claim corrosion extents many orders of magnitude in excess of established scientific views, would cause corrosion of only around one millimetre of copper during the one million year period covered by the safety assessment. Based primarily on the former of these two conclusions, corrosion of copper in pure, oxygen-free water is not further considered in the report, since established thermodynamic data predicts a corrosion depth under repository conditions that is completely negligible during the assessment period.

It is concluded that pitting corrosion due to sulphide exposure can be excluded since pitting requires the formation of a passive copper sulphide film on the copper surface, and such film formation has never been observed on copper in sulphide solutions under naturally corroding conditions (i.e. with no applied electric potential), even in concentrations far above the highest observed and expected in the groundwater at Forsmark (1.2×10^{-4} mol/L). As regards other forms of localised corrosion, there are some laboratory observations that have been interpreted as micro-galvanic corrosion of copper in sulphide solutions. When these laboratory conditions are translated to repository conditions, it cannot be conclusively ruled out that micro-galvanic corrosion could occur for the highest sulphide fluxes that could occur in the repository in the case of eroded bentonite buffer. The occurrence of localised corrosion under a biofilm of sulphate-reducing bacteria (SRB) is also discussed and ruled out, in particular based on the fact the groundwater at repository depth is not sufficiently rich in nutrients to support the formation of a biofilm and/or high metabolic activity of SRB. The conclusions regarding localised corrosion are supported by several new studies.

It is concluded that simultaneous tensile stresses and sulphide exposure are not expected to jeopardise the canister integrity in the repository environment. Tensile stresses cannot be ruled out in parts of the canister during certain periods. In laboratory studies, microscopic fractures have been observed in the surfaces of copper specimens exposed to tensile stresses in combination with high concentrations of sulphide. When the conditions under which these observations were made are evaluated, it is concluded that the sulphide concentrations and fluxes required for the phenomenon to be observed, are such that they will not occur at the canister surface in the repository. Also, it is argued that the observed phenomenon is not an example of "traditional" stress corrosion cracking, SCC, but rather a kind of intergranular corrosion that appears only for very high sulphide fluxes when copper is subjected to high tensile stress. The conclusions are supported by several new studies.

It is concluded that hydrogen embrittlement will not jeopardise canister integrity in a KBS-3 repository. The conclusion is based on assessments of possible influxes of hydrogen generated in corrosion processes and an evaluation of experiments and model calculations of how such influxes would affect the metal. Exposure conditions leading to damaging effects in thin surface layers in laboratory experiments are much more aggressive than in the repository environment.

It is concluded that irradiation will cause insignificant levels of radiation damage in the canister materials. This is concluded on the basis of revised calculations of radiation damage and to some degree also demonstrated by new experiments. Also, earlier pessimistically neglected annealing effects have been shown to reduce the radiation damage considerably. From experimental studies of radiolytic corrosion of copper and theoretical considerations it is concluded that radiation effects will have a negligible influence on localised corrosion (pitting), SCC and hydrogen embtittlement. The theoretical understanding of radiation induced corrosion has been substantially improved.

Consequence calculations

Since localised corrosion in the form of micro-galvanic sulphide corrosion, could not be conclusively ruled out for the highest sulphide fluxes that could be expected in the repository environment, an updated dose consequence calculation based on a pessimistic interpretation of available data on micro-galvanic pit formation was carried out. The results of the calculation demonstrate that the calculated peak dose is only marginally affected compared to the value in the safety assessment SR-Site, meaning that the corresponding risk is still below SSM's risk criterion by about one order of magnitude.

The robustness of the repository system to canister integrity issues is demonstrated in a couple of hypothetical calculation cases. It is demonstrated that even if all canisters are hypothetically assumed to fail by penetration at a very early stage, the calculated risk is still on a par with SSM's risk criterion.

Overall conclusion

The overall result of the work presented in this report is that the main conclusion in the safety assessment SR-Site is unaltered: A KBS-3 repository built at the Forsmark site will fulfil SSM's requirements on post closure safety.

Sammanfattning

Bakgrund

Mark- och miljödomstolen har i sitt yttrande till regeringen om tillåtlighet enligt miljöbalken för ett slutförvar av KBS-3-typ i Forsmark efterfrågat ytterligare underlag om följande fem frågor beträffande kopparkapselns integritet:

a) Korrosion på grund av reaktion i syrgasfritt vatten.

b) Gropkorrosion på grund av reaktion med sulfid, inklusive saunaeffektens inverkan på gropkorrosion.

c) Spänningskorrosion på grund av reaktion med sulfid, inklusive saunaeffektens inverkan på spänningskorrosion.

d) Väteförsprödning.

e) Radioaktiv strålnings inverkan på gropkorrosion, spänningskorrosion och väteförsprödning.

SKB har arbetat med dessa frågor en länge tid. Till följd av domstolens yttrande intensifierades arbetet, och denna rapport sammanfattar och presenterar slutsatser om fenomenen i sig och deras betydelse för slutförvarets säkerhet efter förslutning. Fokus ligger i stor utsträckning på nytt material som inte har använts som grund för domstolens yttrande.

Slutsatser om kapselfrågor

Som bakgrund för utvärderingarna ges en beskrivning av förvarsmiljön där de omättade och mättade buffertfaserna såväl som en situation med eroderad buffert diskuteras. Ett antal nya studier stödjer den utökade beskrivningen av de omättade förhållandena.

Vad gäller saunaeffekten dras slutsatsen att saltackumulering som en konsekvens av förångning av tillflöde av grundvatten från en spricka som skär ett deponeringshål inte kommer att uppstå i ett KBS-3-förvar. Slutsatserna bygger på laboratorieundersökningar, modellberäkningar och fältförsök. Således är slutsatsen att saunaeffekten inte kommer att vara verksam i ett KBS-3-förvar i Forsmark, och processen hanteras därför inte i de fortsatta analyserna i rapporten.

Vad gäller kopparkorrosion i rent, syrgasfritt vatten dras slutsatsen att det inte finns något stöd för att anta att denna korrosionsform sker på något annat sätt än vad etablerad vetenskap förutsäger. Slutsatsen bygger på en detaljerad utvärdering av tillgängligt vetenskapligt underlag i frågan. Vidare skulle data som ett fåtal forskare använder för att hävda att denna korrosion sker i en utsträckning som är många storleksordningar större än den som förutsägs av etablerad vetenskap, orsaka korrosion av endast omkring en millimeter koppar under den miljonårsperiod som säkerhetsanalysen omfattar. Baserat på den första av dessa två slutsatser beaktas inte korrosion av koppar i rent, syrgasfritt vatten vidare i rapporten, eftersom etablerade termodynamiska data förutsäger ett helt försumbart korrosionsdjup under förvarsförhållanden.

Vad gäller gropkorrosion på grund av sulfidexponering dras slutsatsen att detta kan uteslutas, eftersom gropkorrosion kräver bildning av en passiv kopparsulfidfilm på kopparytan och sådan filmbildning har aldrig observerats på koppar i sulfidlösningar under naturliga korrosionsförhållanden (dvs utan applicerad elektrisk potential), inte ens för sulfidkoncentrationer långt över de högsta observerade och förväntade i grundvattnet vid Forsmark ($1,2 \times 10^{-4}$ mol/L). När det gäller andra former av lokal korrosion finns några laboratorieobservationer som tolkats som mikrogalvanisk korrosion av koppar i sulfidlösningar. När dessa laboratorieförhållanden översätts till förvarsförhållanden kan det inte helt uteslutas att mikrogalvanisk korrosion kan förekomma för de högsta sulfidflödena som kan uppstå i förvaret i situationen med eroderad bentonitbuffert. Förekomsten av lokal korrosion under en biofilm av sulfatreducerande bakterier (SRB) diskuteras och utesluts också, särskilt baserat på att grundvattnet på förvarsdjup inte är tillräckligt rikt på näringsämnen för att möjliggöra bildandet av en biofilm och/eller hög metabolisk aktivitet hos SRB. Slutsatserna om lokal korrosion stöds av flera nya studier.

Dragspänningar under sulfidexponering förväntas inte äventyra kapselns integritet i förvarsmiljön. Dragspänningar kan inte uteslutas i vissa delar av kapseln under vissa perioder. I laboratorieundersökningar har mikroskopiska sprickor observerats i ytan hos kopparprover som utsätts för dragspänningar i kombination med höga koncentrationer av sulfid. Sulfidkoncentrationerna och -flödena som krävs för att fenomenet ska uppstå i laboratoriet är emellertid sådana att de inte kommer att inträffa vid kapseln i förvaret. Det observerade fenomenet bedöms inte vara ett exempel på "traditionell" spänningskorrosion utan snarare en slags korngränskorrosion som endast uppträder för mycket höga sulfidflöden när koppar är utsatt för höga dragspänningar. Slutsatserna stöds av flera nya studier.

Väteförsprödning bedöms inte äventyra kapselns integritet i ett KBS-3-förvar. Slutsatsen är baserad på bedömningar av möjlig tillförsel av väte genom korrosionsprocesser och en utvärdering av experiment och modellberäkning av hur sådan tillförsel skulle påverka metallen. Exponeringsförhållanden som leder till skadliga effekter i tunna ytskikt i laboratorieexperiment är mycket mer aggressiva än i förvarets miljö.

Strålningen från det använda bränslet kommer att ge obetydliga strålskador i kapselmaterialen. Slutsatsen grundas på reviderade beräkningar av strålskador och till viss del också på nya experiment. Tidigare pessimistiskt försummade självläkningseffekter har också visats reducera strålskadorna väsentligt. Från experimentella studier av korrosion av koppar från radiolysprodukter och från teoretiska överväganden dras slutsatsen att strålningseffekter kommer att ge försumbar påverkan på lokal korrosion, spänningskorrosion och väteförsprödning. Den teoretiska förståelsen för strålningsinducerad korrosion är väsentligt förbättrad.

Konsekvensberäkningar

Lokal korrosion i form av mikrogalvanisk sulfidkorrosion kan inte kategoriskt uteslutas påverka kapselns integritet för de högsta sulfidflödena som kan förväntas i förvarsmiljön. En uppdaterad doskonsekvensberäkning baserad på en pessimistisk tolkning av tillgänglig data om mikrogalvanisk gropbildning visar att den beräknade maximala risken endast påverkas marginellt jämfört med resultaten i säkerhetsanalysen SR-Site. Den maximala risken ligger under en tiondel av SSM:s riskgräns under hela den en miljon år långa analysperioden.

Förvarssystemet är tåligt mot skador på kapslarna. Detta framgår av två hypotetiska beräkningsfall. Dessa visar att även om alla kapslar hypotetiskt antas ha genomgående skador i ett mycket tidigt skede, är den beräknade risken fortfarande i nivå med SSM:s riskgräns.

Övergripande slutsats

Det övergripande resultatet av genomförda kompletterande studier och analyser är att den viktigaste slutsatsen i säkerhetsanalysen SR-Site är oförändrad: Ett slutförvar som byggs enligt KBS-3-metoden i Forsmark är långsiktigt säkert och uppfyller SSM:s krav på säkerhet efter förslutning.

Contents

1 Introduction

1.1 Context of this report

In March 2011, the Swedish Nuclear Fuel and Waste Management Co., SKB, applied for a permit to build a KBS-3 type final repository for spent nuclear fuel at the Forsmark site in central Sweden. The safety concept is primarily based on complete containment of spent fuel in copper canisters, surrounded by a clay buffer at around 500 m depth in granitic rock. The assessment of post-closure safety in the license application was provided in the SR-Site report (SKB 2011). The Swedish Radiation Safety Authority (SSM) reviews the application under the Act on Nuclear Activities and a Swedish Land and Environmental Court examines it under the Environmental Code.

SSM's review is almost exclusively based on exchange of written material with the applicant, with the opportunity for other stakeholders to challenge the application in writing. The Court's review, in addition to being based on written material, also consists of a thorough, public hearing where the applicant presents its case and where other stakeholders can challenge it.

After completing their reviews, each of the reviewing bodies makes a statement to the Government, whereupon the Government, having first consulted with concerned municipalities and taken any other relevant information into account, makes a decision on permissibility.

On January 23rd 2018, SSM and the Court both issued their statements to the Government. SSM recommended the Government grant permission to proceed, but also identified a number of canister-related issues that SKB needs to resolve in the next phase of the step-wise licensing process according to the Act on Nuclear Activities, i.e. in the Preliminary Safety Assessment Report (PSAR). The PSAR must be submitted by SKB and approved by SSM in order for SKB to obtain a construction licence.

In its statement, the Court approved large parts of the application; parts relating to the Forsmark site, the rock, the buffer and the environmental impact assessment. It also expressed an opinion that supplementary information regarding five issues related to the long-term behaviour of the copper canisters should be presented and evaluated before a licence is considered. The five issues overlap in part with those pointed out by SSM for the next phase of the stepwise licensing process.

The canister related issues in the Court statement are:

a) Corrosion due to reaction in oxygen-free water.

b) Pitting due to reaction with sulphide, including the influence of the sauna effect on pitting.

c) Stress corrosion cracking due to reaction with sulphide, including the influence of the sauna effect on stress corrosion cracking.

d) Hydrogen embrittlement.

e) The effect of radioactive radiation on pitting, stress corrosion cracking and hydrogen embrittlement.

The Court states the following regarding permissibility according to the Environmental Code:

"*In a complete risk assessment, a full investigation is required regarding safety of the final repository during 1 000 years after closure. According to the view of the Land and Environmental Court, a full investigation of the risks for leakage and dispersion of radioactive substances in the environment during 100 000 years and longer is, however, not required. It is reasonable to accept certain uncertainties regarding the protective capacity of the repository in the very long term. The uncertainties must not be considerable in relation to the risk criterion, but it can be acceptable if the uncertainties are small. The requirements on investigation shall be fulfilled at the trial regarding permissibility*

according to the Environmental Code. In the assessment of the safety of the repository in the long term, a potential continued investigation after a decision on permissibility must not be taken into account.[1]

Regarding the requirements on the supplementary information, the Court states the following:

"SKB should according to the assessment by the Land and Environmental Court, in any case provide the following in the trial according to the Environmental Code. A documentation is required as a basis for new assessments regarding the uncertainties that have emerged regarding the protective capacity of the canister. To the extent that the uncertainties remain after this, the uncertainties need to be included in the safety assessment according to the requirements in SSM's regulations. A new scenario may be required where the uncertainties have been included. Finally, a new calculated result of the entire safety assessment that is compared to the risk criterion is required."[2]

Among the issues in the Court statement, SSM in its statement brought up issues related primarily to items b), c) and d) above as areas where SKB is required to provide additional material in the next licensing step. SSM also, based on its integrated assessment, stated that the uncertainties associated with these three phenomena are such that it should be possible for SKB to demonstrate compliance in the coming steps of the step-wise licensing process and hence recommended the Government grant permission in the current step. Issues a) and e) are not particularly emphasized as significant uncertainties in SSM's statement.

SKB argued in the Court hearing that, based on available knowledge, none of the five items jeopardizes the safety of a KBS-3 repository at Forsmark. All the issues were addressed in SKB's original application in 2011 and further results were provided by SKB for most of them in the exchange of written material in SSM's review under the Act on Nuclear Activities, in particular during 2012–2016. SKB also noted that further research is required before full resolution is reached for some of the issues. In SKB's view, no new scientific information on the five issues was provided by any other actor during the hearing.

The matter currently (spring 2019) rests with the Government, which has given SKB the opportunity to submit supplementary information and analyses in the areas identified by the Court. At SKB, work on these issues has long been in progress. In response to the Court statement, SKB has intensified its on-going work in these areas.

1.2 Purpose and structure of this report

The purpose of the present report is to summarise SKB's and other work on the canister integrity issues brought up in the Court statement and to present conclusions regarding the phenomena *per se* and their importance for post-closure safety of the final repository for spent nuclear fuel, in response to the statements by the Court. The focus is to a large extent on new material that has not been used as bases for the statements from SSM and the Court. Safety assessment issues in SSM's statement that do not overlap with those in the Court's statement are not included in this report. These will, in accordance with SSM's statement, be addressed in future safety assessments and RD&D programmes.

---

[1] SKB's unofficial translation of the following text in Swedish: "*Vid en samlad riskbedömning krävs det full utredning om att slutförvaret är säkert under 1 000 år efter förslutning. Enligt mark- och miljödomstolens mening kan det däremot inte krävas full utredning om riskerna för läckage och radioaktiva ämnens spridning i miljön under 100 000 år och längre. Det är rimligt att acceptera vissa osäkerheter om slutförvarets skyddsförmåga på mycket lång sikt. Osäkerheterna får sammantaget inte vara betydande i förhållande till riskkriteriet, men det kan godtas om osäkerheterna är små. Kraven på utredning ska vara uppfyllda vid prövningen av tillåtlighet enligt miljöbalken. Vid bedömningen av om slutförvaret är långsiktigt säkert får inte beaktas en eventuell fortsatt utredning efter ett beslut om tillåtlighet.*"

[2] SKB's unofficial translation of the following text in Swedish: "*SKB bör enligt mark- och miljödomstolens bedömning i vart fall redovisa följande vid prövningen enligt miljöbalken. Det behövs ett underlag som läggs till grund för nya överväganden om de osäkerheter som tillkommit om kapselns skyddsförmåga. I den mån osäkerheterna kvarstår efter detta behöver dessa tas med i den samlade säkerhetsanalysen enligt kraven i SSM:s föreskrifter. Det kan behövas ett nytt scenario där osäkerheterna har medräknats. Slutligen behövs ett nytt beräknat resultat av hela säkerhetsanalysen som jämförs med riskkriteriet.*"

The structure of this report is based on the five canister-related issues. Before addressing these, a description of the repository environment is provided in Chapter 2. There, the development of the buffer surrounding the canister is discussed in general and sulphide fluxes and concentrations in more detail as these are important for the corrosion assessments. Another issue related to the corrosion environment in the final repository, the so called sauna effect, is treated in Chapter 3. The five corrosion issues are then addressed in Chapters 4 to 8. The results are integrated in Chapter 9 and conclusions are presented in Chapter 10.

2 Repository conditions

2.1 Introduction

The KBS-3 safety concept for final disposal of spent nuclear fuel is primarily based on complete containment of spent fuel in copper canisters, surrounded by a clay buffer at around 500 m depth in granitic rock, see Figure 2-1. Should a canister fail, remaining barriers provide considerable protection by preventing and delaying releases of radionuclides to the environment.

The impact of all identified corrosion issues on canister integrity in the environment provided by the Forsmark site were evaluated in the SR-Site assessment (SKB 2011). It was concluded that a 5 cm copper shell is sufficient to provide adequate safety for a KBS-3 repository at Forsmark. The only case where canister failure due to corrosion could not be ruled out was corrosion caused by sulphide in a few deposition holes with the highest groundwater flows, following erosion of the buffer. Here, the remaining barriers provided adequate protection. The calculated dose consequences for this case were with a margin lower than those corresponding to the risk limit in SSM's regulations (SSM 2008). This report is concerned only with the corrosion issues for which the Court considered that additional information is required, meaning that most of the corrosion issues in the SR-Site assessment are not revisited.

An evaluation of the canister integrity issues considered in this report requires information about relevant conditions in the repository, in the present case at the Forsmark site where SKB has applied for a license to build a final repository of the KBS-3 type. In particular, it will often be important to relate the conditions under which laboratory studies have been carried out to those prevailing in the final repository. Here, it is noted that laboratory studies conducted under accelerated conditions over short periods of time do not necessarily simulate processes occurring under repository conditions over much longer timescales. This is because the reported mechanisms may depend on the rate of the process, e.g., the gamma radiation does rate, the rate of transport of sulphide to the canister surface, the rate of hydrogen generation, etc. Acceleration of the test conditions may result in a change in mechanism, in some cases introducing detrimental phenomena that will not occur in the final repository.
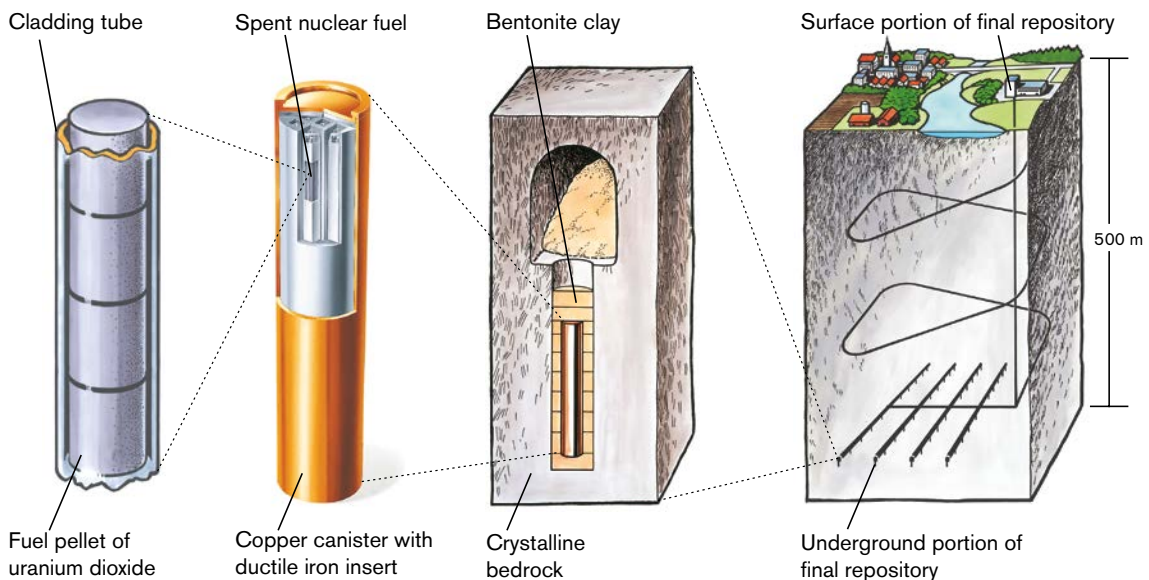
Figure 2-1. *The KBS-3 concept for final disposal of spent nuclear fuel.*

Two of the canister integrity issues, sulphide-induced pitting corrosion and stress corrosion cracking, concern situations where sulphide plays a key role as a corroding agent. As discussed further in Section 5.3, the properties of the copper sulphide film formed on the canister surface may be important in this context. These properties depend on the rate of influx of sulphide to the copper surface. It is, therefore, necessary to understand both the total extent of sulphide induced corrosion and the flux of sulphide to the canister surface, as well as to establish an upper bound on fluxes that may occur. Analysing consequences of upper bound fluxes is an important element in addressing uncertainties in general and some of the sulphide related corrosion processes at hand in this report in particular.

Section 2.2 provides information of relevance for the canister integrity issues regarding temperature, hydraulic and chemical conditions in a final repository at the Forsmark site. This information is a brief summary from the safety assessment SR-Site (SKB 2011) that supported SKB's licence application for the Forsmark site.

Most of the remainder of this chapter concerns sulphide formation and transport to the canister. Emphasis is given to unsaturated repository conditions, both since unsaturated conditions are particularly relevant for a low permeability rock site like Forsmark, and since several new studies have recently been performed in the area that has historically not been as extensively studied as saturated conditions. General information about sulphide in unsaturated clay is provided in Section 2.3. New experimental studies of sulphide formation in unsaturated clay are presented in Section 2.4 and a new modelling study of sulphide fluxes in unsaturated clay is reported in Section 2.5. Conclusions regarding unsaturated repository conditions are given in Section 2.6.

A brief summary of relevant repository conditions in general is provided in Section 2.7.

2.2 General information about conditions in a final repository at the Forsmark site

The long-term development of thermal, hydraulic, mechanical and chemical conditions in a final repository at the Forsmark site were analysed and reported in detail in the safety assessment SR-Site (SKB 2011). A site descriptive model (SKB 2008), based on the findings of several years of surface-based site investigations, was key input to those analyses. The following is a summary of some of the aspects of the development of the site conditions that are of relevance for the issues discussed in this report.

2.2.1 Thermal development of the canister

The background temperature of the host rock at the repository depth of about 470 m is around 11 °C at the Forsmark site. The residual heat of the waste will lead to a transient increase in temperature such that the canister surface reaches a peak temperature of typically 85 °C some 10 years after deposition. The layout of the repository and the residual power in a canister are chosen so that no canister will have a peak surface temperature above 95 °C, see further Section 10.3.4 in SKB (2011). Such a case is shown in Figure 2-2. The canister surface temperature will be around 40 °C after 1 000 years, 20 °C after 10 000 years and will approach the host rock background temperature in around 100 000 years, see Figure 2-2.

2.2.2 Buffer saturation times

A key hydraulic characteristic of the Forsmark site is its low frequency of water-conducting features at repository depth. This is reflected in low groundwater flow rates and hence low fluxes of corrosive agents like sulphide. In addition, the times to reach water saturation in the buffer and backfill of the repository are relatively long.

The saturation time of the buffer is expected to vary between a few tens to a few thousands of years, depending on the position in the repository. Modelling of this natural variability of the times for re-saturation was performed in Sellin et al. (2017) and is presented in Figure 2-3. With the assumption that the rock matrix hydraulic conductivity is 10^{-13} m/s, the saturation time is expected to be more than 1 000 years in most deposition holes. This means that the canister surface can be exposed to unsaturated conditions for a relatively long time.
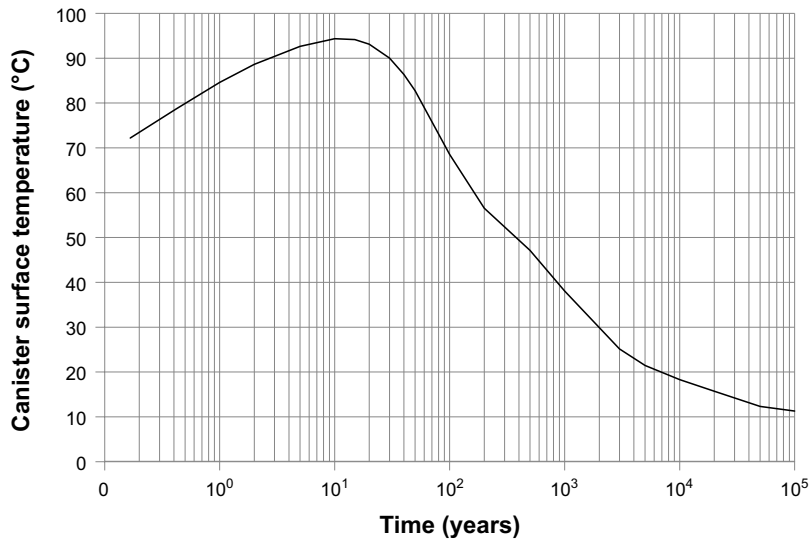
Figure 2-2. Temperature development of the canister surface in a KBS-3 repository at Forsmark. Data from Figure 10-16 in SKB (2011). The case concerns a pessimistic situation where the buffer remains unsaturated. A case where the buffer is saturated results in somewhat lower temperatures.
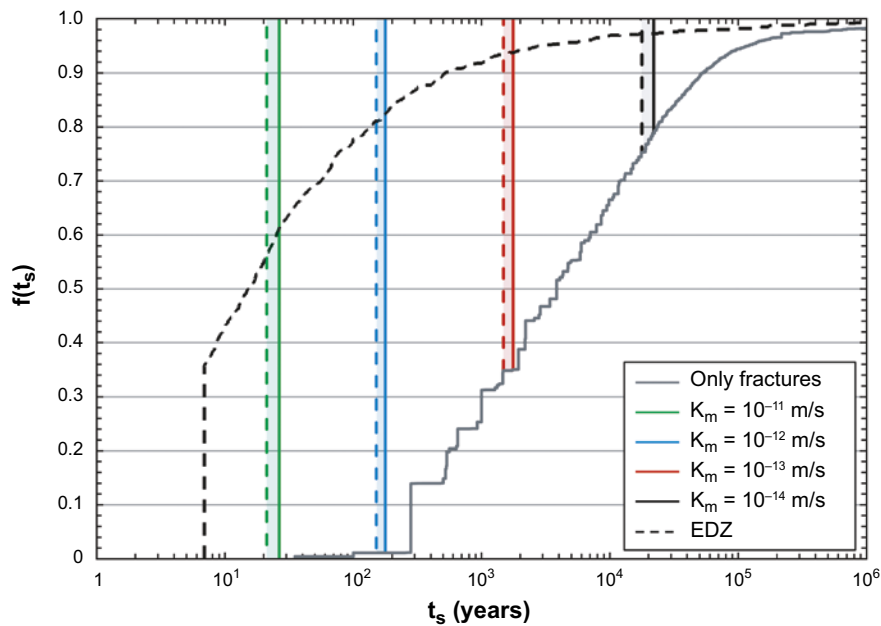
Figure 2-3. The solid grey line identifies the cumulative distribution of saturation times, $f(t_S)$, in the Forsmark repository calculated assuming no matrix flow. The coloured lines identify the time interval within which all deposition holes will reach full saturation if the matrix hydraulic conductivity has the value $K_m = 10^{-exp}$, where exp = {11, 12, 13, 14}. The dashed black line (labelled EDZ) identifies the distribution of saturation times if no flow resistance is present in the tunnels (Sellin et al. 2017). (The coloured thin bands represent intervals of saturation times for given hydraulic conductivities of the rock matrix. The span is caused by different conceptual descriptions of the bentonite in the deposition hole.)

2.2.3 Buffer erosion

Another key aspect of the buffer evolution concerns buffer erosion through colloid formation when the buffer is exposed to dilute groundwaters. Based on extensive evaluations in the safety assessment SR-Site (SKB 2011), it was concluded that this phenomenon could occur to an extent that advective transport conditions would be established in of the order of 100 out of the total of 6 000 deposition holes. This renders the canister surface in direct contact with the groundwater and hence more susceptible to corrosion by sulphide. For the few deposition holes potentially affected, it will take from tens of thousands to hundreds of thousands of years to develop advective conditions through erosion.

2.2.4   Redox conditions and groundwater sulphide concentrations

As for granitic sites in general, the chemical conditions at repository depth at Forsmark are reducing (SKB 2008). After an initial disturbance due to excavation and operation of the repository, the reducing conditions are expected to be re-established and essentially prevail throughout the one million year assessment period.

In the long term, sulphide is the dominating corrosive agent in the groundwater (SKB 2011). Groundwater concentrations of sulphide at repository depth at Forsmark were measured as part of the site investigations. Based on extensive evaluations of the results, a distribution of groundwater sulphide concentrations for use in the SR-Site assessment was derived, see Figure 2-4. The distribution was deemed to be representative, from the point of view of the safety evaluation, both for current conditions and for the long-term future conditions at repository depth.

2.2.5   Peak sulphide fluxes at the canister surface

As regards sulphide fluxes at the canister surface, two main phases of the repository evolution are of relevance: unsaturated buffer conditions when sulphide may be transported in the gas phase, and saturated buffer conditions, when the diffusive transport resistance in the buffer limits the fluxes. For a few depositions holes, also the case of advective conditions in the deposition hole is of relevance. As mentioned above, such conditions may arise after tens of thousands to hundreds of thousands of years as a consequence of buffer erosion.

For unsaturated conditions, a peak sulphide flux to the surface of less than 10^{-10} (7×10^{-11}) mol/(m^2 s) is derived in a modelling study reported in Section 2.5.

For saturated buffer conditions, a peak sulphide flux of around 10^{-11} mol/(m^2 s) is obtained for the highest sulphide concentration in the groundwater (1.2×10^{-4} mol/L) if only the transport resistance in the buffer is taken into account. If the hydraulic conditions in the rock are also considered, the corresponding flux is approximately 1.5×10^{-12} mol/(m^2 s).

For the eroded buffer case the combination of the highest sulphide concentration and the highest flow rate expected at the Forsmark site yield a peak sulphide flux of about 10^{-9} mol/(m^2 s). See Section 5.5 for further data and an illustration of sulphide fluxes for saturated and eroded conditions. Full documentation the calculation of sulphide fluxes at the canister surface is given in SKB (2010a).
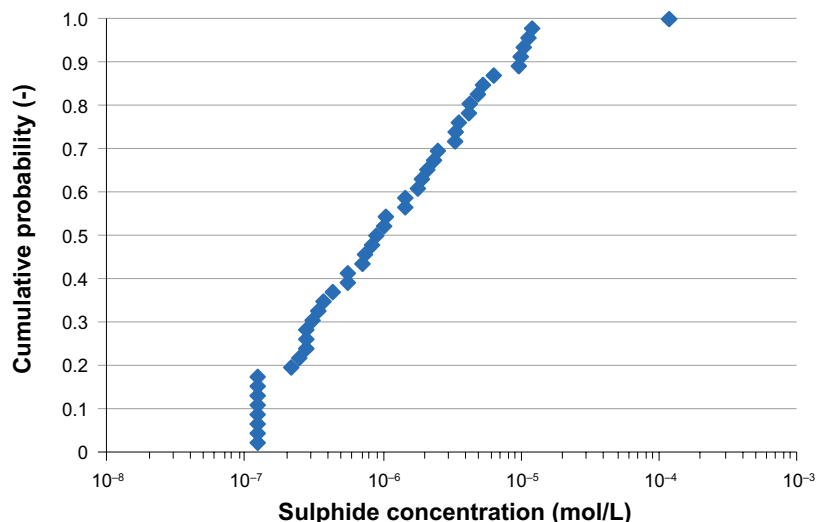
Figure 2-4. Groundwater sulphide concentrations used in the safety assessment SR-Site. Data below the detection limit of the analyses, which is between 9×10^{-7} and 6×10^{-8} mol/L, are set to the lowest value in the distribution, 1.2×10^{-7} mol/L. The maximum value is 1.2×10^{-4} mol/L, whereas all other values are at least one order of magnitude lower.

2.3 General information about the sulphide system in unsaturated clay

2.3.1 Sulphide chemistry

Sulphide is easily oxidised by oxygen and it may also be produced by sulphate reducing bacteria (SRB) if the conditions are favourable (see e.g. Hansen 1993). Because of this, an assessment of sulphide fluxes in the repository must consider sulphate as well. In the initially unsaturated tunnel and deposition-hole system, one must consider two sources of sulphur; that which is located within the buffer and backfill, and the sulphur added by the inflowing groundwater.

In water, hydrogen sulphide acts as a weak acid, and the concentrations of hydrogen sulphide and bisulphide are linked to that of H^+ by an equilibrium constant (K), see for example Section VI.2.1.2 in (Grenthe et al. 1992):

$$H_2S(aq) \rightleftarrows H^+ + HS^- \qquad \log K(298.15 \text{ K}) = \log [H_2S] - \log [H^+] - \log [HS^-] \approx -7.0$$
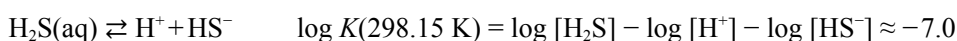
According to this, in neutral aqueous solutions (pH $\approx$ 7), the concentrations of H_2S and HS^- are approximately equal. The forward and reverse reactions are fast and equilibrium can be assumed for all time scales relevant for repository evolution. The solubility of hydrogen sulphide gas in water may be expressed in terms of a Henry's law constant, $H = [H_2S(aq)] / P_{H2S} \approx 1 \times 10^{-3}$ mol/(m^3 Pa) ≈ 0.1 mol/(L bar) (Sander 2015). The rate of dissolution or degassing will depend on the interface area (gas/aqueous solution) and on how far from equilibrium the values of $[H_2S(aq)]$ and P_{H2S} are. During the unsaturated and partially saturated period it is clear that sulphide may exist as three chemical species, $H_2S(g)$, $H_2S(aq)$ and HS^-, in proportions that will depend on temperature, system pressure and pH. The pH will in turn be affected by other reactions, such as calcite precipitation or dissolution, CO_2 degassing, etc, and therefore, the speciation of sulphide will be affected by many processes. Section 2.4 describes experimental studies aiming at determining the sulphide contents of the gas phase in partially saturated backfill and buffer materials.

During the oxic phase of the unsaturated and partially saturated period, sulphide will be quickly oxidised to sulphate (SO_4^{2-}); abiotically, the oxidation proceeds on a time scale of days, while the microbial rate of oxidation is three orders of magnitude greater (Luther et al. 2011). Some of the pyrite present in the bentonite may also undergo some oxidation during this period, even if the reaction is slower. The amount of air initially entrapped in a 6 m section of a deposition tunnel is about 27.7 m^3 (SKB 2011), and this oxygen is more than enough to oxidise all sulphide until saturated conditions are achieved. For example, groundwater flowing into the tunnel section will contain at most a sulphur concentration of $\approx 10^{-3}$ mol/L, and when all the air initially present has been replaced by groundwater, ≈ 28 mol of sulphur will have been added by the groundwater, much less than the initial amount of O_2 from the air entrapped in the backfill. However, in addition to the oxidation of sulphide, oxygen may also be spent in many other reactions: the aerobic corrosion of the Cu canister will scavenge most of the initial O_2 as indicated in Section 2.4.1, and oxygen will also quickly react with Fe(II) in the inflowing groundwater (Pham and Waite 2008). In the safety assessment SR-Site, it is pessimistically assumed that all entrapped oxygen oxidises Cu to Cu_2O, causing a corrosion depth of less than 0.5 mm, see Section 10.2.5 of SKB (2011).

For the assessment of copper corrosion, the initial oxidation of sulphide can be pessimistically neglected, although the initial oxic corrosion of the copper canister cannot be disregarded. When the results of experiments and field tests are interpreted, it may, however, be relevant to include oxidation of sulphide.

As described in more detail in Section 8.6.2, oxygen-containing corrosion products of copper are unstable in sulphide solutions, and the copper oxides are converted to Cu_2S. When this conversion is complete, the sulphide-driven corrosion of copper is controlled by the supply of sulphide.

Once anoxic partially saturated conditions have been achieved, hydrogen sulphide will no longer be oxidised. The results displayed in Figure 2-8 (Section 2.4.1) indicate that the time to reach anoxic conditions will in general be much shorter than the saturation time for the buffer, which is expected to vary between a few tens to a few thousands of years (Section 2.2.2). As mentioned above, at most ≈ 28 mol of sulphur (primarily as sulphate) will be added to the deposition tunnel by the inflowing groundwater; only a fraction of this sulphur will be as sulphide or may be reduced to sulphide by SRB. In addition, a certain amount of sulphate will have its origin in the backfill material; if SRB activity is favourable (see Section 2.3.2), some of this sulphate may be reduced to sulphide.

The partitioning of sulphide between the gas phase in the pores of the backfill (or buffer) and the pore-water is governed by the acid dissociation reaction and by the Henry's law constant. If the concentration of sulphide in the porewater of the backfill increases during the partially saturated period, for example due to SRB activity, so too will the pressure of $H_2S(g)$ in the gas-filled pore space increase according to Henry's law, independently of the total system pressure. It is worth noting however, that the partitioning of a given amount of sulphide between the gas and water phases also depends on the water/gas volume ratio according to the ideal gas law. This means that while groundwater inflow progresses, and the gas phase is compressed, the total amount of sulphide in the system may perhaps increase by the added groundwater and SRB activity, but the total amount of sulphide in the gas phase will decrease because there will be a smaller gas volume. A more detailed analysis of the sulphide fluxes in partly saturated clay is provided by Eriksson and Hedin (2019), and it is summarised in Section 2.5.

2.3.2 Sulphate reducing bacteria

Thermochemical sulphate reduction is not considered in this study as it is significantly slower than biological sulphate reduction and does not occur at temperature below 100 °C (e.g. Machel 2001). Rather, the focus is on biotic sulphate reduction. Oxidized sulphur compounds can be used as terminal electron acceptors for the anaerobic respiration of organic matter by sulphate- and sulphur-reducing bacteria producing hydrogen sulphide (H_2S). These bacteria are commonly heterotrophic, obtaining organic matter from external sources, although some strains can be facultative autotrophs (organisms that, depending on the conditions, can use either inorganic carbon compounds or organic carbon sources) or mixotrophs (i.e. use both organic and inorganic compounds as carbon source). To be used as an electron acceptor, sulphur must have a certain level of oxidation. Among the sulphur compounds, sulphate as well as others such as sulphite, thiosulphate, hyposulphite and elemental sulphur may be used. Sulphate- and sulphur-reducing bacteria obtain energy by coupling the oxidation of organic compounds or H_2 to the reduction of sulphate or other sulphur compounds to sulphide, which may be released as $H_2S(g)$ into the environment:

$$SO_4^{2-} + 2CH_2O \rightarrow 2HCO^- + H_2S$$

$$2H^+ + SO_4^{2-} + 4H_2 \rightarrow H_2S + 4H_2O$$
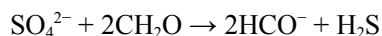
This process is called dissimilatory sulphate reduction and is typical for sulphate reducing bacteria (e.g. Camacho 2009, Madigan et al. 2012). Hydrogen is used by virtually all species of sulphate reducing bacteria whereas use of other electron donors, e.g. lactate, acetate, pyruvate, ethanol, fumarate, propionate is more restricted. In an environment with high sulphate and low H_2, hydrogen (or other electron donors) is rate limiting.

In addition, a few sulphate-reducing bacteria are quite oxygen tolerant meaning that they are inactive but not killed in presence of oxygen (e.g. Kjeldsen et al. 2004, Madigan et al. 2012). There is even at least one species that has been shown to be able to use O_2 as electron acceptor under microaerophilic conditions (Sigalevich and Cohen 2000). This may imply that during unsaturated conditions, certain SRB could at least theoretically be active at moderate oxygen levels and when all oxygen is consumed switch over to respire sulphate. In addition those species that have been inactive could then become active when conditions become anoxic. Unsaturated conditions are expected to prevail during the first couple of thousands of years of the existence of the repository.

In a growth culture of SRB containing ferrous iron, the H_2S that forms will precipitate as FeS. Since the iron binds sulphide, it works as a detoxifying agent and will make growth to higher cell densities possible (Madigan et al. 2012).

The extent to which water activity, a_w, limits microbial activity varies slightly between different microbial species. Bacteria generally need higher a_w than for example moulds. Typically, the lower limit for bacterial growth lies in the range 0.90−0.97 (e.g. Motamedi et al. 1996, Madigan et al. 2012). No microbial activity will occur below 0.60 (e.g. Madigan et al. 2012). However, for bentonite buffer the degree of swelling also needs to be taken into account as it also affects microbial activity (Bengtsson et al. 2015, 2017a, 2017a). In the FEBEX in situ experiment it was obvious that the water content played a major role for microbial activity. Cells could be cultivated in large numbers from moist,

low temperature locations, e.g. in the outer buffer close to the rock and away from the heater in the FEBEX. The absence of cultivable bacteria in the samples from around the heater may be because they were viable but not cultivable due to effects from desiccation, or that viable cells were killed by the absence of water, possibly in combination with the high temperature (Bengtsson et al. 2017b).

Many bacteria, including SRB, can survive without water for long periods of time; therefore bacteria are often described as opportunistic, implying that they take advantage of a situation or environment when the proper circumstances present themselves. For example, a bacterial cell can lie dormant for hundreds or even thousands of years as a spore, or a desiccated cell, and quickly come to life again when suitable conditions reappear (e.g. Potts 1994, Müller et al. 2014). If the barriers work as expected conditions will not favour SRB activity: Either the clay will be too dry or to dense for them to be able to grow.

2.4 Experimental studies of sulphide formation in unsaturated buffer and backfill clay

At the Forsmark site, the saturation time of the buffer surrounding the canister is expected to vary between a few tens to a few thousands of years, depending on the location in the repository (see Section 2.2.2). In most deposition holes the saturation time is expected to be more than 1 000 years. This means that the canister surface can be exposed to unsaturated conditions for a relatively long time. One issue for canister corrosion is the chemical composition of the gas in the unsaturated bentonite and in the engineering voids in the deposition hole. Of particular interest is the content of oxygen (O_2) and hydrogen sulphide (H_2S). Issues of interest include:

- Will O_2 be consumed by the repository components? If yes, what is the reaction rate?
- Will H_2S be generated from accessory minerals in the buffer?
- Can H_2S be generated microbially in an unsaturated buffer?

These issues are addressed in the following, building on results from recent experiments within SKB's R&D programme.

2.4.1 Investigations of gas evolution in an unsaturated KBS-3 repository

Two tests have been designed and conducted at Clay Technology AB, Lund, Sweden in order to investigate the possible evolution of gases in the buffer of an unsaturated KBS-3 repository (Birgersson and Goudarzi 2018). One of the tests included a central heater in the form of a copper tube as well as IBECO RWC bentonite blocks and pellets, configured to form a scaled model of an isolated unsaturated KBS-3 deposition hole (10 cm copper tube, approximately 30 cm bentonite block diameter), Figure 2-5. The second test has no heater and contains only bentonite pellets (apart from a stainless steel container). It was maintained at constant temperature (room temperature or at 50 °C), and is referred to as the isothermal test.

Figure 2-6 shows the evolution of the measured Relative Humidity (RH) and temperature in the thermal gradient test (approximate location of the sensors is indicated in Figure 2-5). It can be noted that although the temperature of the heater is 80 °C, the temperature in the bentonite block near the heater is only approximately 50 °C. There is apparently a large drop in temperature over the inner slot region. In the outer pellets slot, the temperature was about 40 °C throughout the test. Thus, at this position in the set-up, the temperature drops approximately 10 degrees over the bentonite (block and pellets).

The RH close to the heater reached 100 % as the heater was switched on, only to drop to approximately 63 % as the system evolved. The RH in the pellets stayed approximately constant at 80−85 %. This evolution in relative humidity indicates that water has been transported away from the bentonite closest to the heater, while the water content in the pellets slot has basically remained constant.
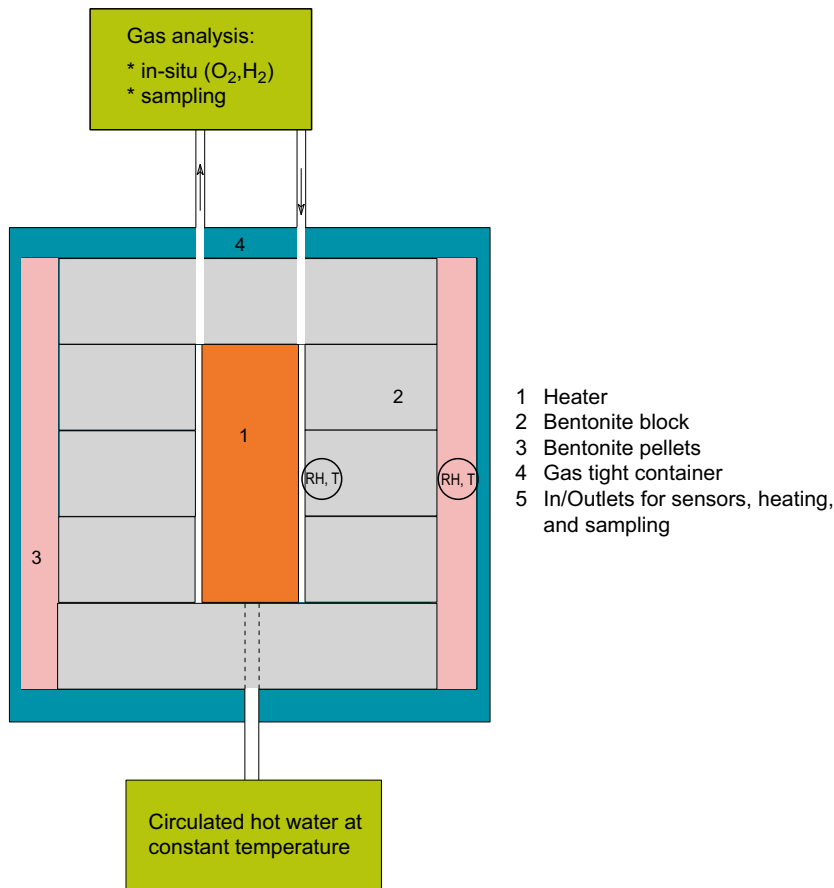
Figure 2-5. *Schematic of the set-up for the thermal gradient test (Birgersson and Goudarzi 2018).*
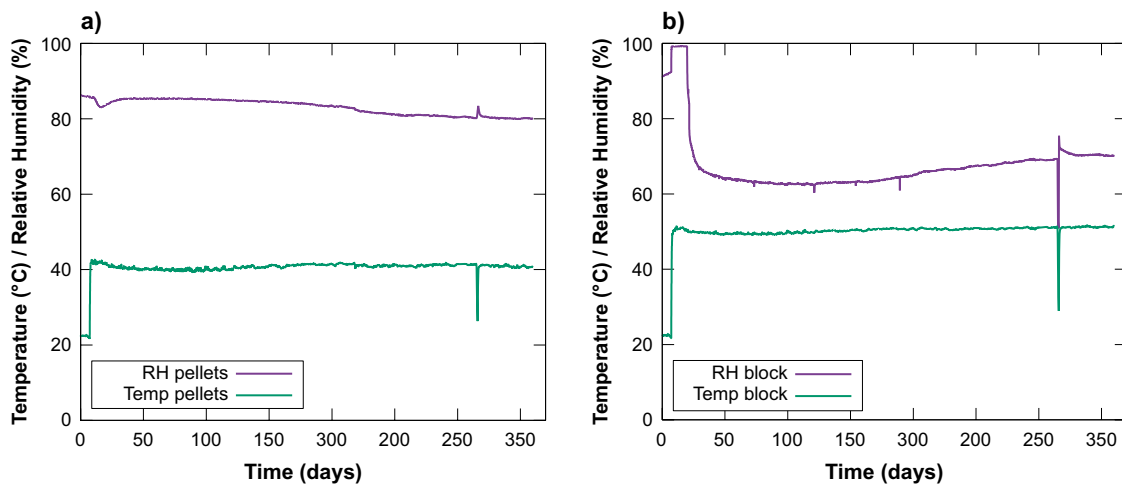
Figure 2-6. *Evolution of temperature and relative humidity in the thermal gradient test, for a) pellets, b) blocks. Approximate positions of the sensors are indicated in Figure 2-5. The spikes seen in all the curves at day 315 are due to an unintentional shut-off of the heating system for a few hours in connection with gas sampling. (Birgersson and Goudarzi 2018)*

At the end of the test, samples were taken for water content determination at various places within the set-up as the bentonite was removed from the container. In general, the bentonite blocks and rings were well preserved, i.e. there were no visible cracks. The recorded water-to-solid mass ratios and the approximate positions where sampling was made are shown in Figure 2-7. The measured water distribution confirms that the system dried significantly next to the heater during the course of the tests, while water accumulated in the pellets slot, particularly in the upper part. Note that the initial water-to-solid mass ratio for blocks and rings was 0.28 and 0.24 respectively, and the initial water-to-solid mass ratio was 0.23 for the pellets. Comparing with the measured RH-evolution, it may be noted that the RH measured in the pellets slot at the end of the test (approximately 80 %) does not correspond to the measured water-to-solid mass ratio; a value of the water-to-solid mass ratio of 0.426 is expected to give an RH value close to 100 %. This discrepancy is interpreted as a sign of a quite uneven water distribution within the pellets slot in this position in the test. Note, for instance, that the measured water-to-solid mass ratio in the adjacent block is 0.124, which corresponds to an RH considerably lower than 80 %.

After termination of the isothermal test, two determinations of the water-to-solid mass ratio of the pellets were made, both giving a value of 0.239, which is in good agreement with the expected value.

The evolution of the oxygen level in the thermal gradient test is shown in Figure 2-8. An immediate drop in oxygen is seen, and the rate of oxygen consumption increased as the heating system was switched on (day 7). This oxygen consumption is reasonably ascribed to aerobic corrosion of the copper. After approximately 60 days, the oxygen level reached a near steady value of approximately 1 %. After about 150 days, a very slow increase of the oxygen level was noted. Towards the end of the test, gas was sampled and analysed externally. The increase in the *in situ* oxygen level corresponds to the times at which gas samples were taken and is believed to be the result of air leakage during sampling.

The evolution of the oxygen level in the isothermal test is displayed in Figure 2-9. For the first 111 days, the test was held at room temperature in the laboratory and no significant oxygen consumption was recorded. At day 111, the test was placed in an oven at 50 °C and a slight continuous drop in oxygen level is observed. After an additional 150 days, the oxygen level reached a steady value. During the last part of the test, gas was sampled and analysed externally.

Two samples were taken from each of the tests. The samples were analysed by an accredited external laboratory using gas chromatography, as well as an optical feedback cavity enhanced absorption spectrometer (for sulphide). The main results from the analysis are presented in Table 2-1.
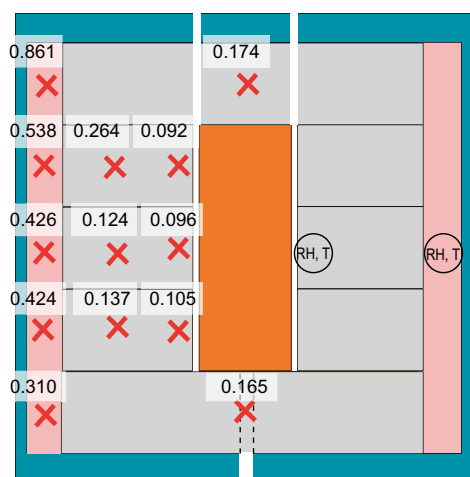
Figure 2-7. *Values of measured water-to-solid mass ratios at different positions in the temperature gradient test at termination. Red crosses indicate approximate positions of where samples were taken (Birgersson and Goudarzi 2018).*
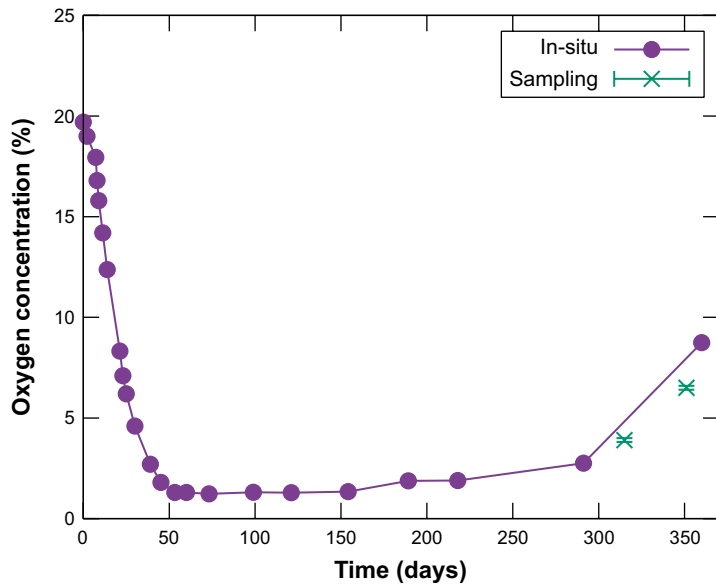
Figure 2-8. *Oxygen evolution in the thermal gradient test. The heater was switched on after 7 days. Sampling was performed at day 315 and day 351 (Birgersson and Goudarzi 2018).*
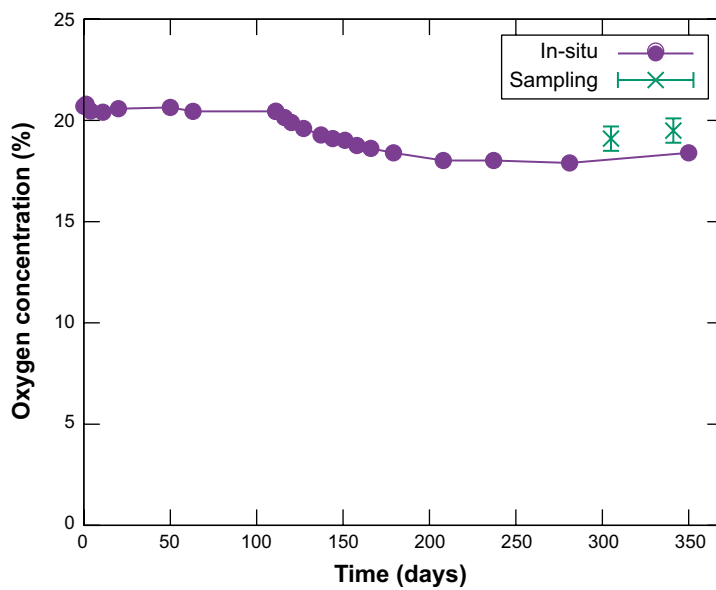
Figure 2-9. *Oxygen evolution in the isothermal test. From day 0 to day 111, the test was kept at room temperature (21 °C–22 °C). From day 111 the test was placed in an oven at 50 °C. Sampling was performed on day 305 and day 341(Birgersson and Goudarzi 2018).*

Table 2-1. Gas composition of the analysed samples. Unit is vol-% except for H₂S, which is given in vol-ppm (Birgersson and Goudarzi 2018).

Sample	Gradient test, day 305	Gradient test, day 341	Isothermal, day 305	Isothermal, day 341
O_2	3.9	5.9	19.1	19.5
N_2	94.6	91.0	79.7	77.8
H_2	0.1	0.1	0.1	0.1
CO_2	1.5	1.3	1.2	0.9
CO	< 0.1	< 0.1	< 0.1	< 0.1
CH_4	< 0.1	< 0.1	< 0.1	< 0.1
H_2S	< 0.1 ppm	< 0.1 ppm	< 0.1 ppm	< 0.1 ppm

The analysed oxygen levels broadly confirmed the on-line measurements; in the temperature gradient test the oxygen level was considerably lower as compared to the isothermal test. The analysed oxygen level in the temperature gradient test was however somewhat higher compared to the in-situ measurements. Furthermore, the oxygen level, at least in the temperature gradient test, was larger in the second sample as compared to the first. This indicates a certain leakage of the test set-up. In all tests, a substantial amount of CO_2 was detected, in the range 0.9–1.5 %, which may be compared to the content in air of 0.04 %, as well as a small, but detectable, amount of H_2. The samples taken at the first samplings were additionally analysed for light hydrocarbons, of which none were detected (detection limit 5 ppm). No sulphide was detected in any of the samples.

The main result of the present study is that no sulphide gas was detected. In the case of the thermal gradient test, this may have been expected, since the copper heater would function as a sink for sulphide even if it was produced (if the reaction rate is sufficiently high). The fact that no sulphide gas was detected in the isothermal test is, however, a good indication that significant amounts of such gases are not to be expected under semi-dry repository conditions. It should be noted that the bentonite used in this study was chosen due to its significant sulphur content (pyrite). But even with this condition, no sulphide gas could be detected (detection limit <0.1 vol-ppm). Another main result is the observed oxygen consumption in the temperature gradient test. It is clear that the main reason for this consumption is due to corrosion processes on the copper heater, since a similar behaviour is missing in the isothermal test, which did not include a copper component.

As a comparison, Giroud (2014) present the results of the O_2 monitoring during the backfilling and early heating phases of the Full-scale Emplacement Experiment (FE Experiment) at the Mont Terri underground laboratory Switzerland, as well as the first results of laboratory experiments which aim at identifying the processes controlling O_2 concentrations. The monitoring shows the disappearance of gaseous O_2 and onset of anaerobic corrosion in sections not affected by O_2 inflow from the access tunnel within weeks after backfilling, and even before closure of the drift for the deepest parts of the experiment. The laboratory experiments show that O_2 can significantly adsorb on granular bentonite exposed to high temperatures and might in principle also adsorb at ambient temperature and relative humidity as low as 55 %. Thus, gas sorption should be considered in the balance of O_2 in the FE experiment.

Previous studies estimated the duration of aerobic conditions in an emplacement drift between a few years and several decades, while the new results from this test show that anaerobic conditions may be reached within a few weeks up to maximum a few months after closure of an emplacement drift for spent fuel in Opalinus Clay.

2.4.2 Further investigations of gas evolution in an unsaturated KBS-3 repository

The tests described in Birgersson and Goudarzi (2018) above gave an indication about the evolution of the gaseous phase in an unsaturated bentonite. There are however still uncertainties remaining: no H_2S was detected, either in the temperature gradient test or in the isothermal test. It cannot be ruled out that the reason could have been that the H_2S reacted with the copper in the temperature gradient test and with oxygen in the isothermal test (Johansson A J 2019a). Therefore, an additional test was conducted to further investigate these issues, in preparation of a more comprehensive experimental study. In this test, a desiccator was filled with Milos bentonite pellets that were heated from below (Figure 2-10) to 50 °C. A flask was placed on the surface of the pellets with a solution of divalent copper ions to capture any hydrogen sulphide formed. On top of the copper solution (dissolved $CuSO_4 \cdot 5H_2O$) a very simple reflux condenser was placed to prevent the evaporation of the water from the solution and to extend the duration of the experiment. The Cu(II) ions in the copper sulphate solution rapidly react with any dissolved hydrogen sulphide by the following principle reaction:

$$Cu^{2+} + H_2S\ (aq) \rightleftarrows CuS(s) + 2H^+$$
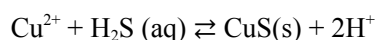
This reaction is extremely fast, and the formed CuS is easily observed visually as a brownish black precipitate, while the blue copper solution slowly loses its colour, see Svensson et al. (2017). The focus of the test was the detection of hydrogen sulphide, and to learn in general about the processes involved.

Figure 2-10. *Test containing bentonite pellets in a desiccator, heated from below, regulated with a temperature probe in the pellets, and also containing a flask with a solution of divalent copper ions to capture any hydrogen sulphide formed.*

During the heating of the bentonite, it was clear that a strong temperature gradient existed within the layer of bentonite pellets between the bottom part closest to the heater and the colder upper part. The appearance of the clay in the lower parts was drier, and at the top lid condensation was taking place. The volume of copper sulphate solution decreased with time, and after some days totally evaporated. After the experiment was turned off no sulphides were observed, only pure bluish crystalline copper sulphate. X-ray diffraction verified the salt present as being the pentahydrate ($CuSO_4 \cdot 5\ H_2O$). In the test *i)* no hydrogen sulphide formation was observed, and *ii)* based on visual inspection water was redistributed from the lower hotter part to the upper colder part, as expected.

An additional, more comprehensive, experiment with two set-ups, one with a stainless steel heater and one with a copper heater, both in unsaturated bentonite and equipped with an on-line gas monitoring system, is in progress. These tests are similar to the ones described in Section 2.4.1 and the purpose is to get more data and gain more understanding on the gas composition in an unsaturated deposition hole. Here both H_2S and SO_2 can be measured on-line, in addition to O_2.

2.4.3 Activity of the sulphate reducing bacterium *Pseudodesulfovibrio aespoeensis* as a function of water activity

Sulphate reducing bacteria respire sulphate, meaning that they use the sulphur in sulphate as an electron acceptor. This results in the formation of sulphide ($S^{2-}/HS^-/H_2S$) which in turn may corrode the copper canisters. The reaction is summarised as:

$$xCu(s) + HS^-(aq) + H^+(aq) \rightleftarrows Cu_xS(s) + H_2(g)$$
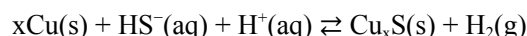
In order to be active, microbes need water, nutrients, electron donors (energy sources), electron acceptors, a carbon source that could be either inorganic or organic and space. The carbon source often serves also as an electron donor, like e.g. lactate. However, hydrogen is the preferred electron donor for most lithotrophic (i.e. living off inorganic energy sources) SRB. In addition, SRB also

generally require reducing conditions in order to be able to perform sulphate reduction, see further Section 2.3.2. In case no energy source (electron donor) is present, the bacteria are unable to respire even if there are enough nutrients and electron acceptors.

During water saturation, bentonite expands and builds up a swelling pressure, and at swelling pressures higher than approximately 2 MPa, SRB are expected to be inactive (Bengtsson and Pedersen 2017). Published data on turgor pressure, i.e. the force within the cell that pushes the plasma membrane against the cell wall, in prokaryotic cells mention pressures between 0.08 MPa and 2 MPa (Potts 1994). An upper limit of 2 MPa turgor pressure would mean that cell integrity is possible though limited, at bentonite swelling pressures below 2 MPa. However, during the early period, i.e. the first couple of thousand years of the repository lifetime, before the bentonite is water saturated, there may be a window of conditions where the bentonite is neither dry, nor wet, when a high enough relative humidity is present where the SRB potentially can be active. A study that aims at finding out if there is a moisture threshold limit for the bentonite when SRB are able to be active is ongoing and preliminary results (Svensson et al. 2019) are presented here.

The experimental set-up consists of a reaction tube containing the bentonite, microbes and various combinations of water, lactate, gypsum ($CaSO_4 \cdot 2\,H_2O$) and nutrients. The experimental conditions are listed in detail in Tables 2-2 and 2-3. The reaction tube is placed in an outer, sealed tube, sharing the atmosphere with the reaction tube, Figure 2-11. The bacterial strain chosen for the study was *Pseudodesulfovibrio aespoeensis* originally isolated from Äspö (Motamedi and Pedersen 1998). This species was chosen because of its ability to use lactate as an energy source. In the outer tube, water or a saturated salt solution was present to set the relative humidity. A pure water solution gives the highest possible relative humidity (RH) in the system, while supersaturated solutions of various salts give rise to lower RH. A small amount of copper sulphate was added to the outer solution as an indicator of formed sulphide, in the same way as for the investigation of gas evolution (Section 2.4.2), so that a brownish black precipitate shows that CuS is formed, while the blue copper solution slowly becomes more pale.

To date (March 2019), two experimental series, here denoted I and II, have yielded results, shown in Table 2-2 and Table 2-3. The positive control conditions are advantageous for microbial activity with added gypsum and a growth medium amended with lactate, macronutrients, nutrient broth and reductants (cysteine-HCl and resazurin) in order to obtain the right anaerobic conditions (<0.1 ppm O_2), as well as the non-compacted bentonite.
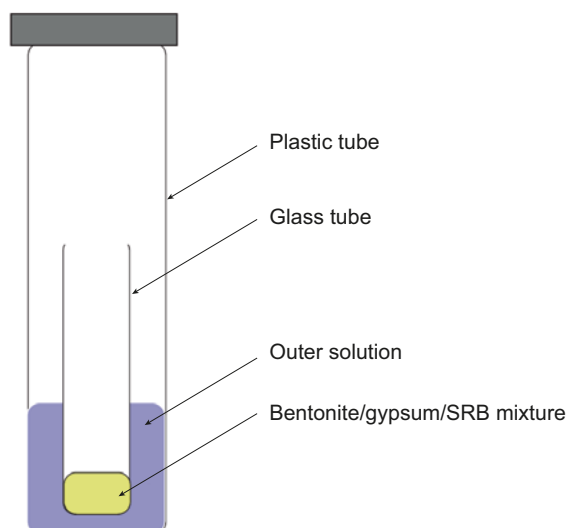
Figure 2-11. Experimental setup containing an inner glass tube within a larger plastic tube. The outer solution sets the relative humidity and also contains divalent copper ions to detect hydrogen sulphide. The experiment was performed in a glovebox with an inert nitrogen atmosphere (Svensson et al. 2017).

Table 2-2. Detailed experimental conditions and results for series I. A1 is a positive control, i.e. with conditions favourable for *P. aespoeensis*. In addition, a control with bentonite and no added bacteria was used for comparison (A2). The bentonite was not sterilized in any of the samples. Duration: 3 months.

No.	CuS formation	~RH (%)	Inner tube				Outer tube		
			Bentonite (g)	Gypsum (mg)	*P. aespo***	Sterile medium (mL)	Salt***	$CuSO_4$ (mg)	Deionized water (mL)
A1	yes	100	–	60	+	5	–	100	15
A2	no	100	2	60	–	5	–	100	15
A3	no	100	2	60	+	0.5	–	100	15
A4	no	11*	2	60	+	0.5	LiCl	100	15
A5	no	76*	2	60	+	0.5	NaCl	100	15
A6	no	97*	2	60	+	0.5	K_2SO_4	100	15

*Choudhury et al. (2011), **100 µL inoculum from culture in late exponential growth phase, ***Supersaturated.

Table 2-3. Detailed experimental conditions and results for series II. S1 and S2 are positive controls, i.e. with conditions favourable for *P. aespoeensis*. In addition a control with bentonite and no added bacteria was used for comparison (S3). The bentonite was not sterilized in any of the samples. Duration: 3 months.

No.	CuS formation	~RH (%)	Inner tube				Outer tube		
			Bentonite (g)	Gypsum (mg)	*P. aespo***	Sterile medium (mL)	Salt***	$CuSO_4$ (mg)	Deionized water (mL)
S1	yes	100	–	60	+	5	–	100	15
S2	yes	100	–	60	+	5	–	100	15
S3	Yes in one of the two replicates	100	2	60	+	5	–	100	15
S4	no	100	2	60	+	0.5	–	100	15
S5	no	97*	2	60	+	0.5	K_2SO_4	100	15
S6	no	76*	2	60	+	0.5	NaCl	100	15

* Choudhury et al. (2011), ** 100 µL inoculum from culture in late late exponential growth phase, *** Supersaturated.

In the test tubes where 5 mL of liquid medium had been added in the inner tube, sulphide formed and was detected as CuS precipitate on the outer surface of the inner tube, Figure 2-12. In the test tubes with 0.5 mL or less medium in the inner tube, no sulphide could be detected and here the outer solution had no impact (pure water or salt water).

These results support what was initially assumed, namely that microbiological reduction of sulphate to sulphide (hydrogen sulphide) occurs when the microbes had access to liquid water (in addition to gypsum, lactate, nutrients and no swelling pressure); while no sulphide production was detected when the microbes were restricted to a relative humidity of 75–100 %, but no liquid water. It cannot be ruled out that sulphate reduction may occur when microbes are in a high relative humidity environment without access to liquid water, although at a very low reaction rate, making it undetectable on the time scale of 3 months used in this study.

The solid material from the inner test tubes in one series was sent to an external laboratory for sulphide analysis. No sulphide could be detected, not even in the samples where CuS was formed in the outer solution. Hence, sulphides are not expected to form in the bentonite or in the internal tube, but rather form gaseous hydrogen sulphide and react with the external copper solution. The pH of the bentonite-water solution (i.e. in the inner tube) is expected to be fairly alkaline which favours $HS^-(aq)$ over $H_2S(g)$. The reaction in the outer solution is, however, extremely fast and CuS is very stable, hence driving the reaction in the direction $HS^-(aq) \rightarrow H_2S(g) \rightarrow CuS(s)$ in this solution.
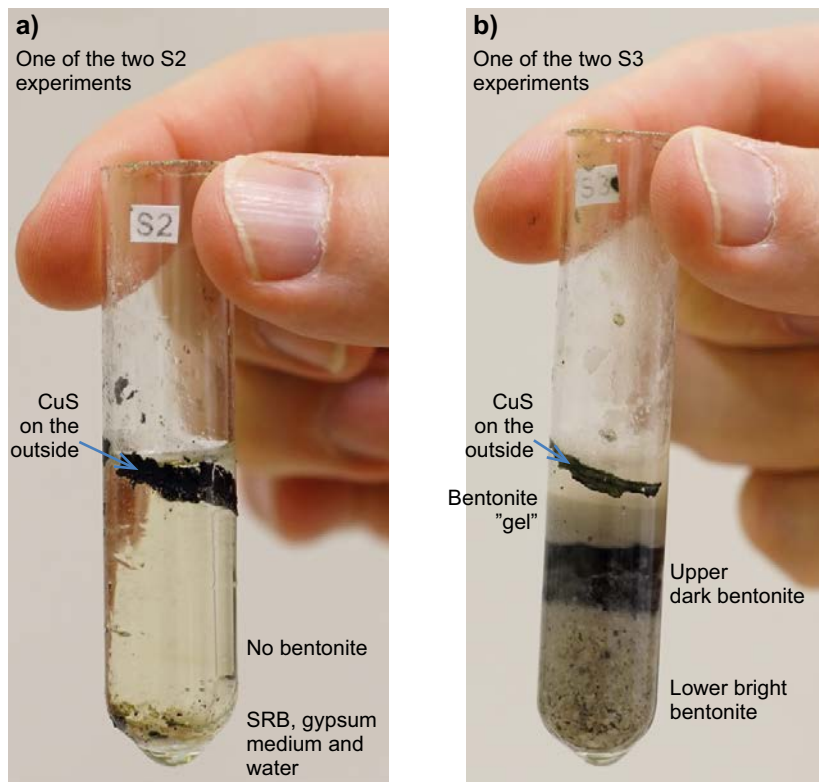
Figure 2-12. Two inner tubes from Series II. Copper sulphide formed on the outside of the inner tube by the reaction of divalent copper ions with hydrogen sulphide: a) in the S2 tubes, without bentonite, b) in one of the S3 tubes, with bentonite. (Svensson et al. 2017)

2.4.4 Summary of experimental results

These experiments concern sources and sinks of molecular oxygen and of sulphide in the form of H_2S and HS^-, which may all corrode the copper canister. Regarding the three questions posed in the beginning of Section 2.4, the results of the experiments that have been performed in unsaturated bentonite show:

1. Rapid consumption of the oxygen if a copper heater is present and limited oxygen consumption in a bentonite-only system

2. No generation of H_2S from sulphide minerals originally present in the buffer

3. No generation of H_2S from microbial processes in unsaturated bentonite, not even at RH=100 %

In particular, it is concluded that the results presented in Section 2.4 further corroborate the conclusion that an SRB-containing biofilm cannot be established on the canister surface under unsaturated conditions, since such conditions are not compatible with microbial activity.

These results confirm SKB's understanding of the evolution of the gas phase under unsaturated conditions. In particular, no evidence of the generation of sulphide in unsaturated bentonite clay has been found under repository-like conditions. The relevance of the results for the issues raised by the environmental court is briefly described at the end of Section 2.6.

2.5 Modelling of sulphide fluxes in unsaturated clay

As a part of the analysis of copper corrosion in a KBS-3 repository, it is of interest to understand the transport of sulphide in the clay system. Transport in saturated clay has been extensively studied as evidenced e.g. by the wealth of buffer diffusion data cited in Section 5.3 of SKB (2010b), whereas this is not the case for an unsaturated clay system. Both the accumulated flux of sulphide to the canister surface and the flux as a function of time are of interest. The latter is of importance since the instantaneous flux has an impact on the properties of the copper sulphide film formed on the surface, see Section 5.3.

Eriksson and Hedin (2019) provide a modelling study of how sulphide diffuses in the gas phase of the unsaturated bentonite backfill and buffer to the copper canister where it is assumed to react with the copper and cause corrosion. Specifically, a case where the initial water content of the clay system is unchanged is considered. This is relevant for low permeability site, as at Forsmark in Sweden, where saturation may take hundreds of years or longer as discussed in Section 2.2.2. As the bentonite saturates, the physical volume of the gas phase in the bentonite will be reduced and the diffusion of sulphide will slow down and finally, when full saturation is reached, the diffusion in the gas phase will stop. Such a case, with an exemplifying water saturation time of 125 years, is also considered.

For modelling purposes, a pessimistic case taking into account only the transport resistance in the buffer and not in the backfill was defined. A detailed model including the pellet filled slot between the buffer and the rock and the slot between the canister and the bentonite was used, see Figure 2-13. For unsaturated conditions, the main gas-phase transport path from the backfill to the canister is through the pellet filled slot between the bentonite and the wall of the deposition hole.

The concentration of sulphide is assumed to be zero at the canister surface, i.e. all sulphide that reaches the canister surface will react instantaneously. At the interface between the deposition tunnel and the deposition hole a sulphide concentration of 1.7×10^{-4} mol/m^3 in the gas phase (approximately 4 ppm) is assumed to be upheld. As further explained in Eriksson and Hedin (2019), this value is based on an equilibrium with an assumed aqueous concentration of sulphide of 10^{-6} mol/L and a pH of 7 in the backfill immediately above the deposition hole. It is noted that this is a pessimistic assumption, since no measurements of sulphide concentrations in bentonite have exceeded the detection limit of 3×10^{-7} mol/L in earlier studies and now also corroborated by the findings reported in Section 2.4. Also, the pH in bentonite is generally 8 or higher, leading to a further reduction in the sulphide concentration.

With the above assumptions and considering the case where no groundwater flows into the system, the highest influx of sulphide to the canister occurs at the top corner of the canister, see Figure 2-14. As seen in the figure, the peak flux is about 6.5×10^{-11} mol/(m^2 s). The temporal development of the flux is determined essentially by the redistribution of water present initially in the buffer, due to the heating of the system by the residual power of the fuel.
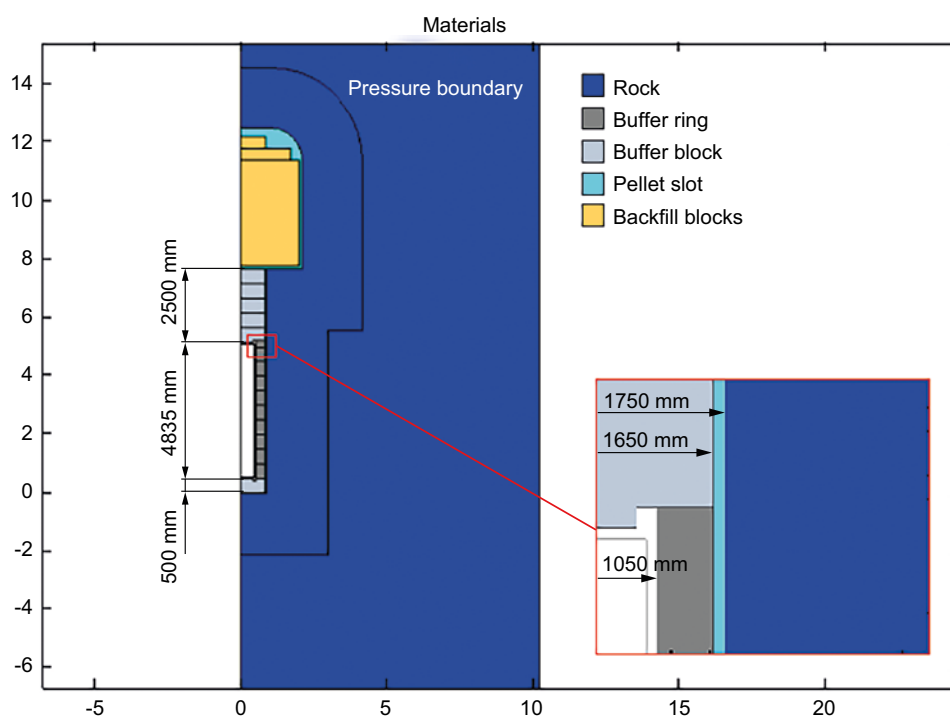
Figure 2-13. *Geometry and the different materials used in the model. The x- and y-axes have units of metres. (Eriksson and Hedin 2019)*
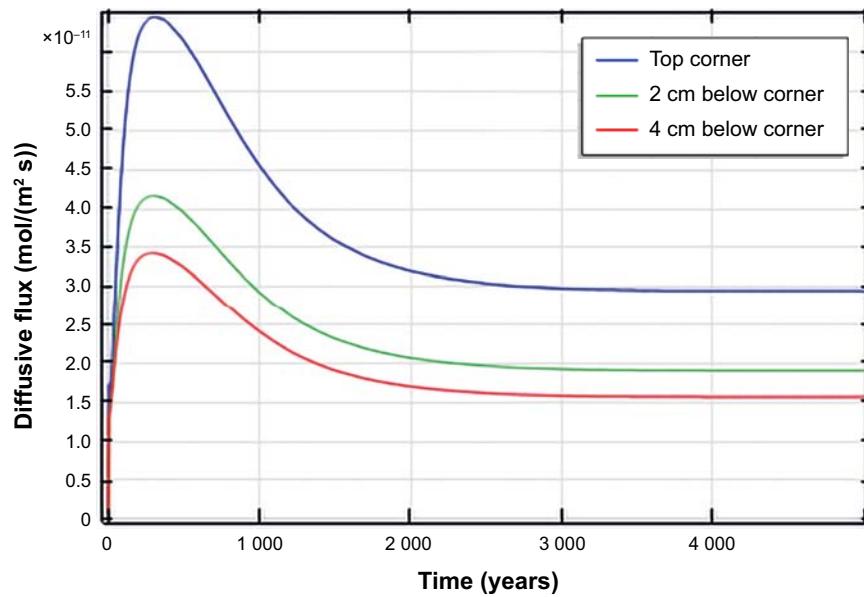
Figure 2-14. *The flux of sulphide to the top corner of the canister, 2 centimetres and 4 centimetres below the top corner (Eriksson and Hedin 2019).*

It is noted that 10^{-10} mol/(m² s) corresponds to a corrosion rate of around 4.5×10^{-6} cm/yr, i.e. the calculated peak corrosion rates of less than 10^{-10} mol/(m² s) would cause negligible general corrosion depths in the 5 cm thick copper canister even if the dry conditions persisted for thousands of years.

The exemplifying case where water saturation is assumed to occur in 125 years yields considerably lower peak sulphide concentrations and fluxes.

The key result in this study is the peak sulphide flux of 6.5×10^{-11} mol/(m² s) for unsaturated conditions. This flux is used in the evaluation of corrosion issues involving sulphide under unsaturated conditions in subsequent chapters.

2.6   Conclusions regarding unsaturated repository conditions

As shown in Section 2.2.2, the saturation time of the buffer surrounding the canister is expected to vary between a few tens and a few thousands of years at the Forsmark site, depending on the position in the rock.

One issue for canister corrosion is the chemical composition of the gas in the unsaturated bentonite. Of particular interest is the content of oxygen (O₂) and hydrogen sulphide (H₂S). Based on the experimental results of oxygen consumption with a copper heater presented in Section 2.4.1 it is realistic to assume that all oxygen initially present in the gas phase will be consumed by reaction with the copper canister before full buffer saturation is reached. This is true even for canister positions with the highest water inflows. This means that aerobic and saturated conditions will not occur simultaneously.

No gaseous H₂S above the detection limit of 0.1 ppm has been detected in the gas phase in unsaturated bentonite. This is consistent with the measurement of aqueous HS⁻ in bentonite porewater presented in Svensson et al. (2017). The assumed gaseous concentration (~4 ppm) in the modelling presented in Section 2.5 can therefore be seen as pessimistic.

The modelling in Section 2.5 shows that the case with no water inflow to either the tunnel or the deposition hole is more pessimistic with regard to fluxes of H₂S than a case with a more rapid saturation. Increasing saturation will have a strong effect on the transport of sulphide since the gas tortuosity will decrease sharply with increasing degree of saturation. The modelling also provides an upper value of 6.5×10^{-11} mol/(m² s) for the sulphide flux to the canister surface under unsaturated conditions.

It is difficult to construct a case that could potentially give higher sulphide fluxes than the dry case where no groundwater enters the deposition hole in Section 2.5. For example, a partially saturated tunnel with microbial sulphate reduction in the saturated low density outer part of the backfill and diffusion in the gaseous phase in the inner unsaturated part does not give higher fluxes than the dry case. Extensive microbial sulphate reduction requires transport of nutrients and sulphate, which will be slow in a partially saturated system. Slow saturation would also lead to a more even distribution of water in the backfill and not a mix between "fully saturated" parts and unsaturated parts.

The results presented in this chapter concern in particular sulphide sources and fluxes during unsaturated conditions that have, as mentioned in Section 2.1, previously not been as extensively studied as saturated conditions. The results are important for the evaluation of most of the issues raised by the environmental court: Since they concern sulphide they relate directly to pitting corrosion and SCC due to reaction with sulphide addressed in chapters 5 and 6, respectively, to hydrogen embrittlement addressed in Chapter 7 since sulphide corrosion of copper is a source of hydrogen, and to the effects of radiation on these corrosion processes addressed in Chapter 8.

2.7 Summary of long-term repository conditions

Based on the material in this chapter, the long-term repository conditions relevant for the canister integrity issues to be addressed in this report are as summarised in Table 2-4. In the following chapters, the concerns regarding canister integrity issues raised by the environmental court are analysed in detail. In Chapter 9, an expanded version of Table 2-4 is presented, where conclusions regarding the canister integrity issues are given for each of the buffer conditions in the table.

Table 2-4. Conditions of relevance for the canister integrity issues in the development of the buffer and canister system in a KBS-3 repository at Forsmark.

	Unsaturated buffer phase	Saturated buffer phase	Eroded buffer case
Time (years)	$0–6\,000$	$(0)–10^6$	$10^5–10^6$
Canisters affected	All 6 000	All 6 000	~ 100
Peak sulphide concentration (mol/L)	10^{-6}*	10^{-4}**,†	$10^{-4,\,†}$
Peak sulphide flux (mol/(m² s))	$\sim 10^{-10}$	$\sim 10^{-12}$	10^{-9}

* In saturated backfill.
** In groundwater in contact with outer buffer boundary.
† Distribution with more than 97 % $< 10^{-5}$ mol/L.

3 The sauna effect

3.1 Introduction

As noted in Chapter 1, the environmental court considered that the impact of the so-called sauna effect on pitting due to reaction with sulphide and on stress corrosion cracking due to reaction with sulphide needs to be further considered. In this context, the sauna effect is defined as the evaporation and vapour transport of water entering a deposition hole followed by precipitation of salt, chloride salts in particular, on, or in the vicinity of, the heat source (the canister). This is illustrated in Figure 3-1.

The residual power in the canister may be as high as 1 700 W at deposition (SKB 2011), which means that the potential for evaporation of water is substantial. Extensive salt enrichment is possible if a large part of the water that enters the deposition hole can leave in the vapour phase. If condensation of vapour occurs in the bentonite within the deposition hole, only a limited part will leave as vapour and the salt enrichment will consequently be limited. If all water that enters the deposition hole condensates, no more salt than what is present in the volume of water needed to saturate the buffer can be enriched in the deposition hole. Water vapour diffusivity in bentonite decreases with increasing degree of saturation and reaches zero at full saturation (at which condition vapour transport does not occur).

In the following, a summary of SKB's experiments regarding the sauna effect is given in Section 3.2, observations from field tests are given in Section 3.3, modelling results are summarised in Section 3.4 and conclusions are presented in Section 3.5.
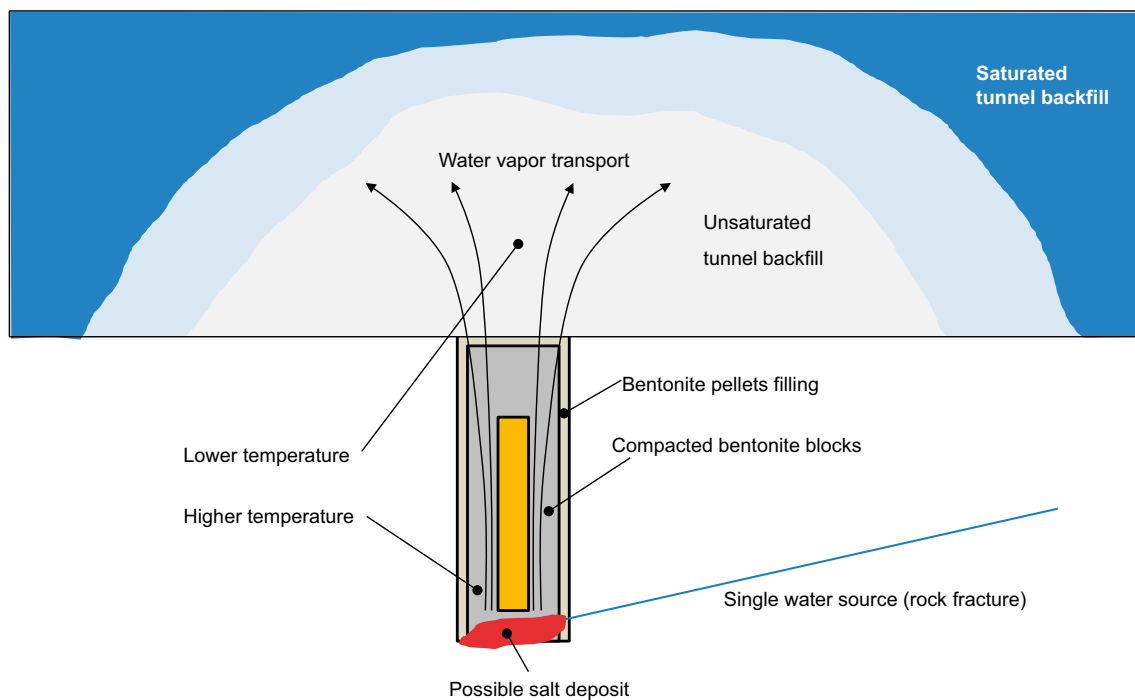
Figure 3-1. *Schematics of the "sauna" effect (Birgersson and Goudarzi 2013).*

3.2 Overview of experimental results

3.2.1 Specific laboratory experiments

Over the last several years SKB has undertaken a number of laboratory experiments specifically focused on the sauna effect. These experiments are reported in Birgersson and Goudarzi, (2013, 2016, 2017).

The first set of tests showed that a substantial amount of vapour was able to flow through the bentonite pellets without apparently being absorbed by a bentonite with a water ratio of 17 %, which can be considered rather dry with respect to vapour transport. Furthermore, water uptake due to water condensation completely dominated in these tests, consequently vapour as such is not readily absorbed by dry bentonite. Condensation of vapour is needed for an efficient absorption.

The second set of tests confirmed that vapour is able to be transported rather far in this type of pellet-filled slot without being substantially absorbed by the bentonite; a substantial amount of water was lost to the environment in tests where the slot was directly opened to the environment. This behaviour agrees with the observation of vapour transported in pellets fillings from the first set of tests (Birgersson and Goudarzi 2013), where major loss to the environment was also observed under certain conditions. The (initial) water content in the bentonite in these tests was low (about 17 %) and the material thus had a large affinity for taking up water – the water chemical potential in the dry bentonite corresponds to a "suction" of the order of 50 MPa. The observations thus strengthen the conclusion that there appears to be a kinetic barrier for dry bentonite to efficiently take up water directly in vapour form (note, however, that bentonite does take up water in vapour form, as evident when e.g. recording retention curves (Dueck 2004)).

Rather than uniform water uptake directly from the vapour phase, the dominating mechanism of water uptake observed in this study is that of localized water condensation: as the present test set-up (as well as a KBS-3 repository) inevitably has variations of temperature and relative humidity, condensation of water vapour occurs locally and, to a certain degree, variably in many of the tests. Once water has condensed somewhere in the system and formed a condensation nucleus, more water uptake is promoted at the same position. This type of localized uptake was observed in the lower bentonite ring in several of the tests, as well as in the massive top block in tests where such a block was present. The observation of water condensation in the massive top block is additional evidence that vapour may be transported relatively far before being taken up by the bentonite. On the other hand, the observation also shows that the presence of such top blocks – which is the case in the KBS-3 concept – effectively inhibits further vapour transport.

The configuration of the most recent test, Test 9 (Birgersson and Goudarzi 2017) was built on the experience from all earlier tests and precautions were taken to, as far as possible, avoid experimental artefacts, especially the pumping of water into the bentonite. Bentonite blocks (rings) were placed on top of each other on the bottom plate, thus creating the inner slot between the copper heater and the clay. Similar to the earlier tests, a massive bentonite block was placed on top of these four rings, and the set-up was encapsulated in a plexiglass tube and the outer slot was filled with bentonite powder. The bentonite used both for blocks, powder and the ring in the bottom was MX-80. The powder and the blocks had an initial water-to-solid ratio of 16 %, while the bottom ring was close to water saturation from the start of the test. Water was fed to the system via in- and outlets at the bottom of the bottom plate. A photograph of the fully configured set-up is shown in Figure 3-2.

The heater was kept at approximately 80 °C. The main variables measured was mass of water fed into the system (referred to as "consumption" in Figure 3-3), and the evolution of the mass of the full set-up, which gives the amount of water taken up by the bentonite (the whole set-up was placed on a scale, as seen in Figure 3-2). Total water consumption, water uptake, and loss as a function of time in Test 9 is plotted Figure 3-3. Over the course of the 50 days of testing, approximately 0.25 kg water was lost to the environment, giving a loss rate of approximately 0.005 kg/day. During dismantling of the test, samples were taken at different places in the set-up and analysed for water content. Figure 3-4 shows the approximate positions for each of the samples taken, and Figure 3-5 displays the measured water-to-solid mass ratios. These data show many of the same trends as in earlier tests. There is a tendency towards higher water-to-solid ratio in the upper parts of the set-up, while there is no evidence of any radial gradients thus, an efficient condensation in the block on top of the canister. This distribution may indicate that vapour condensation also occurred in this test. It can also be noted that the outer part of the massive top block has a lower water-to-solid mass ratio (samples 1 and 2). This is yet another indication that the water which is being lost to the environment in these tests originates from the outer bentonite parts (while the inner slot basically functions as an isolated system).

Figure 3-2. *The configuration of the most recent test, Test 9: a) Four bentonite rings and a massive block stacked on top of each other, b) The full set-up before starting the experiment. (Birgersson and Goudarzi 2017).*
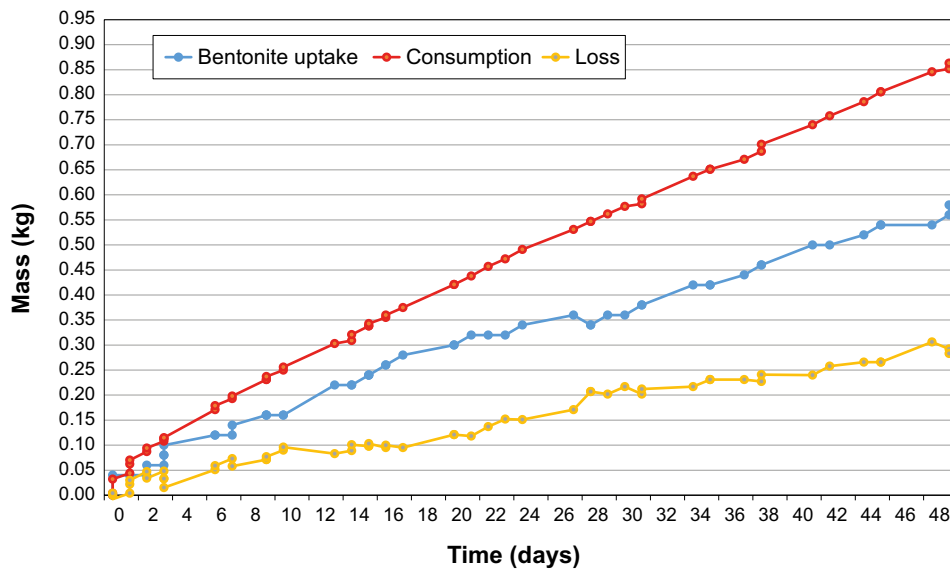
Figure 3-3. *Total water consumption, water uptake in the bentonite, and loss of water to the environment, measured in Test 9 (Birgersson and Goudarzi 2017).*

The overall conclusion from the tests performed is that while water vapour may move relatively freely in slots and dry pellets at constant temperature, condensation will occur rapidly in blocks as well as in pellets when a temperature gradient is present. Therefore, water vapour generated in the vicinity of the canister is not expected to ever leave the deposition hole. Since no water vapour is leaving the deposition hole no accumulation of chloride salts will occur.
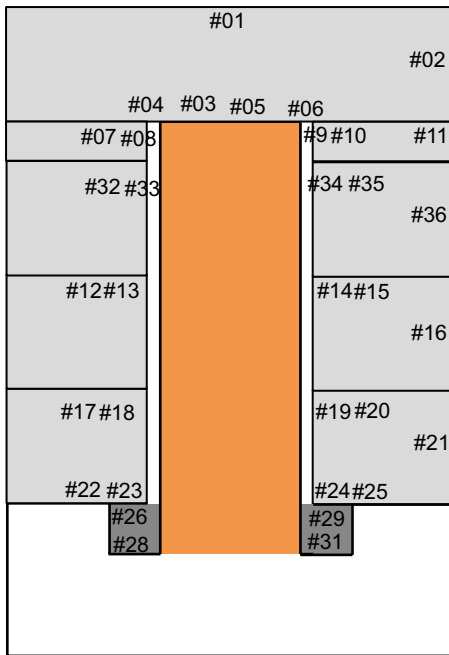
Figure 3-4. *Approximate positions of samples taken for water content determinations in Test 9. The measured water-to-solid mass ratios are shown in Figure 3-5 (Birgersson and Goudarzi 2017).*
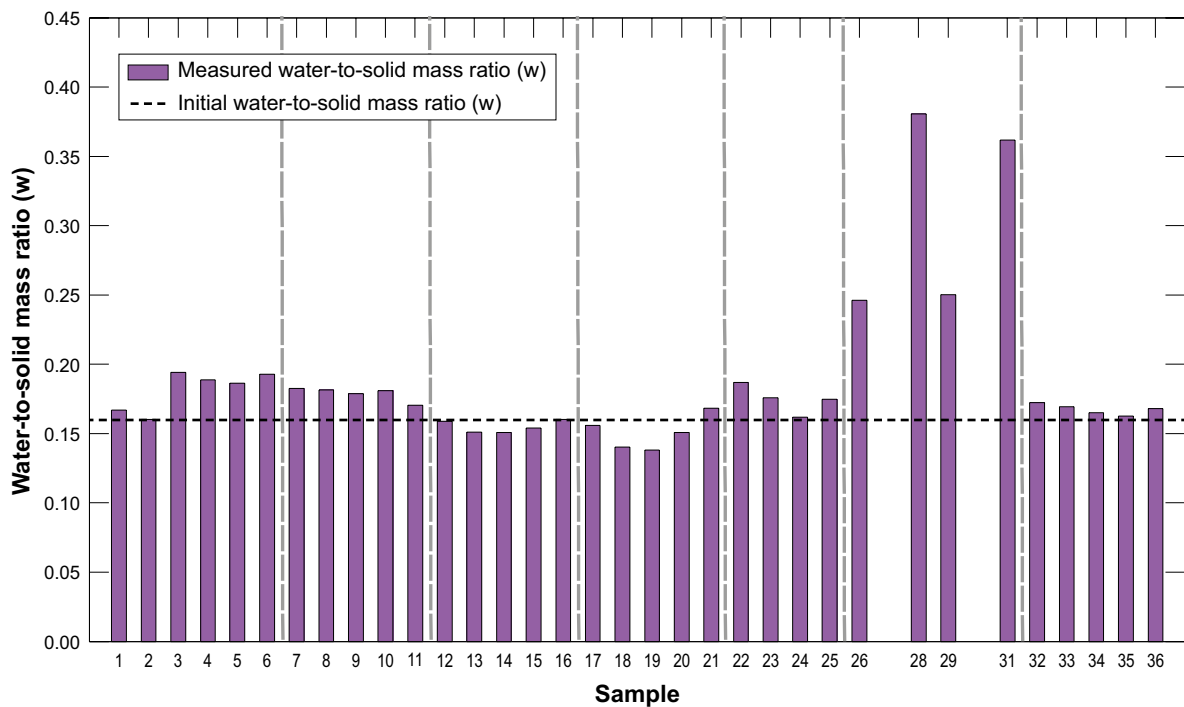
Figure 3-5. *Water-to-solid ratio of all samples in Test 9. The initial water content was 16 % in both powder and blocks. For position of the samples, see Figure 3-4. It was not possible to obtain samples 27 and 30 (Birgersson and Goudarzi 2017).*

3.2.2 Recent tests with vapour transport

Additional experimental studies with vapour transport in bentonite have been performed in the latter part of 2018. The purpose of the tests was to gain additional understanding about the thermo-hydraulic processes that govern the moisture redistribution in partially saturated bentonite blocks and pellets. The objective was to investigate two material properties in particular:

- The vapour transport capacity through the buffer; both through bentonite blocks and through pellets-filled slots.

- The occurrence of equilibrium between the relative humidity in the gas-filled pores and the absorbed water in the bentonite. It is usually assumed that such an equilibrium exists.

The results are presented in Åkesson et al. (2019). Two types of tests have been included in the laboratory test program:

1. Isothermal tests. Test cells including a bentonite sample are placed in a climate chamber with a set temperature and relative humidity. The relative humidity on the lower side of the bentonite sample is set by de-ionized water.

2. Tests with a thermal gradient across the sample. The test cells are placed on an electrical heater with a certain temperature (T1). The relative humidity on the lower side of the bentonite sample is controlled by a saturated salt solution (RH1). The test cell and the heater are then placed in a climate chamber with a set temperature (T2) and relative humidity (RH2).

Specially designed test cells have been manufactured. Each test cell consists of a reservoir made of copper and a sample holder made of PEEK (Figure 3-6). During the test, the reservoir is filled with either deionized water (isothermal tests) or a salt solution (tests including a thermal gradient). In the case of a thermal gradient, the test cells are positioned on a heater.

The isothermal tests were performed with temperatures ranging from 30 to 70 °C and relative humidity from 50 to 85 %. The gradient tests were run with reservoir temperatures between 70 and 90 °C and climate chamber temperatures from 39 to 61 °C. The relative humidity in the reservoir was controlled at ~60 or ~80 % by KI and KCl solutions, while the humidity in the chamber was kept constant at 70 %. All test conditions were selected to avoid condensation.

The tests were run with specimens consisting of blocks, fractured blocks, references without any bentonite specimen or pellets. These can be seen in Figure 3-7.
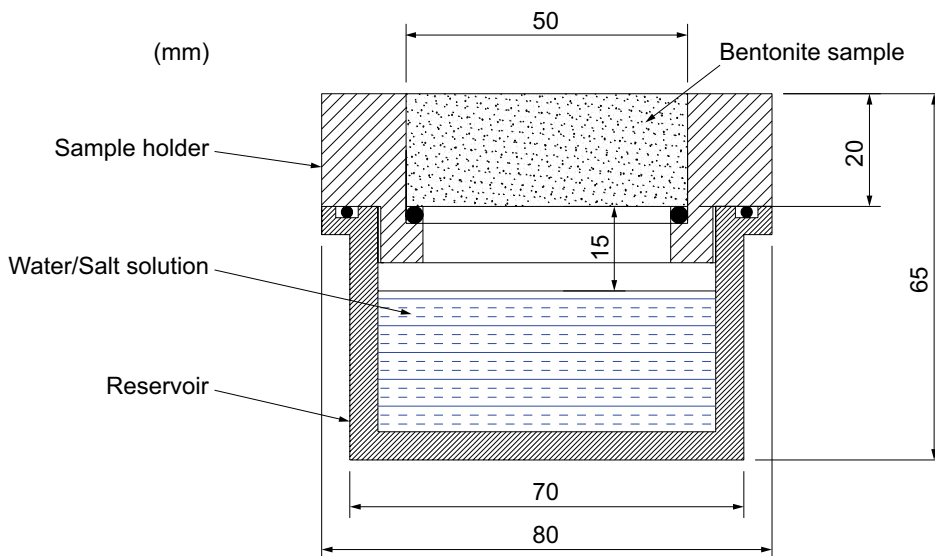
Figure 3-6. *The test cell consisting of a reservoir made of copper and a sample holder made of PEEK (Åkesson et al. 2019).*

Figure 3-7. Photo showing the four different test types included in all test series: 1. Block, 2. Fractured Block, 3. Pellets and 4. Reference. (Åkesson et al. 2019)

For every test, four features were recorded:

- Equilibrium: The specimens are placed in the climate chamber at the specified conditions regarding temperature and relative humidity to reach equilibrium i.e. the water content distribution of the specimen is not changing.

- Test phase: The specimens are exposed to a relative humidity and/or a temperature gradient

- Water content determination: After dismantling, the water content at different levels of the bentonite specimens was determined. Initial water contents of 10, 17 and 20 % were used in the tests.

- Climate chamber: The temperature and relative humidity in the climate chamber is recorded as a function of time.

Figure 3-8 shows the mass changes during the test phase for IT6, which was an isothermal test with an initial water content of 17 %, a sample temperature of 70 °C and an RH of 70 %.

In these experiments, the time dependence of the mass loss of the liquid reservoir due to evaporation was compared with the mass gain of the bentonite due to the absorption of moisture. The mass loss in the reference cell is, as expected, much faster than where bentonite samples are present. The mass loss in the cells with blocks is similar, independent of fracture or not (actually less with a fracture in this particular case), while the pellet-filled cells loses more water. The uptake of water in the bentonite is less than the loss from the cells in all cases. Thus, it is clear that bentonite will not limit vapour transport, to any major extent, unless condensation occurs. All the tests yielded similar results.

The experiments were modelled using a description of the vapour transport as driven by gradients in water vapour content or absolute humidity, and with a vapour permeability as a corresponding moisture flow coefficient. The input parameters for each calculation was the temperature and RH (for reservoir and climate chamber, respectively), lengths of specimen and gaps, cross-sectional areas, dry density, the vapour permeability value for the specimen and the hydration rate coefficient. The vapour permeability value for the gaps was calculated as the vapour diffusion coefficient in air as defined in Code_Bright. The hydration rate coefficient is a fitted parameter. A value of 5 has been used for the blocks and 0.1 for the pellets (1/s). The results of the calculations are, however not very sensitive to the actual value.
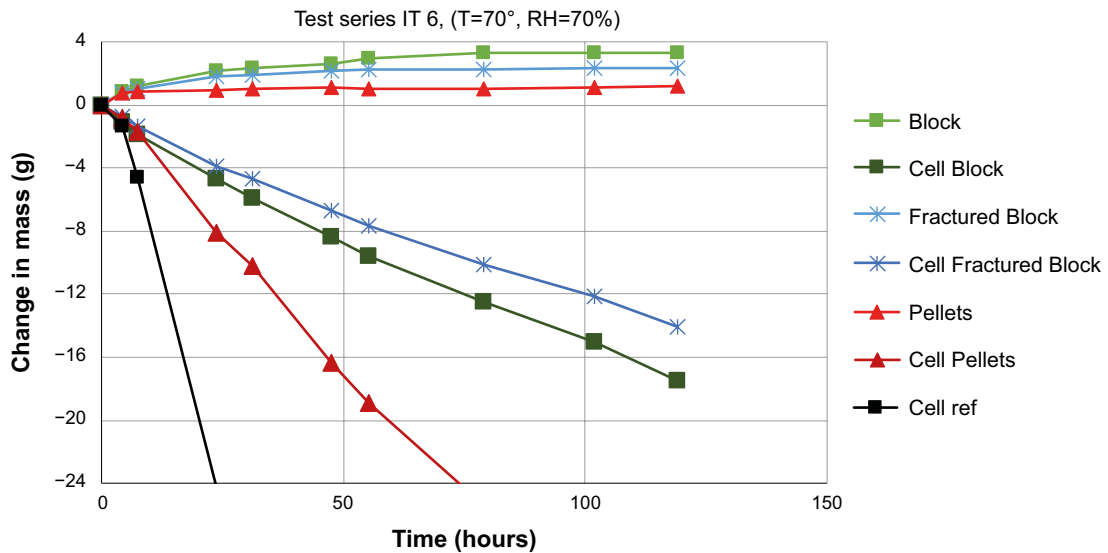
Figure 3-8. *Data determined during the test period for isothermal test series 6. The "cell" lines show the change of weight of the total test cell, including water, while block, fractured block and pellet show the mass change in the bentonite only. (Åkesson et al. 2019)*

The measured time evolutions could be simulated fairly well, especially for isothermal test conditions (Figure 3-9). For the test with pellets a behaviour could be observed in which the water loss from the reservoir and the water uptake in the bentonite deviated at an early stage, and this reflects the temporary absence of equilibrium between vapour content in the pores and the bentonite, respectively.

Evaluated vapour permeability values are apparently consistent with the material model (vapour diffusion coefficient), especially for the isothermal tests with blocks. The behaviour with non-equilibrium conditions between RH in large pores and bentonite water is not included in the established material model, but can be described with a "hydration rate coefficient". This means that blocks can be seen as in equilibrium with vapour, while a kinetic expression is needed for pellets. This slow uptake of vapour by pellets is consistent with other studies; see Section 3.2.1 and Birgersson and Goudarzi (2013).
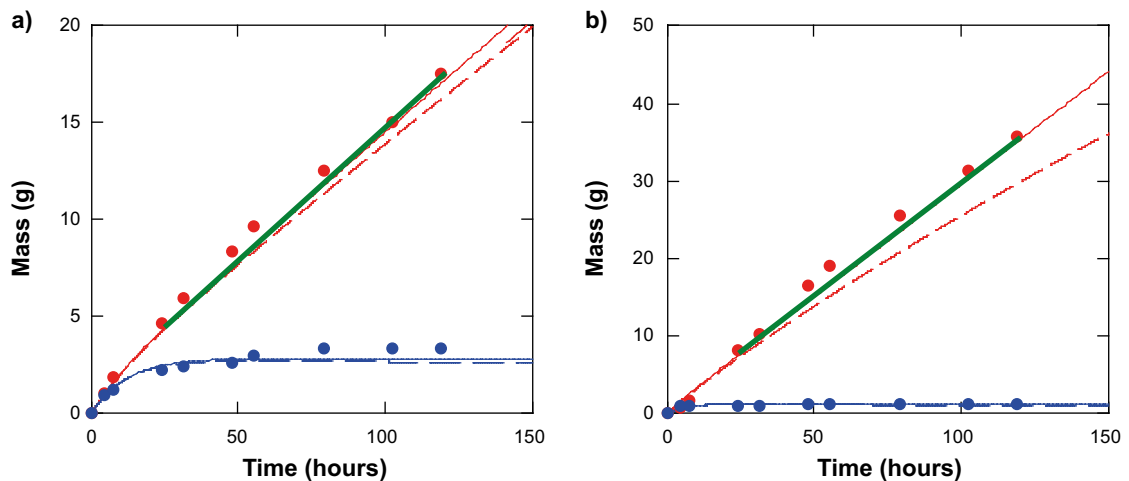
Figure 3-9. *Experimental (dots) and model (lines) results for test IT6. Mass loss from reservoir (red) and water uptake (blue) for a) intact block, b) pellets. The green lines represent evaluated rates of mass loss. (Åkesson et al. 2019)*

3.3 Observations from field tests

The sauna effect has not been specifically studied in any large-scale field test with a bentonite barrier. However, it is still possible to draw conclusions about the phenomenon based on observations from available experiments.

3.3.1 Prototype repository

The Prototype Repository is a full-scale field experiment performed in crystalline rock at a depth of 450 m in the Äspö Hard Rock Laboratory (Äspö HRL). The aim of the experiment is to simulate conditions that are largely relevant to the KBS-3 disposal concept for spent nuclear fuel. The 64 m long experimental tunnel at the very end of the main access ramp of the Äspö HRL contains six deposition holes and the same number of full-scale copper canisters (with heaters) surrounded by MX-80 bentonite buffer. The outer plug was opened and the outer section (23 m long) with two deposition holes (5 and 6) was retrieved after about seven years of operation. The overall objective of the retrieval was to study the actual conditions of canister, buffer, backfill and the surrounding rock after being subjected to natural groundwater inflow and heating for a considerable time. The buffer water content was not homogeneous in either deposition hole after almost 8 years of wetting and large variations in water saturation existed, both between the deposition holes, between blocks from the same hole, and also within a given block. The maximum temperature had never exceeded ~85 °C during the test period. Chemical-mineralogical analyses were carried out in parallel at two different laboratories on four radial profiles from three blocks with variable water content. The analyses included determinations of water-soluble salts, chemical composition, cation exchange capacity, exchangeable cations, and mineralogy. The radial distribution of chloride extracted by dispersion of the bulk samples in deionized water is plotted in Figure 3-10.

The Na-Ca-Cl type groundwater (~8 100 mg Cl/L) responsible for wetting the bentonite buffer during the course of the experiment is the primary source of chloride. The water to solid ratio in the original bentonite was 0.18, which corresponds to a degree of saturation of 66 % while the final water ratios vary between 0.236–0.283 in the different samples. Except for the innermost part of the sampled sector 165 from block P6R05, which had a saturation value below 95 %, the sampled sectors of blocks P6R05 165 and P5R06 050 were more or less fully water saturated at the excavation. The average chloride concentration was ~2 900 mg Cl/L in P6R05 165 and ~2 200 mg Cl/L in P5R06 050. The initial chloride concentrations were ~900 and ~600 mg Cl/L in the water originally present in the bentonite. The values show that the final chloride concentration is a result of a proportional mix between the groundwater and the water originally present. No enrichment of chloride, apart from the mixing of waters, can be seen in the bentonite. The data from P5R06 050 actually indicate the resulting chloride content is slightly below what would be expected from a proportional mix of waters. This could be the result of anion exclusion effects. The data also show that the chloride concentrations are relatively constant over the radius of the buffer. After 8-years test-duration, no chloride enrichment towards the heater can be seen.
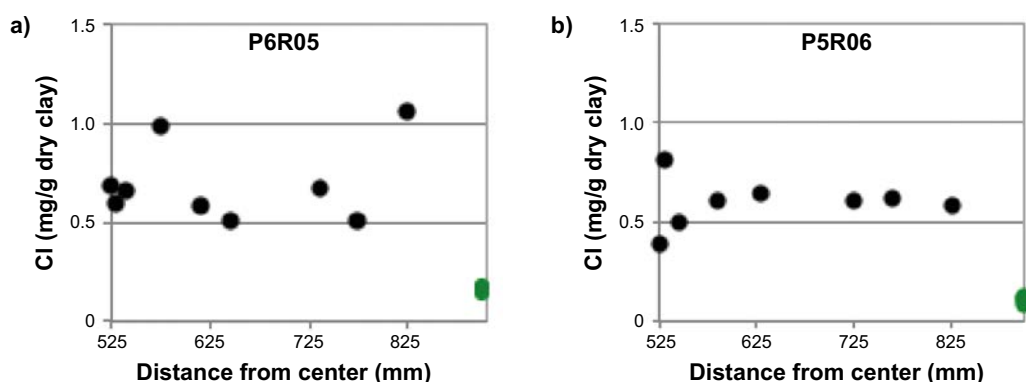
Figure 3-10. *Radial distribution of Cl in profiles for sampled sectors, a) P5R06 050, b) P6R05 165. Reference samples are plotted in green on the right axis. R6 and R5 denotes Ring 6 and Ring 5, which both are located approximately at the canister mid-height The canister surface was located at a distance of 525 mm from the centre (Olsson et al. 2013).*

3.3.2 LOT

The ongoing LOT test series at the Äspö HRL are focused on identifying and quantifying mineralogical alterations in the bentonite exposed to typical repository-like conditions. In total, the LOT project included seven test parcels, which contained a central Cu-tube surrounded by cylindrical bentonite blocks with a diameter of 30 cm, and gauges for temperature, total pressure, water pressure and humidity. Electrical heaters placed inside the copper tube are used to simulate the heat generation from the decaying spent fuel. Three parcels are exposed to standard KBS-3 conditions (maximum temperature below 100 °C) and four parcels to adverse conditions (maximum temperature below $\sim$140 °C). The results discussed here are from the A2 parcel, which was a 6 year test exposed to a maximum temperature of $>$130 °C (Karnland et al. 2009). The radial concentration profile of chloride, expressed as the mol/L concentration of the pore water and mg/g dry bentonite, are presented in Figure 3-11. The pore water concentration of chloride is more or less constant in all three blocks but has increased compared with the chloride concentration of the reference bentonite. Thus, the ground-water must be the primary source of chloride. However, the pore water chloride concentration is still only half of that of the Äspö groundwater, which may be explained by the mixing of the original water in the bentonite with incoming groundwater, or alternatively by ion equilibrium theory (Birgersson and Karnland 2009).

The concentration of chloride in the groundwater at the LOT location was measured to be $\sim$7800 mg/L. The initial concentration in the bentonite was 1350 mg/L as an average of the reference samples. The final concentration in the blocks was on average $\sim$0.11 mol/L which corresponds to $\sim$4000 mg/L. The higher concentrations in LOT compared to Prototype can be explained by a lower initial water ratio in the bentonite. The initial degree of saturation in LOT was about 33 % based on an initial water content of 0.1 and a final mean of 0.3. The assumption that the final chloride concentration should be a proportional mix of the initial concentration and the concentration in the groundwater would yield a concentration of $\sim$5600 mg/L. The actual measured concentration of $\sim$4000 mg/L shows that chloride has been "lost" from the system. This can, however be explained by ion-exclusion effects, or ion equilibrium theory (Birgersson and Karnland 2009).

No indications whatsoever of sauna effects, expressed as enrichment of chlorides in the buffer of on the heater compared to the content in the surrounding groundwater, can be seen in the LOT experiment since there was no signs of concentration of chloride as a function of distance to the heater. The chloride concentration was also lower than the concentration of a mixture between the original porewater and the groundwater.
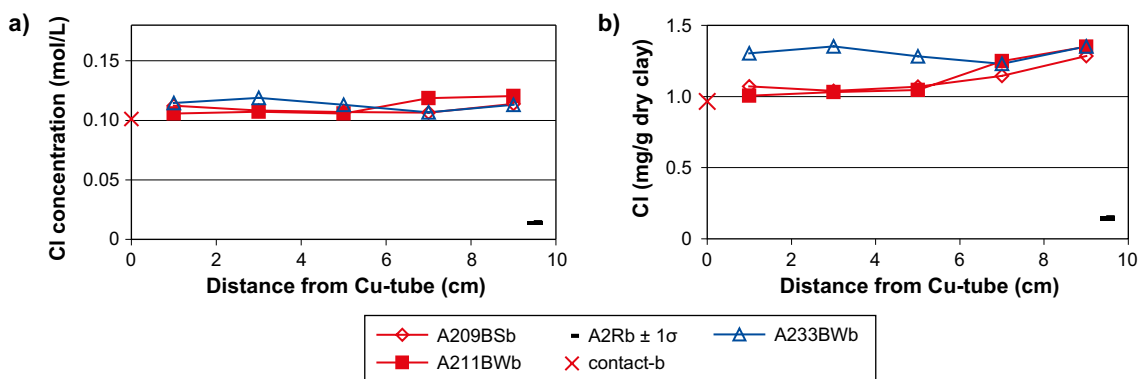
Figure 3-11. The radial distribution of Cl in water extracts of bulk samples from blocks 09, 11 and 33 of the LOT A2 parcel taken at 90, 110 and 330 cm from the bottom of the deposition hole. Blocks 9 and 11 were exposed to the highest temperatures in the test, while block 33 was located in a cold section. The concentration of the reference samples (A2Rb) is shown at position 9.5 cm as the mean ±1 standard deviation of five samples (Karnland et al. 2009). The concentrations are given as a) mol/L, b) mg/g dry bentonite.

3.3.3 FEBEX

FEBEX (Full-scale Engineered Barrier EXperiment in Crystalline Host Rock) (Fernandez et al. 2018) was a research and demonstration project that was initiated by Enresa (Spain) in 1994. The aim of the project was to study the behaviour of near-field components in a repository for high-level radioactive waste in granite formations. The full-scale heating in situ test was performed at the Grimsel underground laboratory in Switzerland, also known as the Grimsel Test Site (GTS).

A horizontal drift with a diameter of 2.28 m was excavated in the Grimsel granodiorite. Two electrical heaters, of the same size and of a similar mass as the reference canisters, were placed in the axis of the drift (Figure 3-12). The gap between the heaters and the rock was backfilled with compacted bentonite blocks, up to a length of 17.40 m, requiring a total 115 716 kg of bentonite. A partial dismantling of the FEBEX in situ test was carried out during the summer of 2002, after 5 years of continuous heating. The Heater #2 was switched off on 24th April 2015. The objective of the second dismantling operation, carried out throughout 2015, was to dismantle all the remaining parts of the in situ test, including the Heater #2. This operation included carrying out a complete sampling of the bentonite, rock, relevant interfaces, sensors, metallic components and tracers to allow the analysis of the barrier condition after 18 years of heating and natural hydration.

The initial compacted bentonite had a water content of 14 % and a dry density of 1.60 g/cm^3 upon emplacement and evolved towards full saturation after 18 years of the experiment, except in the blocks located in contact with the heater, where the degree of saturation was around 85 % (see Villar et al. 2016). Aqueous extracts were obtained to determine the ion inventories and distributions within the bentonite barrier (Fernandez et al. 2018).

The chloride contents obtained from samples taken during dismantling of Heater #2 are shown in Figure 3-13. Chloride ions are clearly leached in zones close to the granitic formation and increase towards the internal part of the barrier. It is interesting to note the different behaviour of these ions in the different sections. In the heated zones, chloride concentrations seem to be concentrated at the heater contact, whereas in Section 59 (non-heated section), the concentration is distributed towards the inner bentonite blocks, possibly due to the advective movement of groundwater towards the internal part of the barrier, saturating the bentonite (Figure 3-13).
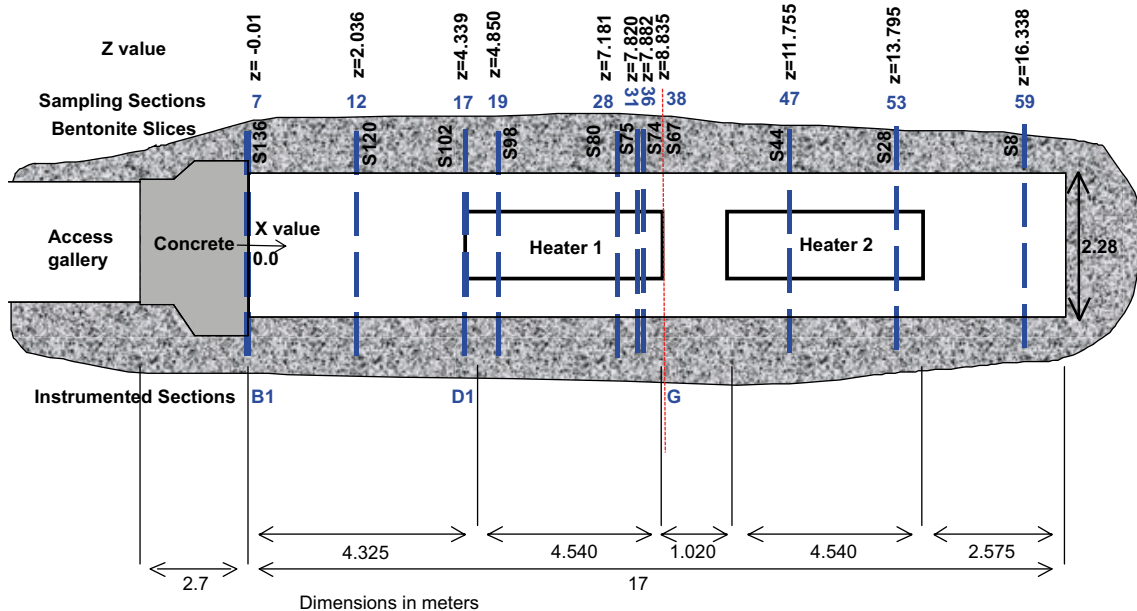
Figure 3-12. *Bentonite Sampling Sections from the FEBEX in situ test analysed for THC studies after dismantling of Heater#1 in 2002 and Heater#2 in 2015.*
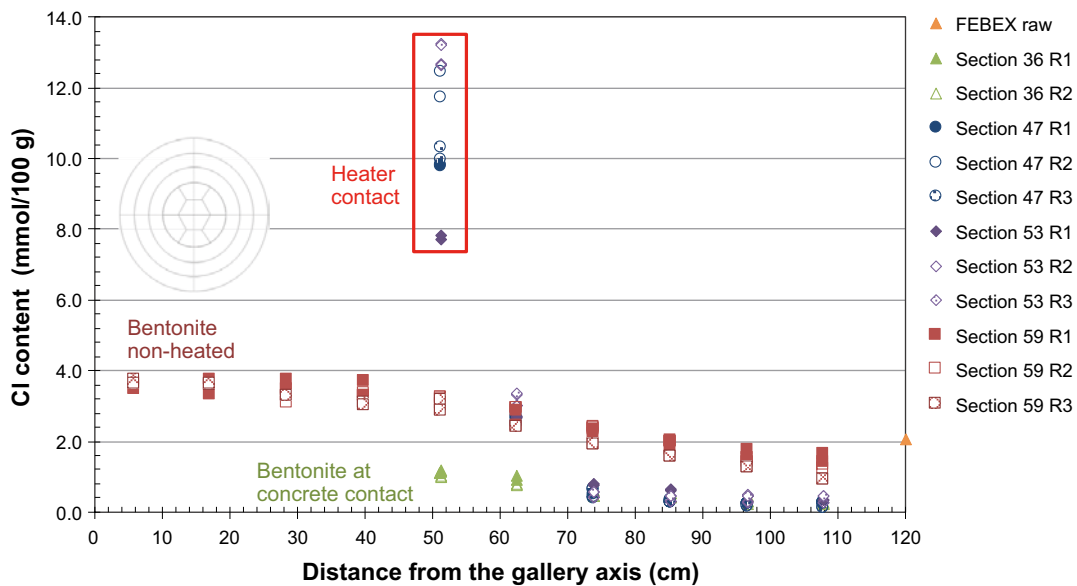
Figure 3-13. *Chloride content (1:4 aqueous leaching) from samples at different sections in three radii after dismantling of Heater #2 in 2015. The initial chloride concentration in the FEBEX bentonite is shown as a yellow triangle far to the right in the Figure (Fernandez et al. 2018).*

In FEBEX an enrichment of chloride on the bentonite/heater contact can be observed. However, in the same sections (47 and 53) the bulk of the bentonite is depleted in chloride compared to the initial values. The enrichment could be caused by the evaporation/condensation that is expected during the saturation process, which would lead to a redistribution of the original chloride content. The enrichment close to the heater could also be an effect of leakage through the cabling system. Giroud (2014) states: "The study of the plug design shows that special care has been taken to make the plug water- and gas-tight during Phase 2. However, while this may reduce the risk of air contamination through the plug, it does not allow us to exclude air contamination from the access gallery, whether through defects in the plug sealing, the EDZ, or the cable and pipe seals." The data show no overall accumulation of chloride in the buffer surrounding the heater, rather a loss to the groundwater in the rock.

3.3.4 Summary of field tests

In Prototype and LOT the chloride concentration profiles are flat over the radius of the buffer and the overall chloride content corresponds to, or is lower than, a proportional mixture between the content in the groundwater and the content originally present in the bentonite.

In FEBEX, there is an enrichment of chloride close to the heater as well as a concentration gradient from the heater towards the rock. The test was not fully saturated close to the heater. Enrichment of salt due to evaporation/condensation in the remaining unsaturated part of the bentonite may be the reason for the increased concentration at the heater contact. The bulk of the bentonite surrounding the heater in FEBEX is depleted in chloride compared to the initial state.

None of the field tests show any accumulation of chloride in the buffer, apart from pure mixing. There is no evidence for the existence of the sauna effect in these tests.

3.4 Overview of modelling results

3.4.1 Introduction

The initial state of the installed buffer according to SR-Site (SKB 2010c) is presented in Table 3-1.

The total void volume in the buffer is 4.95 m³. An additional 1.71 m³ of water is needed for full saturation. The chloride content in the MX-80 bentonite is ~0.1–0.2 mg/g dry weight and the concentration in the present day Forsmark groundwater is 5 500–6 000 mg/L (Laaksoharju et al. 2008). With the assumption that no vapour and no chloride are lost from the buffer, the final amount of chloride in the saturated buffer will be 11.3–14.1 kg from pure mixing at the end of the saturation phase. This would yield a mean concentration of 2 300–2 800 mg/L. If exclusion effects are accounted for (e.g. Birgersson and Karnland 2009), the mean concentration at full saturation would be lower.

Table 3-1. Installed total mass and volume of buffer material, water and air in a deposition hole, assuming nominal blocks and pellets and nominal dimensions of the deposition hole (SKB 2010c).

	Mass (ton)	Volume (m³)
Buffer solid part	19.03	6.85
Water	3.24	3.24
Air	–	1.71
Total	22.27	11.8

3.4.2 Potential for the sauna effect (Birgersson and Goudarzi 2017)

A modelling case where a single fracture intersects a deposition hole providing water for saturation of a substantial amount of the bentonite in the hole is considered in Birgersson and Goudarzi (2017), and summarised below.

When the temperature in the region where water enters is elevated, evaporation of the water is conceivable, which in turn may result in accumulation of salt. The mere evaporation process, however, is not sufficient for drawing the conclusion that any significant salt accumulation occurs. On the contrary, in order for salt to accumulate to any significant degree, it is necessary that the major part of the incoming water is vaporized and transported as a gas some distance. Only in such a case will there be a significant salt concentration increase in the liquid left behind. As an example, consider a liquid-to-vapour conversion rate of 90 % of the inflow rate, which would give a 10-fold increase of the concentration of the incoming water, i.e. the solution being transported in liquid form would have a chloride concentration of 2 mol/L, based on a groundwater concentration of 0.2 mol/L.

As a evaporation process requires elevated temperatures and temperature gradients, it is expected that possible salt accumulation effects will be influential only in the early stages of the repository lifespan. A maximum bentonite temperature of 90 °C is estimated to be reached in a KBS-3 repository already within 10–20 years after closure, see Figure 2-2, while a peak temperature of approximately 60 °C is expected to be reached at the rock wall at canister mid height after about 30–50 years (Åkesson et al. 2010). After approximately 100 years, the corresponding temperatures are ~65 and ~55 °C, respectively, and after 1 000 years, the difference between these temperatures is only a few degrees, both being close to 40 °C. The saturated vapour pressure at 40 °C is approximately 7 kPa, in comparison with 47 kPa at 80 °C. Thus, this 7-fold decrease of the saturated vapour pressure, combined with the fact that only minor temperature gradients remain after 1 000 year, suggest that possible effects of evaporation will be negligible after this time period.

For a given inflow rate (q_{in}), the amount of accumulated chloride in the specified case is

$$nCl = q_{in} \cdot c \cdot t = 1.05 \cdot 10^8 \text{ mol/L} \cdot \text{min} \cdot q_{in}$$

where the inflow rate is given in L/min, $c = 0.2$ mol/L is the chloride concentration in the groundwater, and $t = 1 000$ years is the assumed total time for the process. Table 3-2 gives the calculated amount of accumulated chloride for the considered range of inflow rates. In the table the amount of accumulated chloride is also given in terms of the corresponding total mass of NaCl, in terms of the corresponding mass fraction of NaCl with respect to the total buffer mass (23 600 kg), and in terms of the total chloride concentration if distributed in a fully saturated buffer (6 450 litres).

Table 3-2. Amount of accumulated chloride in the adopted inflow case for different values of inflow rate (q). The second column lists the total amount of water during the 1 000 year duration. The third column lists the calculated amount of chloride accumulated, and the fourth and fifth columns lists the corresponding mass of NaCl, in absolute terms and as a mass fraction of the whole buffer dry mass (23 600 kg), respectively. The last column lists the corresponding concentration of chloride if distributed in the entire pore volume of the deposition hole (values in red corresponds to supersaturation with respect to NaCl).

q (L/min)	Total water volume (L)	Amount Cl (mol)	mass NaCl (kg)	mass fraction NaCl	Cl concentration (mol/L)
10^{-7}	5.26×10^1	1.05×10^1	0.61	0	0.00163
10^{-6}	5.26×10^2	1.05×10^2	6.1	0.03	0.0163
10^{-5}	5.26×10^3	1.05×10^3	61	0.26	0.163
10^{-4}	5.26×10^4	1.05×10^4	610	2.6	1.63
10^{-3}	5.26×10^5	1.05×10^5	6 100	26	16.3
10^{-2}	5.26×10^6	1.05×10^6	61 000	260	163
10^{-1}	5.26×10^7	1.05×10^7	610 000	2 600	1 630

In the saturated state, salt which may have precipitated locally during the saturation process will relatively quickly diffuse out in the entire buffer region (and eventually out of the entire repository). As a criterion for whether a certain amount of accumulated salt in the considered case poses a problem regarding canister corrosion, the corresponding concentration when the precipitated chloride is distributed in the fully saturated buffer is used – if this concentration is one mol/L or less, the effect of salt accumulation on the corrosion process is negligible. This criterion is solely based on the solubilities of $CaCl_2$ and NaCl which both are ~6.7 mol/L and the assumption of some concentration gradient within the buffer. Below an average concentration in the mol/L region no precipitation of chloride salts is expected to occur. Using this criterion, Table 3-2 shows that the amount of accumulated salt in the considered case begins to lead to NaCl concentrations approaching NaCl solubility for rates around around 10^{-4} L/min. Note that the total amount of water entering the deposition hole at an inflow rate of 10^{-4} L/min during 1 000 years corresponds to the pore volume of approximately eight deposition holes. In order to actually deposit the ~600 kg of NaCl given by this analysis, it is thus required that this amount of water is transported exclusively as vapour far out into the overhead tunnel section. Such a process can be judged as highly unlikely by simply noting the strong tendency for vapour condensation occur within the buffer, as observed in many of the tests described in Section 3.2.1. Furthermore, state-of-the-art THM (Thermo-Hydro-Mechanical) simulations of the saturation process from a single fracture intersecting a deposition hole predict that a saturation front reaches the canister within only $2-35$ years for water inflows in the range $10^{-5}-10^{-3}$ L/min (Åkesson et al. 2010, Malmberg et al. 2013). These simulations thus conclude that possible evaporation effects can, at most, only be active during the first few years after closure, giving negligible salt accumulation.

Test 6 in Birgersson and Goudarzi (2016) was performed with restriction of water inflow to 5.5×10^{-6} L/min (8 mL/day), i.e. far below the adopted critical limit of 10^{-4} L/min. Despite this very restricted inflow, Test 6 clearly demonstrated that the bentonite gained water during the entire course of the test (approximately 90 days). This behaviour, in turn, shows that the rate at which water was transported out of the slot region is lower than 5.5×10^{-6} L/min. In fact, since the rate at which water was lost to the environment in this test was no larger than the loss rate recorded in the test where no water was injected (Test 7 in Birgersson and Goudarzi 2016), it can be concluded that the water transport rate out of the slot region is much smaller than 5.5×10^{-6} L/min. Translating this result to a full scale geometry is done by scaling with the ratio between the slot circumferences in a KBS-3 deposition hole and in these tests, i.e. 1.05 m/0.1 m = 10.5. It can thus be concluded that the transport rate out of the slot region in a KBS-3 deposition hole is much smaller than $10.5 \times 5.5 \times 10^{-6}$ L/min $\approx 6 \times 10^{-5}$ L/min. This transport rate is so small that it will limit any possible salt accumulation effect in the slot region to such an extent that it can be disregarded. Note that this conclusion was reached without even considering the possibility of liquid water entering the inner slot region in the first place, which of course is a further requirement for salt accumulation to occur there.

3.4.3 Modelling of vapour transport (Luterkort et al. 2017)

In the design of the deposition hole there is a slot filled with bentonite pellets between the rock and the bentonite blocks. This slot is very permeable to air before it saturates. Therefore, water vapour can be transported through convection in the pellet filled slot. The convection in this case will be driven by the temperature gradient between the inner and the outer part of the pellet slot. The radial gradient is dependent on the vertical position. This convection driven transport could potentially dry out the deposition hole and redistribute moisture to the deposition tunnel.

Modelling of this system has been done in Luterkort et al. (2017). The purpose of this modelling was to investigate how the redistribution of water in the deposition hole affects the temperature in the buffer. Since the process of vapour transport due to convection is included in the model it can be used to draw some conclusions about the possibility of water being transported from the deposition hole up to the tunnel.

The model predicts that a very small amount of water is transported up to the deposition tunnel. In the case modelled in Luterkort et al. (2017), with the assumption of a deposition hole with no inflow the amount that is transported up to the deposition tunnel is 40 kg. The reason for this is that the temperature in the buffer decreases sharply with distance above the canister. The temperature of the air in the pellet slot is assumed to be equal to that of the surrounding pellets which should be true as long as the air flow is low which it is in this modelling. The air flow is of the order of 3 mm/s or less. To get a large transport up to the deposition tunnel it would require a high enough air flow so that the temperature of the air is warmer than the surrounding pellet filling. Such high flow rates are not likely as long as there are pellets in the slot which will reduce the air flow rate due to drag.

If an inflow were to occur it would not increase the temperature in the top of the hole and therefore the vapour transport up to the tunnel would not increase. An inflow would also saturate the pellet slot faster which would reduce the air flow and therefore also the vapour transport. A deposition hole with no inflow could therefore be considered to be the worst case.

3.5 Conclusions

It is concluded that significant salt accumulation as a consequence of evaporation of inflowing water from a fracture intersecting a deposition hole will not occur in a KBS-3 repository. There are several reasons for this:

- For significant amounts of salt to accumulate, the major part of the inflowing water must transform into vapour, rather than continue to flow in liquid form, since chloride concentration only can be increased if water is evaporated. For the relevant inflow geometry, it is highly unlikely that the liquid flow is suppressed to such an extent. It is also verified in state-of-the-art THM models that significant liquid flow is maintained.

- The experimental results strongly suggest that the vapour transport capacity within a KBS-3 buffer is not large enough to support a significant amount of salt accumulation, since condensation will limit the vapour transport.

- The study presented in Section 3.2.2 indicates that gaps and fractures are of limited importance regarding vapour transport. The main part of the vapour seems to go through the bentonite block even if there is a fracture present. Fractured blocks and block joints will not affect the vapour transport the process.

- No relevant signs of salt accumulation have been observed in field experiments. The FEBEX test showed enrichment on the heater, but there was still a total loss of original chloride from the bentonite.

In summary, SKB finds that the sauna effect will be insignificant in a KBS-3 repository at Forsmark and thus this process will not be included in the further analyses of pitting and stress corrosion cracking.

4 Corrosion due to reaction in oxygen-free water

4.1 Introduction

Copper has been chosen as the container material in the KBS-3 repository concept since, based on established thermodynamic data, it has favourable corrosion properties in reducing, i.e. O_2-free, deep granitic groundwaters (SKB 2011). In such waters, sulphide is the primary concern for the longevity of the copper canisters from the point of view of corrosion. Copper is expected to corrode to an infinitesimal extent in pure, O_2-free water. For the same reason, copper is considered as a container material in other national spent fuel programmes, in, for example, Finland, Canada and Switzerland.

Since 2007, this view has been challenged by a group of researchers who claim that hydrogen evolution detected in their studies indicates copper corrosion in pure water to an extent far exceeding that predicted by established thermodynamic data (e.g. Szakálos et al. 2007, Hultquist et al. 2011, 2015). The concern was originally raised in Hultquist (1986) and was also contested at that time (Simpson and Schenk 1987, Eriksen et al. 1989). The renewed claim is based on a two-chamber experiment where copper is immersed in water in a lower chamber separated from an evacuated upper chamber by a palladium foil that allows the passage of hydrogen but no other gases. Hydrogen steady-state pressures of up to 1 mbar were observed in the upper chamber (e.g. Szakálos et al. 2007, Hultquist et al. 2011, 2015). This is about 6 orders of magnitude higher than predicted by established thermodynamic data for the Cu-O-H system. Szakálos et al. (2007) suggest that the hydrogen pressures observed in their experiment may be explained by corrosion of copper by water if a hitherto unknown phase of Cu-O-H exists, which would be the thermodynamic driving force necessary for corrosion.

A fuller introduction to the issue is given in Section 1 of Hedin et al. (2018). In that paper, much of the material summarised in this chapter is discussed in more detail, and there are, therefore, frequent references to the paper in this chapter. The paper also contains a more complete set of references for the material covered in Sections 4.2.1, 4.2.2, 4.2.3 and most of 4.2.4.

In this chapter, theoretical and experimental studies undertaken to evaluate these claims are described in Section 4.2, a calculation of the consequences in terms of corrosion depths in a repository environment, assuming hypothetically that the claims are correct, is presented in Section 4.3 and conclusions are presented in Section 4.4.

4.2 Theoretical and experimental studies to evaluate claims of corrosion

4.2.1 Theoretical and experimental studies in search of hitherto unknown species in the Cu-O-H system

According to established thermodynamic data, the equilibrium pressure of $H_2(g)$ in a closed system with only Cu(s) and $H_2O(l)$ present initially is calculated to be of the order of 10^{-6} mbar at room temperature, when all known solid compounds and solution species of the Cu-O-H system are taken into account, see, e.g., Appendix A in Hedin at al. (2018). Very similar equilibrium calculations have been presented by other authors, see e.g. MacDonald (2011) and Landolt (2007).

This result relies on the assumption that all relevant species in the Cu-O-H system have indeed been identified and included in the calculation. In recent years, considerable computational (Korzhavyi et al. 2012, Li et al. 2015) and experimental (Soroka et al. 2013) efforts have been made to identify potential hitherto unknown species of this system. No stable Cu-O-H compound that could act as the thermodynamic driving force of a continuing corrosion reaction in pure, O_2-free water was found.

Furthermore, surface reactions between water and the copper or copper oxide surface may lead to the oxidation of about one half of a monolayer of copper at most, potentially releasing a corresponding amount of hydrogen. This is far too little to explain the results observed by Hultquist et al. (2011, 2015).

A fuller discussion and an extensive set of references regarding the above issues are provided in Section 2 of Hedin et al. (2018).

4.2.2 The Uppsala experiment

In an SKB-funded experiment at Uppsala University, the two-chamber hydrogen evolution experiment mentioned in Section 4.1 was repeated under more controlled conditions (Figure 4-1). Specifically, the copper specimen surfaces were carefully cleaned and characterised prior to their exposure to water, the water to which the copper was exposed was extremely pure and free of dissolved oxygen, and detailed background measurements were carried out to distinguish hydrogen evolution due to a corrosion reaction from evolution due to experimental artefacts (Boman et al. 2014, Ottosson et al. 2016). The sensitivity of the experiment is fully sufficient to detect the hydrogen evolution rates reported in Szakálos et al. (2007) and Hultquist et al. (2011, 2015). No hydrogen evolution ascribable to copper corrosion was detected in the experiment.

In similar setups, the Uppsala group also looked for oxidised copper, which would be a more direct piece of evidence of copper corrosion (Ottosson et al. 2017). The water and all relevant surfaces in the setups were examined and in total less oxidised copper than the amount corresponding to a monolayer of the copper surface was found after up to 29 months of exposure. There were no indications of accumulation of oxygen at grain boundaries (Ottosson et al. 2016, 2017). In contrast, the hydrogen evolutions reported in Szakálos et al. (2007) and in Hultquist et al. (2011, 2015), if due to copper corrosion, would have caused corrosion depths of tens of monolayers.

A more detailed account of experimental details, results and conclusions is provided in Sections 3.2, 4.4 and 5.2 of Hedin et al. (2018) where all relevant references are also found.

Recently, one of the key publications from the Uppsala group, Ottosson et al. (2017), was commented by Szakálos et al. (2018), criticizing the control of hydrogen and oxygen gas levels in the experiment as well as the way in which the copper surfaces were pre-treated. The comment was readily responded to in all details by Ottosson at el. (2018), pointing, e.g., to misinterpretations of the data presented by the Uppsala group and apparently confused statements about standard methods for the preparation of clean copper surfaces.

4.2.3 The Micans experiment

An alternative method for studying hydrogen evolution from copper in pure, O_2-free water has been developed in an SKB-funded experiment at Microbial Analytics Sweden AB, Micans, Gothenburg, Sweden. In this method, typically two copper pieces with a total surface area of 46 cm^2 are submerged in pure O_2-free water in butyl rubber sealed test tubes, leaving a 6 cm^3 N_2-filled gas volume above the water, see Figure 4-2. The gas volume is sampled and analysed at regular intervals. The test tubes are kept in an inert N_2 atmosphere at a temperature of 70 °C. The sensitivity of the Micans method is far higher than that required to observe the hydrogen evolution rates and pressures reported in Hultquist et al. (2011, 2015).
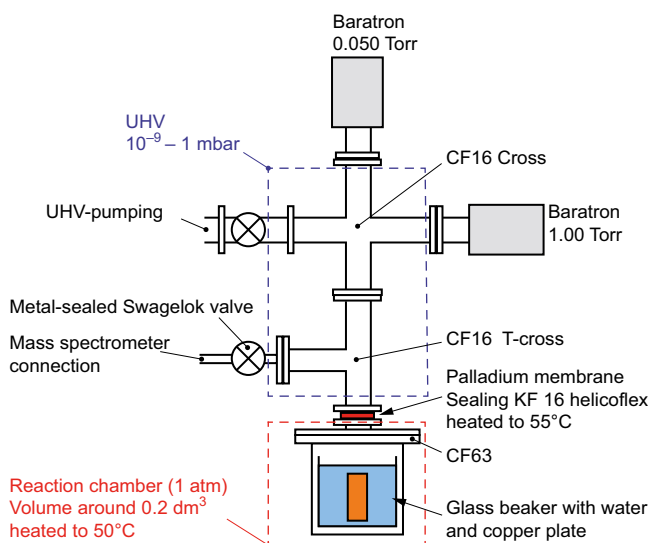
Figure 4-1. *Schematic view of the metal contained set-up at Uppsala University. The reaction chamber is located within the lower dashed rectangle. The tubing within the upper, dashed rectangle constitutes the upper, initially evacuated chamber. (Boman et al. 2014)*

Figure 4-2. Pairs of copper pieces immersed in pure water, contained in butyl rubber sealed borosilicate glass tubes. The 6 cm³ gas phase at the top is sampled and analysed at regular intervals. Two tubes contain only water and gas. The image was taken after 27 months of exposure to pure, oxygen free water at 70 °C. (Johansson et al. 2015)

Several combinations of copper qualities and surface treatment methods were exposed for up to 3 years. As an example, results from the experiment with the copper quality used in Hultquist et al. (2011, 2015), for a number of surface treatments including the "as received" condition used by Hultquist et al., are shown in Figure 4-3. As seen in the figure, none of the samples yield hydrogen evolution above background, whereas the expected H_2 evolution rate according to data from Hultquist et al. would have been easily detected by this method.
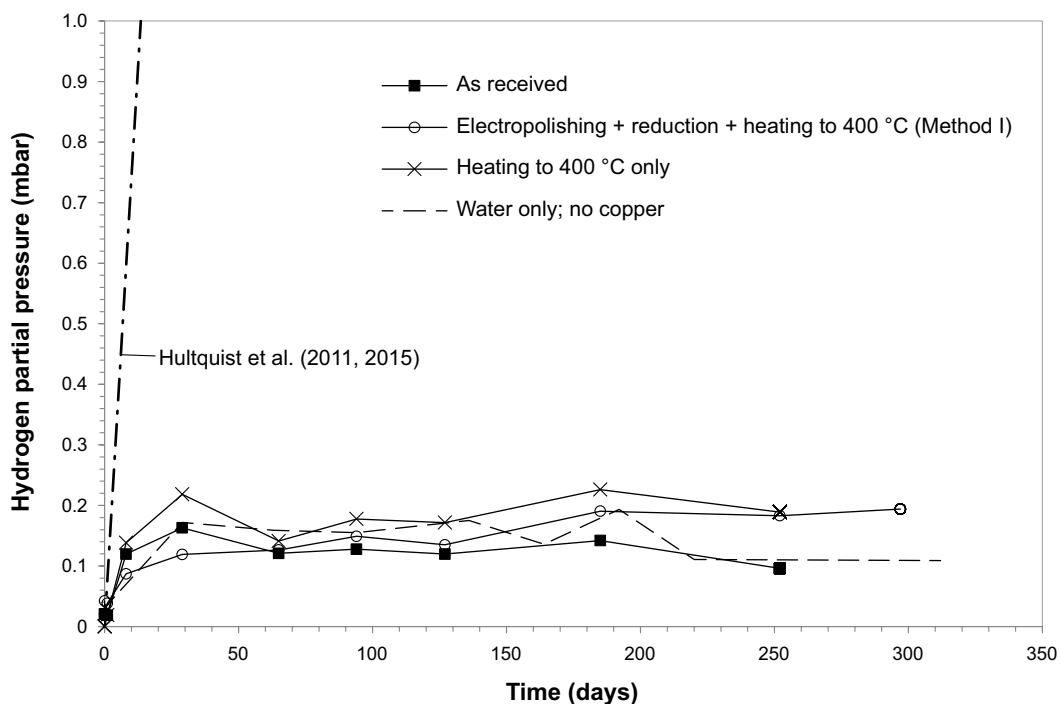
Figure 4-3. Hydrogen evolution from samples of 99.95 % Cu-OF (oxygen free copper) with different surface treatments. The expected hydrogen evolution rate according to Hultquist et al. (2011, 2015) is also shown. (Hedin et al. 2018)

In summary, no continuing hydrogen evolution above background was observed for any of the combinations in the Micans experiment, with one exception: Samples of phosphorous doped oxygen free copper (Cu-OFP), see SKB (2010d, Section 3.2), intended as canister material exhibited hydrogen evolution rates of typically 10^{-15} mol/(cm^2 s). Apart from being the only phosphorous doped samples, they also had a thickness, 2 mm, which was an order of magnitude larger than all other samples. The hydrogen evolution from these samples is, however, not due to copper corrosion since a similar rate of hydrogen evolution is observed for copper samples not in contact with water. Furthermore, when samples of this type were first outgassed at 400 °C in vacuum for 1 hour (with the outgassing of hydrogen explicitly measured), no hydrogen evolution was observed during the subsequent exposure to water. It was thus concluded that for these samples, the detected hydrogen had its origin in the copper material; Cu-OFP has an initial H content of about 0.5 wt.ppm (weight-ppm).

A more detailed account of the method, the results and conclusions is provided in Sections 3.1, 4.1−4.3 and 5.1 of Hedin et al. (2018) where all relevant references are also found.

Recent developments

A selection of the samples studied in the Micans experiment has been stored in an inert atmosphere at 70 °C for up to 6 years after the measurements reported above. Recently, a final set of measurements were made on these samples (Morsing Johansson and Pedersen 2019). In summary, no hydrogen above background was found in any of the vials. It was also found that after the nearly six years storage time the butyl rubber stoppers had deteriorated in several of the test tubes meaning that these had not been tight during the latter period of storage. Elevated O_2 levels were detected in some of the tubes, compatible with leaking stoppers.

As mentioned above, hydrogen was detected from Cu-OFP samples in the Micans experiment, irrespective of whether the copper samples were submerged in water or not. Scoping calculations of the outgassing rate of $H_2(g)$ from Cu-OFP at 70 °C have been made and compared to the experimental results for various assumptions on hydrogen trapping in the material (Hedin 2019). It is shown that the same model and data assumptions that explain the Micans data can also explain the much more rapid outgassing observed when the samples are heated to 600 °C at a rate of 1 °C/min. The result thus further corroborates the conclusion that the slow hydrogen evolution from the Cu-OFP samples in the Micans experiment is due to outgassing from the Cu metal. A detailed understanding of the form in which the 0.5 wt.ppm H occurs in Cu-OFP is, however, lacking.

4.2.4   Comments on other experiments

The experiments at KTH

Issues relating to the experiments reported in Szakálos et al. (2007) and Hultquist et al. (2011, 2015) are discussed in Section 5.4 of Hedin et al. (2018), with references to discussions in the scientific literature. Most notable, measurements of background H_2 from the apparatus is reported only in Szakálos et al. (2007) and in that case likely disturbed by remaining oxygen. No such measurements are reported in Hultquist et al. (2011, 2015). Such measurements are crucial since the hydrogen evolution rates reported in the experiments are comparable to what could be expected from the stainless steel of which the chambers are built. Also, it appears as the palladium foil separating the two chambers is in contact with the exterior, meaning that the steady hydrogen levels attained after long exposure times could be caused by hydrogen releases to the exterior via the foil being balanced by the generation of H_2 in the set-up, rather than by a chemical equilibrium of a corrosion reaction as claimed by the authors.

Two-chamber experiment by Becker and Hermansson

A brief attempt to repeat the two-chamber experiment mentioned in Section 4.1 was made by Becker and Hermansson (2011). Hydrogen gas was detected in a run with copper immersed in water in the lower chamber, but not in a background run without copper. However, about 1 mbar of O_2 remained in the lower chamber at the onset of the measurements. This O_2 is expected to react with any background H_2 emerging from the stainless steel walls of the chambers in the background run, thus preventing its detection. In the run with Cu, the remaining oxygen is expected to be consumed by the copper, thus allowing the detection of H_2 from the apparatus' stainless steel. See Section 5.3 of Hedin et al. (2018) for a further discussion of the results of that experiment.

Kinetic model by Cleveland et al.

Cleveland et al. (2014) presented a kinetic model study of copper corrosion in pure O_2-free water. The discussion that ensued in the scientific literature, however, made it clear that the kinetic data used in the model were taken from systems that had not been demonstrated to be relevant for the study at hand and that the model, as a consequence, yielded results that are not compatible with the established thermodynamic data on which the study was also founded. See Section 5.5 of Hedin et al. (2018) for a more detailed discussion and additional references.

A preliminary report from an effort to clarify the possibilities of formulating a kinetic mixed-potential model for copper corrosion in pure, O_2-free water is provided in King and Orazem (2017).

E-flask experiments

Hultquist et al. (2009) studied corrosion of copper submerged in water in E-flasks stored in air for 15 years. One of the flasks was sealed with a 0.1 mm hydrogen permeable palladium foil and the other with a glass stopper. UHV-glue was used to secure a gas tight seal. In flasks sealed with the palladium foil to allow outflow of any hydrogen generated in the flask, clear evidence of copper corrosion was observed whereas this was not the case for flasks sealed with the glass stopper. Ollila (2013) repeated the experiment under more controlled conditions, most notably by storing the flasks in an inert atmosphere, and did not obtain the observations of corroded copper made by Hultquist et al. (2009). Ollila (2013) also carried out a test with a palladium sealed E-flask in air and then obtained clear evidence of corrosion. It appears clear that an in-leakage of air through the palladium seal caused the observed corrosion in Hultquist's study. A more detailed discussion is provided in Section 5.5 of Hedin et al. (2018).

Recent electrochemical study by He et al.

He et al. (2018) exposed copper (rods and foils) to de-aerated synthetic groundwaters, at 50 and 80 °C, with the solution exposed to air or an inert atmosphere. The investigation consisted of measurement of open-circuit potential, corrosion rate (with electrochemical methods and weight-loss measurements) and measurement of hydrogen generation.

The results indicated that the Cu open-circuit potential and corrosion rates in anoxic waters (with less than 10 ppb of O_2) were very sensitive to the residual O_2 concentration in solution. The corrosion rates ranged from submicrometre to micrometres per year with increasing residual O_2 concentration level in parts per billion. The corrosion product was predominantly Cu_2O. Hydrogen gas was also found to be evolved from the tests, albeit in very small amounts. This small amount of H_2 evolved could not be correlated to the Cu corrosion process since hydrogen evolution from the autoclave material complicated the interpretation of the results.

The authors interpret their results cautiously and do not directly couple the corrosion products or hydrogen gas to corrosion in pure water. Furthermore, there are many factors in the experimental set-up that are not taken into account when interpreting the results. These include *i*) that the observed weight-loss could be due to corrosion by the O_2 initially present in the PTFE lining, and *ii*) that the electrochemical methods used are easily disturbed by the complex solution and not adequate for measuring small corrosion rates.

Recent study by Senior et al.

Senior et al. (2019) recently published a study of hydrogen evolution from bundles of Cu wires submerged in O_2-free water. At 50 °C, no hydrogen evolution was detected although the sensitivity of the method is fully sufficient to detect the hydrogen reported by Hultquist et al. (2011, 2015) at this temperature. Hydrogen that would hypothetically correspond to a corrosion rate of 1 nm/yr is observed at 75 °C, but the authors point out that alternative sources of H_2 have not been eliminated. Also, the observed rate of hydrogen evolution is much smaller than that observed by Hultquist et al. (2011, 2015) and the authors point out that the measurements represent a conservative upper bound on the corrosion rates.

Recent study by Ollila

In a recent report, Ollila (2019) presented *i)* additional measurements from the E-flask experiment (Ollila 2013) and *ii)* results from a study similar to the Micans test tube experiment discussed in Section 4.2.3.

In the E-flask experiment, a Cu sample exposed to pure O_2-free water for almost seven years had similar surface properties as both the sample exposed for 2 years in Ollila (2013) and to unexposed reference samples, i.e. the surface was not affected by a corrosion reaction.

The test tube experiment was similar to the Micans experiment, but conducted at room temperature rather than 70 °C. Samples of Cu-OFP and of 99.9999 % Cu (6N-Cu) were exposed to pure, O_2-free water for times ranging between 1 week and 6.5 months. The results were qualitatively similar to those reported in the Micans experiment. Ollila (2019) writes "The detected hydrogen concentrations suggest difference between the two copper types. The H_2 concentration increased with the duration of the test in the test vials with OFP-Cu rods, while it remained at the same level with blank tests in the test vials with 6N-Cu rods." It is noted that the hydrogen evolution rates from the Cu-OFP is about two orders of magnitude lower than that observed in Micans' experiment, compatible with the lower diffusivity of H in Cu at room temperature compared to 70 °C. Regarding surface examinations by XPS, the author concludes that "...the presence of oxidized layers, Cu_2O, $Cu(OH)_2$ or CuO, was not observed by XPS on the exposed copper surfaces suggesting that corrosion reactions of copper did not occur." It is also noted that the background level in Ollila's experiment appears to be around 0.2 μmol/L (around 5 μbar) at room temperature, i.e. at least one order of magnitude lower than in the Micans experiment. This further lowers the limit above which no hydrogen emanating from a corrosion process is observed in the Micans type of experiment.

4.3   Application to repository conditions – what if calculation

Even if the material in the above sections suggests that the basis for claiming that copper corrodes to an extent that is not compatible with established thermodynamic data is very weak, it is of interest to examine what the data presented by Hultquist et al. (2011, 2015) would mean in terms of corrosion depths in a final repository.

Based on the data available in the cited references, two approaches to such a calculation can be taken: One is to assume that the equilibrium aqueous concentrations of H_2 corresponding to the partial pressures of hydrogen reported in Hultquist et al. (2011) for the proposed corrosion reaction are always upheld at the canister surface. The extent of corrosion can then be calculated through the available hydrogen sinks in the repository, both in the form of volumes available for hydrogen "storage" and by rates at which hydrogen, at the concentration corresponding to the presumed equilibrium partial pressure, can be transported away from the canister. Another, and bounding approach, would be to directly consider the hydrogen evolution rates reported in Hultquist et al. (2015) and transform these into hypothetical corrosion rates.

Both approaches have been investigated, as reported in section III in Hedin et al. (2017). It is shown that the latter approach yields a corrosion depth of around 1 mm in the one million year period that needs to be covered in a post-closure safety assessment, when the effect of the elevated temperatures expected during the first few thousand years is also taken into account. The first approach, based on the assumption of equilibrium pressures, yields even smaller corrosion depths when considering only the transport resistance offered by the clay buffer surrounding the canister. The approach based on hydrogen evolution rates is seen as more robust since hydrogen would be free to leave the copper surface essentially unimpeded in the cited experiments, meaning that it is difficult to conceive of a situation where the evolution rates would be higher. This approach also obviates the need to quantify transport rates and sinks of H_2 in the repository.

In Hedin et al. (2017) it is also noted that the claim made in Hultquist et al. (2015) that their measured hydrogen evolution rates indicate corrosion rates in the range 10−100 nanometres/yr at room temperature lacks support in those authors' own data.

In this context, it is also noted that the corrosion rates calculated above would be impossible to observe in large-scale *in situ* field tests, where typical average corrosion depths are $0.2-10$ μm. Furthermore, the corrosion observed in field tests (corrosion depth and corrosion products) is fully compatible with processes and parameters included in traditional safety assessment corrosion models, such as the amounts of residual O_2 present in the experiments initially, the thermodynamics of the system, and in some cases the influx of sulphide through the clay (Johansson A J 2019b).

Finally, it is noted that it is not sufficient to dismiss the claims by Szakálos et al. (2007) and Hultquist et al. (2011, 2015) as being irrelevant for repository conditions based solely on the type of what-if calculations discussed above. Even if the process *per se* would not lead to unacceptable consequences, its existence would indicate a lack of fundamental understanding of copper corrosion in aqueous environments, which would not be satisfactory. Hence all the efforts to evaluate the alleged existence of the process described in the preceding sections.

4.4 Conclusions

Based on the account of the issue of copper corrosion in pure, O_2-free water given in this chapter, it is concluded that there is no support for claiming that the extent of this process exceeds that predicted by established thermodynamic data.

Experiments on which claims of far higher extents of corrosion are made have been repeated under more-controlled conditions. The hydrogen evolution claimed as evidence of copper corrosion was not observed, despite fully sufficient detection levels. Nor was any evidence of oxidised copper found. Also different experimental approaches were used, with the same result.

No hitherto unknown stable species of the Cu-O-H system has been found despite both theoretical and experimental efforts.

It has also been demonstrated that even if the claims of corrosion of copper in pure O_2-free water were correct, they would correspond to a corrosion depth of about 1 mm in 10^6 years in a final repository.

5 Pitting due to reaction with sulphide, including the influence of the sauna effect on pitting

5.1 Introduction

Pitting is one type of localised corrosion that could appear on a metal surface, following the formation of a film of corrosion products on the surface. Sulphide is the main long-term corroding agent in a repository at Forsmark, meaning that it is relevant to address the possibility of pitting under a film of copper sulphide. This was done in the safety assessment SR-Site with the conclusion that this type of pitting will not occur. The morphology and properties of the copper sulphide film are key issues in the possible occurrence of pitting. These will in turn be determined by the interfacial concentration of sulphide, which is a result of the balance between the influx of sulphide to the surface and the consumption rate (corrosion rate) at the surface. It should be noted, therefore, that under mass-transport limited conditions, the interfacial concentration is close to zero.

In the statement by the Land and Environmental Court (Section 1.1), it was suggested that pitting due to reaction with sulphide needed to be further addressed. This is done in the present chapter. It was also suggested that the influence of the sauna effect on pitting needs to be included. Since it was concluded in Section 3.5 that the sauna effect will be insignificant in a KBS-3 repository at Forsmark, this effect is not included in the evaluation to follow. This chapter is structured as follows.

- The concept of localised corrosion, and especially pitting, is briefly reviewed in Section 5.2. Parts of the mechanistic descriptions are also valid for the discussion of stress corrosion cracking (SCC) in Chapter 6.

- The nature of copper sulphide films formed under various conditions of exposure to sulphide is discussed in Section 5.3.

- Investigations of localised corrosion under copper sulphide films are discussed in Section 5.4.

- In Section 5.5, possible future repository conditions are compared to those leading to sulphide films of various types and to those for which localised corrosion has been observed.

- Finally, conclusions regarding the occurrence of pitting and other forms of localised corrosion under repository conditions are presented in Section 5.6.

5.2 Localised corrosion in sulphide solution

Localised corrosion is a term used for corrosion mechanisms which have in common that the oxidation of the metal is focused on just parts of the surface. This is in contrast to general or uniform corrosion where the anodic oxidation of the metal and the cathodic reduction process is evenly spread over the corroding surface. The properties of a solid film of corrosion products are central to the origin of several forms of localised corrosion. If the film prevents or drastically reduces further general corrosion it is often called a "passive film".

The formation of a passive film can be identified by cyclic voltammetry (CV); a type of electrochemical investigation where the current at an electrode is recorded when changing the applied potential. If a non-passivating film is formed, the current remains significant, indicating continuing metal dissolution, when scanning back to lower potentials. The presence of a non-passivating corrosion film or deposit could lead to a negative current peak when the film is reduced back to metal. For a passive film the anodic current is significantly suppressed when the potential scan is returned to lower values because the formed film is blocking metal oxidation.

For the specific form of localised corrosion called pitting, increasing the potential first leads to the formation of a passive film , but above a certain value results in a sudden increase in positive current, indicating that the film has been locally ruptured allowing localised attack to start, i.e. that pits have started to form in the underlying metal surface. The potential at which this occurs is called the breakdown potential.

Copper metal reacts with soluble sulphide species to form the corrosion product, Cu_2S (Chen J et al. 2010), which is highly insoluble and remains as a corrosion film on the copper surface. The morphology of the film is dependent on the conditions under which the film is grown (Section 5.3). Numerous experiments performed by a group at the University of Western Ontario, Canada, show that both compact and porous films can form, depending on the experimental conditions. A compact structure is a prerequisite for a film to have passivating properties. Porous films, on the other hand, do not have passivating properties. In general, copper sulphide films tend to be porous and non-protective (Sharma 1980, Speight 2014 Chapter 8.2.5).

In addition to the more well-known form of corrosion called pitting, there is another form of localised corrosion described as micro-galvanic corrosion. There are important mechanistic differences between pitting and micro-galvanic corrosion. Pitting corrosion is the result of microscopic defects which act as local anodes that appear in an otherwise passive film that protects the surface from metal dissolution but is sufficiently conductive to act as a cathode. As a result of a very small anode-to-cathode area ratio, local corrosion damage can become distinct and deep compared to the average corrosion depth. Micro-galvanic corrosion, on the other hand, occurs through the coupling of anodic and cathodic areas of the same order of magnitude, and typically leads to local penetrations which are not much deeper than the average corrosion depth. A schematic illustration of the morphological differences between these forms of localised corrosion is presented in Figure 5-1 (Chen J et al. 2019).

During the long-term sulphide corrosion phase, the environment near the copper canister will be anoxic and shift towards lower temperature and slightly alkaline conditions. In SR-Site, it was concluded that the risk of pitting in sulphide solutions is small because the value of the corrosion potential is much lower than the values of the film breakdown potential available at that time (King et al. 2010). As discussed in more detail below, since SR-Site our understanding of the mechanisms of the corrosion of copper in sulphide environments has increased and has reinforced the belief that the probability of localised corrosion is low.
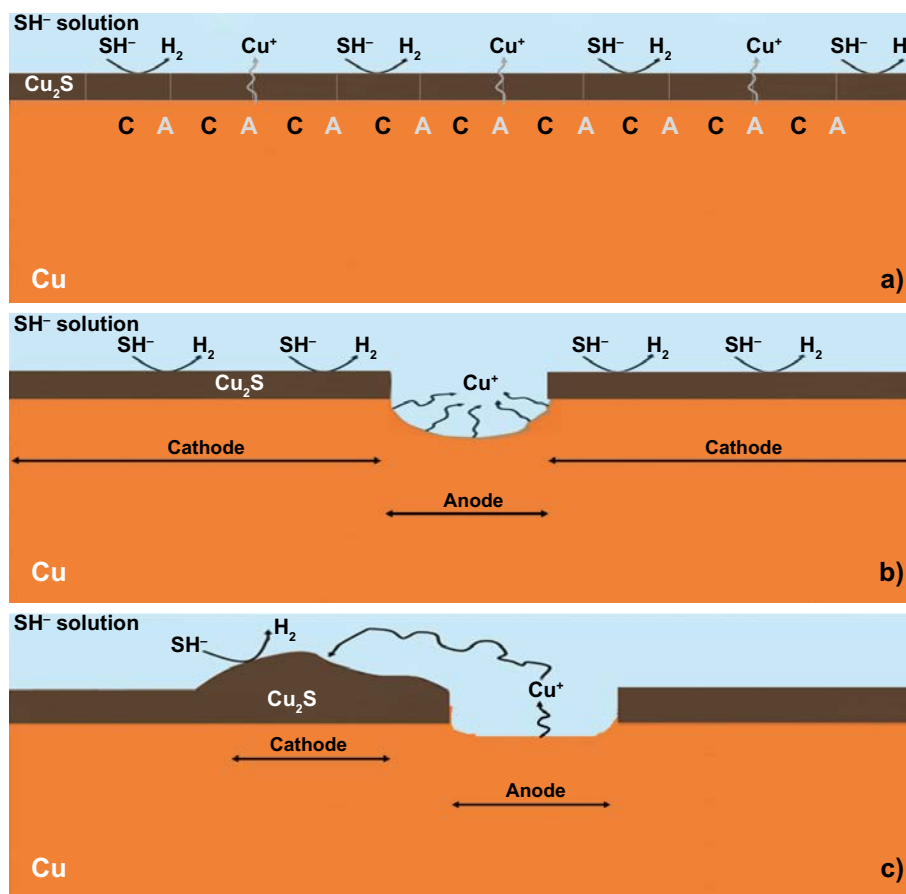
Figure 5-1. *Schematic illustration of the differences in corrosion morphology between a) general, b) pitting, and c) micro-galvanic corrosion (Chen J et al. 2019).*

5.3 Copper sulphide film formation and properties

5.3.1 Naturally corroding conditions

A series of experiments was performed under naturally corroding conditions (no potential is applied to the specimens) in which canister copper was exposed to sulphide concentrations from 5×10^{-5} to 1×10^{-3} mol/L, and chloride concentrations in the range 0 to 5.0 mol/L (Chen J et al. 2017a, King et al. 2017). Cross sections of the films were studied with SEM (scanning electron microscopy), see Figure 5-2 to 5-4. The experiments show that at low bulk concentration of sulphide ($\leq 1 \times 10^{-4}$ mol/L) the film is always porous, while an increase of bulk sulphide concentration gives a compact film, see Figure 5-5. Most experiments were performed with chloride present and increasing the concentration of chloride changes the morphology toward more porous films. At very high concentrations of sulphide (10^{-3} mol/L) and chloride (5 mol/L) a porous film is formed but it has a more columnar structure than those formed at lower chloride concentrations.

The concentrations in the experiments above are the bulk concentrations of sulphide and chloride, but it is the interfacial concentration near the copper surface that is important for the corrosion mechanism. Under stagnant conditions and/or at low sulphide concentrations, the corrosion rate is transport limited and the interfacial sulphide concentration will be close to zero. Using a rotating disc electrode the sulphide flux to the surface is increased by decreasing the diffusion layer thickness. If the sulphide flux is larger than the consumption rate, the sulphide concentration at the surface will be non-zero. It is this situation that results in the formation of a compact film, see Figure 5-6.
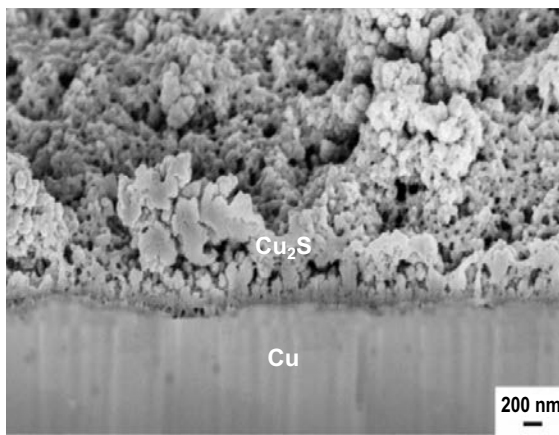
Figure 5-2. Cross section of a porous copper sulphide film formed under stagnant conditions, in 5×10^{-5} mol/L sulphide and 0.1 mol/L chloride after 4000 h (King et al. 2017).
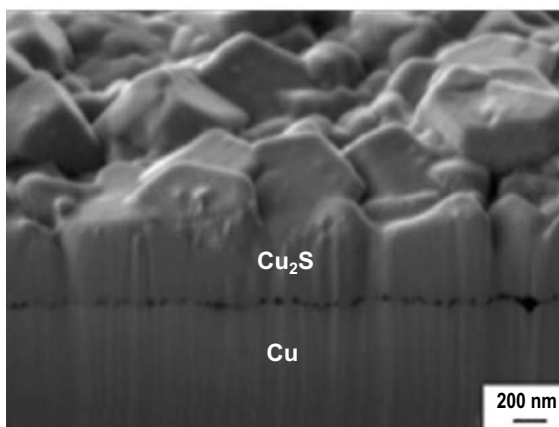
Figure 5-3. Cross section of a compact copper sulphide film formed under stagnant conditions, in 5×10^{-4} mol/L sulphide and 0.1 mol/L chloride after 1691 h (Chen J et al. 2010).
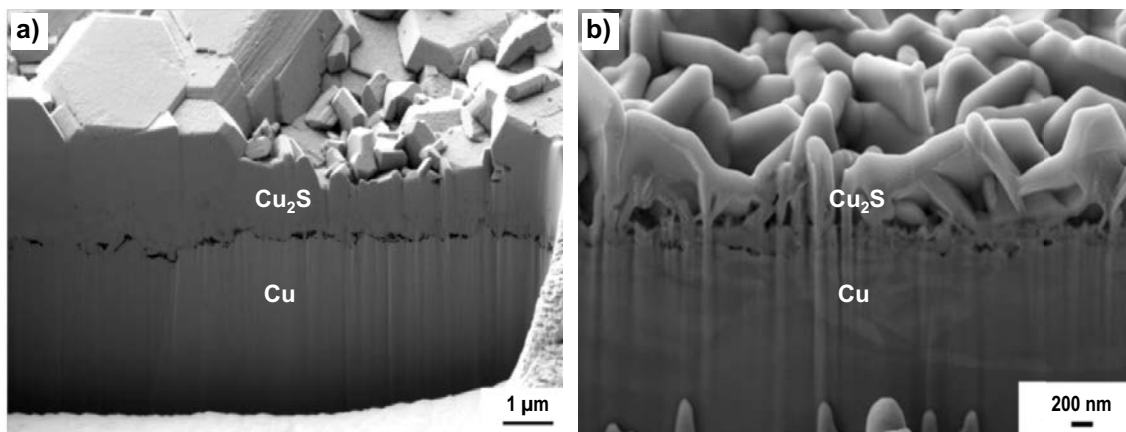
Figure 5-4. Cross section of copper sulphide films formed under stagnant conditions, in 1×10^{-3} mol/L sulphide at 1 691 h. a) A compact film in 0.1 mol/l chloride M: b) a porous and columnar film in 5.0 mol/L chloride (Chen J et al. 2017a). (The features at the bottom right in a) are remnants from the preparation of the cross section.)
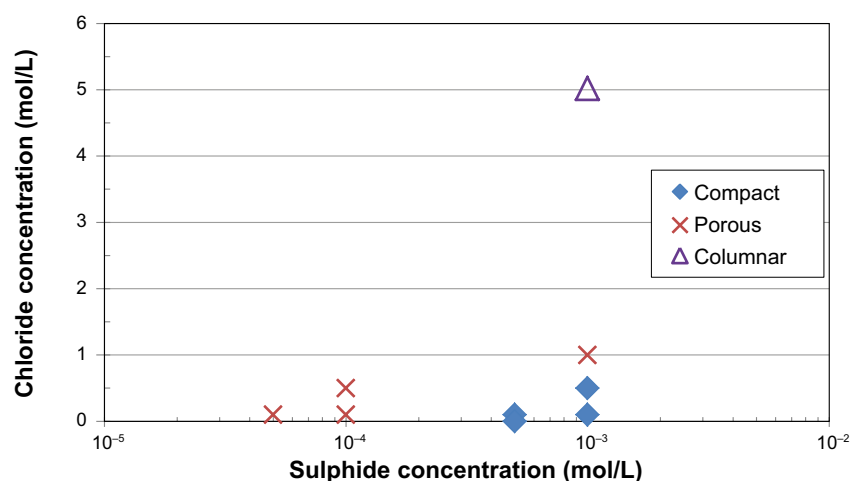
Figure 5-5. Morphology of copper sulphide films as interpreted from cross sections studied with SEM, as a function of bulk sulphide and chloride concentrations in solution. Data from Chen J et al. (2014) and King et al. (2017).
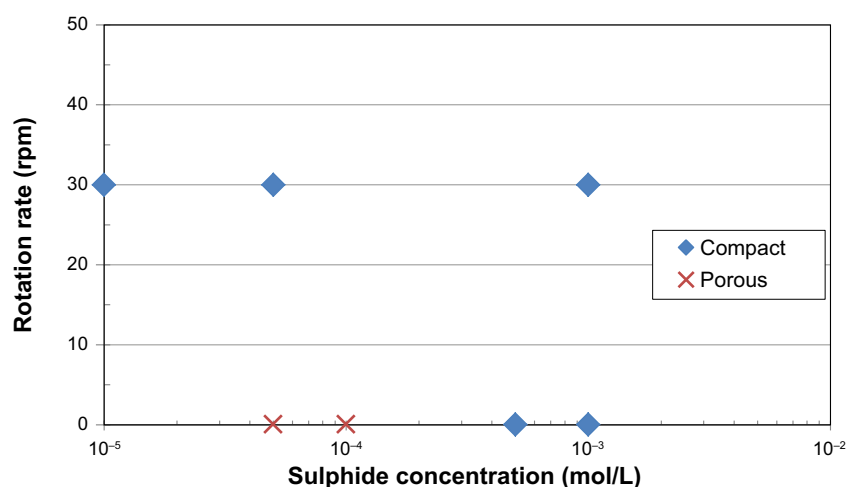
Figure 5-6. Morphology of copper sulphide films as interpreted from cross sections studied with SEM, as a function of bulk sulphide concentration and electrode rotation rate, at a constant chloride concentration of 0.1 mol/L. Data from Chen J et al. (2014) and King et al. (2017).

To identify the location of the Cu$_2$S film growth, an experiment with a gold marker was performed (Martino et al. 2017). A Cu sample was first corroded in a solution with 5×10^{-4} mol/L sulphide and 0.1 mol/L chloride to form a thin (200 nm) film, the gold was deposited and the sample was further exposed for 1 530 h. Analysis of the cross section showed that the film beneath the gold marker was unchanged, and new film had grown on top of it. The results show that the film growth occurs at the Cu$_2$S/electrolyte interface. It was also noted the film was compact, which is in accordance with Figure 5-5.

Film growth at the film/solution interface means that the reactants (Cu$^+$ and HS$^-$) must be transported to this interface, i.e. there must be a transport of copper ions through the film. If the process is mass transport limited there are two alternatives: the diffusion of HS$^-$ in solution (and pores of the film) or the diffusion of Cu$^+$ through the film. For the latter case, a growing film would decrease the growth rate, and e.g. give a growth rate following a power law. If the transport of sulphide through the solution is limiting, the film would grow linearly with time (for a constant diffusion rate). The film thickness has been measured as a function of time, see Figure 5-7, and for experiments in a 0.1 mol/L chloride solution the linear growth rate corresponds to a porous film (5×10^{-5} mol/L sulphide), while a power law growth (nearly parabolic) corresponds to compact films (5×10^{-4} and 10^{-3} mol/L sulphide).

A more detailed evaluation of the possible mechanisms for the growth of the film is discussed in Chen J et al. (2011, 2018), taking into account that the diffusion of Cu$^+$ could also be along the grain boundaries in the film or in the solution in the pores, and that the diffusion of HS$^-$ could be within the pores of the Cu$_2$S film and not only diffusion in the bulk solution. Diffusion of Cu$^+$ may also be assisted by complexation with Cl$^-$ at high chloride concentration (Chen J et al. 2018). It can be concluded that a compact and protective film that can decrease the rate of further film growth, is only formed at high sulphide and low chloride concentrations under naturally corroding conditions.

5.3.2 Experiments under applied potential

The mechanism of film formation can also be studied in experiments under potential control (i.e., in electrochemical experiments), which have also been performed at the University of Western Ontario.

Cyclic voltammetry was used to investigate the mechanism of sulphide film formation. The detailed description of the experimental set-up and interpretation of the results can be found in Martino et al. (2014, 2017). From cyclic voltammograms (CVs), EIS (Electrochemical Impedance Spectroscopy) spectra and SEM-analyses it can be concluded that 3 types of films are possible. The film types are illustrated in Figure 5-8:

- Type I film with a single porous layer of Cu$_2$S

- Type II film consisting of a dual layer of Cu$_2$S, with an inner thin film and an outer porous film. The inner film breaks because of interfacial stresses due to the large Pilling-Bedworth ratio (the ratio of the volumes of the elementary cells, Cu$_2$S/Cu).

- Type III film with a partially-passivating layer in which the pores in the film are blocked. At the bottom of the pores a passivating film may exist.
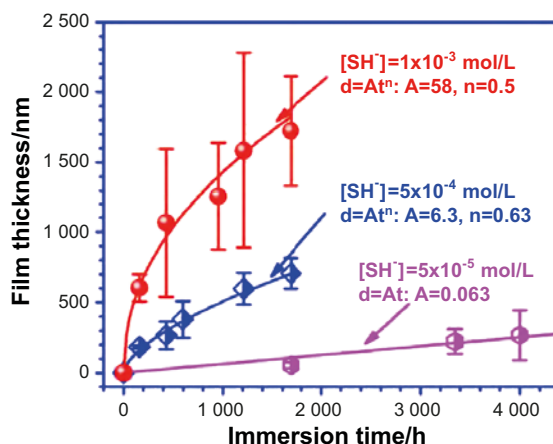
Figure 5-7. Film thickness as a function of time, for copper exposed to 0.1 mol/L chloride and various sulphide concentrations (Chen J et al. 2017b).
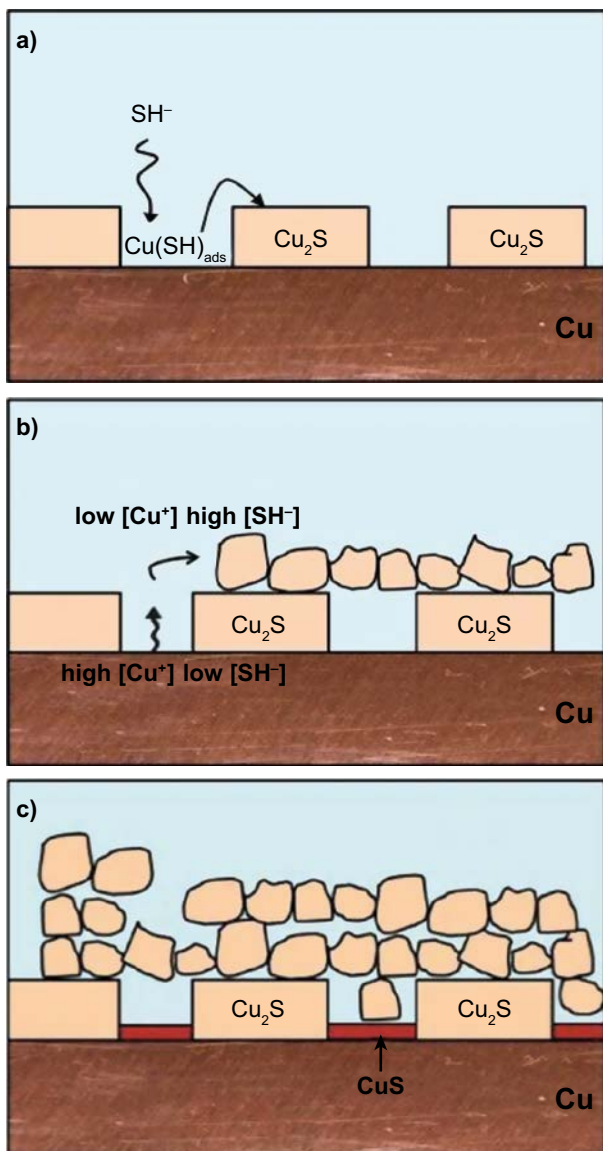
Figure 5-8. *Illustration of the different film types, a) Type I b) Type II, c) Type III, observed under various solution conditions. Note that the pore dimensions and the film thickness are not to scale, as the pores in reality are much narrower and the outer films are thicker. (Martino et al. 2014)*

The experiments were also performed with a rotating electrode, which increases the flux of sulphide ions to the surface and thus their interfacial concentration. Figure 5-9 summarizes the conditions under which each type of film is formed. For the two lower sulphide concentrations studied (5×10^{-5} mol/L, 10^{-4} mol/L HS$^-$), a Type I film is formed irrespective of the sulphide flux (controlled by the rotation rate of the electrode). Type III films are only formed at high sulphide flux ($\geq 1 \times 10^{-3}$ mol/L HS$^-$ and rotation rate ≥ 50 rad/s). Type II films are formed under intermediate conditions. Increasing the chloride concentration extends the Type II film formation range to lower sulphide fluxes for intermediate sulphide concentrations. The sulphide concentrations and fluxes required for the formation of a type III film do not change with increasing chloride concentration.

Unlike the films grown under naturally corroding conditions, however, it must be remembered that the development of the films, and the film types, are influenced by their growing while the potential is changing in the experiment, and not under open circuit conditions (natural corrosion). Still, the understanding of mechanisms for film growth and the film properties can be used when interpreting the films formed under naturally corroding conditions, e.g. in determining the rate-controlling factors for the corrosion.
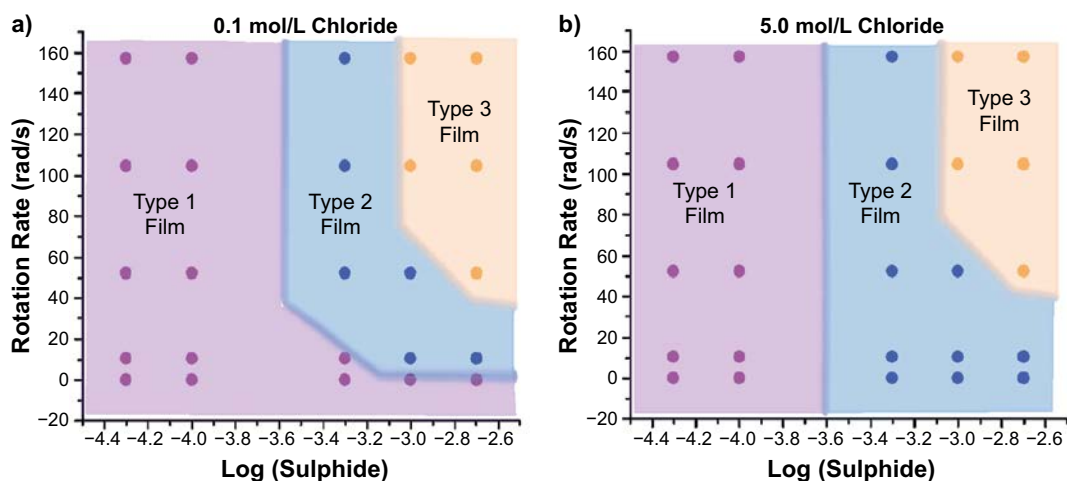
Figure 5-9. *Summary of the conditions under which porous (Type I and II) and compact, possibly passive (Type III) films are formed, as a function of sulphide concentration and electrode rotation rate (a measure of the flux of sulphide to the electrode), for a) 0.1 mol/L chloride, b) 5.0 mol/L chloride (Martino et al. 2017).*

The influence of mass transport of sulphide in solution can also be seen in the voltammogram in Figure 5-10, where convective conditions using a rotating electrode (red curve) are compared to stagnant conditions (black curve). The anodic current in the region -0.8 V to -0.1 V is for the growth of a film under transport-limited conditions, with an increased growth rate indicated by the higher current for the rotated electrode. The additional amount of corrosion products formed is also manifested in the larger cathodic peak for the rotated electrode. Irrespective of the rotation rate, the current in the potential region -0.8 to -0.1 V is reversible, which shows that the growing film does not influence the rate of further film growth, i.e. the film growth is controlled by mass transport and does not lead to passivity. Further studies with films grown at different potentials (Martino et al. 2019a) showed that no passive layer was involved in the film formation, but that a thin porous layer and a thicker outer deposit determines the sulphide flux and thereby the film morphology.

In other experiments, under conditions of high sulphide flux, accomplished by combining high sulphide concentrations with a rotating electrode, an anodic peak is observed in the cyclic voltammogram at the beginning of the current plateau (i.e., ~ -0.8V). When the potential is subsequently reduced, the current is considerably lower indicating that the film formed is blocking further film formation (Martino et al. 2014). It was concluded that, if a passive film form, it would only be at high sulphide concentration ($\geq 1 \times 10^{-3}$ mol/L), and then only at high sulphide flux accomplished with a rotating electrode when a high interfacial concentration is maintained.
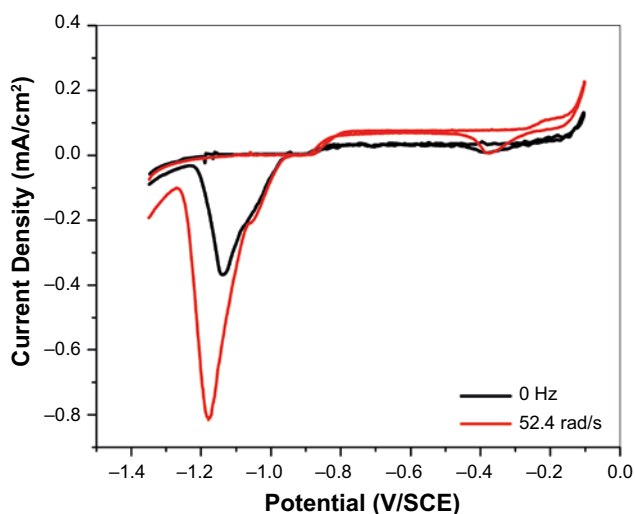
Figure 5-10. *Cyclic voltammograms under stagnant conditions and with increased sulphide flux (rotating electrode, 52.4 rad/s), in 10^{-4} mol/L HS$^-$ and 0.1 mol/L Cl$^-$ (Martino et al. 2017).*

5.3.3 Effect of anions – chloride, sulphate and bicarbonate

The effect of chloride and other anions such as sulphate and carbonate, which are expected to be present in groundwaters, has been studied with cyclic voltammetry (Martino 2018, Chapter 7).

Chloride influenced the film formation processes in different ways depending on sulphide concentration:

- At low sulphide concentration, chloride appeared to have two different effects on the anodic formation of Cu_2S films. At low chloride concentration, film formation occurred at a rate identical to the diffusion-controlled limit indicating that film growth was transport controlled. At high chloride concentration, film formation was suppressed, which was interpreted as a result of competition between chloride and sulphide for adsorption sites on the Cu surface.

- At high sulphide concentration the Cu_2S film formed was more compact at low chloride concentration with the growth rate governed by diffusion of Cu^+ within the film. An increase in chloride concentration led to an increase in film growth rate, controlled by ion migration within solution-filled pores in the growing film. The higher ionic strength of the solution led to a reduction of the electric field within the pores. Thus, a larger fraction of the applied potential was available to anodically oxidize the Cu leading to the increased film growth rate.

- The ability of Cl^- to suppress the Cu_2S film growth rate decreased as the $[SH^-]/[Cl^-]$ ratio increased further supporting the idea that the two anions competed for adsorption sites on the Cu surface at the base of pores in the film.

In the presence of sulphate, the Cu_2S film formation was effectively suppressed. This was most likely due to the strong adsorption of SO_4^{2-} on Cu, reinforced by the co-adsorption of H_2O, leading to the displacement of SH^- from surface adsorption sites. At high sulphide concentration the film remained porous in nature and no active-to-passive transition was observed during anodic film formation.

Voltammetric data showed that the effect of HCO_3^- appeared to be intermediate between that of Cl^- and that of SO_4^{2-}. While some aspects of the influence of SO_4^{2-} and HCO_3^- remain unresolved their dominant influence is to suppress the oxidation of Cu and, in the case of SO_4^{2-} to inhibit the tendency to form protective films at high sulphide concentration.

5.3.4 Other claims of passivity

In a series of papers (e.g. Mao et al. 2014, Dong et al. 2016, Kong et al. 2018), a group of researchers describes the copper sulphide film formed electrochemically on copper as a passive layer, with the sharp increase in current at higher potentials being a breakdown potential. This potential decreases with increasing chloride concentration (first mentioned in Mao et al. 2014) and increasing temperature (Dong et al. 2016).

Martino et al. (2017) showed that what these authors interpret as a breakdown potential is actually the onset of active dissolution of Cu accelerated by Cl^- complexation in the pores of the Cu_2S film, which is observed both in the presence and absence of sulphide. The marked area in Figure 5-11 shows this onset potential occurs for potentials ≥ 0.25 V/SCE on a rotating copper electrode. The onset potential shifts to lower potential with increasing chloride concentration and increasing temperatures (Martino et al. 2019b).

In a paper by Huttunen-Saarivirta et al. (2018), the Point Defect Model (PDM) is used to quantify the properties of the Cu_2S film developed on the surface of copper in simulated groundwater in the presence of sulphate-reducing bacteria. The film properties are investigated with EIS, with the data then fitted to the PDM. The authors conclude that a thin passive film is formed (0.3 % of the total film thickness), with the remaining film being a porous outer film. On the other hand, they also note that no sharp increase in current was seen with increasing potential, which would be typical of passivity breakdown, and no hysteresis loop between the forward and backward scan of the cyclic polarisation curve was seen, which would be indicative of a passive film.
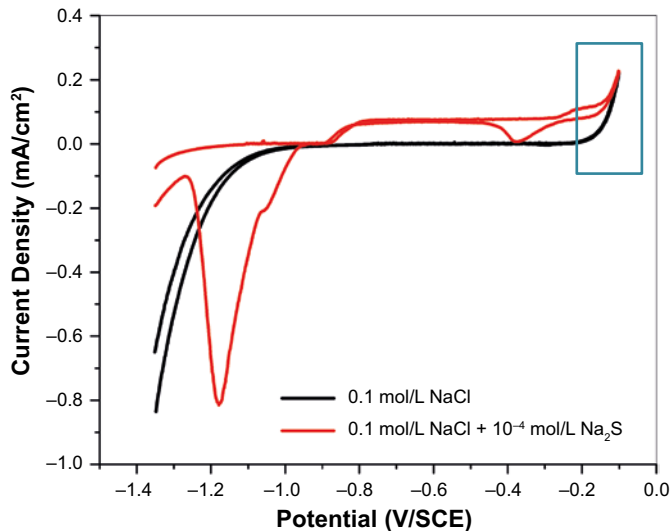
Figure 5-11. *Cyclic voltammograms in 0.1 mol/L chloride concentration, with and without added sulphide, using a rotating electrode (52.4 rad/s).*

In a critical review (Martino et al. 2019b), several objections to this interpretation are presented. Overall, the Huttunen-Saarivirta et al. study offers no undisputed evidence regarding the presence of a passive Cu_2S film, with the main arguments being:

- The authors misinterpreted both electrochemical and surface analysis data, ignoring the abundance of literature that concludes that Cu_2S films grown under similar conditions are in fact porous in nature.

- The cation vacancy concentration at the interface between the barrier layer and the outer layer, calculated from the fitting of EIS data to the PDM, is presented to be of the order of 10^4 mol/cm^2, which is more than 10 orders of magnitude more than e.g. the surface concentration of copper atoms on a pure copper surface (typically 10^{-8} mol/cm^2). Using these vacancy concentration values to express the Cu vacancy flux supporting film growth and dissolution leads to a non-physical output from further calculations.

- The majority of the argument regarding the barrier layer is based on the analysis of EIS data together with the application of the PDM, a combination which presupposes a passive surface.

5.3.5 Conclusions on film formation and passivity

The results from natural corrosion and polarization experiments show that the formation of a passive, and thus protecting film, requires a high interfacial concentration of sulphide at the film/electrolyte interface, where the film formation takes place. In turn, the interfacial sulphide concentration depends on the relative rates of supply by transport and consumption by film formation.

For a stagnant solution and natural corrosion conditions, a compact and protective film has only been observed at sulphide concentrations $\geq 1 \times 10^{-4}$ M, when the sulphide flux causes the film formation rate to become controlled by the interfacial reaction rate. At lower sulphide concentrations, the film growth is controlled by the transport of sulphide in solution (and in the pores of the film), resulting in a porous and non-protective film.

There is no unequivocal evidence for the formation of a passive film under natural corrosion conditions. The arguments for passivation by sulphide films from experiments under potential control are questionable as the interpreted breakdown potential is the same as the onset potential for chloride assisted general corrosion. Furthermore, interpretations of experimental data with the Point Defect Model are biased because of the inherent assumption of passivity in the model.

5.4 Localised corrosion under copper sulphide films

5.4.1 Methods to study localised corrosion

In addition to the studies of corrosion films in Section 5.3, a number of studies initiated by SKB have been devoted to the direct study of the topography and roughness of the copper surface beneath the copper sulphide film formed during corrosion. While the studies reviewed in Section 5.3 were aimed at improving the understanding of the conditions necessary for passivation, the studies reviewed in this section are focused on evidence of localised corrosion, i.e. alterations in the copper surface topography or roughness, for a range of exposure conditions. Reference to a few other relevant studies, not initiated by SKB, will also be made.

A general challenge when examining corroded specimens for localised corrosion is to achieve a sufficient information depth, without affecting the surface topography too much. Cross sections of the corroded surface can be analysed with metallographic techniques without removing the corrosion film, and this approach can give very detailed information of the surface topography locally. However, to achieve a globally representative description of the surface requires extensive sampling and analysis of cross sections. On the other hand, removing the corrosion film chemically allows microscopic examination of larger surface areas, albeit with the risk of affecting or disturbing the copper surface topography during film removal. For both approaches, it is essential to either characterise the surface prior to exposure to the corroding environment or, alternatively, to use representative reference specimens.

5.4.2 Corrosion morphology of copper in sulphide solutions

Chen and co-workers at the University of Western Ontario, Canada, exposed Cu-OFP to anoxic sulphide solutions in the concentration range 5×10^{-5} to 10^{-3} mol/L and examined the copper surfaces for localised corrosion damage (Chen J et al. 2019). The exposures lasted for several months and resulted in Cu_2S films of up to ca 1 μm average thickness, depending on the exposure conditions. Prior to exposure, the copper specimens were polished to a mirror finish, resulting in a planar surface with very low initial roughness.

At low sulphide concentrations, examination of cross sections prepared by focused ion beam (FIB) milling revealed a porous Cu_2S film and only general corrosion (Figure 5-2), while at a sufficiently high concentration ($[HS^-] > 5 \times 10^{-4}$ mol/L) a compact film is formed (Figure 5-3). In agreement with electrochemical studies, there were no indications of the formation of a passive barrier layer, and there were no signs of localised corrosion in the FIB-cut cross-sections for sulphide concentrations ranging from 5×10^{-5} to 10^{-3} mol/L.

In order to examine the whole surface and to verify the conclusions drawn from the examination of cross sections, two chemical procedures were developed using either NH_4OH or HCl to remove Cu_2S corrosion product deposits from the corroded copper surfaces without causing significant local corrosion damage. Exposure of uncorroded copper specimens using these two methods for film removal showed a surface morphology with low roughness and very shallow pits or surface defects, < 0.4 μm (Chen J et al. 2018). These experiments were, thus, very sensitive even to the most minor initiation of localised corrosion and changes of the surface topography. An important conclusion from this work was that, while several of the methods tried were efficient enough to remove the copper sulphide film, they also caused some localised corrosion of the underlying copper surface (Chen J et al. 2019).

Examination of corroded copper surfaces by profilometry after film removal confirmed the observations of the FIB-cut cross sections for low sulphide concentrations, i.e. only rough uniform corrosion occurred when the sulphide concentration was 5×10^{-5} mol/L or lower. However, pits or localised corrosion features were observed for sulphide concentrations of 5×10^{-4} mol/L or above (Chen J et al. 2019). These localised corrosion features have been interpreted as arising from micro-galvanic corrosion (Chen J et al. 2017b).

The occurrence of micro-galvanic corrosion, measured as the number of locally corroded sites per unit area, and the maximum depth of penetration, depended on the sulphide concentration, the duration of exposure, and the concentration of chloride (Table 5-1). Longer immersion time and higher chloride concentration resulted in an increase in the maximum depth, although the maximum depth was similar

for sulphide concentrations of 5×10^{-4} and 10^{-3} mol/L. As seen in Table 5-1 the relation between average corrosion depth and maximum pit depth varies for the different exposure conditions. The average corrosion depth is calculated with film thickness data from Figure 5-7 (Chen J et al. 2017b) and King et al. (2014), using a Cu_2S density of 5.6 g/cm^3, a molar mass of 159.14 g/mol, and assuming a compact crystalline film. The deepest relative penetration occurred for 5×10^{-4} mol/L sulphide and 0.1 mol/L chloride, for which the deepest pit was nearly twenty times deeper than the average corrosion depth after both 597 and 1 691 hours exposure. This relation was smaller for 10^{-3} mol/L sulphide, but it should be noted that the standard deviation of the film thickness measured for 10^{-3} mol/L sulphide is rather high (Figure 5-7), reflecting the uneven nature of the corrosion film, while the thickness of the film formed at 5×10^{-4} mol/L sulphide is more even.

Based on the proposed mechanism of micro-galvanic corrosion (Figure 5-1), the transport of sulphide into the pit (for the anodic reaction) and of Cu^+ out of the pit (for the deposition of solid Cu_2S) will eventually make the process self-limiting as the transport resistance increases with increasing pit depth (see further Section 6.3 and Bhaskaran et al. 2013).

Table 5-1. General and localised corrosion of copper surfaces exposed to sulphide solutions. The film thickness is taken from Figure 5-7 and King et al. (2014), while pit depths are taken from Chen J et al. (2019).

[HS⁻]	[Cl⁻]	Time	Average Cu₂S film	Average corr. depth	Max pit depth	Max pit/average corr. depth
(mol/L)	(mol/L)	(days)	(µm)	(µm)	(µm)	
5×10^{-4}	0	1691	1.3	0.65	0.8	1.2
5×10^{-4}	0.1	597	0.38	0.19	3.7	19.5
5×10^{-4}	0.1	1691	0.71	0.35	6	16.9
10^{-3}	0.1	1691	1.72	0.86	6.5	7.5

5.4.3 Corrosion morphology of copper exposed to H₂S(g) under humid and heated conditions

In order to simulate unsaturated conditions that exist before the bentonite clay is completely water saturated, Cu-OFP coupons were exposed to $H_2S(g)$ at 75 % RH (relative humidity) and 85 °C in a study reported in Gordon et al. (2018). The gas-phase concentration of $H_2S(g)$ was either 10 ppm or 1 % (per volume) with a total pressure of around 1 atm (balance N_2), and the duration of the exposures was either 10 or 30 days. Much effort was made to control the humidity and $H_2S(g)$ concentrations in the experimental set-up, and the gas-phase conditions were stable during the exposures (Gordon et al. 2018). The copper coupons were polished, albeit not to a mirror finish as in the study by Chen J et al. (2019) discussed above, meaning that surface defects of up to 20 µm (a few even deeper) were present in the coupon surfaces from the start.

After the exposure, the corroded copper coupons were cross-sectioned and examined with SEM-EDS. As expected, the Cu_2S film thickness increased with both sulphide concentration and duration of the exposure. The copper surface beneath the Cu_2S film appeared rough, but none of the cross sections inspected revealed any surface defects deeper than the average corrosion film thickness or corrosion depth (Gordon et al. 2018). In the longest exposure with the highest concentration, i.e. 1 % $H_2S(g)$ for 30 days, the average film thickness was ca 5 µm but the surface defects observed were around 1 µm or less (Figure 5-12). In the exposure with 10 ppm $H_2S(g)$ for 30 days, the average film thickness was ca 0.7 µm and the surface defects seen in the cross-section were of the same depth (Figure 3-17 in Gordon et al. 2018). The surface beneath the film was rough, however, no distinct deep defects or pits were seen. As discussed in Section 5.4.2, cross-sections of this type cannot be taken as representative of the entire surface, and obviously none of the initially present up to 20 µm deep surface defects were encountered in the cross-sections. In order to verify the conclusions drawn from inspection of cross-sectioned specimens, examination of the whole surface should be done after gentle removal of the Cu_2S film. An attempt to remove the Cu_2S film (with sequential alkaline and acidic solutions) was made but failed since it was found that the chemical method used to remove the Cu_2S film caused localised corrosion of the underlying copper surface to such an extent that examination of corrosion damage caused by the $H_2S(g)$ exposure became meaningless (Gordon et al. 2018).
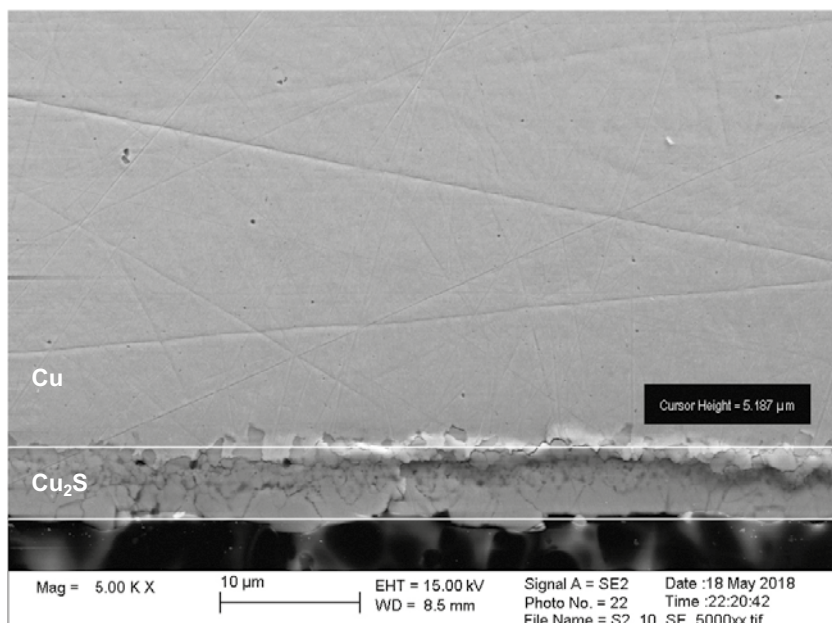
Figure 5-12. Cross-section of the copper sulphide film formed after 30 days exposure to 1 % H₂S(g) at 75 % RH and 85°C. The copper surface beneath the Cu₂S film has a rough appearance (Gordon et al. 2018).

5.4.4 Corrosion morphology of copper beneath an SRB biofilm

In the safety assessment SR-Site, the possibility that some of the 6 000 canister positions will experience groundwater with concentrations of cations low enough to cause partial erosion of the bentonite buffer could not be excluded. For the deposition holes exposed to the highest groundwater flows, this could lead to the development of advective conditions at the canister surface after 10^5 years or more after closure of the repository (see Table 2-4 and SKB 2011). The influx of sulphide to the canister would then no longer be limited by the diffusion resistance of the buffer but become controlled by the groundwater flow rate at the deposition hole and the groundwater concentration of sulphide. Also, the high swelling pressure of the buffer suppresses microbial activity in the vicinity of the canister and prevents the formation of a biofilm at the canister surface; a function that could be lost in the case of buffer erosion. While the possibility and effect of accelerated abiotic sulphide corrosion in the case of eroded buffer was assessed in SR-Site, the possibility and consequences of the formation of a biofilm directly on the canister surface was not explicitly included.

In order to mimic the situation in which the canister surface is exposed directly to advective groundwater, Cu-OFP coupons were immersed in glass vials in media supporting the metabolic activity of sulphate reducing bacteria (SRB). Two different media were used, a minimal medium representing repository conditions with low levels of sulphate (4×10^{-3} mol/L) and organic carbon (0.1×10^{-3} mol/L lactate), and a rich medium representing more SRB supportive conditions with higher levels of sulphate (20×10^{-3} mol/L) and organic carbon (47×10^{-3} mol/L lactate), as well as added yeast (1 g/L). Copper coupons were immersed together with pre-grown SRB in both media, for periods of both 10 and 32 days. Reference experiments were also performed in which copper coupons were immersed in the same media without SRB, and an abiotic control experiment was performed in which the copper coupons were exposed to the same media, without SRB, but with 3×10^{-3} mol/L added sulphide. Further details of these experiments can be found in Gordon et al. (2018).

In the vials with SRB in a rich medium and in the abiotic control experiment with added sulphide, corrosion became visible within a few days of immersion with a black deposit appearing over the copper coupons (Figure 5-13). At the end of the exposure, coupons immersed in rich media and in the abiotic control experiment were more or less covered by a black deposit. Immediately after terminating the exposures, the surface of one copper coupon from each exposure condition was examined with optical microscopy and a staining technique using acridine orange, which allows evaluation of cell activity and cell growth rate. It was found that only a few inactive cells were attached to the copper surfaces exposed in minimal medium, while a large number of cells had colonized the copper surfaces exposed to the rich medium. This result was interpreted as the formation of a biofilm on the copper surfaces exposed in rich media. The sulphide concentrations in the solution measured at the end of

the exposure were 12×10^{-3} to 16×10^{-3} mol/L in the vials with rich media and around 0.2×10^{-3} mol/L in the minimal media (Johansson L 2019, Stahlén 2019). Three copper coupons from each exposure condition were used for evaluation of mass loss and average corrosion depth. It was found that the corrosion depth increased with the richness of the cultivation media and with duration, as expected. While the corrosion was not measurable in the ten days exposure to minimal conditions and just about measurable in the 30 days exposure, the mass-loss corresponded to ca 0.1 μm after ten days exposure to rich medium and 0.2 μm after 32 days exposure (see Table 3-2 in Gordon et al. 2018).

One coupon from each exposure was cross-sectioned and examined with SEM. Generally, the surface beneath the Cu_2S film appeared smooth, although some variation in the topography could be observed (Figure 5-14).
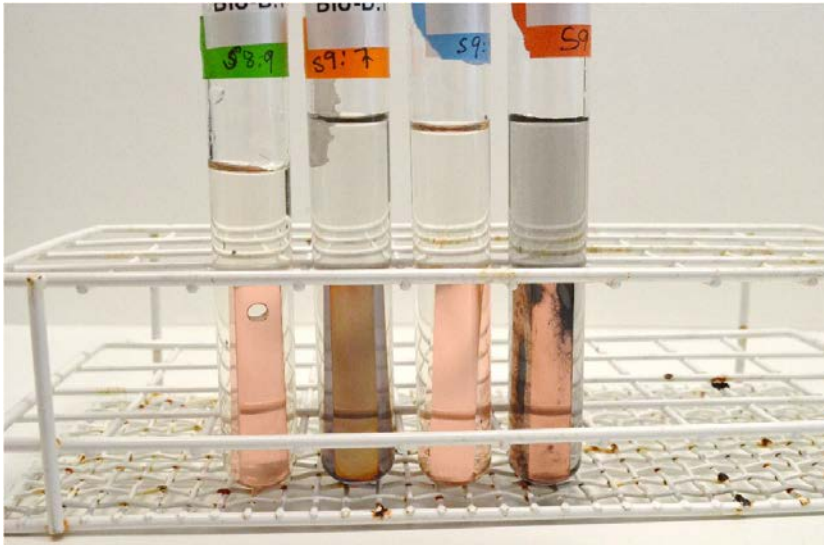
Figure 5-13. *Copper coupons after five days of immersion. From the left: minimal medium with SRB, rich medium with SRB, minimal medium without SRB, and rich medium without SRB but with 3×10^{-3} mol/L added sulphide (Johansson L 2019).*
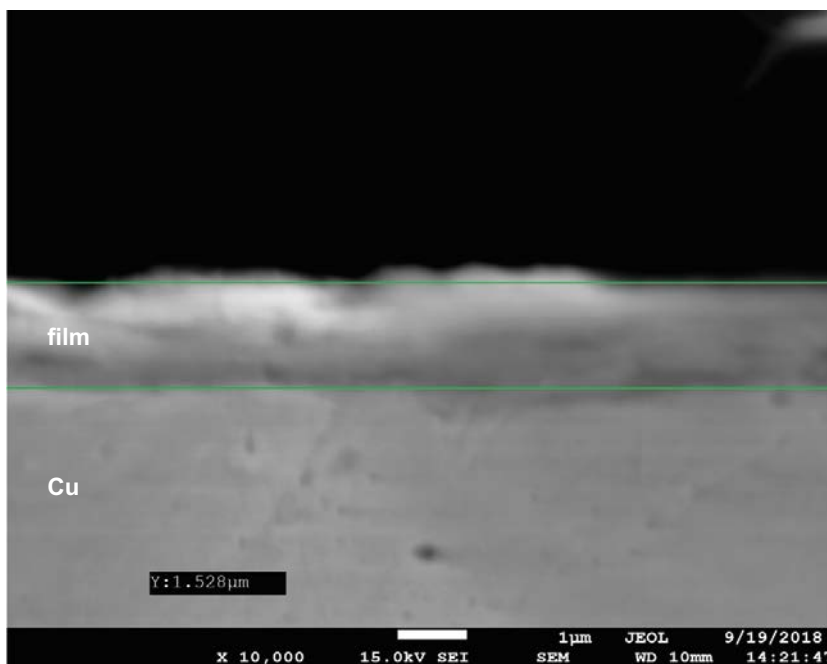
Figure 5-14. *Cross-section of a copper coupon exposed to SRB in rich medium for 32 days (Gordon et al. 2018). (The photo is out of focus, but is used for looking at the topography of the Cu-Cu_2S interface.)*

After removal of the Cu₂S films the surfaces were examined with optical microscopy in order to count and measure any pits formed during the exposures. The copper coupons were polished before starting the experiment, but not to the same depth and degree of fineness as in the study by Chen J et al. (2019) described in Section 5.4.2, meaning that surface defects of tens of μm were present over the coupon surfaces from the start of the experiment. As a consequence, only a statistical evaluation of the surface topography can be made. During microscopic examination of the surfaces, all surface defects deeper than 5 μm were counted in order to estimate a defect density. The five deepest defect found on each side of each coupon were measured and documented by photography.

The observations revealed surface defects that could be categorised into one of two types: 1) deep defects occurring on all samples, with no significant difference in frequency or depth when compared to defects present on the unexposed reference samples, and 2) a higher density of shallow surface defects for some exposures interpreted as signs of localised corrosion:

- Comparison of the deepest surface defects found on the coupons from the different SRB exposures showed that there were no statistically significant differences between the coupons that had been exposed in minimal medium for 10 days and the coupons exposed in rich medium for 32 days. This comparison is where the most pronounced difference would have been expected if there was any effect of the SRB exposure on the deepest defects or if the exposures would have caused localised corrosion damage of the order of tens of μm. Similarly, there was no significant difference between the abiotic control experiment with 3×10^{-3} mol/L sulphide and the SRB exposures with rich medium, which had developed 12×10^{-3} to 16×10^{-3} mol/L sulphide at the end. These results show that the deepest pits and defects found on the surfaces are not affected by, or even related to, the corrosion occurring during the SRB exposure. Instead, the presence of deep pits and defects indicate that the surfaces of the copper coupons had a topography at the 10 μm-scale from the start, which is confirmed by the presence of equally deep surface defects on the reference coupons. This surface finish resembles the roughness and topography of the machined copper canister after production (Taxén et al. 2012, Taxén 2013, Högberg et al. 2017). Inspection of the photographs of the deepest pits, confirms that most of them result from different types of mechanical damage and wear of the surface. Some of the deepest defects appear to be due to grain fallout from the surface. This is further discussed in Gordon et al. (2018).

- Two observations were made that could be interpreted as signs of localised corrosion. First, the abiotic control experiment with 3×10^{-3} mol/L sulphide had a pit density that was two orders of magnitude higher than any other coupon, including the reference coupons. A similar, but less-pronounced increase in the pit density was observed for one of the coupons exposed to rich medium for 32 days, but not the other. An example of pits found on the coupons immersed in rich medium with SRB is shown in Figure 5-15. Since the abiotic control experiment had 3×10^{-3} mol/L sulphide from the start, and since the rich medium had developed 12×10^{-3} mol/L sulphide by the end of the 32-day exposure, both observations are compatible with the localised corrosion damage reported in Chen J et al. (2019), and interpreted there as due to micro-galvanic corrosion.
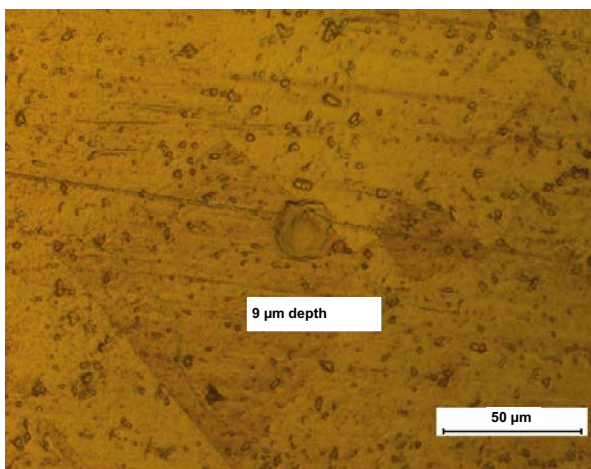
Figure 5-15. *The central circular feature is a pit found on one of the coupons immersed in rich medium with SRB for 32 days, which could possibly be attributed to corrosion. Marks from polishing and smaller pits and surface defects are also visible on the surface (Gordon et al. 2018).*

Two other studies of copper exposed to SRB in media containing high levels of lactate and yeast have indicated localised as well as general corrosion, albeit with unrealistic levels of nutrients for the Forsmark deep groundwater.

In a study by Chen S et al. (2014), localized corrosion was reported on copper under an SRB biofilm in rich medium with sulphate (4×10^{-3} mol/L), lactate (47×10^{-3} mol/L) and yeast (1g/L), although without any evaluation of mass-loss and the extent of general corrosion. This means it is not possible to compare the relative importance of general and localised corrosion. The pits observed on the corroded specimens were up to a few μm wide (depths were not measured) after two weeks of exposure in a rich medium which developed ca 2.6×10^{-3} mol/L sulphide.

Another study of copper corrosion under an SRB biofilm in nutritious solutions revealed localised as well as general corrosion (Dou et al. 2018). The corrosion exposures were made for ten days with various amounts of nutrients. In the most-aggressive exposures, the amount of organics was similar to that used in Chen S et al. (2014). However, here both lactate and citrate were added. It was found that the deepest pits were of similar depth as the average corrosion depth calculated from mass-loss, giving a pitting factor close to two. For example, for copper exposed to the most-aggressive conditions for ten days, i.e. those samples with the highest levels of organic nutrients, the average corrosion depth determined by mass-loss was ca 45 μm, while the deepest pit found was 44 μm deep. It may be noted that the appearance of the pits, as shown for example in Figure 4 in Dou et al. (2018), has some resemblance to the deepest pit in Figure 5-15.

Even though the corrosion morphologies observed in Chen S et al. (2014) and Dou et al. (2018) were attributed to SRB and biofilm formation, it is worth noting that in both experiments the sulphide concentrations evolved to concentrations near or above those at which abiotic localised corrosion in the form of micro-galvanic corrosion has been reported (Chen J et al. 2017b).

5.4.5 Summary of observations during exposures

The corrosion morphology of copper was studied in three different types of sulphide environment: 1) aqueous sulphide solutions at room temperature, 2) humid hydrogen sulphide gas at elevated temperature, and 3) nutritious growth media containing sulphate reducing bacteria. The corroded copper coupons were studied by SEM examination of surface cross-sections with the copper sulphide film still present at the copper surface, as well as with optical microscopy of the entire copper surface after removal of the copper sulphide film. A summary of the exposure conditions and the results is given in Table 5-2, with the following observations:

- In aqueous sulphide solutions, only general corrosion was observed when the sulphide bulk concentration was 5×10^{-5} mol/L. Locally damaged areas, interpreted as micro-galvanic corrosion, were observed in solutions with bulk sulphide concentrations of 5×10^{-4} mol/L or higher. High chloride concentrations were found to enhance the degree of localised corrosion. These conclusions are supported by inspection of surface cross-sections as well as of the whole surface after removal of the copper sulphide film.

- On copper coupons exposed to humid heated hydrogen sulphide gas there were no signs of localised corrosion. However, the information is limited since only cross-sections could be examined. In order to confirm these results, more careful examination of the copper surface after removal of the copper sulphide film is required.

- Examination of copper coupons after exposure to sulphate reducing bacteria indicated that localised corrosion had occurred on the copper coupons immersed in rich media. This finding is in agreement with two other studies of copper in rich SRB media, in which the authors attributed the observed corrosion to SRB metabolism and the formation of a biofilm on the copper surface. However, since the concentrations of sulphide in these experiments were similar to or much higher than what has been found to cause micro-galvanic corrosion, the possibility of abiotic localised corrosion cannot be disregarded (see the first bullet). In growth media with SRB and nutrients more representative of repository conditions, neither the formation of a biofilm nor localised corrosion has ever been reported.

Table 5-2. Summary of results from studies of localised corrosion of copper in sulphide environments.

Study	General conditions	$[SO_4^{2-}]$ (mol/L)	[lactate] (mol/L)	Sulphide exposure*	Temp. **	Duration	Corrosion morphology
Chen J et al. 2017b, Chen J et al. 2019	Aq.	–	–	5×10^{-5}	RT	Several months	Rough uniform
	Aq.	–	–	5×10^{-4}	RT	Several months	Micro-galvanic
	Aq.	–	–	10^{-3}	RT	Several months	Micro-galvanic
Gordon et al. 2018	Gas	–	–	10 ppm H_2S(g)	85 °C	10 days	Uniform
	Gas	–	–	1 % H_2S(g)	85 °C	10 days	Uniform
	Gas	–	–	10 ppm H_2S(g)	85 °C	30 days	Uniform
	Gas	–	–	1 % H_2S(g)	85 °C	30 days	Rough uniform
	SRB in aq. medium	4×10^{-3}	10^{-4}	–	RT	10 days	Uniform
	SRB in aq. medium	4×10^{-3}	10^{-4}	–	RT	10 days	Uniform
	SRB in aq. medium	2×10^{-2}	4.7×10^{-2}	1.5×10^{-2}	RT	32 days	Uniform
	SRB in aq. medium	2×10^{-2}	4.7×10^{-2}	1.2×10^{-2}	RT	32 days	Possibly localised
	Aq. medium	2×10^{-2}	4.7×10^{-2}	3×10^{-3}	RT	32 days	Possibly localised
Chen S et al. 2014	SRB in aq. medium	2×10^{-2}	4.7×10^{-2}	2.6×10^{-3}	RT	14 days	Localised
Dou et al. 2018	SRB in aq. medium	2×10^{-2}	Up to 5×10^{-2}	2×10^{-4}–3.6×10^{-3}	RT	10 days	Uniform and localised

* In units of mol/L HS^- unless otherwise noted. Concentration in gas phase given as ppm or % per volume.
** RT = room temperature.

5.5 Application to repository conditions

In the following sections, the rate of transport of sulphide to the canister surface and how this might impact the corrosion behaviour is discussed for different environmental conditions that might occur during the evolution of the repository. These conditions are then compared to the conditions under which localised corrosion has, and has not, been observed.

5.5.1 Mass transport limitation and sulphide flux thresholds

As discussed in Sections 5.3 and 5.4 above, as well as in Section 6.4 below, it is the flux of sulphide to the surface/solution interface that determines the properties of the sulphide film that forms on copper in anoxic sulphide environments. These properties include the protectiveness of the film, its morphology and electrochemical properties, as well as the topography of the corroded copper surface. From the experiments in which copper has been exposed to sulphide solutions it is possible to compile the lowest fluxes at which different types of films are formed and different types of localised corrosion are observed. These threshold fluxes can then be compared with the fluxes that could exist in the repository. Such a comparison was made in King et al. (2017), and an extended comparison, including the unsaturated phase, is made in this section. The comparisons are illustrated in Figure 5-16.

As described in Section 5.3 the formation of a compact film indicates that the corrosion is not limited by the mass transport of sulphide, while a porous film displaying linear growth (constant rate) is consistent with sulphide mass transport control. In Figure 5-7, the linear growth of the porous film in a solution with [HS]= of 5×10^{-5} M is equivalent to a sulphide flux of 3×10^{-10} mol/(m^2 s) (assuming a Cu_2S density of 5.6 g/cm^3, molar mass of 159.14 g/mol, and a film porosity of 0.5). This is one way of determining a threshold flux for sulphide transport control of the corrosion reaction and is indicated by the green square in Figure 5-16. As described in King et al. (2017), the threshold flux can also be determined from a sulphide depletion experiment, which gives a flux of 2×10^{-8} mol/(m^2 s). This is illustrated by the green line in Figure 5-16.
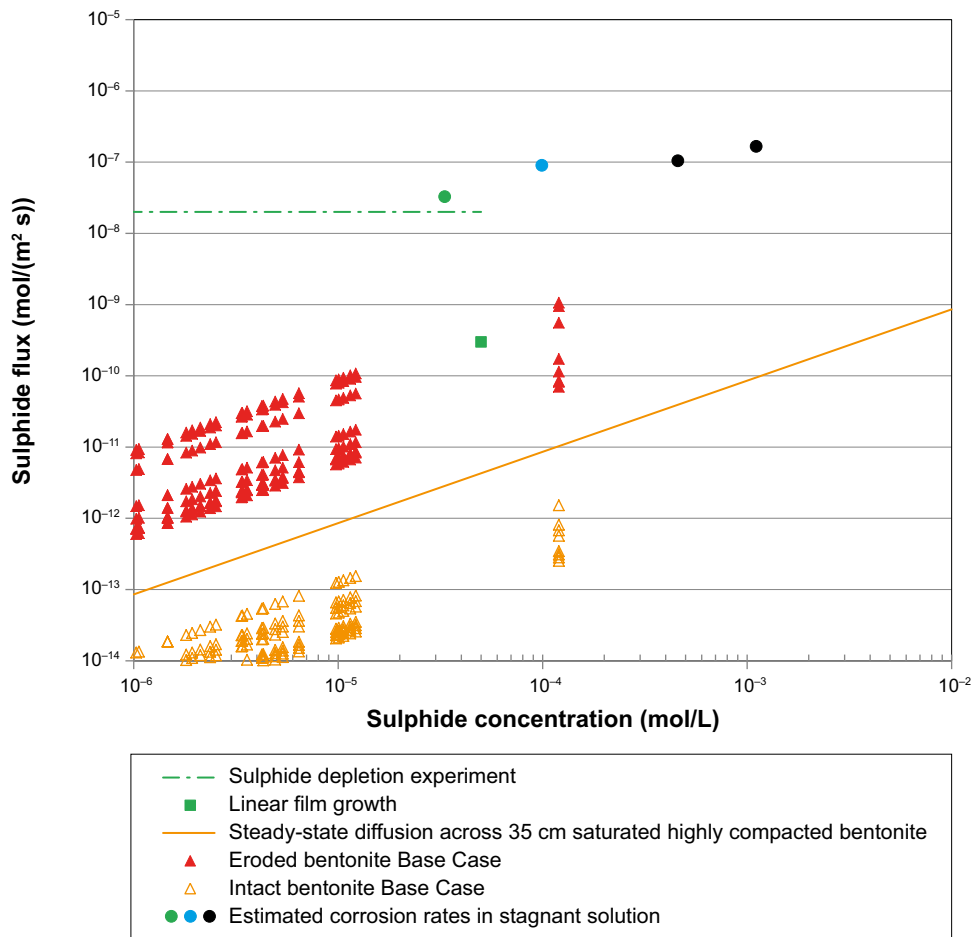
Figure 5-16. *Comparison of the flux of sulphide to the canister in the repository (orange and red) with the estimated threshold flux for sulphide-transport control (green) of the overall corrosion reaction. Repository fluxes for intact and eroded bentonite are taken from the Base Case analyses performed for SR-Site. Only the 8 deposition positions with the highest fluxes out of the 6 000 are shown. The sulphide flux corresponding to the estimated corrosion rates for experiments in stagnant bulk solution are also shown (circles: green – transport control, blue – mixed control, black – kinetic control).*

In King et al. (2017), the nature of the rate-controlling steps for the reaction of copper in sulphide solutions is discussed in detail. In stagnant solution the rate-controlling step for the anodic reaction under freely corroding conditions depends on the sulphide concentration. At low sulphide concentration the overall corrosion reaction becomes limited by the rate of supply of sulphide, most likely because the anodic reaction becomes transport limited. With increasing sulphide concentration, the reaction gradually changes to joint kinetic-transport control at intermediate concentrations to complete kinetic control of the anodic reaction at approximately 5×10^{-4} mol/L sulphide. In King et al. (2017) the sulphide flux (from estimated corrosion rates) for a set of measurements of corrosion potential was calculated, and is given in Figure 5-16 as dots: green – mass transport control, blue – mixed control, black – kinetic control.

However, transport control of the anodic reaction can be readily established at high groundwater sulphide concentrations if the rate of mass transport (sulphide flux) at the canister surface is externally restricted by e.g. diffusion through a bentonite buffer, see further Section 5.5.2.

Pitting corrosion requires the formation of a passive film on the copper surface. As described in Section 5.3, a truly passive film has never been confirmed on copper in stagnant sulphide solutions. Instead, it is generally observed that copper sulphide corrosion films are rather porous and non-protective. Compact films have been observed for sulphide concentrations of 5×10^{-4} mol/L or higher, but passive films have only been observed using rotating electrodes (≥ 50 rad/s) to increase the flux and for sulphide concentrations $\geq 10^{-3}$ mol/L. On the other hand, localised corrosion has been reported in the scientific literature (Chen J et al. 2017b, 2019, Dou et al. 2018, Chen S et al. 2014), albeit under conditions that are rather extreme compared with realistic repository conditions.

5.5.2   Saturated compact clay system

When the bentonite buffer is fully saturated it has a density of $2\,000$ kg/m³, a high swelling pressure of around 15 MPa, and a very low water activity. This is an environment that effectively suppresses microbial activity in the clay, see further Section 2.3.2, meaning that the sulphide concentration at the canister/clay interface is determined by the sulphide concentration in the groundwater, the transport of the sulphide ions from the groundwater into and through the dense clay, and the rate of sulphide consumption by corrosion of the copper surface. Here it is pessimistically assumed there are no other sinks for sulphide, such as e.g. the precipitation of iron sulphide. The sulphide flux at the canister surface by steady-state diffusion through a 35 cm bentonite buffer (with $D_{eff} = 3 \times 10^{-11}$ m²/s) is illustrated by the orange line in Figure 5-16. In SR-Site, the hydraulic conditions in the rock were also considered (SKB 2010a), using the distribution of measured sulphide concentrations at Forsmark and the groundwater flow from the hydro-modelling. In Figure 5-16 the open orange triangles represent the sulphide fluxes of the 8 deposition holes with the highest groundwater flow (out of the $6\,000$ deposition positions) and the sulphide concentrations in the range covered in the diagrams. The highest sulphide flux is thus 1.5×10^{-12} mol/(m² s) corresponding to the highest sulphide concentration observed at Forsmark.

Thus, there is a difference of 2 to 4 orders of magnitude between the highest sulphide flux at Forsmark and the threshold flux for transport control (derived from film growth rates and the depletion experiment, respectively) and for the formation of compact films. Since a compact film is a prerequisite for the formation of a passive film, it is concluded that passivity and pitting corrosion of copper in sulphide solutions relevant to the repository has no support in the scientific literature.

The lowest sulphide concentration for which localised corrosion has actually been observed under naturally corroding conditions (5×10^{-4} mol/L, Chen J et al. 2017b) is higher than the maximum value observed in the groundwater at Forsmark. More importantly, the flux of sulphide at the bare copper surface in these experiments (5×10^{-7} mol/(m² s) assuming a diffusion layer of 1 mm) is 4 orders of magnitude higher than what could be established at the copper/bentonite interface with an intact buffer, so that the sulphide concentration at the canister surface will be close to zero.

5.5.3   Unsaturated clay system

The dryness of the Forsmark site, resulting from relatively few water-bearing fractures and low advective flow of groundwater, is in principle an inherent limitation for corrosion. In order for a galvanic cell to establish, water must be present and serve as an electrolyte, but liquid water also transports corrosive agents like sulphide to the canister surface. During the very earliest period of the unsaturated phase the temperature on the outer canister surface rises to ca 95 °C (see Figure 2-2), meaning that there might be a period when the canister surface is so dry that electrochemical corrosion is not supported. However, when the temperature falls, a liquid film will form on the canister surface due to humidity and condensation. Since full saturation of the bentonite clay may take hundreds or even thousands of years in the driest deposition holes, there will be a period during which hydrogen sulphide gas (H_2S) could be transported through the clay system. This sulphide gas will dissolve in the water film at the canister surface and the flux of sulphide at the canister surface is then controlled by the transport of gaseous sulphide through the unsaturated clay system. Since there is no evidence for the generation of H_2S from microbial processes in experiments with unsaturated bentonite (Section 2.4.3), the only source of sulphide during the unsaturated phase will be the transport of H_2S from the groundwater.

As was discussed in Section 5.3, the highest flux of $H_2S(g)$ that could possibly be established in the unsaturated repository environment is of the order of 7×10^{-11} mol/(m² s). This is about a factor of 50 higher than the flux for the case of the diffusion of dissolved HS^- through intact buffer (1.5×10^{-12} mol/(m² s)), but still about 2 orders of magnitude lower than the threshold flux for corrosion limited by mass transport. This means the interfacial concentration will be close to zero, and the concentration for which micro-galvanic corrosion has been observed cannot be maintained. It can be concluded that even for the highest sulphide concentration and the highest groundwater flow that could appear at Forsmark, there is a considerable margin to conditions supporting localised corrosion due to micro-galvanic coupling as long as the bentonite clay is in place.

Some initial corrosion due to the entrapped oxygen is expected in the repository, but as noted in Section 2.3.1, with reference to further details in Section 8.6.2, the copper oxides will be transformed to copper sulphides when sulphide exposure commences.

5.5.4 Eroded buffer case

As was concluded in SR-Site, the bentonite buffer may erode when contacted by groundwater with low cation concentration. On a timescale of tens of thousands to hundreds of thousands of years, this may lead to loss of a sufficient amount of buffer to cause advective conditions in the most exposed deposition holes, leaving the copper surface directly exposed to the groundwater. This situation has two consequences for the sulphide corrosion process. First, without the bentonite clay, the flux of sulphide at the canister surface is controlled directly by the groundwater flow rate and the sulphide concentration. Second, without the bentonite there is in principle nothing that prevents a biofilm containing SRB to become established on the copper surface. The formation of an active biofilm has, however, never been reported for experiments as scarce in nutrients as deep groundwater.

The sulphide flux in the eroded buffer case was evaluated in King et al. (2017). In Figure 5-16, the solid red triangles represent the sulphide flux at the canister surface for the 8 deposition holes with the highest groundwater flow combined with the highest sulphide concentration measured at Forsmark (in the range covered in the diagram). It is noted that the highest sulphide flux is about 10^{-9} mol/(m^2 s), which is in the same range as the threshold flux derived for porous film growth (3×10^{-10} mol/(m^2 s)), but one order of magnitude lower than the flux derived from the depletion experiment where transport control is demonstrated. Thus, the corrosion rate would be under mass transport control with porous films formed for the overwhelming majority of sulphide fluxes possible in the repository.

The lowest concentration where pits of the micro-galvanic corrosion type have been observed (5×10^{-4} mol/L) is higher than the highest observed sulphide concentration (1.2×10^{-4} mol/L) at the Forsmark site. As seen from Figure 5-16 (and Figure 2-4), the highest measured sulphide concentration is one order of magnitude higher than the next highest concentration, with the remainder of the distribution of measured sulphide concentrations below the concentration where no localised corrosion has been observed (5×10^{-5} mol/L). The pessimism in using the very highest value for the whole assessment period has been discussed in SR-Site (SKB 2011, Section 12.6.2).

Since the highest sulphide flux for the case of eroded bentonite is close to the threshold flux for transport control and because the highest groundwater concentration is close to the sulphide concentration at which evidence for localised corrosion has been observed experimentally (5×10^{-4} mol/L), some consideration of the possibility of localised corrosion for the case of eroded bentonite is warranted. The proposed mechanism for localised micro-galvanic corrosion involves the coupling of anodes and cathodes of similar surface area. Therefore, in contrast to pitting, for which a small anode-to-cathode area ratio could give very deep pits, the "pitting factor" for micro-galvanic corrosion would be expected to be small. As discussed in Section 5.4.2, the deepest pits found experimentally were ca 6 μm for both experiments in 5×10^{-4} and 10^{-3} mol/L sulphide. Furthermore, the deepest relative penetrations found were less than 20 times deeper than the average corrosion for 5×10^{-4} mol/L sulphide, independent of whether the exposure time was 597 or 1 691 hours. For the assessment of the consequences of localised corrosion (due to micro-galvanic coupling), it appears pessimistic to apply a pitting factor of 20 for canisters in those deposition holes for which buffer erosion would cause advective conditions, and where the sulphide flux exceeds 3×10^{-10} mol/(m^2 s). This approach will be used in an assessment in Chapter 9.

Metabolically active SRB biofilms on copper in laboratory studies are reported only for nutrient-rich environments, i.e. with high concentrations of sulphate and organics. Examination of copper coupons after exposure to nutrient-rich media containing sulphate reducing bacteria, has shown signs of localised corrosion in several studies (Section 5.4.4). It is important to note, however, that since the concentrations of sulphide in all of these experiments were 2×10^{-4} mol/L or higher, the possibility that the localised corrosion damage is micro-galvanic in nature, and thus abiotic (Section 5.4.2), cannot be disregarded. In minimal growth media, with pre-grown SRB and nutrient concentrations similar to those in deep groundwater, neither biofilms nor localised corrosion has ever been reported.

5.6 Conclusions

The following conclusions can be drawn concerning the risks and consequences of localised corrosion of the copper canister during the long-term sulphidic phase of the repository, based on film growth kinetics, metallographic examination of surfaces and cross-sections with SEM, as well as cyclic voltammetry:

* Compact copper sulphide films that could possibly become passive (though passivity has never been seen in stagnant solution) can only be achieved at sulphide fluxes that are at least 2 orders of magnitude higher than what could ever occur in the repository with an intact buffer irrespective of whether the bentonite clay is saturated or unsaturated. For localised corrosion of copper in the form of pits interpreted as micro-galvanic corrosion the margin is nearly as large.

* For the case of eroded buffer, the corrosion rate is limited by sulphide mass transport except for the pessimistic combination of the highest possible groundwater flow rate and the highest sulphide concentration measured at Forsmark. The sulphide fluxes are below the threshold fluxes for formation of a compact film (a prerequisite for a passive film to give pitting).

* Localised corrosion of copper due to the presence of a metabolically active biofilm of SRB on the canister surface exposed directly to the ground water seems unlikely, since neither biofilm formation nor localised corrosion in the presence of SRB have been observed under repository conditions.

6 Stress corrosion cracking due to reaction with sulphide, including the influence of the sauna effect on stress corrosion cracking

6.1 Introduction

Stress corrosion cracking (SCC) may occur when a metal is subjected to a combination of chemical and mechanical loads. In earlier safety assessments, SCC has primarily been discussed in the context of ammonia, nitrite or acetate under oxidising conditions. For SR-Site (SKB 2010e), SCC during the long-term anaerobic period was ruled out as there would be an insufficient flux of sulphide ions in the crack to support any known crack growth mechanism. In recent years, there have also been a few studies in which micro fractures observed on copper surfaces exposed to a combination of sulphide in aqueous environments and high tensile stresses have been interpreted as evidence of SCC. SKB has conducted several new studies in this field.

In the statement by the Land and Environmental Court (Section 1.1), it was suggested that stress corrosion cracking due to reaction with sulphide needed to be further addressed, in particular for unsaturated conditions. This is done in the present chapter. It was also suggested that the influence of the sauna effect on this process needs to be included. Since it was concluded in Section 3.5 that the sauna effect will be insignificant in a KBS-3 repository at Forsmark, this effect is not included in the evaluation to follow. This chapter is structured according to the following.

- Experimental studies of surface effects that could be interpreted as evidence of SCC in the presence of sulphide are discussed in Section 6.2.

- An assessment of the phenomenon is given in Section 6.3.

- Implications of these studies for repository conditions are discussed in Section 6.4.

- Conclusions are drawn in Section 6.5.

Many of the investigations of stress corrosion cracking have been performed with slow strain rate testing (SSRT), where a copper specimen is strained at a constant rate, usually until the specimen fails (ruptures). Examples of tensile specimen are shown in Figure 6-1. The gauge length is the thinner part of the specimen, and where metallographic investigations are performed, both along the specimen to search for cracks and on the fracture surface to look at rupture type (ductile or brittle).

Figure 6-1. *Examples of tensile specimens used for slow strain rate testing (SSRT), a) round specimens, before and after drawn to rupture, b) a flat rectangular specimen (Taxén et al. 2018).*

6.2 Experimental studies

6.2.1 Taniguchi and Kawasaki (2008) and Taniguchi et al. (2007, 2008)

Taniguchi and Kawasaki (2008) were the first to suggest that pure copper might be susceptible to SCC in the presence of high concentrations of sulphide. This conclusion was based on the results of SSRT using flat tensile specimens prepared from phosphorus-deoxidised (PDO) copper and exposed to artificial seawater containing between zero and 0.01 mol/L sulphide added as Na_2S. The PDO copper is a commercial grade in which phosphorus is added to remove oxygen impurities during alloy manufacture, resulting in residual P contents of a few tens of wt.ppm. At sulphide concentrations less than 0.005 mol/L, the specimens were said to be susceptible to intergranular attack, whereas SCC was said to have occurred at a concentration of 0.01 mol/L. The evidence for SCC was based on the observation of cracks along the gauge length of the specimens away from the fracture surface, although the ductility (as measured by the elongation to failure relative to that in an inert environment) and material strength (as measured by the reduction in ultimate tensile strength relative to that in the inert environment) were also reduced at the highest sulphide concentration. Metallography was performed on cross sections along the gauge length of the specimens, which confirmed intergranular attack at the lower sulphide concentration and a crack-like feature extending perpendicular to the loading direction to a depth of approximately 50 µm at the highest concentration.

The results presented by Taniguchi and Kawasaki (2008) were part of a larger study that also included SSRT experiments on the weld metal and heat-affected zone of electron-beam welded PDO copper (Taniguchi et al. 2007). In contrast to the apparent susceptibility to SCC of the base material at high sulphide concentrations, neither the weld nor the heat-affected materials exhibited a loss of ductility or strength during SSRT, although there was still some cracking at the highest sulphide concentration. Thus, at least for electron-beam welding, there did not appear to be any increase in susceptibility to cracking caused by the metallurgical changes introduced by welding.

In an extension of the original work, Taniguchi et al. (2008) also considered the effect of the grade of copper and of the electrochemical potential on the SCC of copper. Additional tests were conducted using oxygen-free copper to complement those performed earlier using PDO copper and, for both materials, the effect of anodic polarisation of up to +700 mV was also investigated. Anodic polarisation would be expected to increase the susceptibility to SCC if the cracking process involved the dissolution of the material. Based on the extent of crack formation along the gauge length, Taniguchi et al. (2008) suggested that anodic polarisation of up to 300 mV reduced the susceptibility to SCC, although it was claimed that susceptibility increased again at higher polarisation. The oxygen-free copper was found to be more susceptible than PDO copper, the latter having a chemical composition more like that of the Cu-OFP proposed for the canister. However, the conclusions drawn from the extent of cracking were inconsistent with the effect of potential on the ductility and strength of the specimens, both of which showed progressive degradation with increasing polarisation of the specimens. The decrease in strength could have been a result of increasing corrosion of the specimens with increasing polarisation, which would have reduced the load-bearing cross-sectional area of the specimens and the measured (engineering) stress. However, as pointed out by Bhaskaran et al. (2013), the corrosion rate should be transport limited by the supply of HS^- in this potential range and the corrosion rate would not be strongly dependent on the potential. In contrast to the appearance of cracks along the gauge length, the fracture surfaces exhibited some degree of plasticity and of ductile failure, even for the most susceptible conditions.

Taniguchi et al. (2008) also conducted a single experiment in the presence of compacted bentonite buffer material. The test, using PDO copper and an electrochemical potential of -420 mV$_{SCE}$, said to be equivalent to the corrosion potential of copper in the presence of compacted bentonite, was performed in a special cell that allowed continuous straining of the specimen. A sulphide concentration of 0.001 mol/L was used. Although both the ultimate tensile strength and elongation to failure were reduced compared with a blank experiment without a chemical environment, no cracking was observed. The fracture surface exhibited significant plasticity and indications of ductile failure.

Because of the fact that specimens are typically strained to failure, it is difficult to determine at what point during the test the cracks actually formed. Figure 6-2 shows a failed PDO copper specimen exposed to the highest sulphide concentration used by Taniguchi and Kawasaki (2008). The cracks exhibit a large displacement at the mouth (Figure 6-2a), almost equal to the crack depth (Figure 6-2b), which suggests that the cracks were subject to a significant degree of strain.
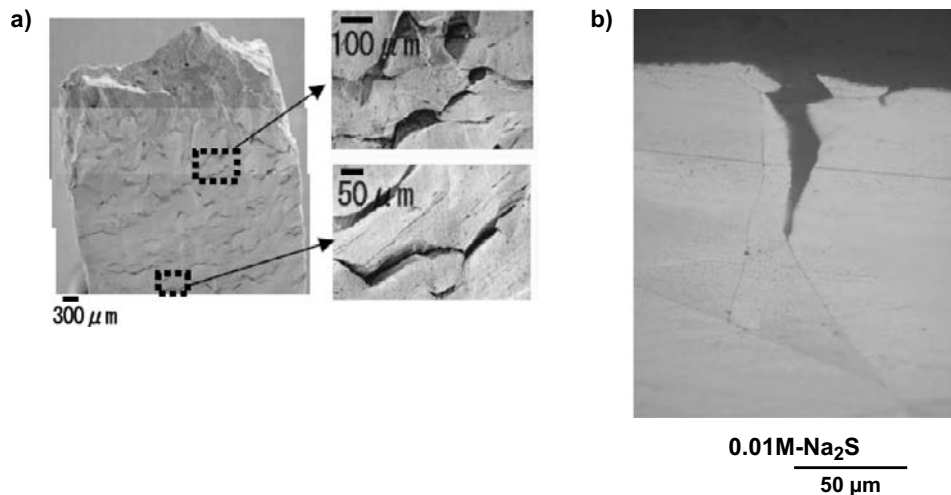
Figure 6-2. Images of cracks along the gauge length of a phosphorus deoxidised copper tensile specimen following SSRT to failure in synthetic seawater containing 0.01 mol/L sulphide; a) Scanning electron microscopic images of cracks along the gauge length (the fracture surface is at the top of the image on the left-hand side of the figure), b) optical micrograph of the cross section of a single crack (Taniguchi and Kawasaki 2008).

The cracks in Figure 6-2 are clearly intergranular in nature. Copper is known to be susceptible to intergranular corrosion (IGC) in sulphide solutions (Al Kharafi et al. 2008) and it is interesting to note that clear intergranular attack was observed on a specimen exposed to synthetic seawater containing 0.001 mol/L sulphide at a potential of -180 V_{SCE} (Figure 6-3). This potential is approximately 20 mV more positive than the potential at which Al-Kharafi et al. (2008) suggested that IGC becomes the primary mode of corrosion in 3.5 wt.% NaCl solution containing 0.001 mol/L sulphide at 25 °C. Intergranular corrosion can also occur at more negative potentials, albeit at a slower rate than at higher potentials (Al-Kharafi et al. 2008). It is possible, therefore, that the relatively shallow crack-like features reported by Taniguchi and Kawasaki (2008) and Taniguchi et al. (2007, 2008) are simply corroded grain boundaries that have been opened up by excessive strains, and not SCC.

6.2.2   Bhaskaran et al. (2013)

Bhaskaran et al. (2013) attempted to replicate the findings of Taniguchi and co-workers using Cu-OFP from manufactured canister parts from SKB, and a range of environmental conditions and mechanical loading methods. No evidence for SCC was found in any of the experiments. Neither was there evidence for significant intergranular attack. The range of test conditions employed included:

- Cu-OFP from two different sources and from different locations on the canister.
- Round tensile specimens, U-bend specimens, and flat specimens with stress-raising indentations.
- Electropolished and SiC-polished surfaces.
- Constant extension rate testing to either a limited strain (to represent what a canister might experience) or straining to failure, as well as testing under constant strain.
- Strain rates of 10^{-5}, 10^{-6}, or 10^{-7} 1/s.
- 0.1 mol/L chloride as well as synthetic seawater, both containing $0.005-0.050$ mol/L sulphide.
- pH $7-12$.
- Room temperature and 80 °C.
- Open-circuit potential and either modest cathodic or anodic polarisation (in the range ± 100 mV).
- Most test solutions were nominally deaerated by bubbling nitrogen for at least one hour, whereas others were either rigorously deaerated or not deaerated at all, in the latter case to investigate the possible effects of contamination by elemental sulphur or thiosulphate ions.
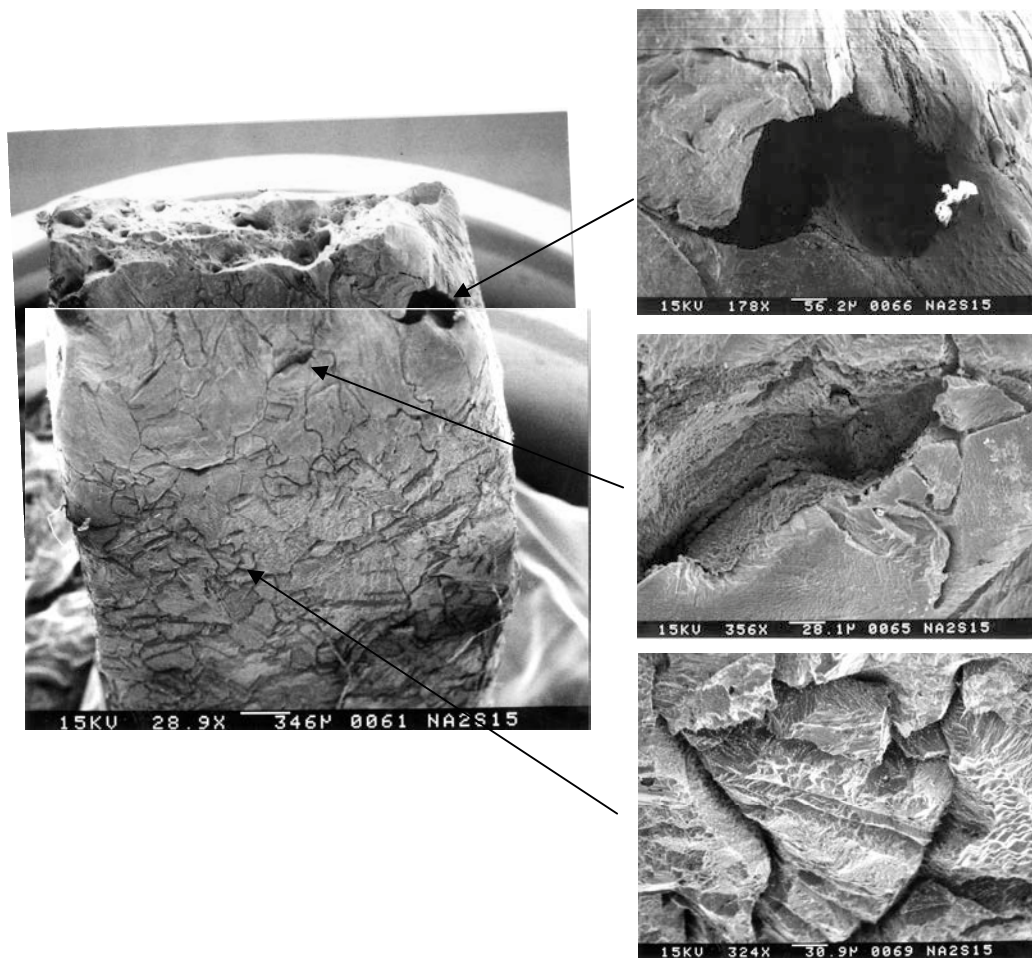
Figure 6-3. *Scanning electron microscope images of an oxygen-free copper tensile specimen strained to failure in synthetic seawater containing 0.001 mol/L sulphide at a potential of -180 mV$_{SCE}$ exhibiting evidence for intergranular corrosion (Taniguchi et al. 2008).*

Corrosion products were removed from the specimens prior to examination for SCC or IGC. Although the underlying metal surface exhibited zig-zag patterning, Bhaskaran et al. (2013) considered this to be the result of preferential corrosion of the copper at the base of zig-zag cracks in the Cu_2S film (see Figure 6-4) caused by the straining of the specimen, rather than an indication of preferential grain boundary attack. The results of electrochemical impedance spectroscopy (EIS) and polarisation scans suggested the corrosion rate was limited by "inward-diffusion" of sulphide, either through the solution or through a porous Cu_2S layer. Notwithstanding the indications of transport control of the corrosion rate, differences were also observed in the extent of film growth on different crystal planes, but only one instance of superficial attack around a grain boundary was observed.

Bhaskaran et al. (2013) were unable to explain their inability to replicate the observations of Taniguchi and Kawasaki (2008) despite studying a wide range of environmental and loading conditions. However, they did argue that SCC and any form of localised corrosion would not be expected under transport-limited conditions as the interfacial sulphide concentration will be very small, meaning that there would be no diffusive driving force for sulphide transport into a crack, pit, or crevice.

6.2.3   Arilahti et al. (2011) and Sipilä et al. (2014)

Arilahti et al. (2011) also tried to replicate the observations of Taniguchi and Kawasaki using pre-cracked specimens under constant load. This study, therefore, was focussed on crack growth rather than crack initiation. Compact tension specimens were used in an attempt to simulate the plane strain conditions that would be experienced by the canister, rather than the excessive strains of an SSRT test. Because of the ductility of the Cu-OFP the specimens were probably too small to ensure linear-elastic behaviour,
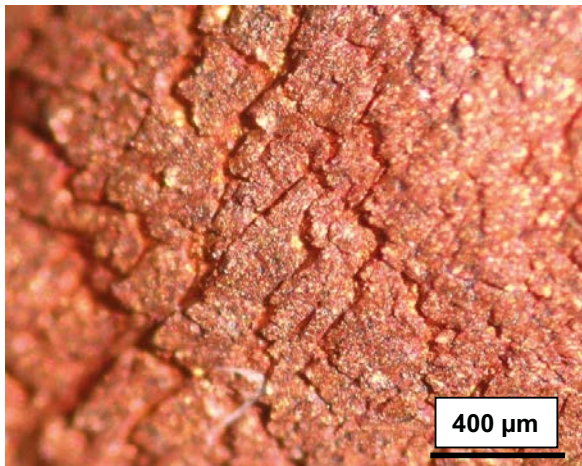
Figure 6-4. *Morphology of the exposed surface of copper SSRT specimens after removing the sulphide film formed during exposure to 0.01 mol/L HS⁻, synthetic seawater at 80 °C. The zig-zag patterns are thought to be due to enhanced corrosion at sites of film fracture. (Bhaskaran et al. 2013).*

but Arilahti et al. (2011) nevertheless estimated a crack-tip stress intensity factor of 9 MPa m$^{1/2}$. This level of stress intensity is similar to that estimated by King (2004) for a 7–8 mm deep single edge crack in a semi-infinite plate loaded at the typical yield strength of annealed Cu-OFP of 60 MPa. Arilahti et al. (2011) did not observe any crack growth over a period of 6 weeks exposure to an artificial Finnish groundwater solution containing either 100 or 200 mg/L sulphide (0.003 or 0.006 mol/L), but they did report rapid grain boundary diffusion of sulphide ahead of the tip of the fatigue pre-crack. However, these observations were later shown to be an artefact of the method used to open up the specimen ahead of the pre-crack after the test, as only small concentrations or no sulphur could be detected on the fracture surfaces (Sipilä et al. 2014).

In a continuation of this work, Sipilä et al. (2014) exposed plain and notched tensile specimens to sulphide-containing artificial bentonite pore-water solution for periods of up to 14 weeks and subjected them to SSRT or constant load tests. The aim was to determine whether exposure to sulphide would change the mechanical properties of the Cu-OFP due to the grain boundary diffusion of sulphide as previously proposed by Arilahti et al. (2011). Although some reduction of the ductility was suggested at a sulphide concentration of 200 mg/L (0.006 mol/L), the yield strength and ultimate tensile strength increased after exposure. Given the typical scatter of tensile testing results, there was no significant impact of sulphide exposure on the mechanical properties of the copper and no evidence for enhanced grain boundary diffusion as previously suggested.

6.2.4 Becker and Öijerholm (2017) and Forsström et al. (2017)

The aims of the study by Becker and Öijerholm (2017) were to identify a threshold stress and a threshold concentration for the initiation of SCC of Cu-OFP in sulphide solutions. A tapered-tensile specimen design was used to determine the threshold stress and sulphide solutions of nominally 10^{-5} to 10^{-3} mol/L were used to determine the threshold concentration. The base solution in which the tests were performed consisted of deaerated 0.1 mol/L NaCl with the pH maintained at a value of pH 7.2 through the addition of a phosphate buffer (concentration 0.01 mol/L). The specimens were strained to a maximum true strain of 9 %. The corresponding true stress (determined by the actual cross-sectional area of the specimen), as a function of distance along the tapered gauge length was estimated from a stress-strain curve on a blank specimen using FE-modelling. The position of crack-like indications was determined from cross-sections of the specimen using SEM and the corresponding stress calculated.

A total of eight crack-like features were identified from the two specimens tested at a nominal sulphide concentration of 0.001 mol/L, although there might have been additional cracks revealed if the defects not attributed to cracks had been studied in further detail. The maximum depth of these eight features was approximately 50 µm. Based on the location of these cracks along the tapered gauge length, the threshold stress for crack initiation at this sulphide concentration was estimated to be 160 MPa.

Some features were observed on the two specimens exposed to 10^{-4} mol/L sulphide, but the authors did not attribute them to SCC, since similar defects were observed also deeper inside the material where effects from the surface exposure could be excluded. The specimen exposed to 10^{-5} mol/L sulphide was not examined for cracks. On the basis of these results, Becker and Öijerholm (2017) proposed a threshold sulphide concentration for SCC of copper between 10^{-4} and 10^{-3} mol/L.

Forsström et al. (2017) measured the hydrogen content of three of the specimens tested by Becker and Öijerholm (2017), specifically one sample for each of the three sulphide concentrations used. Forsström et al. (2017) reported an approximate doubling of the hydrogen concentration from 0.5 wt.ppm in as-received material to 1.0 wt.ppm in the tapered-tensile specimens. Interestingly, there was no effect of sulphide concentration on the amount of hydrogen after exposure, despite presumably a difference of two orders of magnitude in the rate of formation of adsorbed hydrogen on the surface of the copper. Furthermore, samples taken from the unexposed threaded portion of the specimens contained the same amount of hydrogen as sections directly exposed to the solution. It would seem unlikely that H absorbed in the exposed section of the specimen could have diffused to the threaded region in the time available. The diffusion coefficient of H in copper at the experimental temperature of 90 °C is approximately 10^{-12} m²/s (Ishikawa and McLellan 1985). Thus, H would only diffuse a maximum of 1 mm during the 2-week exposure period, which is significantly less than the distance between the threaded portion of the sample and that exposed to solution (see for example Figure 27 in Becker and Öijerholm 2017). Neither is it likely that the absorbed H diffused through the sample following the test since it would take 30 years for H to diffuse the approximate distance of 10 mm between the threaded region and exposed section at the room temperature diffusivity of 10^{-13} m²/s. It has also been shown that measurements of H in copper are challenging, with reported values in as-received material varying between 0.33 wt.ppm and 2.3 wt.ppm (Granfors 2017). Nevertheless, Forsström et al. (2017) proposed a role for absorbed H in the reported SCC of copper due to either the formation of micro-voids on grain boundaries or the stabilisation of vacancies and vacancy clusters.

6.2.5 Taxén et al. (2018, 2019)

Taxén et al. (2018, 2019) have further attempted to replicate the observations of both Taniguchi and Kawasaki (2008) and Becker and Öijerholm (2017). No evidence for SCC was observed by Taxén and co-workers in either study, although evidence for shallow intergranular attack was found (Taxén et al. 2019).

Taxén et al. (2018) closely followed the experimental conditions of Taniguchi and Kawasaki (2008) but using SKB Cu-OFP. Experiments were conducted using round and flat tensile specimens, some of the latter being heat treated to replicate the apparent hardness of the PDO specimens used by Taniguchi and Kawasaki (2008). Slow strain rate testing was performed in artificial seawater containing 0.01 mol/L sulphide at room temperature and 80 °C. Unlike the earlier work, Taxén et al. (2018) did not control the potential of the specimens at a previously determined open-circuit potential but instead monitored this potential during the course of the test. Tensile testing showed no significant effect of exposure to sulphide on either the elongation to failure or the ultimate tensile strength of the specimens. Nor was there any effect of sulphide exposure on the mechanical properties of the cold-worked flat tensile specimens with or without subsequent heat treatment. Optical and scanning electron microscopic examination revealed ductile fracture surfaces. Some indications of intergranular attack (see Figure 6-5) and cracked corrosion products were observed and which were of similar appearance to features reported by others to be SCC. However, there was no evidence for cracking of the underlying copper.

In order to replicate the experimental conditions of Becker and Öijerholm (2017), Taxén et al. (2019) added phosphate buffer to sulphide-containing chloride solutions to maintain a near-neutral pH. Slow strain rate tests were performed on Cu-OFP with sulphide concentrations between 2×10^{-5} mol/L and 0.002 mol/L in 0.01 mol/L Cl⁻ solution (and, in one experiment, 0.1 mol/L Cl⁻). A phosphate concentration of 0.01 mol/L was used and was sufficient to maintain a pH close to the theoretical value of pH 7.2 at the lower sulphide concentration and a pH of 7.3−7.6 at the higher sulphide concentrations. Shallow (10−30 μm deep) crack-like features were observed in solutions containing 0.001 and 0.002 mol/L sulphide, but not in 2×10^{-5} mol/L sulphide, see Figure 6-6. However, these features initiated early on in the overall straining process and away from the site of final rupture. Their depth did not seem to increase significantly with time, and the fracture surfaces exhibited the dimpled,

cup-and-cone appearance of ductile failure. For these reasons, Taxén et al. (2019) considered these features to be intergranular corrosion where the excessive strain had opened up the grain boundaries, rather than SCC. No such crack-like features were observed in solution containing 2×10^{-5} mol/L sulphide.

Therefore, despite careful replication of the techniques of Taniguchi and Kawasaki (2008) and of Becker and Öijerholm (2017), Taxén et al. (2018, 2019) were unable to reproduce the indications of SCC reported in the two earlier works.

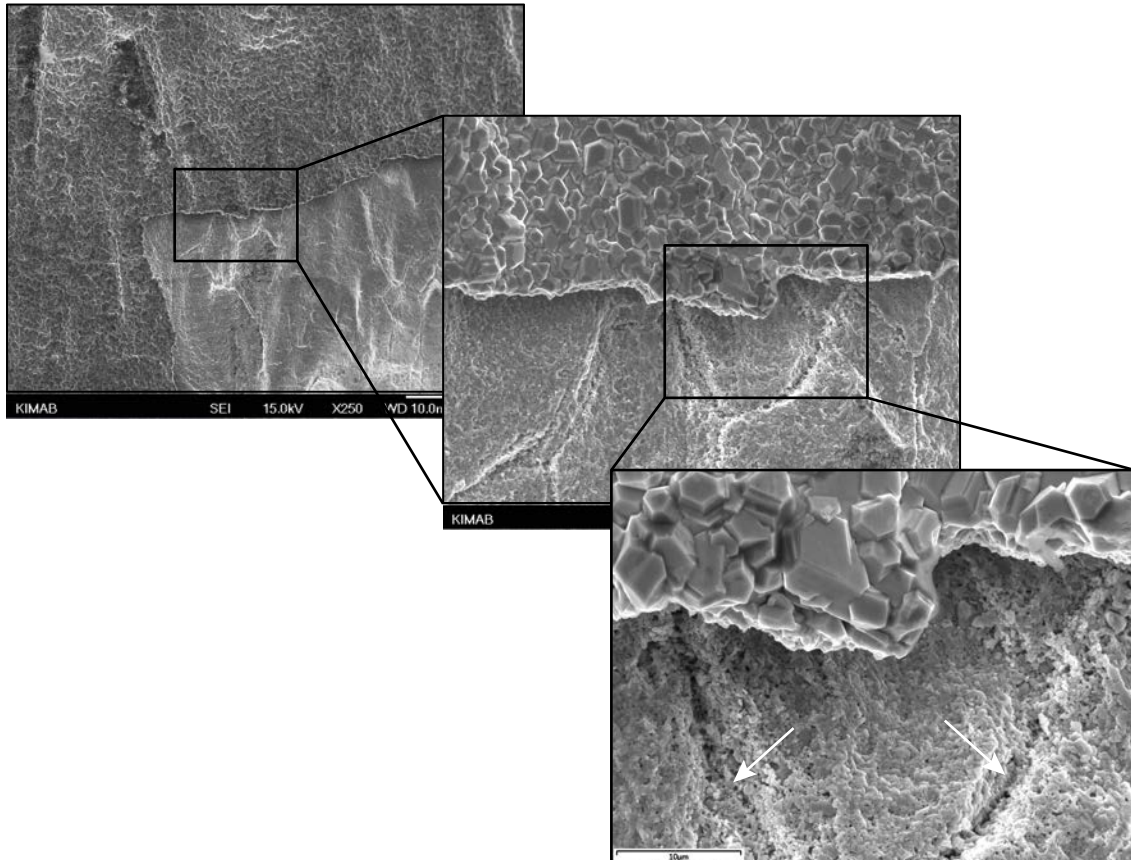**Figure 6-5.** *Surface features found after SSRT test in 0.01 mol/L sulfide at 80 °C (Taxén et al. 2018). The arrows point at some intergranular attacks.*

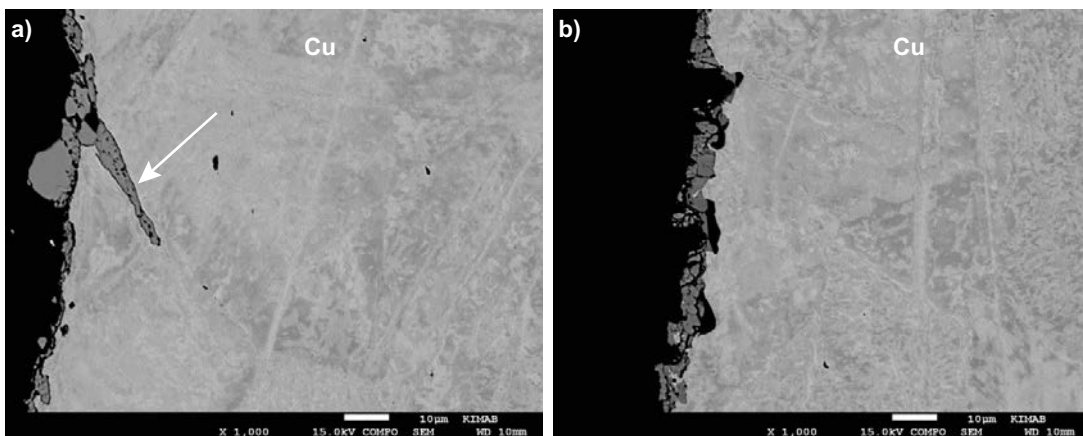**Figure 6-6.** *Longitudinal cross sections of test rod from a) Run #1 in 0.001 mol/L sulphide, 0.01 mol/L chloride, 90 °C, b) Run #2 in 2×10^{-5} mol/L sulphide, 0.01 mol/L chloride, 90 °C (Taxén et al. 2019). The arrow in a) points at a crack.*

6.2.6   The Aaltonen mechanism

The Aaltonen mechanism has been mentioned as one mechanism to describe SCC of copper (e.g. King and Newman 2010). SKB has initiated a more thorough review of this mechanism, presented in Huotilainen et al. (2018). The Aaltonen mechanism is based on the concept that excess vacancies in the metal can activate dislocations within the material leading to strain localisation at the crack tip and crack propagation (Aaltonen et al. 1998, 2003, Jagodzinski et al. 2000). Huotilainen et al. (2018) have characterised the Aaltonen mechanism as a variant of the well-known slip-dissolution mechanism, in which discontinuous crack advance occurs as a result of repeated slip (film rupture) and dissolution steps (King and Newman 2010). Absorbed hydrogen can enhance the Aaltonen mechanism, either by stabilizing the vacancies and preventing their annihilation, or by forming microvoids as a result of the formation of hydrogen gas. The generation of the excess vacancies is typically achieved in the laboratory by anodic polarization of the specimens in order to produce rapid rates of dissolution and film (oxide) formation. Once the polarizing current is removed, however, the effect of the excess vacancies (typically demonstrated by the enhanced creep rate, Aaltonen et al. 2003), disappears within an hour or so as the vacancy concentration returns to the equilibrium value.

Although there is no intrinsic reason why excess vacancies could not be generated in copper exposed to sulphide solutions, there is no evidence for it occurring under laboratory conditions and it is even less likely to occur in the repository. Experimentally, the effect of vacancy injection has been demonstrated at applied current densities of the order of 1 mA/cm^2 (Aaltonen et al. 1998, 2003). In contrast, as already described in Section 5.5.2, the highest sulphide flux to the canister for intact buffer in the SR-Site safety assessment is of the order of 10^{-12} mol/(m^2 s) (King et al. 2017), equivalent to a corrosion current density of 10^{-8} mA/cm^2. Even for the case of eroded buffer, the highest sulphide flux would only produce a corrosion current density of 10^{-5} mA/cm^2. Thus, the maximum vacancy generation rate due to sulphide corrosion of the canister is five to eight orders of magnitude lower in the repository than that used in laboratory tests. It is probable that the annihilation rate would be comparable and even larger than the vacancy generation rate at low corrosion rates as under repository conditions, and that there would be no excess vacancies generated (Huotilainen et al. 2018).

Also, in an new evaluation of published reports on mechanical tests of copper specimens under various conditions (Björkblad and Faleskog 2018), no mechanism has been identified that could cause crack propagation during the conditions and the time periods that are of relevance for the final repository.

6.3   Summary of studies and assessment of sulphide-related "SCC"

Of the five groups that have studied the SCC of copper in sulphide-containing environments, only two have definitively reported cracking with the other three groups failing to replicate the observations. The maximum depth of the reported cracks is of the order of 50 μm, which could be compared with an average grain size for the Cu-OFP of 78 μm and 156 μm in manufactured lids and tubes, respectively (SKB 2010d). Thus, the reported cracks have a maximum depth in the order of, or less than, the size of a single grain.

It's been difficult to reproduce cracking in spite of the testing being performed under extreme mechanical loading and environmental conditions. In most of the studies described above, the copper has either been strained to failure or to strains in excess of what the canister is expected to experience. Furthermore, no consistent correlation has been presented between the occurrence of cracks and the reduction in cross-sectional area or elongation to failure, which are the two common measures of SCC susceptibility from SSRT (Parkins 2010). Instead, the susceptibility to SCC has been largely based on the observation of cracks along the gauge length away from the fracture location. There is though no strict and common definition of what consists of "a crack", and as noted in Taxén et al. (2018), cracks in copper can appear both as singular branching cracks and as a multitude of cracks in the surface under strain.

As will be explored in more detail in Section 6.4, these apparently inconsistent experimental observations may be explained by differences in the relative rates of sulphide supply and consumption at the copper surface. A low sulphide flux and/or high rate of consumption will lead to a low interfacial sulphide concentration and vice versa, as discussed in Chapter 5 in the context of passivity and localised corrosion. From a corrosion point-of-view, a low sulphide flux and a near-zero interfacial concentration

will have a number of effects. First, Cu$_2$S films grown under these conditions tend to be porous, non-adherent, and consist of relatively large grains. Low concentrations of dissolved sulphide will favour grain growth over the rapid nucleation observed at high concentrations. In turn, the growth of large grains causes the development of in-film stresses which leads to friable, poorly adherent and non-protective films. Second, as argued by Bhaskaran et al. (2013), any form of SCC or localised corrosion that relies on the transport of sulphide to the tip of a crack, crevice, or pit is not possible as the diffusive driving force down the occluded region is negligible because of the restricted geometry and the near-zero sulphide concentration at the mouth (Figure 6-7).

These effects of low sulphide flux may explain some of the differences in cracking and localised corrosion observed in the various studies described above. Bhaskaran et al. (2013) presented evidence that, under their experimental conditions, the corrosion rate was transport limited based on the results of EIS and polarisation scans which suggested transport control over a wide range of potentials. In contrast, Taniguchi et al. (2008) reported a reduction in both the ultimate tensile strength and elongation to failure with increasing anodic polarisation, despite the fact that the severest cracking was observed at the lowest levels of polarisation. The reduction in strength and ductility would be consistent with a greater general corrosion loss with increasing potential which, in turn, would suggest that the corrosion rate was not sulphide transport limited under the conditions of their tests because otherwise the corrosion rate would not be a function of potential.

The need for sulphide transport into a crack or along a grain boundary is also consistent with the observation of a threshold sulphide concentration. The lower the bulk sulphide concentration, the more likely the corrosion rate is to be transport limited and the resulting interfacial concentration low. Thus, the threshold sulphide concentration may simply be a reflection of the inability to transport sufficient sulphide into the crack or grain boundary to sustain SCC or IGC. Also the observation of maximum crack depth in the order of the size of a grain is consistent with a process limited by transport of sulphide into the crack, as the transport resistance increases when the directions of the grain boundaries starts to divert from being nearly perpendicular to the surface.

The competition between the rate of supply of sulphide and the rate of interfacial consumption is also affected by the kinetics of the interfacial electrochemical reactions. This may explain the observation of crack-like features or, perhaps more correctly, intergranular corrosion, in the presence of phosphate in solution (Becker and Öijerholm 2017, Taxén et al. 2019). As well as buffering the pH, phosphate is also known to inhibit the rate of copper corrosion under oxidising conditions (Ha and Scully 2013). As discussed in Section 5.3.3 other anions like e.g. sulphate will suppress film formation, most probably by strong adsorption. Therefore, the corrosion rate is more likely to be under kinetic control for the same sulphide concentration and mass-transport conditions in the presence of phosphate than without phosphate. In turn, this will lead to a higher interfacial sulphide concentration and the possibility of transport of sulphide along a crack or grain boundary.
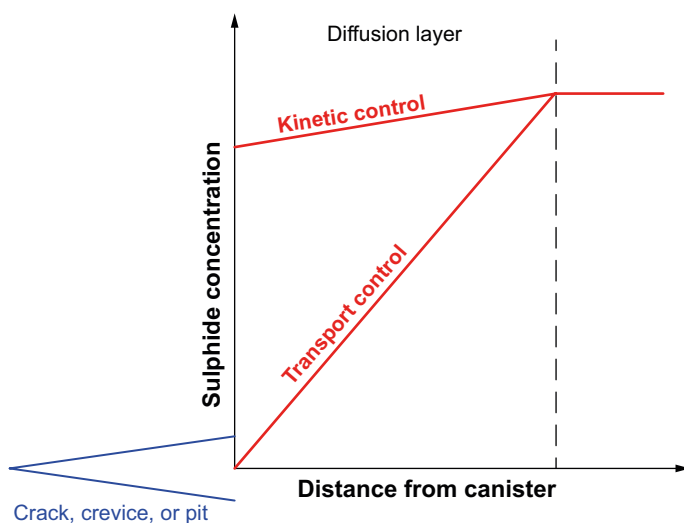

Figure 6-7. Schematic of the difference in surface concentration of sulphide and the resulting driving force for transport into a crack, crevice, or pit depending upon the rate-controlling process for canister corrosion.

This concept of the absence of cracking or intergranular attack under externally transport-limited conditions is also consistent with the absence of SCC in the presence of compacted bentonite-based buffer, as reported by Taniguchi et al. (2008). In studies of the rate of general corrosion, Taniguchi and Kawasaki (2008) reported that the films formed on copper specimens embedded in buffer material were less adherent and composed of larger crystals than those formed on specimens exposed to bulk solution. As a result, corrosion rates were higher in compacted buffer despite the lower sulphide flux, while the lower corrosion rates obtained in bulk solution were due to the protectiveness of the more compact sulphide film formed at high sulphide flux. This is a strong indication that under the conditions of their experiments in solution, including the SSRT tests, the copper corrosion reaction was under kinetic control, leading to a non-zero interfacial sulphide concentration.

The proposal that SCC and localised corrosion are not possible for conditions under which the corrosion rate is transport limited applies especially to those mechanisms that require the presence of sulphide at the crack tip (or along the grain boundary). The supply of sulphide will also determine the rate of vacancy generation due to anodic dissolution of the copper. It would seem, however, that the maximum rate of corrosion due to the supply of sulphide to the canister surface will be five to eight orders of magnitude lower than that typically used to observe effects due to the injection of excess vacancies in the laboratory based on the Aaltonen mechanism. The argument is less applicable to mechanisms associated with the absorption of hydrogen and subsequent micro-void formation, as proposed by Forsström et al. (2017). Nevertheless, the rate of formation of hydrogen adsorbed on the surface, the precursor to atomic hydrogen absorbed in the bulk, would be proportional to the flux of sulphide under transport-limited conditions. Thus, it is reasonable to argue that H-related cracking mechanisms should also be less likely in systems with low sulphide fluxes. The involvement of absorbed H in the reported SCC of Taniguchi and Kawasaki (2008) and Becker and Öijerholm (2017) has not been proven and it is important to note that Bhaskaran et al. (2013) did not observe cracking when they cathodically polarised specimens. Possible effects of hydrogen in copper are discussed and analysed further in Chapter 7.

6.4 Application to repository conditions

As mentioned in Section 6.1, stress corrosion cracking (SCC) may occur in some metals and alloys when the material is simultaneously subjected to certain chemical environments and tensile stress. In the sections below, the chemical and mechanical conditions of the canister in the repository will be discussed in terms of their possible support for SCC in copper.

6.4.1 Tensile stresses in the copper shell

The imposition of an isostatic load results in a compressive stress state in the cylindrical part of the copper shell. However, especially if the temperature is elevated, the external pressure can deform the copper shell even below the yield strength (creep) and cause local tensile stresses to be built up. The creep strain could be higher if the copper shell is not in contact with the insert. Finite element simulations of stress and strain of the canister illustrate how stresses are built up and how they change with time. For example, as seen in Figure 6-8, the maximal principal stresses are localised at the outer surface of the canister close to the lid and base. The level of stress depends on the gap between the insert (not shown in the figure) and the copper shell (shown) (Hernelind 2019b). Simulations have also been performed for a zero gap (Figure 6-9) between the insert and the copper shell, to clarify whether minor alterations to the design could lead to reduced tensile stress levels (Hernelind 2019b). Here the levels of the principal stress on the canister surface are lower and it can be seen that the stress range decreases.

In the finite element simulations of the isostatic load case, all inelastic strains are calculated as equivalent creep strain and thus the plastic strain is included in the creep strain. Only the base flange of the copper shell, as discussed above, has tensile stresses (axial) penetrating through the wall thickness (Hernelind 2019a, b).
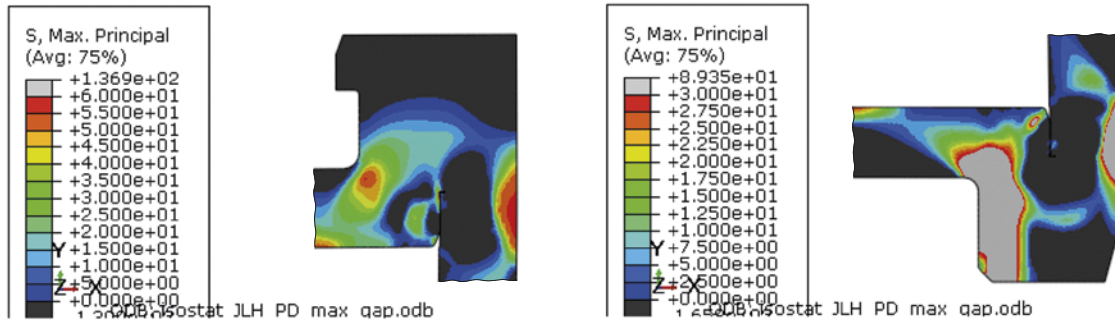
Figure 6-8. Finite element simulation of the maximum principal stresses in the copper lid and base due to the isostatic pressure and creep strain, with maximal gap (drawing scale 1:5). For clarity, all compressive stresses are shown as black. (Hernelind 2019 b)
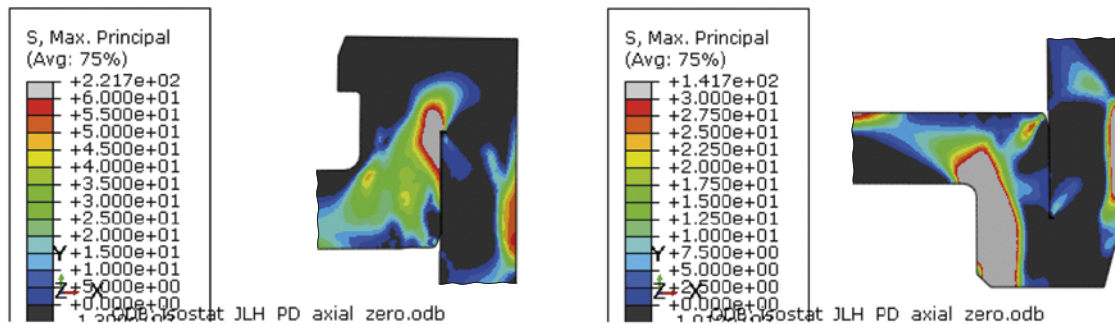
Figure 6-9. Finite element simulation of the maximum principal stresses in the copper lid and base due to the isostatic pressure and creep strain, with zero gap (drawing scale 1:5). For clarity, all compressive stresses are shown as black. (Hernelind 2019 b)

6.4.2 Environmental conditions

The environmental conditions for which cracks have been reported are generally harsh compared with those to which the canisters will be exposed. In the same way as in Section 5.5 and Figure 5-16 the sulphide concentrations and sulphide fluxes in the experiments could be compared to those possible in the repository. Not only is the minimum sulphide concentration at which cracking has been observed (10^{-3} mol/L, Becker and Öijerholm 2017) a factor of 10 to 100 times higher than that measured in the groundwater at Forsmark, but more importantly the flux of sulphide to the copper surface is orders of magnitude lower than the experimental fluxes, as long as the buffer is in place. In stagnant solutions, the diffusion layer thickness adjacent to the copper surface is assumed to be approximately 1 mm (King et al. 2017). (The slowly refreshed solutions used by Becker and Öijerholm (2017) and Taxén et al. (2018, 2019) might have resulted in a thinner diffusion layer.) For a typical diffusivity in bulk solution of 10^{-9} m²/s (King et al. 2017), the flux of sulphide to the copper surface in an experiment with 0.001 mol/L HS⁻ would be of the order of 10^{-6} mol/(m² s). In contrast, the maximum sulphide flux with the buffer in place is 1.5×10^{-12} mol/(m² s) for saturated buffer (Section 5.5.2) and 7×10^{-11} mol/(m² s) for unsaturated buffer (Section 5.5.3), i.e. a factor of 10^4 lower than the experimental flux for which some indication of cracking or SCC has been reported. Further, as discussed in Section 5.5.4 the threshold sulphide flux for transport control of the corrosion reaction is estimated to be in the range 3×10^{-10} to 2×10^{-8} mol/m² s (King et al. 2017), and the canister corrosion rate is expected to be transport limited, meaning that the interfacial concentration of sulphide at the canister surface will approach zero (Figure 6-7). Therefore, there will be an insufficient external flux of sulphide to the canister surface to support intergranular corrosion or any SCC mechanism with the buffer in place.

Even for the eroded buffer case, in which advective conditions arise at the canister surface, the highest flux calculated in the SR-Site safety assessment was of the order of 10^{-9} mol/m² s (Section 5.5.4), i.e. still three orders of magnitude lower than the lowest experimental flux for which any indication of SCC has been observed. The corrosion would be under mass transport control for the overwhelming

majority of sulphide fluxes possible in the repository (Section 5.5.4) with the same lack of driving force for intergranular corrosion or SCC as with the buffer in place. For intergranular corrosion and cracks growth also the mass transport limitation of sulphide to the tip of the crack needs to be taken into account, which will depend on the sulphide concentration at the mouth of the crack as well as corrosion products filling up a narrow crack. As discussed in Section 6.3, this internal transport limitation leads to an inability to transport sufficient sulphide into the crack or grain boundary to sustain SCC or IGC, and the process would be self-limiting.

The flux of sulphide is important, not only as it determines the interfacial sulphide concentration, but also the rate of the electrochemical reactions, including the generation of adsorbed H.

Overall, therefore, given the extreme loading and environmental conditions under which shallow crack-like features have been observed, it is concluded that the copper canisters will not be subject to this form of attack due to sulphide exposure in the repository.

6.5 Conclusions

Although some studies have reported superficial cracks in copper exposed to high sulphide fluxes and under high tensile stress, there are no studies in the literature that have demonstrated that copper is subject to SCC in sulphide environments.

It cannot be excluded that some locations on the copper canister will be subjected to local tensile stresses arising from creep deformation in the final repository. The levels of tensile stresses can be though be reduced by decreasing the gap between the copper shell and the insert.

However, the sulphide peak fluxes that may occur in the repository with intact buffer under both unsaturated and saturated buffer conditions as well as for the overwhelming majority of the deposition in the case of eroded buffer, are too small to sustain a non-zero concentration at the canister surface (mass transport limited corrosion) which is a prerequisite for a crack to grow. For the few deposition holes in the case eroded buffer, where higher sulphide fluxes to the canister surface are possible, the transport resistance in the crack would restrict the sulphide flux to the crack tip and render the process self-limiting. It is also noted that these fluxes are at least three orders of magnitude lower than the flux in any of the studies in which cracks or other indications of SCC-like phenomena have been reported.

It is thus concluded that the possibility of SCC in copper, even at high sulphide fluxes has questionable scientific support. Even if copper is susceptible to SCC in the presence of sulphide, the sulphide fluxes in the repository environment are far too low to induce the phenomena observed and sometimes interpreted as SCC.

An evaluation of published results on the Aaltonen mechanism to describe SCC in copper shows that it would require conditions that will never be prevailing in the final repository.

7 Hydrogen embrittlement

7.1 Introduction

Atomic or molecular hydrogen in copper may, if present in sufficient concentrations, negatively influence the mechanical properties of the metal. This is a well-known phenomenon that applies to metals in general. Atomic hydrogen has a very low solubility in the undisturbed copper lattice, but may be trapped at grain boundaries, in lattice dislocations and vacancies or bind to impurities in the lattice or in grain boundaries. In addition, atomic hydrogen may form molecular hydrogen in micro voids in the metal. This could have a negative effect on mechanical properties and is generally referred to as hydrogen embrittlement (HE). In particular, H reacting with oxygen in the metal may form molecular water in micro-voids, which could also have a negative effect on mechanical properties. The latter phenomenon is sometimes called hydrogen sickness.

In the statement by the Land and Environmental Court (Section 1.1), it was suggested that there are uncertainties concerning the effect of hydrogen embrittlement on canister integrity in the final repository. The court pointed to the need to further demonstrate that oxide formation during welding can be kept at a sufficiently low level, and the need to quantify the amount of hydrogen that could enter the canister in the repository environment and to assess whether this could have any detrimental effect. The largest uncertainty as regards sources of hydrogen generating processes in the repository was considered to be copper corrosion by pure, O_2-free water. As seen in Section 4.3, it is SKB's clear conclusion that this is a negligible process in the final repository, and this source of hydrogen is, therefore, not further discussed in the following.

Copper and many other types of face centred cubic alloys such as aluminium alloys, fully austenitic stainless steels and nickel are not particularly susceptible to HE, and HE is not in general considered to be a problem for these types of materials in industrial applications (Lynch 2012) and that applies to oxygen free copper qualities as well. Consequently, it is mainly special conditions for the copper canister that should be considered, for example the possibility of a slow hydrogen charging mechanism possibly acting for thousands of years.

According to the requirements for the oxygen free phosphorous doped copper, Cu-OFP, to be used for the KBS-3 canister, the initial content of hydrogen and oxygen in the material should be less than 0.6 wt.ppm and 5 wt.ppm, respectively. These requirements serve to prevent hydrogen sickness and hydrogen embrittlement. Similar requirements on oxygen content have been applied for many years for copper in various applications. They have been so successful that hydrogen sickness is not considered to be a technical problem in copper any more. This is illustrated by the fact that hardly any scientific paper on hydrogen sickness in copper has been published during the last 40 years. As regards the requirement on hydrogen content, it is noted that there is a variation at least in the range 0.3−0.6 wt.ppm in samples of Cu-OFP (SKB 2010d). The requirement on hydrogen content can likely be relaxed to at least 1 wt.ppm, but this has not been systematically investigated.

Oxygen could be introduced into the copper canister material through the welding of the canister lid and base, and to reduce this phenomenon to harmless levels, the welding is performed in an inert atmosphere.

The Cu-OFP to be used for the canister material typically contains around 0.5 wt.ppm H. Several studies with the specific aim of increasing the hydrogen content in copper have demonstrated that extreme electrochemical conditions in specially prepared aqueous environments are required to force hydrogen into copper (Martinsson and Sandström 2012, Leijon et al. 2018, Yagodzinskyy et al. 2018). Some of these studies have also demonstrated the impact on the mechanical properties of the increased hydrogen content. Simply exposing copper to hydrogen gas at the highest pressures and temperatures expected under repository conditions (see further Section 7.4.1) would not lead to any significant increase in H content, since the solubility of H in Cu is very low. In two relatively recent studies, it has been suggested that the H content may increase by about a factor of two in thin samples when subjected to a combination of aqueous sulphide and tensile stresses (Forsström et al. 2017), as discussed in Section 6.2.4, or a gamma radiation dose that is representative for the repository (Lousada et al.

2016). The overwhelming part of the H in Cu-OFP is bound to traps in the form of voids, vacancies, dislocations or impurities, in the bulk or at grain boundaries. Leijon et al. (2018) studied the influence of hydrogen charging on the creep properties of Cu-OFP. A hydrogen content of up to 10 wt.ppm was achieved. The focus in the study was on changes of the microstructure.

This chapter is structured according to the following.

- SKB's experience of welding in inert atmospheres in order to reduce the introduction of oxygen in the material during welding is summarised in Section 7.2.

- Introduction of hydrogen into copper in laboratory experiments and the resulting mechanical effects are discussed in Section 7.3.

- Hydrogen introduction and associated mechanical effects under repository conditions are discussed in Section 7.4.

- Conclusions are summarised in Section 7.5.

7.2 Welding in inert atmospheres

In the encapsulation plant, fuel will be emplaced in the insert, inside the copper shell, and the canister will then be sealed by Friction Stir Welding (FSW) of the copper lid to the copper tube. During welding, heat generated in the stir zone will be transported to the surrounding material. The joint surfaces will therefore experience a temperature increase prior to joining. If the process is conducted in an atmosphere containing oxygen, such as air, oxide films will grow on the joint surfaces prior to consolidation of the joint. These oxide films will, to some degree, be broken up by the stirring action of the tool and become embedded into the final weld. The thickness of the oxide films will depend on the temperature history prior to joining. The largest amount of embedded oxides is found at the overlap sequence, see Figure 7-1, where the hot joint line is exposed to the environment during most of the welding sequence (Björck et al. 2017).

In the literature there is evidence that oxygen in copper can affect the ductility of the material (measured as area reduction at rupture or the elongation to failure). Oxides were located either at grain boundaries (Nieh and Nix 1981) or present as larger particles (Camurri et al. 2011). Also, oxide particles formed during FSW of copper can affect the ductility in a negative manner (Savolainen 2012, Rantala et al. 2015). It is also known from FSW of aluminium that oxide particles in the weld can cause a reduction in the mechanical strength (Chen et al. 2006, Zhou et al. 2006). Another possible detrimental effect of oxides is hydrogen embrittlement where oxide particles are reduced by hydrogen and form molecular water which creates blisters in the material (Mattson and Schücker 1958). Standardised procedures have been developed to test a material's susceptibility to this type of hydrogen embrittlement. One of these tests is ASTM B577-16 method B (ASTM 2016), in which the material to be tested is heated to 850 ± 25 °C in an atmosphere of at least 10 % hydrogen gas for 20-40 min, after which the microstructure of the material is examined using optical microscopy. These types of tests are part of the acceptance testing of oxygen free copper material.

In order to reduce the amount of oxide particles in the weld material, SKB has developed a gas shield in the current FSW process (Björck et al. 2017). Formation of oxide particles can be strongly suppressed using a suitable cleaning method of the joint surfaces prior to welding together with a gas shield during welding. None of the tested welds were then susceptible to hydrogen embrittlement according to ASTM B577-16 method B. In order to further analyse the experimental results they were complemented by calculations with a model describing the oxidation kinetics (Björck and Elger 2013). Trial welds and subsequent analysis (Björck et al. 2017) showed that the optical response of a copper oxide is highly sensitive to very thin oxide layers. Layers as thin as 10 nm can be detected by the human eye as a colour change of the surface. Inspecting the colour of the resulting outer surface can be used as an additional quality control, complementing monitoring of the oxygen level in the gas shield during production.
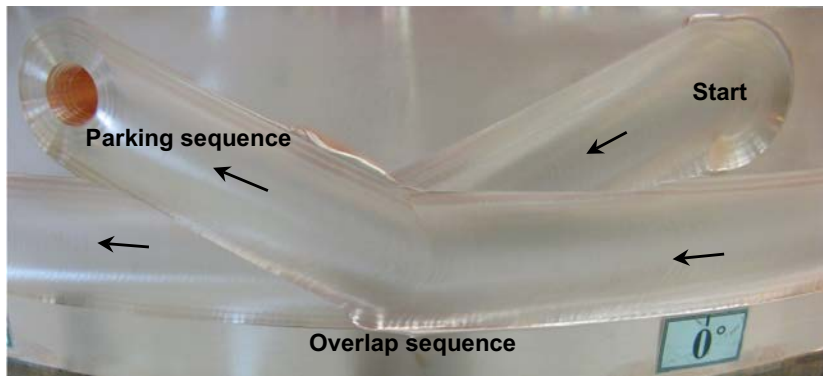
Figure 7-1. *An overview of the different sequences during welding. The welding starts above the joint line. The tool then traverses down to the joint line and continues around the canister until it overlaps the initial part of the joint line. The tool is then moved upward in a parking sequence and is finally retracted leaving an exit hole in the upper part of the lid. This part of the lid is machined to remove the exit hole. The arrows show the direction of the tool. The colour of the copper surface is a result of the cleaning procedure prior to welding.*

The effects of oxides on material properties were investigated further by Björck et al. (2019). The identified properties that could be affected by the presence of oxide particles were the aforementioned ductility and the corrosion resistance. Different segments of a joint line were pre-oxidized to different thicknesses between 0 μm (a freshly cleaned joint surface) and 8 μm (worst case for the outer surface of a weld made under air) and subsequently welded under an inert gas atmosphere with an oxygen level known not to produce any detectable oxides (Björck et al. 2017). From these segments, samples for tensile and creep testing were cut. The samples were especially prepared to locally measure the response around the streaks of oxide particles. It was found that the ductility remained unchanged, as compared to the base material, for an oxide thickness of up to 0.1 μm. For an oxide thickness of 0.1 μm and thicker a reduction in the ductility, from 86-87 % to 66-69 % at 75 °C, could be detected. Pictures of the ruptured surfaces are shown in Figure 7-2 as a function of oxide film thickness where the enlargement in area between the 0.1 μm and 1 μm samples shows the loss of ductility. When comparing the segments with metallographic tests for detecting copper oxides (ASTM 2016) as well as macro-etched cross-sections, see Figure 7-2, a clear connection between the appearance of a streak of oxide particles in the metallographic pictures and the resulting ductility can be seen. In welded samples where oxides were detected the ductility was decreased. Likewise, the ductility was similar to the parent material in welded samples where no oxides were identified. This verifies that metallographic tests developed for the base material can be used to assess the quality of the welded material as well.

In order to investigate the corrosion properties, the apparent nobility of the welded material was measured (Taxén et al. 2017). No significant difference in the apparent nobility between the welded material and base material was found (Björck et al. 2019).

In conclusion, oxides can be detected with standard metallographic tests, and welds essentially oxide free can be produced using a properly designed gas shield. Welding under an inert gas atmosphere is commonly employed in industrial applications. The oxygen level inside the gas shield can be monitored by sensors, and it is expected that the colour of the final outer weld surface can be used as an additional acceptance criterion to indirectly monitor the process. The exact oxygen level in the gas shield to be used during welding in the actual encapsulation process remains to be determined. However, based on the current tests (Björck et al. 2019) oxygen levels below 100 volume ppm in the gas shield would be sufficient. The retrofitted gas shield available today is capable of achieving oxygen levels <50 volume ppm.
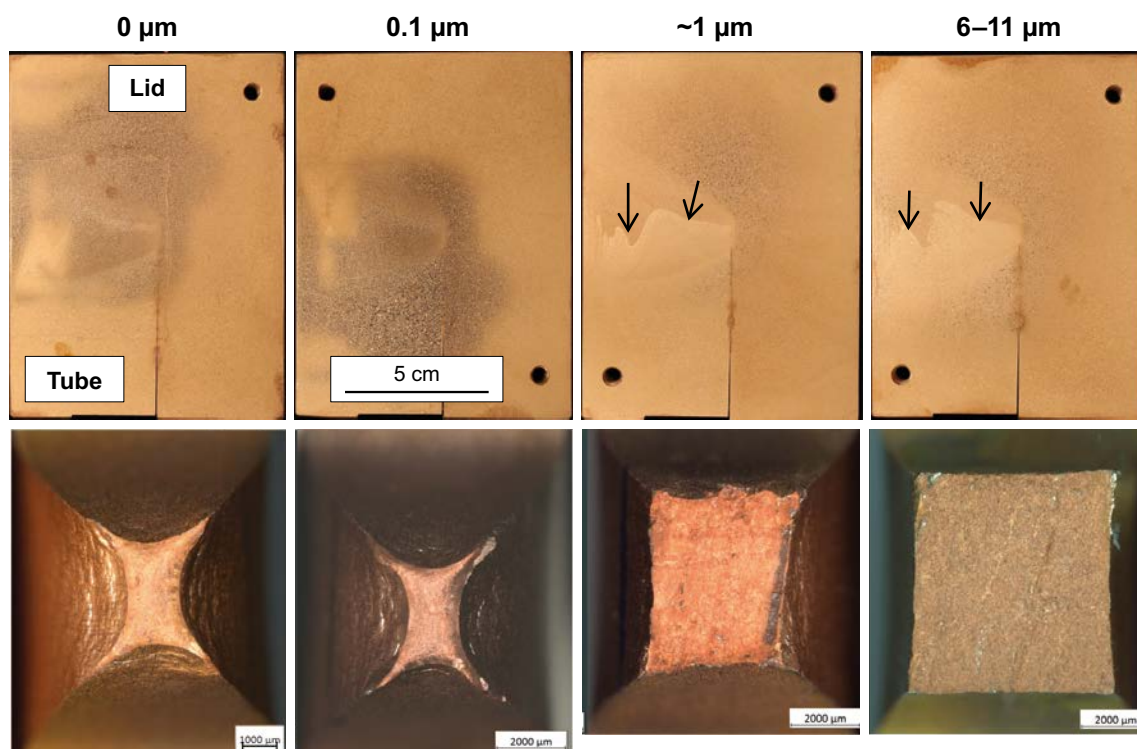
Figure 7-2. An example of different pre-oxidised samples described in the text. The oxide thickness is given in the insets in each column. The top row shows pictures of macro etched weld cross sections, canister surface to the left and the vertical slit is the border between the tube and lid. Upwards in the figure is towards the lid top surface. The processing line where the oxide particles are located is more visible in the last two columns, marked with black arrows. The bottom row shows the fractured tensile test conducted at 75 °C. A decrease in ductility is readily seen going from left to right by an increase in the area of the fracture. (Björck et al. 2019)

7.3 Introduction of hydrogen into copper in laboratory experiments

7.3.1 Wampler et al. (1976)

Wampler et al. (1976) observed that pores in the form of spherical "bubbles" were formed in copper loaded with H by equilibration with H_2 gas at temperatures between 600 and 1 000 °C at a pressure of 3 MPa and then cooled to room temperature. Alternative names for bubbles in the literature are pores, blisters and cavities. The concentration of H in the samples after loading was 300 at.ppm (atom-ppm) or around 5 wt.ppm. Micrographs show bubbles with radii of the order of 0.1 µm. The bubbles formed preferentially at grain boundaries and dislocations. The authors report 0.2-0.4 µm bubbles with a density of around $10^9/cm^3$. The internal H_2 pressure of the bubbles is estimated at 100-200 MPa, meaning that the density of hydrogen is near that of liquid H_2.

7.3.2 Okinaka and Straschil (1986)

Electroless copper deposition is mentioned here for the completeness of the discussion because in the past it has been used to study the influence of hydrogen on ductility. Electroless copper deposition involves the simultaneous reduction of copper and hydrogen. Therefore, high atomic and/or molecular hydrogen contents can be found in the powder metallurgical deposits. Electroless copper is characterized by high porosity and low ductility. For example, Okinaka and Straschil (1986) found that the elongation to failure was below 5 % when the hydrogen content exceeded 10 to 25 wt.ppm. Due to its high porosity and impurity contents, electroless copper has poor mechanical properties and is therefore not relevant when discussing the properties of the canister material (Cu-OFP). Electroless copper will thus not be considered further in this report.

7.3.3   Panagopoulos and Zacharopoulos (1994)

Panagopoulos and Zacharopoulos (1994) charged tensile specimens of pure copper in a solution of 75 % methanol, 22.4 % water, 2.6 % sulfuric acid with 10 mg/L arsenic trioxide as a hydrogen recombination inhibitor with charging currents up to 100 mA/cm^2. The thickness of the tensile specimens was 1.5 mm. The influence of charging time on tensile properties is illustrated in Figure 7-3. The charging gave a modest reduction of the tensile strength and of the elongation to failure. A higher charging current than the one used in the figure did not generate any further reduction in the properties. No measurement of the hydrogen content and no microstructural study were performed.

7.3.4   Martinsson and Sandström (2012)

Martinsson and Sandström (2012) observed formation of near-surface hydrogen bubbles in Cu-OFP that had been electrolytically charged with H with a current density of 10 mA/cm^2 for up to three weeks in a 10 % H_2SO_4 electrolyte containing 30 mg/L As_2O_3 to supress hydrogen recombination. These conditions were chosen to obtain maximum charging and are referred to here as full charging. The hydrogen bubbles are preferentially formed at grain boundaries within 50 μm from the surface and have sizes of the order of 1 μm (see Figure 7-4). An increase in the hydrogen content in comparison to the value for uncharged specimens was only observed for depths of up to 100 μm. This means that the observation of bubbles is an approximate indication of how deep into the material the hydrogen content has been raised. The authors find through modelling that the internal H_2 pressure in the bubbles can at most be around 400 MPa. It is noted that a pressure of 400 MPa corresponds to a molecular density of 0.16 mol/cm^3 at room temperature, whereas metallic copper has a density of around $8.9/63.5 \approx 0.14$ mol/cm^3. The authors write: "During 3 weeks of charging, the average hydrogen content in the topmost 50 μm increased from 0.6 to almost 100 wt.ppm in as-received copper."

One important conclusion from the work of Martinsson and Sandström (2012) is that the enhanced hydrogen content is located near the surface even after extensive charging. Modelling results show that a steady-state distribution is soon reached and deeper penetration of hydrogen does not take place even if the charging goes on for years (Martinsson et al. 2013). The reason is that the outflow of hydrogen increases with time and soon matches the inflow.

From the modelling performed by Martinsson and Sandström (2012), it was concluded that the influx of H was around 1×10^{-10} kg/(m^2 s), i.e. 1×10^{-11} mol/(cm^2 s). The charging current 10 mA/cm^2 corresponds, with F = 96 485 C/mol, to 10^{-7} mol/(cm^2 s), meaning that a fraction of $\sim 10^{-4}$ of the generated H seems to have entered the metal. It is noted that this is for a charging situation with a clean surface and using a recombination poison to enhance the charging rate.
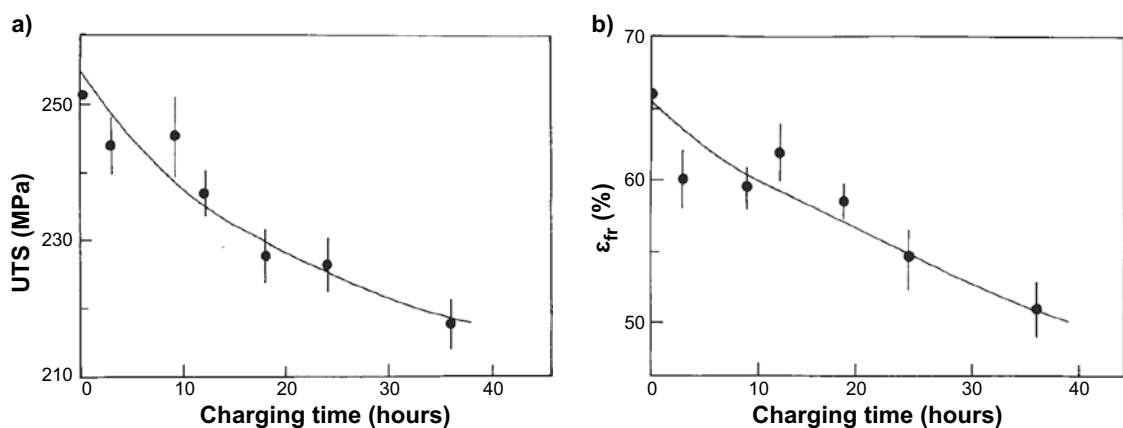
Figure 7-3. *Influence of charging time on the a) ultimate tensile strenghth (UTS) and b) elongation to failure ε_{fr} of copper for a current density of 25 mA/cm^2(Panagopoulos and Zacharopoulos 1994).*
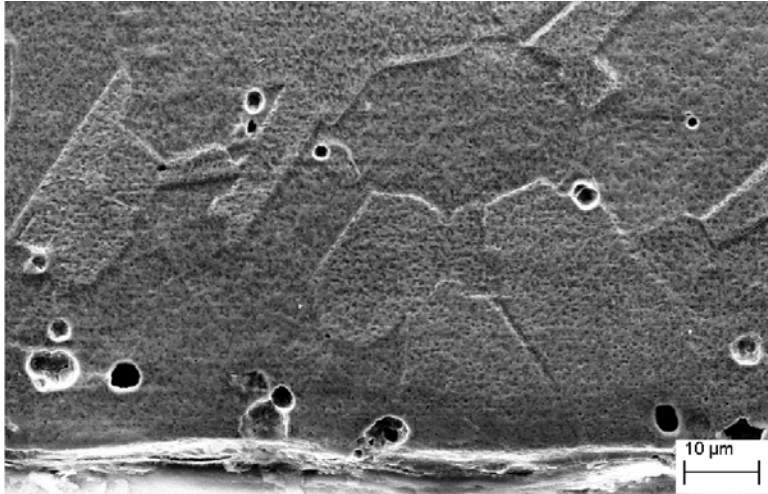
Figure 7-4. Hydrogen bubbles formed close to the surface, located at the bottom of the image, and at grain boundaries (Martinsson and Sandström 2012).

7.3.5 Yagodzinskyy et al. (2012)

Yagodzinskyy et al. (2012) continuously charged Cu-OFP with hydrogen at 20 and 50 °C during slow strain rate tensile tests. The specimen thickness was 1.5 mm. Pores and intergranular cracks were found to a depth of 110 μm. In comparison to uncharged specimens, the tensile strength at 50 °C was reduced by about 7 % and the elongation to failure by 10 %. No explanation of the observations is presented in the paper, but the following is suggested: The cracked surface layers can be expected to have a much reduced load bearing capacity. If it is reduced by 50 % which is a reasonable value, the drop in tensile strength would be equivalent to that observed based on the relative cross-sectional areas of the embrittled surface layer and uncharged central core. If the flow stress[3] versus strain is known, the ductility (elongation value) can be computed with a classical plasticity criterion (Considère's criterion). It states that when the plasticity limit (and thereby the uniform elongation) is reached, the work hardening is equal to the flow stress. The reduction in tensile strength is accompanied by a lower work hardening (a lower slope of the stress strain curve). According to Considère's criterion, this automatically means that the elongation value is reduced, in agreement with the observations.

Yagodzinskyy et al. (2012) also performed a few creep tests with or without continuous charging. The creep results for specimens without charging are very different from other published results. For example, they reported an exponent for the stress dependence of the creep rate of 3 whereas other literature gives a value above 50 (for a review of creep properties see Andersson-Östling and Sandstrom 2009). This difference represents many orders of magnitude in the creep rate. The testing conditions appear to have been quite different from the ones mentioned in the paper, and it is therefore rather difficult to interpret the results. A discrepancy of the same order of magnitude is also found for the tests with continuous charging in comparison to the results of Leijon et al. (2018).

7.3.6 Lousada et al. (2016)

Lousada et al. (2016) studied the influence of gamma irradiation (total dose of 69 kGy over 6 days at a dose rate of 486 Gy/h) on copper surfaces in pure water. An increase in the hydrogen content to up to 0.4 wt.ppm hydrogen was found after the irradiation exposure using thermal desorption spectroscopy (TDS). This was around twice the initial concentration of the specimens (~0.2 wt.ppm H). Since neither the uptake of 0.2 wt.ppm hydrogen, nor the absolute final value of 0.4 wt.ppm hydrogen after uptake is larger than the hydrogen concentration already present in the Cu-OFP (ca 0.5 wt.ppm), and since the effect is measured for a repository representative gamma dose (about 100 kGy at the canister surface), it is not regarded as a risk for hydrogen embrittlement. Also, the thickness of the copper canister is 50 mm whereas that of the foils in Lousada et al. (2016) was 0.25 mm. If the same

---

[3] Flow stress is a measure of how the stress of a stress/strain curve varies with strain. Flow stress thus depends on strain contrary to yield strength which is the flow stress for a fixed strain, usually 0.2 %.

amount of hydrogen was generated in the final repository, and if the hydrogen would be distributed in a 0.25 mm surface layer, then only a small fraction of the canister cross section would see a mildly increased hydrogen concentration. If the hydrogen would be distributed further into the 5 cm copper shell, the concentration increase would be correspondingly smaller.

It is also noted that the TDS spectra of the H release as a function of temperature from irradiated and non-irradiated samples are very similar in shape, suggesting that H exists in the same form and is similarly distributed in the two samples. This is somewhat unexpected since if the difference in total content stems from the irradiation, the additional H would be expected to be closer to the surface whereas the original H would be homogeneously distributed in the sample. The form in which H occurs could also be different. This suggests that it could be premature to draw firm conclusions regarding the extent of hydrogen introduction from this single measurement.

7.3.7 Forsström et al. (2017)

As described in Section 6.2.4, Forsström et al. (2017) measured the hydrogen content in Cu-OFP before and after exposure to sulphide solutions of various concentrations while straining the samples in SSRT tests. The authors report an increase in hydrogen content from initially around 0.5 wt.ppm to around 1 wt.ppm after the exposure. As also noted in Section 6.2.4, *i)* the increase in hydrogen content was independent of sulphide concentration which is unexpected if the source of H is believed to be the corrosion reaction caused by the sulphide and *ii)* a sample taken from an unexposed part of the specimen shows the same apparent increase although it was far too distant from the exposed region for H to diffuse to the sample location in the time available.[4]

7.3.8 Yagodzinskyy et al. (2018)

Yagodzinskyy et al. (2018) electrolytically charged $1 \times 3 \times 10$ mm single crystal copper samples of 99.9999 wt.% purity. The electrolyte was 1 N H_2SO_4 aqueous solution with 20 mg/L $NaAsO_2$ recombination poison and the charging was carried out under controlled electrochemical potential of -350 mV (SHE) at 50 °C for 250 ks (ca 70 h).

The average concentration of hydrogen in the charged samples was determined by thermal desorption spectroscopy (TDS) to be about 240 at.ppm, i.e. around 4 wt.ppm. Positron annihilation spectroscopy indicated void formation, and indications of near-surface voids were also observed as spikes in the TDS spectra in Figure 7-5. The hydrogen was thus believed to be present in part as molecular hydrogen in the voids formed by the electrolytic charging.

The H charging rate is 240 at.ppm in 1 mm during 250 ks i.e. $240 \times 10^{-6} \times 8.9/63.5 \times 0.1/250\,000$ mol/(cm^2 s) $\approx 1.3 \times 10^{-11}$ mol/(cm^2 s). The charging current is not given. If it is assumed that it is around 10 mA/cm^2 as in similar experiments, i.e. 10^{-7} mol/(cm^2 s), then in this experiment, as in that of Martinsson and Sandström (2012) described in Section 7.3.4, a fraction of the order of 10^{-4} of the generated H appears to enter the metal. This assumes that there are no losses of H over the boundaries.

The authors found that the hydrogen introduction caused strain hardening with about 6 % increase of the flow stress at the nominal strain of about 2 % in stage I of the plastic deformation, i.e. the very first part of the plastic deformation. The observed increase in the flow stress is very small, only up to 2 MPa. Hydrogen is known to stabilise the formation of vacancies (Ganchenkova et al. 2014, Korzhavyi and Sandström 2014). This mechanism is assumed to explain the small increase in the flow stress. Stage I does not occur in the polycrystalline material that is used for the copper canisters. If the effect also exists in polycrystalline copper, it would be expected to be quite small as well and without technical significance due to the small effect of vacancies.

---

[4] At 90 °C, the diffusivity of H in Cu is around 10^{-12} m^2/s (e.g. Ishikawa and McLellan, 1985). With an approximate diffusion distance of 1 cm between the exposed part of the specimen and the unexposed sample, the diffusion time is of the order of $0.01^2/(4 \times 10^{-12})$ s or almost 300 days, whereas the duration of the exposure was only about 14 days. The time between exposure and H measurements is not known, but it is reasonably assumed that the samples were stored at room temperature during this period, meaning that the diffusivity was at least an order of magnitude lower and the diffusion time hence an order of magnitude longer compared to 90 °C. Also, the unexposed sample was located in a part of the test specimen that was not strained, meaning that the diffusivity should not have been affected by the straining.
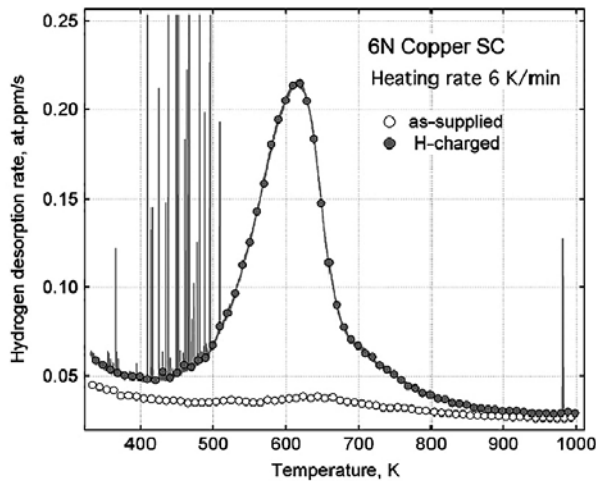
Figure 7-5. Temperature dependence of hydrogen desorption rate in ultra high vacuum from high purity copper in as-supplied state (open circles) and after electrochemical hydrogen charging (filled circles). The heating rate was 6 K/min. (Yagodzinskyy et al. 2018)

7.3.9 Leijon et al. (2018)

In Leijon et al. (2018), creep tests for Cu-OFP were carried out at 23, 50 and 75 °C with and without continuous charging. The hydrogen charging was performed in an electrolyte of 1 N H_2SO_4 solution with 10 mg $NaAsO_2$ (or 5 mg As_2O_3) recombination poison per litre at a controlled potential of −1.1 V (Hg/Hg$_2$SO$_4$).

The experimental set up is illustrated in Figure 7-6. In the centre, there is a copper specimen being charged. It is surrounded by a double-wall glass compartment. Electrodes, filters and sensors are used in the set-up. From the presence of the bubbles on the surface of the specimen, it is evident that much of the electrolytically generated hydrogen recombines into molecular hydrogen (H_2) instead of entering the material as atomic hydrogen (H).

Creep tests were first performed applying the same tensile stress of 140 MPa as was used by Yagodzinskyy et al. (2012); however, no surface cracks were observed after these tests. The stress level was then raised to 170 MPa or above. After the creep testing, the hydrogen content of all charged specimens was measured to ensure that a significant amount of hydrogen had entered the material. Up to 12 wt.ppm was measured. For some charged specimens, intergranular cracks with a maximum depth of 100 μm were found. On the crack surfaces bubbles were frequently observed. Creep deformation was recorded only for two specimens, which showed higher and lower creep rates than for ordinary creep tests in air. This shows that the hydrogen charging had a limited effect on the creep properties.
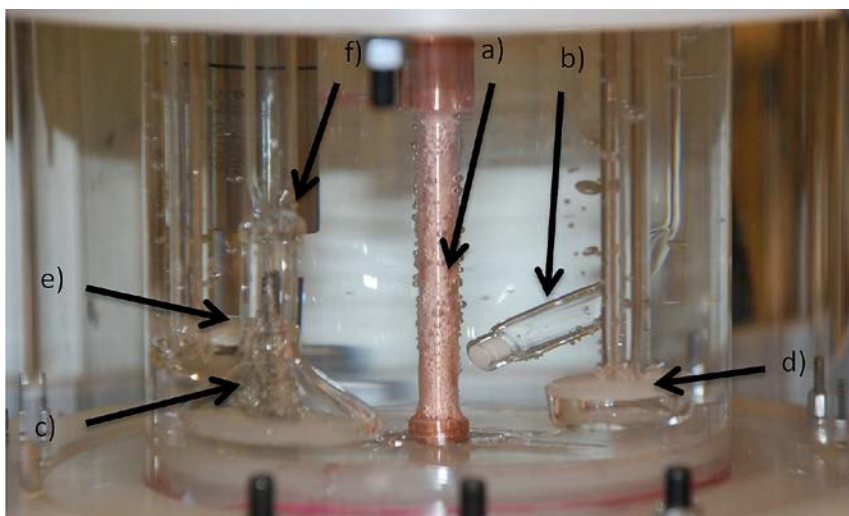
Figure 7-6. Reaction chamber for creep tests with continuous charging a) specimen, b) Luggin-probe, c) Pt reference electrode, d) e) filter tubes, f) oxygen sensor (Leijon et al. 2018).

7.3.10 Summary of studies and observations

A brief summary of the listed references in Section 7.3 is given in Table 7-1. For each reference the analysed material is specified. When it is available in the report, the longest charging time as well as the measured hydrogen content is provided. In a number of the reports the microstructure has been studied after charging. A brief summary is given. If mechanical properties were measured, some main findings are shown in Table 7-1.

Table 7-1. Main findings in studies on H charging of copper.

Charging method	Material	Max charging time (h)	Max H content (wt.ppm)*	Microstructure	Mechanical properties	Comment
Wampler et al. (1976)						
High pressure at T > 600 C	Pure Cu		5	Fine bubbles 0.2-0.4 µm		
Okinaka and Straschil (1986)						
Electroless deposition	PM Cu		39	Porous copper	Low ductility above 10-25 wt.ppm H	No relevance for canister Cu
Panagopoulos and Zacharopoulos (1994)						
Full charging	Pure Cu	36			30 % reduction of tensile strength and elongation to failure after 25 h charging	
Martinsson and Sandström (2012)						
Full charging	Cu-OFP	500	5	Bubbles and increased hydrogen content < 50 µm from surface		H pick-up factor 10^{-4}
Yagodzinskyy et al. (2012)						
Full charging, slow strain rate tests	Cu-OFP	14		Intergranular surface cracks < 110 µm from surface	Up to 7 % reduction in tensile strength and 10 % in ductility	
Lousada et al. (2016)						
Gamma radiation (69 kGy) in water	HP Cu		0.4	Crystals and localized corrosion features to < 1µm depth		
Forsström et al. (2017)						
Corrosion in sulphide solution, SSRT	Cu-OFP	340	1	Surface cracking		
Yagodzinskyy et al. (2018)						
Full charging	6N Cu	69	4	Fine slip bands observed	6 % increase in flow stress	H pick-up factor thought to be 10^{-4}
Leijon et al. (2018)						
Full charging	Cu-OFP	1000	12	Cracks down to < 100 µm		

*Assuming homogeneous charging of the sample

7.4 Hydrogen introduction and associated mechanical effects under repository conditions

7.4.1 Introduction

As mentioned in Section 7.1, exposing the canister to the highest H_2 pressures that could occur in the repository would result in negligible H concentrations in the Cu matrix. As analysed in the safety assessment SR-Site, the highest gas pressures that need to be considered at the canister wall during the life time of the repository is pessimistically assessed to be 20 MPa (SKB 2011, Section 13.8). According to Sieverts' law and data according to Magnusson and Frisk (2017), this corresponds to an atomic fraction of H in the Cu matrix of 2.6×10^{-10} at room temperature, i.e. many orders of magnitude lower than the original H content of around 3×10^{-5} in the material.

The only other identified source that could potentially cause introduction of hydrogen in the copper material is a corrosion process in which atomic H is generated. Here, corrosion by sulphide during unsaturated buffer conditions, during saturated buffer conditions and for the less likely case of saturated conditions with an eroded buffer need to be considered. As discussed in Section 2.2.2, unsaturated conditions could occur for about 6 000 years at most, and saturated conditions would then prevail during the remainder of the one million year assessment period. For approximately 100 deposition holes, the possibility that the buffer erodes to the extent that advective conditions arise somewhere around the canister cannot be excluded. The onset of advective conditions is expected to take of the order of 100 000 years to occur. The peak sulphide influxes for the unsaturated, saturated and eroded cases have been estimated to be 10^{-10}, 10^{-12} and 10^{-9}, mol/(m² s), respectively (see Section 2.2.5). This would lead, for each of the case, to the same peak generation rate of H on the canister surface if it is assumed that all inflowing HS^- is transformed to atomic H in the corrosion process. A certain H generation due to radiation induced processes in water outside the canister is also possible.

As regards the fraction of the generated H that actually enters the metal, there are several aspects to consider. As is evident from the account of the experiments above, only a small fraction is expected to enter, and this pick-up factor was estimated at 10^{-4} e.g. for the experiment by Martinsson and Sandström in Section 7.3.4, which was in agreement with Yagodzinskyy et al. (2018) (Section 7.3.8). Another way of addressing this is by considering the energetics of H on the copper surface versus H in an interstitial position in the Cu matrix. The energy difference between these two states, the segregation energy of H to a Cu surface, has recently been calculated by Lousada and Korzhavyi (2019). They find that the segregation energy is at least 0.5 eV for surface coverages of both 25 and 100 %. This suggests that the H concentration in the bulk material in equilibrium with a surface with a high H coverage can be estimated at $\exp(-0.5eV/k_BT) \approx 3.5 \times 10^{-3}$ at.ppm. For a more sparsely covered surface, the corresponding H concentration would be even lower. A concentration of 3.5×10^{-3} at.ppm is a very low value and many orders of magnitude smaller than the initial concentration of H in Cu-OFP. However, it is noted that the latter concentration still corresponds to a pore pressure of around 500 MPa according to Sieverts' law, which is of relevance when considering the possibility of bubble formation.

In the following, repository conditions will be addressed both for a situation where bubbles are assumed to be formed near the Cu surface and a situation where this is not the case.

7.4.2 Assuming bubble formation

As was discussed above, the surface layers of specimens that have been electrolytically charged with hydrogen are affected in a characteristic way. Bubbles filled with molecular hydrogen are formed particularly at the grain boundaries. Eventually this can lead to cracks being created along the grain boundaries. The observed depth of this damaged surface layer where the microstructure is changed is 20 to 100 μm. Martinsson and Sandström (2012) showed that the zone of altered microstructure corresponds approximately to the layer with increased hydrogen content. This has also been implicitly assumed in several of the studies in Section 7.3.

For the charging experiments that have been performed, the increase in the hydrogen content is restricted to a thin surface layer. The reason is that with increasing charging time, the number of bubbles and cracked grain boundaries increases with an increased outflow of hydrogen. Eventually a steady state between the inflow and outflow is reached. In the reports summarised in Section 7.3, the longest

charging times are three to six weeks. Modelling shows that the total hydrogen content in the material is not changed very much even if very long charging times exceeding one year are considered (Martinsson et al. 2013).

Mechanical properties of charged copper have been measured in a few publications (Panagopoulos and Zacharopoulos 1994, Yagodzinskyy et al. 2012, 2018, Leijon et al. 2018). In the first three of the investigations, some reduction of the ductility or a small change in the flow stress was observed. In all three papers, specimens with a thickness of 1.5 mm or less were used. This means that micro-structural damage in the surface layer with a depth up to 110 μm (Section 7.3.5) would have an influence on the mechanical test result. Even for these thin specimens, the observed influence on mechanical properties was small and not of technical significance. Leijon et al. (2018) used a specimen diameter of 5 mm. In their tests in which the creep rate was measured, the rate was either above or below results from standard creep tests in air indicating that the influence of hydrogen was limited and presumably smaller than the variation between samples.

To date, all experimental studies show that the hydrogen after electrolytical charging is found in a narrow surface layer. The mechanical properties are only affected in this thin layer. However, for other fcc materials like Ni, Al-alloys and austenitic stainless steels it seems possible to achieve a homogeneous distribution of hydrogen in the material. As mentioned above, hydrogen embrittlement is still not considered as a technical problem for these materials.

The reason that the increase in hydrogen content is restricted to a narrow surface layer is that hydrogen filled bubbles are formed which eventually provide an easy path for the outflow of hydrogen. It is noted that the amount of metallic Cu is not affected by the bubble formation, meaning that the amount of matter available as a corrosion barrier, or at least as a sink for sulphide, is not altered. It is also noted that all the above observations have been made at charging conditions that are much more aggressive than in a repository environment, as is discussed further below.

7.4.3 Assuming no bubble formation

If bubbles and cracks were not formed, the copper matrix could be more extensively charged. Although at present it is a hypothetical situation, the case of no bubble formation will now be analysed.

As shown in Section 2.2.5, the maximum estimated influx of sulphide for *unsaturated conditions* is of the order of 10^{-10} mol/(m^2 s) and could last for a few thousand years in the longest cases. This would lead to a maximum hydrogen generation rate of the same order of magnitude as the sulphide flux. Only a fraction of this hydrogen would enter the copper. This pick-up factor was estimated to be 10^{-4} in Sections 7.3.4 and 7.3.8 above for two of the charging experiments. It is noted that this factor was obtained in experiments with a clean surface and using a recombination poison. Also, for the hydrogen generating corrosion reaction in the repository, sulphide corrosion, the hydrogen is thought to be generated at the interface between the copper sulphide layer and the solution, i.e. the atomic hydrogen would also have to migrate through the copper sulphide layer to reach the metal. All these conditions should reduce the pick-up factor for sulphide corrosion in the repository compared to the conditions in the charging experiments. On the other hand, it is not known how the lower hydrogen generation rate would affect the pick-up factor.

With a pick-up factor of 10^{-4}, the hydrogen charging rate, φ, of the outer copper surface under unsaturated conditions would thus be at most 10^{-14} mol/(m^2 s). If it is pessimistically assumed that outflow of hydrogen can occur only over the inner copper surface and not over the outer surface where hydrogen is introduced, then after a transient build-up period, the hydrogen flux in the canister will approach a steady state and be equal to the charging rate. With a zero concentration boundary condition at the inner surface, the maximum concentration in the canister, C_{Max}, will occur at the outer surface and be given by

$$C_{Max} = \frac{\varphi L}{D}$$

where φ is the H charging rate, L is the thickness of the canister and D is the diffusivity of hydrogen in Cu. With $L = 0.05$ m and $D = 3.3 \times 10^{-14}$ m^2/s, corresponding to the approximate H diffusivity in Cu at 25 °C according to Ishikawa and McLellan (1985), one obtains a C_{Max} of 0.015 mol/m^3, corresponding to a hydrogen content of 1.7×10^{-3} wt.ppm. It is again noted that this is for the pessimistic assumption

that no outflow occurs over the outer boundary. Even with a pick-up factor as high as 10 % and no outer-boundary outflow, the maximum increase in H concentration is limited to around 1.7 wt.ppm. The transient phase is described by Eq 5 in Section 3.8 of Carslaw and Jaeger (1959). From that equation it can be seen that the transient time is of the order of $L^2/4D$, i.e. about 600 years in this case. Note also that the Cu temperature will be considerably higher than 25 °C for hundreds of years after deposition, meaning that the diffusivity is also pessimistically under estimated, and the maximum concentration C_{Max} thus overestimated, in this calculation.

As was shown in Section 2.2.5, the estimated peak influx of sulphide is one order of magnitude lower for the case of a long-term *saturated buffer* than for the case of unsaturated buffer analysed and discussed above. Thus, the case with unsaturated buffer is also bounding for the case of saturated buffer.

For the case with an *eroded buffer* and the canister directly exposed to the groundwater, the maximum estimated influx of sulphide is an order of magnitude higher, i.e. around 10^{-9} mol/(m^2 s), see Section 2.2.5. This would thus yield a maximum H concentration of 1.7×10^{-2} wt.ppm with a pick-up factor of 10^{-4}.

Concerning the further fate of H for the eroded buffer case, it is noted that in this case the maximum inflow of water to the deposition hole is estimated to be 100 L/yr (SKB 2011, Table 13-4) and the highest sulphide concentration is 1.2×10^{-4} mol/L. This extreme case thus suggests a hydrogen generation rate of about 0.01 mol/year if all sulphide passing the deposition hole generates H through sulphide corrosion of the copper canister. The void volume in the canister interior with the insert and the fuel in place is around 1 m^3 (SKB 2010b, Section 4.1) and the molar volume of H$_2$ is 22.4 L at STP. It would thus take more than 4 000 years to generate a hydrogen partial pressure of 1 atm in the canister void if all generated H is assumed to enter the copper canister and subsequently emerge as H$_2$ at the inner copper surface. With a pick-up factor of 10^{-4}, this time would be far longer than the one million years covered by the safety assessment. This estimate shows that there is a large margin to generating H pressures in the canister insert that would be detrimental for the insert properties during the one million year assessment time.

An alternative way of addressing the case of no bubble formation would be to consider the case of an outer Cu surface fully covered by H. It was noted in Section 7.4.1 that this corresponds to a matrix concentration of around 3.5×10^{-9} in the bulk (atom fraction). A corrosion process generating H can never lead to more than full coverage at the surface, and if it is also assumed the concentration corresponding to full coverage can always be upheld in the bulk near the surface, the flux of hydrogen would be negligible for all cases considered above.

In conclusion, the less realistic case of hydrogen uptake without bubble formation leads to hydrogen concentrations in Cu and hydrogen pressures in the canister interior that are not detrimental to canister integrity.

7.5   Conclusions

A range of experiments have been performed on hydrogen charging of copper. In most cases direct electrolytic charging has been used with a recombination poison present to maximize the inflow of hydrogen. In the charged specimens, hydrogen filled bubbles and intergranular cracks were found in a thin surface layer. The thickness of this layer was 20 to 110 µm from the outer exposed copper surface. The strength and ductility of the surface layer was reduced in comparison to uncharged copper. However, the bulk of the material is unaffected. It is evident from the mechanical testing that even for specimens with a thickness of 1.5 mm or less, the reduction of strength and ductility is modest.

The longest charging times that have been used are 6 weeks. Modelling results suggest that the surface layer with bubbles and cracks will not grow much even if very long times are considered. The reason is that bubbles and cracks create easy paths for the outflow of hydrogen and a steady state is eventually reached between inflow and outflow. For the copper canisters, only a very thin layer would be affected even if hydrogen charging comparable to the rate in the experiments were to occur. However, under repository conditions, the generation rate of hydrogen on the canister surface would be many orders of magnitude lower than in the experiments.

If bubbles and cracks were not formed, the copper matrix could be more extensively charged. Although this has not been observed, the hypothetical situation has been analysed by theoretical considerations. It is assumed that the influx of sulphides that controls the extent of sulphide corrosion also controls the maximum hydrogen generation. Taking into account the fact that only a small fraction of the generated hydrogen is expected to enter the metal, the maximum inflow of hydrogen is estimated at 1×10^{-14} mol/(m^2 s) for unsaturated conditions. For a canister wall with a thickness of 50 mm, such an inflow would produce an additional 1.7×10^{-4} wt.ppm of hydrogen near the entry surface when a stationary flow through the canister is reached. For saturated conditions with the buffer in place, the concentration would be an order of magnitude lower and for the small fraction of canisters that can be expected to experience advective conditions due to buffer loss, it is an order of magnitude higher. In addition, if these cases are alternatively analysed under the assumption that the copper surface is fully covered by H and that this corresponds to a bulk concentration of 3.5×10^{-3} at.ppm as recent calculations have shown, the bulk hydrogen concentration would be completely negligible.

Based on these results, it is concluded that hydrogen embrittlement will not jeopardise canister integrity in a KBS-3 repository.

8 The effect of radiation on pitting, stress corrosion cracking and hydrogen embrittlement

8.1 Introduction

In several safety assessments of the KBS-3 concept, it has been concluded that the radiation from the encapsulated spent nuclear fuel will cause a certain amount of corrosion of the copper canister, but that the impact is negligible as regards the integrity of the canisters and the post-closure safety of the repository. Recent experimental studies have confirmed the earlier view that corrosion due to radiolysis of water is a minor effect (Björkbacka 2015). The detailed mechanism of radiolytic corrosion was, however, not fully understood, which has motivated further research on the matter. Furthermore, it was suggested during the hearing in the Land and Environmental Court (Section 1.1), that the radiation from the spent fuel could affect the defect- or micro-structure of the copper material, which could in principle have negative effects on corrosion by possibly enhancing the risks for localised corrosion (pitting), stress corrosion cracking (SCC), and hydrogen embrittlement. Radiation enhanced effects have been deemed negligible in earlier safety assessments but are here evaluated again, in response to the statement from the Court. This chapter is structured as follows:

- A background to the matter is provided in Section 8.2.

- Further studies on the mechanism of corrosion under gamma radiolysis are discussed in Section 8.3.

- Revised calculations of radiation induced damage in copper (and iron) under exposure to gamma and neutron radiation from the encapsulated fuel are described in Section 8.4.

- An experimental search for microstructural changes in copper after exposure to gamma radiation is described in Section 8.5.

- A discussion on the impact of radiation on pitting, SCC and hydrogen embrittlement is provided in Section 8.6.

- Conclusions are presented in Section 8.7.

8.2 Background

8.2.1 Handling of radiation effects in SR-Site

The radiation fields from the encapsulated spent nuclear fuel, could, in principle, cause radiation damage (vacancies) that affect the mechanical properties of the canister materials, as well as the corrosion process at the copper surface in the repository environment.

In the safety assessment SR-Site, the evaluation of the radiation damage rates in the canister materials was based on calculations combining interaction cross-sections with experimentally measured minimum atomic displacement energies and damage efficiency (Guinan 2001). This was done for both PWR (pressurized water reactor) and BWR (boiling water reactor) fuels and for different relevant burnups. Neutron and gamma radiation fields were considered, and radiation damage rates were computed for both iron and copper. For both materials and all positions evaluated in the canister assembly, the initial damage rate at the time of encapsulation, i.e. after ca 30 years of decay during interim storage prior to deposition in the final repository, was of the order of 10^{-11} to 10^{-9} dpa/y (displacements per atom and year). As expected, the highest damage production rate was found on the inside of the cast iron insert (near the source), and the lowest rate was found at the outer surface of the copper shell (Guinan 2001).

The accumulated radiation damage in the canister materials under repository conditions was evaluated using computed neutron and gamma dose rates as functions of time up to 3×10^5 years. The accumulated damage due to neutron radiation is of the order of 10^{-7} dpa in all positions in a canister, while the accumulated damage due to gamma radiation varies from 10^{-7} dpa at the inside of the iron insert to 10^{-10} dpa at the outer surface of the copper shell (Guinan 2001). The accumulated radiation damage estimated is thus very low and also pessimistic since thermal annealing of defects was

neglected in the calculations. For the first 300 years, accounting for 99.9 % of the total radiation dose absorbed by the canister materials, the canister is also heated by the encapsulated fuel, and the temperature of the copper shell will vary between 50 and 95 °C during this period.

From comparison with the experimental literature on effects on yield strength in copper under radiation, it was concluded that the pessimistically estimated levels of accumulated radiation damage (computed without accounting for thermal annealing) are at least one order of magnitude too small to have any measurable effects on the mechanical properties of the canister materials (Guinan 2001). Similarly, it was concluded that since the radiation damage is much smaller than the concentration of any impurity in the material, the effects of radiation on segregation and redistribution of impurities in the material will be negligible (Guinan 2001). As will be discussed further below in Section 8.5, due to efficient thermal annealing of vacancies and other defects (Padovani et al. 2019), the margin to measurable effects of radiation damage on material properties is even larger than what was concluded in SR-Site.

The possible effects of radiation on processes like SCC and hydrogen embrittlement that were mentioned during the hearing in the environmental court, depend ultimately on the level of radiation damage accumulated in the copper material in the repository. Since the work underlying the assessment of radiation damage in SR-Site was performed nearly twenty years ago, and since the computer codes and data bases in the field of radiation damage have developed since, it was decided to re-examine the earlier work and to compute the accumulated radiation damage using modern software and data. This work is summarised in Section 8.5. In addition, attempts have also been made to verify the estimated low levels of gamma radiation damage in the copper shell experimentally, which is summarised in Section 8.6.

After emplacement of the canister in the repository, the corrosion environment will be determined by the groundwater chemistry at Forsmark, together with the chemical properties of the bentonite clay. In addition, for the first few hundered years, the corrosion will also be influenced by the radiation field present initially at the canister surface. The gamma radiation from the spent fuel is dominated by the decay of ^{137}Cs, with a half-life of ca 30 years. Other gamma emitters have a weaker contribution to the total gamma activity of the fuel and/or a shorter half-life.

The radiation field at the canister surface has been evaluated in several reports, and in SR-Site it was concluded that the gamma dose rate, present at the canister surface at the time of encapsulation, is at most 0.18 Gy/h, while the average dose rate at the canister surface is ca 0.055 Gy/h (SKB 2010f).With a half-life of 30 years, the dose rate decreases to $\sim 10^{-4}$ Gy/h in around 300 years, meaning that the canister materials have then been exposed to 99.9 % of the total repository dose. The total repository dose of gamma radiation is of the order of 100 kGy at the canister surface. The neutron dose rate at the canister is initially only 10^{-4} to 10^{-3} of the gamma dose rate, depending on the type of fuel and degree of burnup (Håkansson 2000). Its effect on radiolysis can thus be regarded as negligible as compared with gamma radiolysis.

The most important effect of gamma radiation on the corrosion behaviour of the copper canister will be radiolysis of gases and aqueous species near the canister surface. The major component of air is nitrogen gas, which during radiolysis can form nitric acid (HNO_3). Since nitric acid is a corrosive agent for copper, it was accounted for in the corrosion assessment of SR-Site. Assuming, pessimistically, an initial gamma dose rate of 1 Gy/h, a half-life of 30 years, and a G-value of 0.02 molecules/eV for nitrogen gas, it was shown that less than 0.015 moles of nitric acid will form due to gamma radiation in the repository. This amount of nitric acid would, if consumed uniformly over the copper surface, correspond to a corrosion depth of 7 nm and is thus a negligible effect, see Section 5.1.1 in SKB (2010a).

The major component of groundwater is water itself (55 mol/L). The radiolytic species formed during irradiation of water include oxidising species, e.g. the OH-radical and H_2O_2, but also reducing species, like H_2 and solvated electrons. In SR-Site, a pessimistic approach was used to derive an upper bound of the amount of copper corrosion due to gamma radiolysis of water. In this approach it was assumed that the kinetics of copper oxidation was very efficient and that all oxidants formed by radiolysis within 5 mm of the canister surface will reach the copper surface, although a significant fraction of the oxidants will in fact react and combine with other species in the solution, e.g. the reducing species

formed during radiolysis of water and groundwater components, before they reach the canister surface by diffusion. The bounding amount of oxidized copper under these assumptions was calculated to be 35 moles, which, if assumed to occur uniformly over the canister surface, would correspond to 14 µm of copper corrosion, see Section 5.1.2 in SKB (2010a).

8.2.2 Experimental studies of radiolytic corrosion conducted after SR-Site

To reduce the pessimism in the safety assessment concerning corrosion due to the radiolysis of water, an experimental programme was conducted with the aim to provide a more detailed mechanistic understanding. Several experiments were performed in which copper samples were immersed in anoxic water and exposed to gamma radiation doses up to 95 kGy, i.e. doses representative of the repository (Björkbacka et al. 2012, 2013, Björkbacka 2015). The experiments were made using a ^{137}Cs gamma source and dose rates ranging between 0.02 and 0.3 Gy/s. These dose rates are considerably higher than the dose rate at the canister surface in the repository, which is at most 5×10^{-5} Gy/s (or 0.18 Gy/h) and decreasing with the decay, but were used in order to study the effects of full repository dose on a reasonable experimental time scale and to assess the amount of corrosion. The oxide film formed at the copper surface was mainly composed of cuprite (Cu_2O), although minor amounts of tenorite (CuO) were also identified. The oxide films were of varying thickness and on average at most a few hundred nm thick, as determined by cathodic reduction. For example, for a dose of 69 kGy (dose rate of 720 Gy/h) the oxide film was on average 307 nm thick (calculated assuming a compact Cu_2O film). Since the samples from this particular experiment were pre-oxidized and had an initial oxide layer of ca 46 nm, the oxide growth due to irradiation of water was on average 261 nm which corresponds to a corrosion depth of ca 157 nm (data from Table 4 in Björkbacka 2015). In addition, copper in the solution always corresponded to less than 10 nm of corrosion. Examination of the irradiated surfaces revealed circular localised corrosion features with diameters of up to a few tens of µm and depths of around 1 µm (Figure 8-1). When the copper specimens were pre-oxidised before irradiation, more irregular localised corrosion features were found after irradiation in water.

It can be concluded that the new set of experiments confirm that the approach used in the assessment of radiolytic corrosion in SR-Site was indeed pessimistic, overestimating the average corrosion depth due to radiolysis of water by at least one order of magnitude (~ 14 µm in SR-Site versus ~ 0.2 µm in Björkbacka 2015). It is noted that the corrosion observed in these experiments, both the oxide film thickness and the degree of localised corrosion, are finite and negligible contributions to the total corrosion of the canister, and that this corrosion corresponds to a repository-representative dose of gamma radiation. The impact of radiolytic corrosion on canister integrity is further discussed below in Section 8.6.
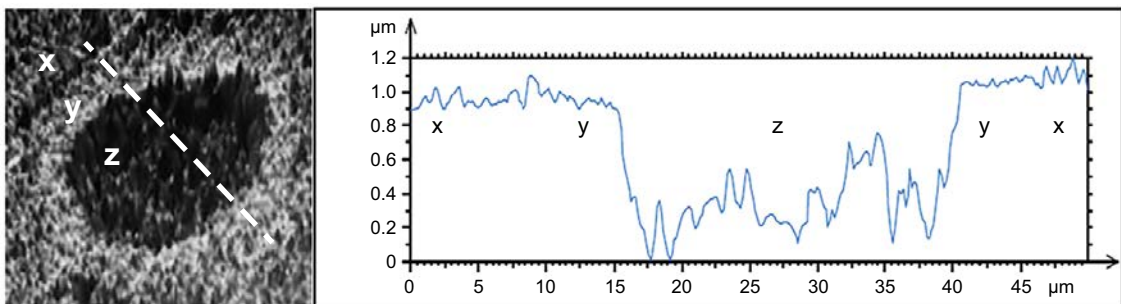

Figure 8-1. *Localised corrosion feature with a diameter of ca 20 µm and a depth of 1 µm. Features like this were formed on copper samples immersed in anoxic water and exposed to a gamma radiation dose of 62 kGy (Björkbacka et al. 2012).*

8.3   Further experimental studies of radiolytic corrosion and development of a mechanistic understanding

In the experiments performed by Björkbacka (2015) and referred to above, copper was exposed to gamma doses of ca 10−100 kGy, and cathodic reduction was used to measure the amount of oxide formed at the copper surface. It was found that the actual amount of oxide on a polished copper surface after irradiation was hundreds of times higher than the amount of oxide estimated by numerical models of the radiolytic formation of oxidants in solution. If the copper samples were pre-oxidised in air at elevated temperature before irradiation, resulting in an oxide layer much thicker than the native oxide film present on the polished copper, then the formation of oxide during irradiation was even more enhanced (Björkbacka 2015, Björkbacka et al. 2016). As a possible explanation for this mismatch between model and experiment, it was suggested that the radiation chemical yield of OH-radicals on the copper surface might be enhanced due to the presence and porous nature of the oxide film at the interface (Björkbacka et al. 2016).

It has recently been found that, contrary to what was earlier believed, neither the OH-radical nor H_2O_2 are the most important oxidants controlling the radiolytic corrosion of copper in water. In experiments with H_2O_2 of different concentrations, it was found that when leaving the copper samples in solution after the H_2O_2 had been quantitatively consumed, corrosion and growth of the oxide film continued for several days (Figur 8-2). In another experiment, for copper specimens of the same surface area, a given initial concentration of H_2O_2 and a given exposure time, the amount of oxide formed during exposure correlated with the volume of the experimental solution (Soroka and Jonsson 2019). Further-more, when exposing copper to H_2O_2 in solution and purging the solution with nitrogen gas, the cor-rosion was reduced (Soroka and Jonsson 2019). While the first result shows that there is an oxidant other than H_2O_2 that is involved in the corrosion, the third result suggests that this oxidant is volatile. Taken all together, these results point towards O_2 as being the dominating oxidant in the system.

In the earlier computational model attempting to describe the radiolytic corrosion of copper in water, it was assumed that the direct oxidation of copper by H_2O_2 by formation of Cu(II) and OH^- was kinetically more efficient than the catalytic decomposition of H_2O_2. This assumption has been used successfully to model the radiolytic surface reactivity of other materials, e.g. uranium. The formation of O_2 by catalytic decomposition was therefore not predicted by the earlier model. Molecular oxygen is not a direct radiolysis product of water, but forms during catalytic decomposition of H_2O_2 on oxide surfaces ($H_2O_2 \rightarrow H_2O + \frac{1}{2}O_2$). This reaction occurs via the reactions:

$H_2O_2 \rightarrow 2OH_{ad}$

$OH_{ad} + H_2O_2 \rightarrow H_2O + HO_2$
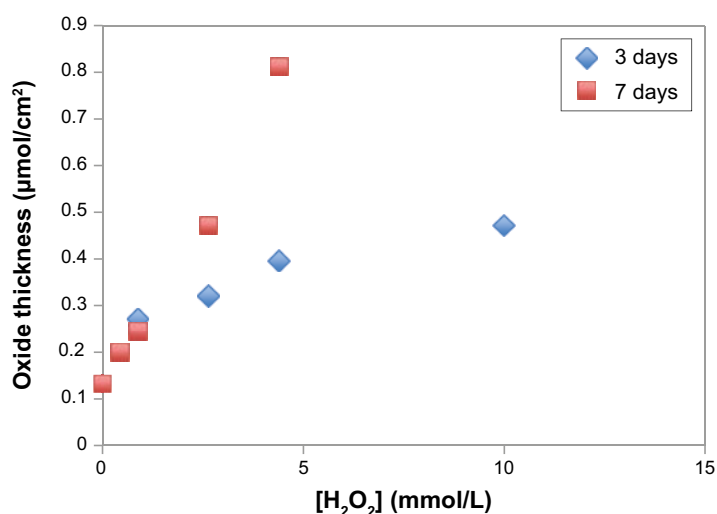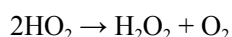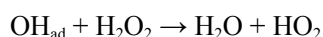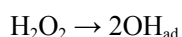
$2HO_2 \rightarrow H_2O_2 + O_2$

Figure 8-2. *Oxide thickness as a function of initial concentration of H_2O_2 measured after 3 and 7 days (Soroka and Jonsson 2019).*

Since the new experiments clearly point towards the formation of O_2 when H_2O_2 reacts with copper, a revised model have been set up such that the formation of O_2 via catalytic decomposition of H_2O_2 and the subsequent corrosion of copper by O_2 are included. The new model predicts oxide formation in much better agreement with experimental findings. For example, 62 nm oxide was formed on polished copper cubes (assuming a compact Cu_2O film) after exposure to a dose of 69 kGy given at a dose rate of 720 Gy/h (Table 5 in Björkbacka 2015), which can be compared to the prediction of the revised model of 54 nm oxide after exposure to 70 kGy given at a dose rate of 540 Gy/h (Soroka and Jonsson 2019).

For a dose of 100 kGy given at a dose rate of 1 Gy/h, i.e. only slightly higher than the initial dose rate at the canister surface, the new model predicts the formation of ca 1.4 μm Cu_2O, which corresponds to an average corrosion depth of ca 850 nm, due to gamma radiolysis of water. Since the new model is still being developed regarding details on the reactions to be included, this value should be regarded as preliminary. It is noted that the result corresponds to at least one order of magnitude less corrosion than what was pessimistically estimated due to radiolysis of water in SR-Site (~ 14 μm in SR-Site versus 0.85 μm in Soroka and Jonsson 2019).

8.4 Computational re-examination of the radiation induced damage estimated in SR-Site

The magnitude and effects of radiation damage in the KBS-3 canister materials, handled in SR-Site on the basis of the work by Guinan (2001), has been re-examined. Neutron and gamma radiation damage have been computed for both iron and copper in the configuration of the KBS-3 assembly (Yang et al. 2019).

These revised calculations take into account different types of photon-electron and neutron-ion interactions in a more complete manner than the approach used in earlier assessments. For example, the software used for computation of neutron-ion interactions (SPECTRA-PKA), allows a complete consideration of different reaction channels, whereas the code used by Guinan (SPECTER) had inherent simplifications. The work by Yang et al. also makes use of an updated nuclear database (TENDL). As input data for the revised neutron damage calculations, the neutron fluxes used in earlier assessments were compared with more recent data from SKB. Both PWR and BWR fuels, and different burnups were considered. The calculations of gamma radiation damage were also revised with improved methods. The gamma decay of fuel with a burn-up of 55 MWdays/kg U after 15 years of interim storage has been re-evaluated and was used in calculations of gamma radiation induced damage in the cast iron insert of the KBS-3 canister (Toijer 2014). In the case of elastic electron-nucleus scattering, sub-threshold effects were taken into account, not properly accounted for by Guinan (2001). These effects lead to some additional damage, however, the transferred energy is low enough to only create single Frenkel pairs (Yang et al. 2019). The effect of thermal annealing was, however, still not accounted for in these updated calculations.

The initial gamma damage rate in copper is of the order of 5×10^{-11} dpa/y (Yang et al. 2019), which is slightly lower than the initial damage rate estimated by Guinan (2001). The total integrated gamma radiation damage is calculated to be 2.4×10^{-9} dpa, which is also slightly lower than the accumulated gamma damage of 4×10^{-9} estimated by Guinan (2001). The most important aspect of these results is not that the revised calculations give lower values of gamma damage, but that the results are of the same order of magnitude and thus not sensitive to the choice of computer code or which data base that is used.

In agreement with earlier work, the revised calculations show that radiation damage due to neutron radiation is two orders of magnitude larger than the damage due to gamma radiation. Comparing the revised calculations by Yang and co-workers with the work by Guinan, the accumulated radiation damage in both copper and iron is of the same order of magnitude for all positions evaluated (inside and outside of both copper shell and iron insert) and any deviations are of the order of 3 % or less (Table 3-2 in Yang et al. 2019). It is important to note that neither Yang et al. (2019) nor Guinan (2001) took into account any effects of thermal annealing, which as discussed further in Section 8.5, has a pronounced affect by lowering the accumulated radiation damage by several orders of magnitude (Padovani et al. 2019).

Yang et al. (2019) analysed the possible impact of vacancy diffusion, which could potentially lead to the formation of irregular structures and surface reconstruction, and if so, could affect the corrosion morphology of the copper canister. It was concluded that even for an assessment time of 10^5 years, the mean diffusion distance would only be a few µm, which can be regarded as a negligible effect for the material properties of the copper shell. The authors also discussed the possibility of transmutation resulting in the formation of H and He atoms in the canister materials. In all cases considered in the analysis, regarding both canister materials and all positions, the formation of H and He due to transmutation were found to be of the order of 10^{-12} to 10^{-11} at.ppm after 10^5 years, which is many orders of magnitude lower than the hydrogen content of any copper or iron material.

8.5 Experimental attempts to verify low levels of damage in copper due to gamma radiation

Parallel with the work to re-examine the computational estimates of radiation damage, attempts were made to possibly verify very low levels of radiation damage experimentally (Padovani et al. 2019). Fully aware of that the estimated levels of accumulated damage in both Guinan (2001) and Yang et al. (2019) are extremely small, and that the actual damage is even lower due to thermal annealing of the material, the strategy was to examine irradiated copper material with sensitive methods and to verify the computational estimates of very low levels of radiation damage as best as possible considering the detection limits of the methods. The methods applied were both of a direct nature, i.e. methods that give structural information at the micro-structural or crystallographic level, and indirect methods, i.e. methods measuring some material property that could be affected by changes in the defect structure.

Copper samples made of high purity copper were irradiated with a ^{60}Co gamma source under argon atmosphere (Padovani et al. 2019). The samples were given a dose of 100 kGy gamma radiation, a dose that is representative for the copper canister in the spent fuel repository. In order to perform the irradiations on a reasonable timescale, the dose rates were enhanced to ca 10^3 Gy/h, meaning that a dose of 100 kGy could be achieved in less than a week of irradiation. Since the defect concentration in the irradiated material depends on the damage production rate (function of dose rate) as well as the thermal annealing of defects (function of temperature), the experimental conditions are highly accelerated as compared with the situation in the repository. The dose rate in the experiment is three orders of magnitude higher than the dose rate in the copper canister, and while the experiments were performed at room temperature, the temperature in the copper canister will be 50 to 95 °C for the period of significant irradiation. Theoretical considerations show that thermal annealing has a significant effect on the damage accumulation. The steady-state vacancy concentration will peak short after encapsulation and at levels many orders of magnitude lower than predicted in the calculations by Guinan (2001) and Yang et al. (2019), after which the concentration decreases due to the decay of the radioactive source. A detailed discussion of the effects of annealing is provided in Padovani et al. (2019).

After irradiation the copper samples were examined using High-Resolution Transmission Electron Microscopy (HR-TEM) and Positron Annihilation Lifetime Spectroscopy (PALS), in order to reveal any changes in the micro- or crystal-structure of the material. Nano-indentation measurements were performed in order to detect any changes in mechanical hardness or the elasticity modulus (Young's modulus), and electrical resistivity measurements were made in order to reveal effects on the material's electrical conductivity properties due to the irradiation.

Examination with HR-TEM showed no obvious difference in the micro-structure of the irradiated and reference samples. However, it was also noted that the reference material contained a relatively high concentration of dislocations, dislocation loops and stacking faults, which would have made it difficult to detect any differences if these were present at the low levels estimated computationally. The level of defects found in the reference material was probably due to cold work during fabrication of the commercial copper rods from which the samples were made.

The investigation with PALS detected no changes in the population or nature of defects after gamma irradiation. However, just like the measurements with HR-TEM, PALS also indicated a high concentration of dislocations in the samples (irradiated and reference material). A theoretical analysis indicated that the sensitivity required is about one or two orders of magnitude beyond the current capability of the technique.

Electrical resistivity measurements did not show any differences between irradiated and reference samples, meaning that the electrical conductivity properties of copper are not affected by absorption of 100 kGy gamma radiation. Regarding the defect structure of the material, a theoretical analysis of the merit of these measurements indicated that they are unlikely to have sufficient sensitivity to detect changes at the expected level. Rather, the detection limit of the resistivity measurements under the current conditions seems to have been of the order of 10^{-4} to 10^{-3} dpa (Padovani et al. 2019).

The nano-indentations did not reveal any significant difference in hardness or modulus (Figure 8-3) between irradiated and reference copper samples. Although the sensitivity to defects was insufficient to verify the very low numbers estimated computationally, the nano-indentations confirm the earlier conclusion that the radiation damage accumulated in copper by the repository dose is too small to give any measurable effects on the mechanical properties of the material (Guinan 2001).

In summary, the gamma radiation given to the copper material (100 kGy at a rate of 10^3 Gy/h) was found to have no measurable effects on the defect structure or properties of the material, within the sensitivity of the techniques applied. The damage estimates made by Guinan (2001) and Yang et al. (2019), and the damage levels remaining after thermal annealing of vacancies, are so minute that the experimental methods applied are unable to verify the estimated levels quantitatively. Nevertheless, these measurements confirm that the radiation damage in copper due to the repository dose is very low, and does not affect the mechanical or electrical conductivity properties of the material.

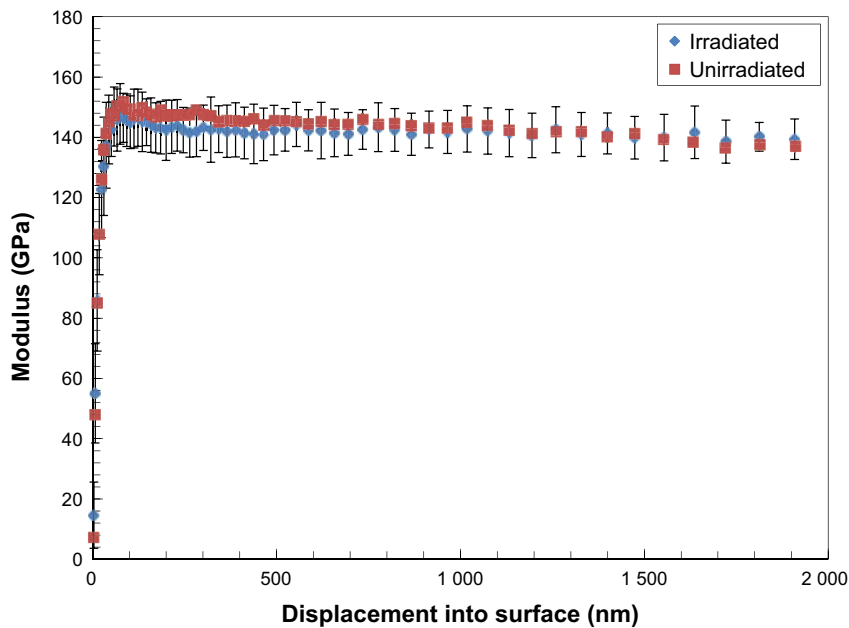***Figure 8-3.*** *Young's modulus of the copper material from the surface and 2 μm into the bulk, measured by nano-indentation. The measurements showed no significant difference between the irradiated and reference materials (Padovani et al. 2019).*

8.6 Assessment of the possible influence of radiation on material properties, localised corrosion, stress corrosion cracking and hydrogen embrittlement

8.6.1 Influence on material bulk properties

The damage accumulation in copper due to gamma and neutron irradiation in the KBS-3 canister assembly was computed independently by Guinan (2001) and Yang et al. (2019) to be of the order of 10^{-7} dpa. Since neither of the computational models applied accounted for thermal annealing of vacancies, the estimated level of damage is pessimistic. Theoretical analysis shows that thermal annealing of vacancies will have a significant effect on the vacancy concentration in the copper material (Padovani et al. 2019). The initial damage production rate is of the order of 10^{-10} dpa/y, but due to the efficiency of annealing the steady-state vacancy concentration will peak at levels many orders of magnitude below the computationally estimated 10^{-7} dpa within a month after encapsulation, after which the vacancy concentration will decrease with the decay of the source and the decreasing dose rate.

Comparison with earlier experimental investigations of the effects on the yield strength of copper after radiation exposure, showed that even the pessimistically estimated levels of radiation damage, computed without accounting for annealing, are at least one order of magnitude too small to have any measurable effects on the mechanical properties of the canister materials (Guinan 2001). Accounting for the efficiency of thermal annealing, as described above, the accumulated radiation damage in the copper canister material will be several orders of magnitude lower than that required to affect the mechanical properties of the copper shell.

Since the radiation damage is several orders of magnitude smaller than the concentration of any impurity in the material, the effects of radiation on segregation and redistribution of impurities in the material must be negligible (Guinan 2001). The maximum level of any impurity in the Cu-OFP is of the order 10^2 at.ppm and the radiation induced vacancy concentration will not exceed 5×10^{-11} dpa. Assuming first order kinetics, with respect to impurities and vacancies, the rate of interaction would depend on the product of these two low concentrations, i.e. a very small number ($10^{-4} \times 5 \times 10^{-11} = 5 \times 10^{-15}$), meaning that such interactions are very rare events and without any significance for the material properties. Overall it can be concluded that radiation from the spent fuel will not have any significant effects on the bulk properties of the copper material.

8.6.2 Influence on localised corrosion and SCC

The observation of shallow pits on the corroded copper surfaces after gamma irradiation might indicate that the surface has become passive during the exposure to very high gamma dose rates in water (Björkbacka et al. 2012). However, in the absence of the radiation field, the copper surface is very unlikely to passivate or remain passive under repository conditions. Literature studies of electrochemical data of copper electrodes in aqueous solutions have shown that conditions that support passivation of copper in aerobic environments, i.e. high concentration of carbonate in combination with low chloride concentrations, are far from repository conditions (King and Lilja 2014).

In addition to the requirement of high tensile stresses for the initiation of stress corrosion cracking (SCC), there are at least three aspects to consider when assessing the potential impact of radiation on the risk of SCC in the copper canister:

- Does the radiation from the spent fuel cause radiation damage (vacancies) in the copper material to such extent that its susceptibility to SCC is increased as compared with un-irradiated copper?

- Are potential SCC agents produced by radiolysis of the environment?

- Does irradiation induce passivation of copper and is the corrosion potential ennobled above the threshold potential for cracking?

In assessing these factors, it is also important to consider the role of the radiation dose rate, since effects observed at the high dose rates typically applied in laboratory experiments may not be relevant for the comparatively low dose rates experienced by the copper canister.

Concerning the effect of radiation on the susceptibility of copper to SCC due to changes of the microstructure or material properties, it was shown above that the extent of such damage is minimal. Therefore, it is not expected that radiation damage would increase the susceptibility of the copper canister material to SCC.

In principle, it is possible that ammonia and nitrite ions, known SCC agents for copper (King et al. 2010), could be produced by gamma irradiation of the repository environment since some residual air is present initially. Earlier studies of the corrosion of copper in humid aerobic environments under irradiation were reviewed in King (1996). Although small amounts of ammonia have been reported (at most 26 volume-ppm in vapour), the predominant radiolytic nitrogen-containing species detected was nitrate (NO_3^-), a species which is not known to cause SCC of copper. More recent studies of copper exposed to irradiated humid air confirm the formation of nitrate species but neither ammonia nor nitrite were reported (Björkbacka et al. 2017, Ibrahim et al. 2018). These later studies used gamma dose rates of between 0.35 and 10^3 Gy/h and the total doses ranged from 0.4 kGy to 100 kGy. Thus, irradiation experiments have been performed for both realistic and accelerated conditions and for total doses representative for the canister in the repository.

Stress corrosion cracking of copper under aerobic conditions is associated with a threshold potential (King and Newman 2010). Gamma irradiation can sometimes affect (ennoble) the corrosion potential of metals and alloys to more positive values as a result of the production of oxidising radiolysis products at the metal-solute interface. However, although Glass et al. (1986) reported a positive shift of ca 100 mV at a very high dose rate of 33×10^3 Gy/h, King and Litke (1987) observed no shift of the corrosion potential of copper specimens which were exposed to saline synthetic groundwater and a gamma dose rate of 27 Gy/h (i.e. two orders of magnitude higher than the gamma dose rate at the canister surface). In summary, gamma irradiation of copper at dose rates relevant to the copper canister in the repository, appear to produce neither significant amounts of SCC agents, nor oxidising radiolysis species to shift the corrosion potential of copper into the range for cracking.

In addition to the mechanistic arguments against SCC in copper due to gamma radiolysis at repository dose rates, perhaps the strongest argument against SCC is the absence of cracking in stressed copper specimens exposed to radiolytic environments in laboratory tests. Yunker (1990) and Yunker and Glass (1987) did not observe SCC of tear-drop specimens of two commercial oxygen-free grades of copper after exposure to irradiated moist air environments at 95 and 150 °C or in a dilute synthetic ground-water at 95 °C for exposure periods of up to 16 months. Dose rates of between 19 and 4.9×10^3 Gy/h were used with total doses exceeding 10^4 kGy, i.e. approximately 100 times higher than the dose absorbed by the copper canister in the repository. Similarly, no sign of cracking was observed on copper U-bend specimens exposed to either a moist vapour phase, synthetic groundwater, or compacted bentonite material at a more representative dose rate of 5 Gy/h (Johnson et al. 1996). These experiments were performed for periods up to 5 years, representing a total dose of the order of 40 kGy. The use of plastically deformed specimens in both of the studies referred to here, either in the shape of tear-drops or a U-bends, ensured the presence of high tensile stresses and represent a severe loading condition. In summary, both the lack of experimental indications of SCC in copper under simultaneous irradiation and tensile stress, and mechanistic considerations regarding the degree of radiation damage in the material and the corrosion potential under realistic dose rates, strongly points against any risk for SCC in the copper canister due to irradiation.

After absorption of 99.9 % of the gamma dose, the gamma dose rate has decreased to insignificant levels, and the repository has long since become anoxic. Corrosion will then be controlled by the diffusive transport of corroding species through the compact bentonite clay and specifically by the sulphide flux at the canister surface. Numerous studies have shown that oxygen containing corrosion products of copper (e.g. Cu_2O, CuO, and $Cu_2Cl(OH)_3$) are unstable in sulphide solutions, and that the copper oxides are converted to Cu_2S by chemical substitution of oxygen for sulphur (Smith et al. 2007, Höllmark et al. 2012, Kristiansen et al. 2015, Stenlid et al. 2017). When the sulphidation of oxygen containing corrosion products is complete, the sulphide driven corrosion of copper proceeds as described in SR-Site, controlled by the sulphide flux and with the morphology discussed in Chapter 5. Thus, on a longer time scale, passivity dependent localised corrosion phenomena, such as pitting or SCC, are not expected to be affected by the initially occurring radiolytic corrosion.

8.6.3 Influence on hydrogen embrittlement

The extent of radiation induced corrosion observed experimentally for a repository representative dose of 69 kGy was around 2 μmol electrons/cm^2 according to Björkbacka (2015). Assuming that the total dose is absorbed over a period of ca 100 years, this amount of corrosion corresponds to an average radiation induced corrosion rate of around 0.02 μmol/(cm^2 y) $\approx 6 \times 10^{-12}$ mol/(m^2 s). This flux is much smaller than the fluxes considered when discussing the possibility of hydrogen embrittlement due to

sulphide corrosion in Section 7.3.6. There, it was found that hydrogen embrittlement in copper due to sulphide corrosion is not a concern under repository conditions; the flux of hydrogen at the copper surface is too low due to the low concentration of sulphide and the transport resistance of the bentonite clay. Due to the even lower flux of hydrogen during radiolysis, the same conclusion can thus be drawn, however, with a larger margin for the possibility of radiation induced hydrogen embrittlement.

Lousada et al. (2016) reported on an uptake of hydrogen in 0.25 mm thin copper foils after gamma irradiation of up to 69 kGy at a rate of 486 Gy/h in anoxic water. The uptake of hydrogen was ca 0.2 wt.ppm, starting at a concentration of around 0.2 wt.ppm and resulting in a total concentration of 0.4 wt.ppm after gamma irradiation in water. As pointed out in Section 7.3.6, since neither the uptake of 0.2 wt.ppm hydrogen, nor the final value of 0.4 wt.ppm hydrogen after uptake is larger than the hydrogen concentration already present in the Cu-OFP (ca 0.6 wt.ppm), and since the effect is measured for a repository representative gamma dose, these results are not regarded as a risk for hydrogen embrittlement of the copper canister under repository conditions.

On the basis of experimental observations of hydrogen uptake in copper during gamma radiation, and the analysis of the hydrogen flux and uptake in Section 7.4, it is concluded that the flux of atomic hydrogen at the copper surface is too small to pose a risk for significant uptake of hydrogen and for embrittlement of the canister material.

8.7   Conclusions

The estimate of radiation damage underlying the safety assessment SR-Site have been verified using improved computer codes and an updated data base. Previous and revised calculations result in estimates of radiation damage of the same orders of magnitude. The initial damage production rate is of the order of 10^{-10} dpa/y for both neutron and gamma radiation. Neglecting effects of thermal annealing, the total accumulated radiation damage in the copper shell is pessimistically estimated to 10^{-7} dpa and is dominated by neutron radiation damage. The computed damage in the copper shell due to gamma radiation has a contribution of only 10^{-9} dpa. It is important to note here that thermal annealing will be very efficient, lowering the actual radiation damage by several orders of magnitude. It can thus be concluded that the estimate of radiation damage made in SR-Site was very pessimistic.

By theoretical considerations and comparisons with experimental literature data, it is concluded that radiation damage in copper will be several orders of magnitude too low to give measurable effects on mechanical properties of the material. Similarly, the vacancy concentration induced by radiation will not have any significant effect on the distribution or segregation of impurities in the Cu-OFP. These conclusions are further supported by measurements of the indentation hardness, elasticity modulus and the electrical resistivity of high purity copper before and after absorption of a repository representative dose of 100 kGy gamma radiation.

Corrosion due to gamma radiolysis is a very minor contribution to corrosion in the repository, corresponding to a few hundred nm for a repository representative dose of gamma radiation. This can be compared with the initial canister thickness of 5 cm. The degree of localised corrosion that has been observed is also minor and not much deeper than the average corrosion depth of a few hundred nm.

The lack of experimental observations of cracking in copper under simultaneous application of tensile stress and irradiation, strongly points against any risk for stress corrosion cracking (SCC) in the copper canister due to irradiation. Several mechanistic considerations support this view, e.g. the very low degree of radiation damage in the material and the absent effect on the corrosion potential under realistic dose rates.

The oxide film formed by radiolytic corrosion is unstable in sulphide solution and will be converted to copper sulphide. Whether localised corrosion occurs in the long run, is thus not determined by the gamma radiation exposure, but by the sulphide flux, as described further in Chapter 5. Thus, on a longer time scale, passivity dependent localised corrosion phenomena, such as pitting or SCC, will not be affected by the initially occurring radiolytic corrosion.

Applying the analysis of hydrogen flux and uptake developed in Section 7.4, and using experimental data from radiation exposure of copper in water, it was concluded that the flux of atomic hydrogen at the copper surface during gamma irradiation is too small to give a significant uptake of hydrogen.

9 Integration and evaluation of results

9.1 Introduction

In this chapter, findings regarding the five canister integrity issues are summarised in Section 9.2. An updated compliance calculation for the safety assessment of a KBS-3 repository at Forsmark is presented in Section 9.3. Further calculation results to demonstrate the robustness of the KBS-3 system against earlier-than-expected canister failures are provided in Section 9.4.

9.2 Summary of findings regarding canister integrity issues

The canister integrity issues brought up in the statement from the Land and Environmental Court to the Swedish Government (Section 1.1) are:

a) Corrosion due to reaction in oxygen-free water.

b) Pitting due to reaction with sulphide, including the influence of the sauna effect on pitting.

c) Stress corrosion cracking due to reaction with sulphide, including the influence of the sauna effect on stress corrosion cracking.

d) Hydrogen embrittlement.

e) The effect of radioactive radiation on pitting, stress corrosion cracking and hydrogen embrittlement.

In the preceding Chapters 3 to 8 these issues have been addressed with conclusions summarised in the following text and in Table 9-1.

As a background for the evaluations, a description of the repository environment is provided in Chapter 2 where the unsaturated and saturated buffer phases, as well as the eroded buffer case are discussed. A number of new studies support the extended description of the unsaturated conditions.

In Chapter 3 it is concluded that the sauna effect, in the form of significant salt accumulation as a consequence of vaporization of inflowing water from a fracture intersecting a deposition hole will not occur in a KBS-3 repository. The conclusions are based on laboratory studies, model calculations and field experiments. Thus, the conclusion is that the sauna effect will not occur in a KBS-3 repository at Forsmark and the process was, therefore, not included in the further analyses in this report.

In Chapter 4 it is concluded that there is no reason to assume that copper corrodes in pure, O_2-free water to an extent that exceeds that predicted by established thermodynamic data. The conclusion is based on a thorough evaluation of available scientific evidence on the matter. It was also concluded that data used by a few researchers to claim corrosion extents many orders of magnitude in excess of established scientific views would cause corrosion of only around one millimetre of copper during the one million year period covered by the safety assessment. Based primarily on the former of these two conclusions, corrosion of copper in pure, O_2-free water is not further considered in the present report, since established thermodynamic data predicts a corrosion depth under repository conditions that is completely negligible during the assessment period.

In Chapter 5 it is concluded that pitting corrosion due to sulphide exposure can be excluded since pitting corrosion requires the formation of a passive copper sulphide film on the copper surface, and such film formation has never been observed on copper in sulphide solutions under naturally corroding conditions (no applied electric potential), even in concentrations far above the highest observed and expected in the groundwater at Forsmark (1.2×10^{-4} mol/L). As regards other forms of localised corrosion, there are a few laboratory observations that have been interpreted as micro-galvanic corrosion of copper in sulphide solutions. When these laboratory conditions are translated to repository conditions, it cannot be conclusively ruled out that micro-galvanic corrosion could occur for the highest sulphide fluxes that could occur in the repository in the case of eroded bentonite buffer, as is further elaborated in Section 9.3.2. The occurrence of localised corrosion under a biofilm of SRB is also discussed and ruled out in Chapter 5, in particular based on the fact the groundwater at repository depth is not sufficiently rich in nutrients to support the formation of a biofilm and/or high metabolic activity of SRB. The conclusions in Chapter 5 are supported by several new studies.

In Chapter 6 it is concluded that simultaneous tensile stresses and sulphide exposure are not expected to jeopardise the canister integrity in the repository environment. Tensile stresses cannot be ruled out in parts of the canister during certain periods. In laboratory studies, microscopic fractures have been observed in the surfaces of copper specimens exposed to tensile stresses in combination with high concentrations of sulphide. When the conditions under which these observations were made are evaluated, it is concluded that the sulphide concentrations and fluxes required for the phenomenon to be observed, are such that they will not occur at the canister surface in the repository. Also, it is argued that the observed phenomenon is not an example of "traditional" stress corrosion cracking, SCC, but rather a kind of intergranular corrosion that appears only for very high sulphide fluxes when copper is subjected to high tensile stress. The conclusions in Chapter 6 are supported by several new studies.

In Chapter 7 it is concluded that hydrogen embrittlement will not jeopardise canister integrity in a KBS-3 repository. The conclusion is based on assessments of possible influxes of hydrogen generated in corrosion processes and an evaluation of experiments and model calculations of how such influxes would affect the metal. Exposure conditions leading to damaging effects in thin surface layers in laboratory experiments are much more aggressive than in the repository environment.

In Chapter 8 it is concluded that irradiation will cause insignificant levels of radiation damage in the canister materials. This is concluded on the basis of revised calculations of radiation damage and to some degree also demonstrated by new experiments. From experimental studies of radiolytic corrosion of copper and theoretical considerations it is concluded that radiation effects will have a negligible influence on localised corrosion (pitting), SCC and hydrogen embrittlement.

Table 9-1 shows the conclusions regarding the canister integrity issues for the unsaturated and saturated buffer phases of the repository development, as well as for the case of eroded buffer that may affect a few deposition holes in a 100 000 year perspective. In summary, four of the mentioned issues are assessed to not affect canister integrity, in line with the reasoning in SR-Site and supplementary information given to SSM during its review of SR-Site, and now supported by a range of new studies. One of the issues, the possibility of localised corrosion in the form of micro-galvanic effects during sulphide corrosion at high sulphide flux, cannot be categorically excluded at this time. This is further addressed in the next section.

9.3 Updated compliance calculation

9.3.1 Introduction

One of the localised corrosion mechanisms under consideration in this report (micro-galvanic corrosion) could not be conclusively ruled out according to Section 9.2, and it was not quantified in the safety assessment SR-Site. It should, therefore, as a cautious interpretation of available knowledge, be examined how it could affect the consequence and risk calculations of the safety assessment for a KBS-3 repository at Forsmark.

Two scenarios contributed to the calculated risk in SR-Site; the shear load scenario and the erosion/corrosion scenario, with the latter giving a tenfold higher risk contribution than the former, see Chapter 13 in SKB (2011) where the consequence and risk calculations for the SR-Site assessment are reported. In the erosion/corrosion scenario, the buffer is gradually lost to the flowing groundwater in fractures intersecting a deposition hole during periods when the groundwater is dilute. After a certain loss, requiring tens of thousands to hundreds of thousands of years, the hydraulic conditions in the deposition hole may become advective and the canister is directly exposed to the flowing groundwater. Corrosion due to sulphide is enhanced as a consequence and, after an additional period of typically several hundred thousand years, a few highly exposed canisters may fail. This scenario is analysed in detail with regard to canister integrity in Section 12.6 of SKB (2011) and with regard to dose consequences in Section 13.5 of the same report.

Table 9-1. Evaluation of canister integrity issues during the development of the buffer and canister system in a KBS-3 repository at Forsmark.

	Unsaturated buffer phase	Saturated buffer phase	Eroded buffer case
Time (years)	0–6 000	(0)–10^6	10^5–10^6
Canisters affected	All 6 000	All 6 000	~100
Peak sulphide concentration (mol/L)	10^{-6}*	10^{-4}**,†	$10^{-4,\,†}$
Peak sulphide flux (mol/(m² s))	~10^{-10}	~10^{-12}	10^{-9}
Sauna effect	Negligible	Not relevant	Not relevant
Corrosion in pure, O_2-free water	Excluded, based on evaluation of scientific evidence.		
"Pitting corrosion" (localised corrosion) — Pitting	Excluded, since conditions necessary for passive sulphide film formation do not occur.		
"Pitting corrosion" (localised corrosion) — Micro-galvanic corrosion	Excluded, based on sulphide flux and concentration.	Excluded, based on sulphide flux and concentration.	Excluded, except pessimistically for a few deposition holes with highest sulphide flux and concentrations.
"Pitting corrosion" (localised corrosion) — Biotic origin	Excluded based on buffer properties and lack of nutrients.	Excluded based on buffer properties and lack of nutrients.	Excluded based on lack of nutrients.
Stress corrosion cracking, SCC	Excluded based on lack of tensile stresses, sulphide concentration and flux.	Excluded based on sulphide concentration and flux.	Excluded based on sulphide flux.
Hydrogen embrittlement	Excluded based on low hydrogen flux at surface and absorption only to limited depth near surface.		
Radiation effects	Excluded due to insignificant levels of radiation damage and due to minor and finite corrosion effects.	**Gamma radiation** Excluded due to negligible radiation beyond ~300 years. **Neutron radiation** Effects on canister material and radiolysis of water negligible.	Excluded due to negligible radiation.

* In saturated backfill.
** In groundwater in contact with outer buffer boundary.
† Distribution with more than 97 % < 10^{-5} mol/L.

The compliance calculations for the erosion/corrosion scenario in SR-Site can be briefly summarised as follows:

- Three hydrogeological models, differing in the degree of correlation between fracture transmissivity and fracture size, were considered, see Section 10.3.6 in SKB (2011) for further details. These are termed the correlated, the semi-correlated and the uncorrelated hydrogeological models, respectively.

- Three variants of the handling of buffer erosion due to exposure to dilute groundwater were considered: *i*) no buffer erosion, *ii*) buffer erosion according to a quantitative model developed within the SR-Site project and *iii*) a bounding, pessimistic case where it was assumed that advective conditions prevailed in all deposition holes already at the time of repository closure.

- The case with no buffer erosion resulted in no canister failures. Therefore, only six corrosion variants, combining the three hydrogeological models with the two buffer erosion cases leading to canister failures, were quantified as regards dose consequences. Of these six, the combination of the correlated hydrogeological model with the assumption of no buffer initially resulted in the highest dose. This can be seen in Figure 13-40 of SKB (2011), reproduced as Figure 9-1 below. The curves represent mean values of probabilistically calculated cases.

- The probabilistically calculated mean dose consequences should be compared to the annual dose (14 µSv) corresponding to SSM's limit on annual risk (10^{-6}) for harmful effects on individuals living in the vicinity of the repository (SSM 2008). In principle, the result of several calculation cases could be weighted by their probability of occurrence, whereas in SR-Site the pessimistic approach of assigning a probability of one to the case with the highest consequences was taken.

The calculated dose consequences in SR-Site for the six combinations that resulted in canister failures are shown in Figure 9-1. In the following, the cases yielding the highest consequences in SR-Site for initial advection and for the SR-Site erosion model, i.e. the two cases applying the correlated hydrogeological model (the brown and yellow curves in Figure 9-1), are updated such that localised corrosion is taken into account. The modifications done to the two SR-Site cases to accomplish this are described in the next section.

9.3.2 Handling of localised corrosion under repository conditions

Sulphide concentrations

The lowest sulphide concentration at which pit formation interpreted as micro-galvanic corrosion is observed (5×10^{-4} mol/L, see Section 5.4.2) is a factor of 4 higher than the highest concentration expected in the groundwater at repository depth (1.2×10^{-4} mol/L, see Section 2.2.4). No pits have been observed at 5×10^{-5} mol/L, a concentration that is higher than 97 % of the sulphide concentrations analysed in the groundwaters at repository depth at Forsmark. Furthermore, micro-galvanic corrosion is related to the formation of a compact (albeit not passivating) film, and such film formation has not been observed for sulphide concentrations up to 10^{-4} mol/L.

The highest groundwater sulphide concentration (1.2×10^{-4} mol/L) might be an outlier as compared with the set of measurements from the Forsmark site, but was still cautiously included in the corrosion calculations in SR-Site. With a strict combination of available experimental results with measured sulphide concentrations at Forsmark, micro-galvanic corrosion can thus not be conclusively ruled out at the Forsmark site, based on groundwater concentrations.
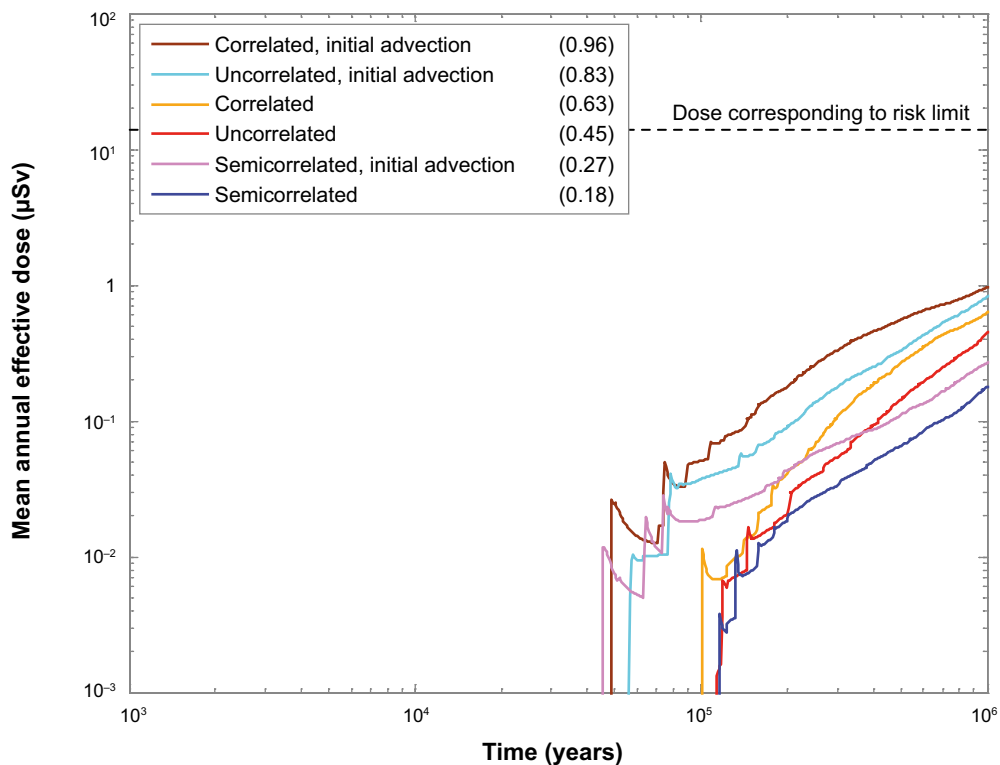

Figure 9-1. *The six cases of the erosion/corrosion scenario used to demonstrate compliance with SSM's risk criterion in SR-Site. The numbers within parentheses in the legend are the peak annual doses for the curves. (The figure is identical to Figure 13-40 in SKB (2011), except that, for clarity, two curves that were used for other purposes have been removed here.)*

Sulphide fluxes

The groundwater concentration of sulphide is, however, not a sufficient factor to consider when evaluating the potential occurrence of micro-galvanic corrosion in a repository, since the canister will generally not be in direct contact with the groundwater, and will hence not be exposed to the sulphide concentrations of the groundwater. It is rather the sulphide flux to the canister surface that is of interest, and this is determined by the transport conditions in the buffer together with the abundance of sulphide. When this is taken into account, the sulphide flux above which micro-galvanic corrosion cannot be excluded (3×10^{-10} mol/(m^2 s), see Section 5.5.1) is higher than the highest expected flux under unsaturated buffer conditions (7×10^{-11} mol/(m^2 s)) and much higher than the highest flux expected under saturated buffer conditions (around 1.5×10^{-12} mol/(m^2 s)). However, a few deposition holes exposed to the highest sulphide fluxes for the eroded buffer case could experience fluxes that exceed the lowest threshold (3×10^{-10} mol/(m^2 s)) for formation of compact films. Thus, based also on a consideration of sulphide fluxes, micro-galvanic corrosion needs to be included for the eroded buffer case, but not for the other two phases of repository evolution.

Pitting factor

As shown in Section 5.4.2, an evaluation of pit depths from the experimental results shows that the deepest observed pits are less than 20 times deeper than the general corrosion depth, with most pits being much shallower. The deepest pits observed were ca 6 μm. A pessimistic way of addressing micro-galvanic corrosion would thus be to apply a pitting factor of 20, for the period that the sulphide flux in the repository exceeds the threshold value of 3×10^{-10} mol/(m^2 s) for the eroded buffer case. This is pessimistically assumed to apply all the way to penetration of the 5 cm copper shell. No lateral expansion of the pit is assumed, which is also pessimistic.

In the probabilistic consequence calculations in SR-Site, distributions of sulphide concentrations are combined with the distribution of groundwater fluxes at deposition holes to yield a distribution of sulphide fluxes and hence canister failure times. It is only the highest sulphide concentrations combined with the highest flow rates that yielded failures within the one million year assessment time.

For the few canisters experiencing a flux exceeding 3×10^{-10} mol/(m^2 s), a pitting factor of 20 is now applied in the corrosion calculations. A flux of 3×10^{-10} mol/(m^2 s) corresponds to a corrosion penetration time of 5 cm copper of roughly 350 000 yr without pitting, assuming that Cu$_2$S is the formed corrosion product.

Buffer conditions

One additional modification is made to the SR-Site calculations. When selecting the three buffer erosion variants, it was possible in SR-Site to very pessimistically choose a bounding case where the buffer was already lost for all canisters at the time of deposition (together with the more realistic case where the extent of buffer loss over time was modelled). It was possible to apply this pessimistic, bounding case since the canister failure times were of the order of hundreds of thousands of years. In comparison, the modelled times required to reach advective conditions due to buffer erosion were much shorter so that the difference between including them as modelled or neglecting them was relatively insignificant, as shown in the results in Figure 9-1. If, however, micro-galvanic corrosion is included as described above, several canister failure times will become considerably shorter than the time to reach advective conditions in these deposition holes. To address this, the bounding pessimistic case is set to a buffer erosion time of 20 000 years for the cases that include micro-galvanic corrosion.

This time of 20 000 years was the length of the initial temperate climate period used in SR-Site. This time is much shorter than the shortest modelled time for buffer erosion (around 75 000 years for the correlated hydrogeological model, which produced the highest consequences in the SR-Site calculations) and the modelled times to reach advective condition are in general considerably longer than 75 000 years. The reason for relating the selected time for the pessimistic bounding case to the duration of the current temperate period is that it may be expected that future glacial conditions could lead to changes in groundwater chemistry (decreased salinity) that favour buffer erosion. For the initial 20 000 years of temperate conditions, the analyses in SR-Site showed that groundwater salinity is sufficient to prevent buffer erosion although a certain decrease in salinity occurs during this period.

In addition, the case with modelled times to reach advective conditions as in SR-Site will be calculated.

9.3.3 Calculation results

The results of the updated calculations, with the procedures described in Section 9.3.2 are shown in Figure 9-2. The two curves represent updates of the cases "Correlated, initial advection" and "Correlated" in Figure 9-1. As seen, the peak annual doses (given in units of μSv within parentheses) do not differ much from the values of the corresponding SR-Site cases, and they are well below the dose corresponding to SSM's regulatory risk limit. The case combining early advection with micro-galvanic corrosion leads to notably earlier releases than the corresponding case without micro-galvanic corrosion. This is expected since the penetration times for a few canisters experiencing the highest sulphide fluxes are reduced by a factor of 20 due to localised corrosion penetration. For the case where the buffer erodes according to the SR-Site model, the penetration times are reduced in the same way, but the onset of corrosion is delayed by the calculated time to reach advective conditions, meaning that the shift towards earlier failure times is less pronounced. The results represent a statistical mean value taken over the distribution of sulphide concentrations and groundwater flow rates at the 6 000 deposition holes. As a statistical average, less than one canister contributes to the calculated dose.

The following points are noted.

- In all consequence calculations in this report, Rn-222 and Po-210 are included in the U-238 decay chain as implemented and described in a supplementary report (Appendix 1 in SKB 2015) to SSM during the review of SR-Site. (These nuclides were omitted in the original SR-Site calculations, and the increase in calculated dose by including them is less than 15 %.)

- The calculation is done for steady state groundwater flow rates occurring during temperate conditions. Higher transient groundwater flow rates could occur temporarily when an ice sheet margin passes over the repository area in the future. During such periods, the groundwater is expected to be diluted by glacial meltwaters (free of sulphide) to an extent comparable to the increase in flow rate, meaning that the sulphide flux should be essentially unaltered.

- The handling of micro-galvanic corrosion in the calculations is, as seen in Section 9.3.2 pessimistic, in particular regarding the pitting factor. The phenomenon will be further studied in order to be able to address it in a more realistic manner in future safety assessments.
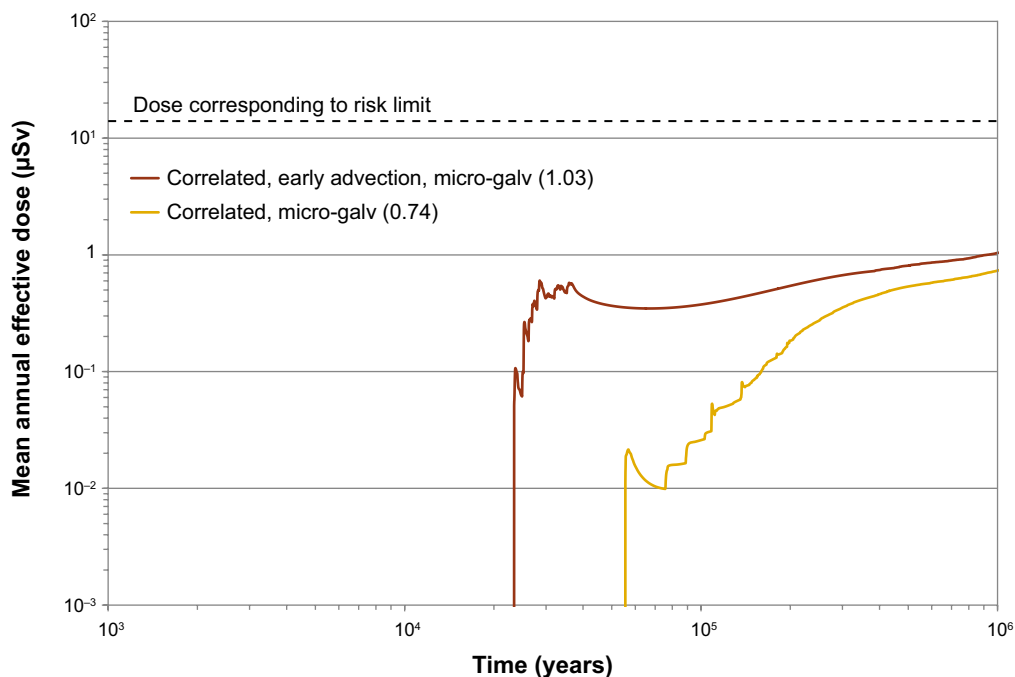

Figure 9-2. Probabilistically calculated mean annual effective dose for the case with a pessimistic representation of micro-galvanic corrosion. The numbers within parentheses in the legend are the peak annual doses for the curves.

9.4 Robustness calculation

In the context of this report it is also of interest to illustrate the robustness of the KBS-3 system to canister failure mechanisms and canister integrity in general. Such illustrations are provided in this section. A bounding case where all canisters fail at an early stage is analysed, as well as a variant, in which the buffer is also assumed to fail as a result of erosion. Neither of the variants is in any way compatible with the findings in the preceding chapters, and are only discussed here to put the canister integrity issues in an overall safety perspective. A range of cases with a similar purpose were analysed in the safety assessment SR-Site.

9.4.1 Failure modes

In the safety assessment SR-Site, a number of so called "what if" cases, illustrating the consequences of hypothetical losses of barrier function, were analysed, see Section 13.7.3 in SKB (2011). Cases illustrating hypothetical losses of canister integrity included one where all canisters were assumed to have large (tens of centimetres in diameter) penetrating holes initially and one where the initial defects were assumed to be millimetre-sized penetrating defects or fractures.

It is difficult to conceive of a naturally occurring failure mechanism that would immediately lead to a large failure. Even failures due to mechanical impacts of earthquakes as analysed in SR-Site would start as a fracture in the copper shell and gradually develop into a larger failure. Therefore, the hypothetical case with initial, small penetrating defects or fractures is used here.

In this case, the buffer is assumed to be water saturated, meaning that a slow ingress of water into the canister interior starts immediately. Based on earlier modelling of the buffer and canister interior (Bond et al. 1997), the canisters are assumed to be water filled after 1 000 years, so that a continuous path for radionuclide transport is established and by which radionuclides may leave the canister. The intruding water will also cause the cast iron insert of the canister to corrode and the corrosion products are expected to exert a pressure on the canister parts. Based on extensive modelling (Bond et al. 1997), this is pessimistically assumed in the SR-Site assessment (SKB 2010b, Section 4.2) to lead to a sudden widening of the initially small defect in the copper shell after 10 000 years. The widening is assumed to be such that neither the insert nor the copper shell offers any transport resistance for radionuclides after this point in time.

Radionuclides embedded in the fuel matrix and as activation products in metal parts of the fuel are released congruently with the dissolution of the fuel matrix and the corrosion of the metal parts, respectively. A minor fraction of the nuclides is more readily accessible and released immediately when water contacts the fuel. Radionuclides released from the canister are retarded by sorption in the buffer and the geosphere, before a fraction of the release may reach the biosphere.

Another barrier failure considered in SR-Site regards bentonite loss due to erosion, as mentioned in Section 9.3.1. When the buffer is exposed to dilute groundwater, it may be eroded. In the deposition holes experiencing the highest groundwater flow rates, the extent of erosion may be such that advective conditions arise in the deposition holes after tens of thousands to hundreds of thousands of years. This type of buffer failure is also considered in the following.

9.4.2 Biosphere model

The what-if cases in SR-Site were calculated with *i*) pessimistically selected constant peak dose conversion factors, so called landscape specific dose conversion factors (LDFs, used in the calculations in Section 9.3) and *ii*) with less pessimistic temporally developing biosphere models where the temporal development of the biosphere due to land-uplift is explicitly modelled in the consequence calculations. This latter dynamic biosphere is a considerably more realistic representation of the biosphere development than the pessimistically chosen constant conversion factors, in particular for cases where a large number of canisters are involved. The development covers the land-uplift during the present temperate climate period and then reaches an essentially steady state.

Since the SR-Site assessment, additional site-specific data for the biosphere at the Forsmark site have been obtained and applied in an assessment of the repository for short-lived low and intermediate level waste at Forsmark (SKB 2014), thus replacing much of the generic biosphere data used in SR-Site. These data are also used in the present what-if analysis. The updates concern biosphere distribution coefficients (K_d values) and concentration ratios (CR values), see further Saetre (2019a,b). In particular, the updated parameters for iodine and selenium are more favourable for post-closure safety, whereas those for radium, the element that dominates in the very long-term compliance cases in the SR-Site assessment through the isotope Ra-226, is slightly less favourable.

The dynamic model with updated input data is used in the "what if" calculation where all canisters fail. It is stressed that the more pessimistic approach with LDF values taken from SR-Site was used in the compliance calculations in Section 9.3.

9.4.3   Case definitions

In the following, two cases, A and B, are modelled to illustrate the consequences of early canister failures.

A. All canisters are assumed to have an initial, penetrating hole of diameter 4 mm, i.e. they are already failed at deposition. The rest of the system is assumed to be intact throughout the assessment period.

B. All canisters are assumed to have an initial, penetrating hole of diameter 4 mm, i.e. they are already failed at deposition. The buffer surrounding the canisters is assumed to be eroded according to the model for buffer erosion used in the safety assessment SR-Site.

In both cases, as in the SR-Site assessment, the small, initial failure is assumed to lead to the development of a continuous transport path after 1 000 years and the initially small defect is assumed to develop into a large (10 cm diameter) hole after 10 000 years.

As mentioned in Section 9.3.1, three hydrogeological models for the geosphere were considered in the SR-Site assessment, distinguished by the way in which fracture transmissivities were modelled to be correlated to fracture sizes in the network of discrete, water-bearing fractures in the geosphere. The so called semi-correlated model, which was considered to be the closest representation of reality, is applied in the "what-if" cases here, as was done in the SR-Site what-if cases.

The biosphere is modelled dynamically, making use of the site-specific data derived after SR-Site, as discussed above.

All other data are the same as in the safety assessment SR-Site. The assessment time is one million years after closure, as in SR-Site, and the modelled consequences are compared with SSM's risk criterion. The risk criterion corresponds to a dose that is about one percent of the natural background radiation in Sweden. It is applicable for 100 000 years after repository closure and SSM's regulations also suggest that the criterion should be used together with other indicators to assess the protective capacity of the repository up to one million years after closure.

9.4.4   Results

Figure 9-3 and Figure 9-4 show results of the calculated consequences of case A and B, respectively. The following points are noted:

•   The calculated risk is below the risk criterion throughout the one million year assessment period for both cases.

•   The differences between cases A and B are small, in part because only around 20 deposition holes out of the 6 000 lose buffer due to erosion to the extent that advective conditions arise, whereas the release from the remaining canisters evolve in the same way in cases A and B.

•   The continuous rise of Cs-135 is due to accumulation in the biosphere throughout the assessment time, which is not realistic. In reality, the biosphere is expected to be more or less eradicated by glaciers at least every 100 000 year or so.

- The result of case A is, beyond ~50 000 years, quite similar to that of a "what if" cases in the SR-Site assessment calculated with constant dose conversion factors that take the distribution in the landscape into account, Figure 13-62 in SKB (2011). The only notable exceptions concern the I-129 and Se-79 doses, that are lower due to the use of site specific biosphere data obtained after the completion of the SR-Site assessment as described above. This also affects the total dose since these two nuclides dominate the SR-Site case in the long term. The updated biosphere data are expected to affect the values of the constant conversion factors in a similar way when they are updated in future assessments.

The cases are not comparable to strict compliance cases, since uncertainties concerning e.g. the hydrogeological modelling and the extent of buffer erosion have not been fully explored. Neither are such cases foreseen to be included as compliance cases in SKB's forthcoming safety assessments of a KBS-3 repository, since they are based on completely unrealistic assumptions regarding early canister failures.

The cases do, however, give a clear indication that, even with such assumptions, the performance of the repository is on a par with SSM's risk criterion. Also, there are several pessimistic assumptions behind the biosphere model in that e.g. the landscape features to which the releases occur are expected to be fully exploited by local populations, thereby maximizing the doses.

In summary, it is concluded that a considerable protective capacity is provided by other parts of the repository if hypothetically all canisters fail prematurely.
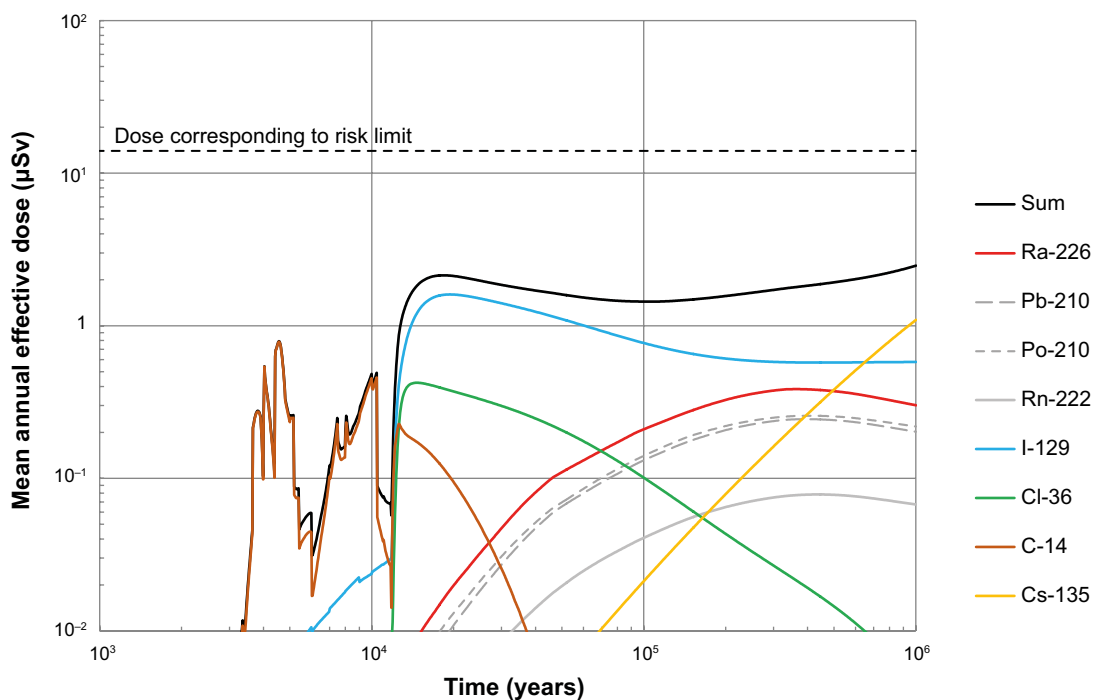
Figure 9-3. *Consequences of what-if case A where all canisters have an initial, small penetrating defect. The relatively rapid variations of the C-14 dose are due to the biosphere development caused by land up-lift in the first few thousand years after repository closure.*

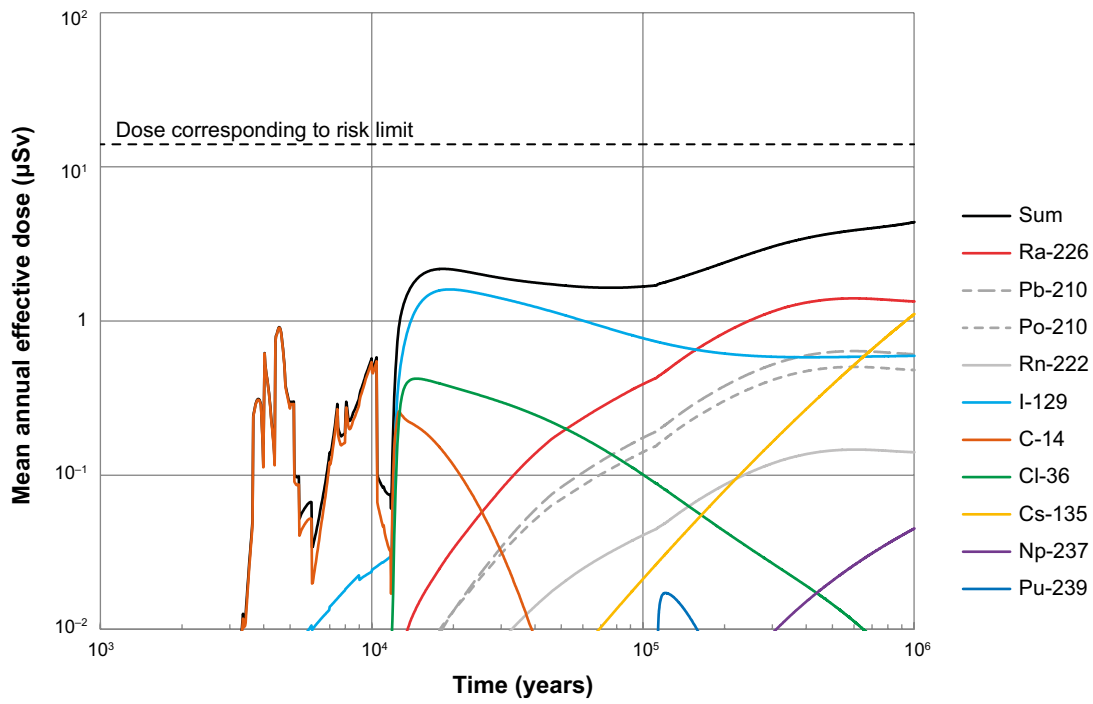***Figure 9-4.*** *Consequences of what-if case B where all canisters have an initial, small penetrating defect and where the buffer is gradually lost in the deposition holes with the highest groundwater flow rates.*

10   Conclusions

As described in Section 1.1, the Land and Environmental Court has in its statement to the Swedish Government expressed that supplementary information regarding five issues related to the long-term integrity of the copper canisters be presented and evaluated before a licence for a final repository for spent nuclear fuel at the Forsmark site is considered. It was also stated that if uncertainties in terms of the protective capacity of the canister remain after evaluation of such supplementary information, these need to be included in the safety assessment calculations for the final repository.

Supplementary information on the five canister integrity issues has been presented in this report. The presentation builds on around 20 new reports and Memoranda from a range of experimental and theoretical investigations. It has been possible to present the material within about a year of the Court's statement since work was on-going in all the areas, as the issues were identified and subject to studies and reviews long before the Court hearing. Also, in response to the Court statement, the efforts in these areas were intensified.

As summarised in Section 9.2, the conclusion from the evaluation of the new and earlier studies is that four of the five issues are assessed to not have any significant impact on canister integrity. This concerns copper corrosion in pure, O_2-free water, stress corrosion cracking during sulphide exposure, hydrogen embrittlement and radiation effects on corrosion phenomena. For some phenomena, detrimental effects may have been observed in relatively aggressive laboratory tests, whereas the final repository provides an environment where the effect would not occur or be much milder.

One issue, localised corrosion in the form of micro-galvanic sulphide corrosion, could not be conclusively ruled out for the highest sulphide fluxes that could be expected in the repository environment. An updated dose consequence calculation based on a pessimistic interpretation of available data on micro-galvanic pit formation was carried out in Section 9.3. The results of the calculation demonstrate that the calculated peak dose is only marginally affected compared to the value in the safety assessment SR-Site, meaning that the corresponding risk is still below SSM's risk criterion by about one order of magnitude.

The robustness of the repository system to canister integrity issues is demonstrated in a couple of hypothetical calculation cases in Section 9.4. It is demonstrated that even if all canisters are hypothetically assumed to fail by penetration at a very early stage, the calculated risk is still on a par with SSM's risk criterion.

Some of the issues will be further pursued in SKB's RD&D programme. Among other things, it is of interest to be able to handle the issue of micro galvanic corrosion less pessimistically in the safety assessment, and this requires further studies of the phenomenon.

The overall result of the work presented in this report is that the main conclusion in the safety assessment SR-Site is unaltered: A KBS-3 repository built at the Forsmark site will fulfil SSM's requirements on post closure safety.

References

SKB's (Svensk Kärnbränslehantering AB) publications can be found at www.skb.com/publications.
SKBdoc documents will be submitted upon request to document@skb.se.

Aaltonen P, Jagodzinski Y, Tarasenko A, Smouk S, Hänninen H, 1998. Low-frequency internal friction of pure copper after anodic polarisation in sodium nitrite solution. Corrosion Science 40, 903–908.

Aaltonen P, Jagodzinski Y, Hänninen H, 2003. Vacancy generation in electrochemical oxidation/dissolution of copper in $NaNO_2$ solution and its role in SCC mechanism. Hydrogen effects on material behavior and corrosion deformation interactions. In Moody N R, Thompson A W, Ricker R E, Was G W, Jones R H (eds). Proceedings of the International Conference on Hydrogen Effects on Material Behavior and Corrosion Deformation Interactions, Jackson Lake Lodge, Wyoming, 22–26 September 2002. The Minerals, Metals & Materials Society, 597–606.

Al Kharafi F M, Ghayad I M, Ateya B G, 2008. Rapid intergranular corrosion of copper in sulfide-polluted salt water. Electrochemical and Solid-State Letters 11, G15–G18.

Andersson-Östling H C M, Sandstrom R, 2009. Survey of creep properties of copper intended for nuclear waste disposal. SKB TR-09-32, Svensk Kärnbränslehantering AB.

Arilahti E, Lehtikuusi T, Olin M, Saario T, Varis P, 2011. Evidence for internal diffusion of sulphide from groundwater into grain boundaries ahead of crack tip in Cu OFP copper. Corrosion Engineering, Science and Technology 46, 134–137.

ASTM, 2016. ASTM B577-16: Standard test methods for the detection of cuprous oxide (hydrogen embrittlement susceptibility) in copper. West Conshohocken, PA: ASTM International.

Becker R, Hermansson H-P, 2011. Evolution of hydrogen by copper in ultrapure water without dissolved oxygen. Stockholm: Swedish Radiation Safety Authority. (SSM 2011:34)

Becker R, Öijerholm J, 2017. Slow strain rate testing of copper in sulfide rich chloride containing deoxygenated water at 90 °C. Stockholm: Swedish Radiation Safety Authority. (SSM 2017:02)

Bengtsson A, Pedersen K, 2017. Microbial sulphide-producing activity in water saturated Wyoming MX-80, Asha and Calcigel bentonites at wet densities from 1 500 to 2 000 kg m^{-3}. Applied Clay Science 137, 203–212.

Bengtsson A, Edlund J, Hallbeck B, Heed C, Pedersen K, 2015. Microbial sulphide-producing activity in MX-80 bentonite at 1 750 and 2 000 kg m^{-3} wet density. SKB R-15-05, Svensk Kärnbränslehantering AB.

Bengtsson A, Blom A, Hallbeck B, Heed C, Johansson L, Stalén J, Pedersen K, 2017a. Microbial sulphide-producing activity in water saturated MX-80, Asha and Calcigel bentonite at wet densities from 1 500 to 2 000 kg m^{-3}. SKB TR-16-09, Svensk Kärnbränslehantering AB.

Bengtsson A, Blom A, Taborowski T, Schippers A, Edlund J, Kalinowski B, Pedersen K, 2017b. FEBEX-DP: Microbiological report. Nagra Arbeitsbericht NAB 16–15, Nagra, Switzerland.

Bhaskaran G, Carcea A, Ulaganathan J, Wang S, Huang Y, Newman R C, 2013. Fundamental aspects of stress corrosion cracking of copper relevant to the Swedish deep geologic repository concept. SKB TR-12-06, Svensk Kärnbränslehantering AB.

Birgersson M, Goudarzi R, 2013. Studies of vapor transport from buffer to tunnel backfill (Sauna effects). SKB R-13-42, Svensk Kärnbränslehantering AB.

Birgersson M, Goudarzi R, 2016. Vapor transport and sealing capacity of buffer slots ("sauna" effects). SKB TR-15-09, Svensk Kärnbränslehantering AB.

Birgersson M, Goudarzi R, 2017. Summary report on "sauna" effects. SKB TR-17-07, Svensk Kärnbränslehantering AB.

Birgersson M, Goudarzi R, 2018. Investigations of gas evolution in an unsaturated KBS-3 repository. SKB TR-18-11, Svensk Kärnbränslehantering AB.

Birgersson M, Karnland O, 2009. Ion equilibrium between montmorillonite interlayer space and an external solution – Consequences for diffusional transport. Geochimica et Cosmochimica Acta 73, 1908−1923.

Björck M, Elger R, 2013. Oxidation kinetics of copper at reduced oxygen partial pressures. SKBdoc 1410172 ver 1.0, Svensk Kärnbränslehantering AB.

Björck M, Pehkonen H, Vuori L, Tigerström M, Lahtonen K, Valden M, Purhonen T, Cederqvist L, 2017. Evaluation of a gas shield for friction stir welding of copper canisters. Posiva SKB Report 02, Posiva Oy, Svensk Kärnbränslehantering AB.

Björck M, Taxén C, Vuoristo T, Elger R, Zavalis T, Wikström L, Sparr M, 2019. Embedded oxide particles in FSW. Posiva SKB Report 10, Posiva Oy, Svensk Kärnbränslehantering AB.

Björkblad A, Faleskog J, 2018. Evaluation of Cu-OFP creep crack growth and theoretical fracture models for Cu-OFP. Posiva SKB Report 03, Posiva Oy, Svensk Kärnbränslehantering AB.

Björkbacka Å, 2015. Radiation induced corrosion of copper. PhD thesis. Royal Institute of Technology, Sweden.

Björkbacka Å, Hosseinpour S, Leygraf C, Jonsson M, 2012. Radiation induced corrosion of copper in anoxic aqueous solution. Electrochemical and Solid-State Letters 15, C5–C7.

Björkbacka Å, Hosseinpour S, Johnson M, Leygraf M, Jonsson M, 2013. Radiation induced corrosion of copper for spent nuclear fuel storage. Radiation Physics and Chemistry 92, 80−86.

Björkbacka Å, Johnson C M, Leygraf C, Jonsson M, 2016. Role of the oxide layer in radiation-induced corrosion of copper in anoxic water. The Journal of Physical Chemistry C 120, 11450−11455.

Björkbacka Å, Johnson C M, Leygraf C, Jonsson M, 2017. Radiation induced corrosion of copper in humid air and argon atmospheres. Journal of The Electrochemical Society 164, C201–C206.

Boman M, Ottosson M, Berger R, Andersson Y, Hahlin M, Björefors F, Gustafsson T, 2014. Corrosion of copper in ultrapure water. SKB R-14-07, Svensk Kärnbränslehantering AB.

Bond A E, Hoch A R, Jones G D, Tomczyk A J, Wiggin R W, Worraker W J, 1997. Assessment of a spent fuel disposal canister. Assessment studies for a copper canister with cast steel inner component. SKB TR 97-19, Svensk Kärnbränslehantering AB.

Camacho A, 2009. Sulfur bacteria. In Likens G E (ed). Encyclopedia of Inland waters. Amsterdam: Elsevier/Academic Press.

Camurri C, Carrasco C, Leite R, Mangalaraja R, Dille J, 2012. Influence of impurities in Cathodic Copper on the ductility of copper wires. Journal of Materials Engineering and Performance 21, 1474−1478.

Carslaw H S, Jaeger J C, 1959. Conduction of heat in solids. 2nd ed. Oxford: Oxford University Press.

Chen H-B, Yan K, Lin T, Chen S-B, Jiang C-Y, Zhao Y, 2006. The investigation of typical welding defects for 5456 aluminum alloy friction stir welds. Materials Science and Engineering A 433, 64−69.

Chen J, Qin Z, Shoesmith D W, 2010. Kinetics of corrosion film growth on copper in neutral chloride solutions containing small concentrations of sulfide. Journal of The Electrochemical Society 157, C338–C345.

Chen J, Qin Z, Shoesmith D W, 2011. Long-term corrosion of copper in a dilute anaerobic sulfide solution. Electrochimica Acta 56, 7854−7861.

Chen J, Qin Z, Shoesmith D W, 2014. Key parameters determining structure and properties of sulphide films formed on copper corroding in anoxic sulphide solutions. Corrosion Engineering, Science and Technology 49, 415−419.

Chen J, Qin Z, Martino T, Shoesmith D W, 2017a. Effect of chloride on Cu corrosion in anaerobic sulphide solutions. Corrosion Engineering, Science and Technology 52, 40−44.

Chen J, Qin Z, Martino T, Shoesmith D W, 2017b. Non-uniform film growth and micro/macro-galvanic corrosion of copper in aqueous sulphide solutions containing chloride. Corrosion Science 114, 72−78.

Chen J, Qin Z, Martino T, Guo M, Shoesmith D W, 2018. Copper transport and sulphide sequestration during copper corrosion in anaerobic aqueous sulphide solutions. Corrosion Science 131, 245–251.

Chen J, Guo M, Martino T, Ramamurthy S, Noël J J, Shoesmith D, Lilja C, Johansson A J, 2019. The distribution of corrosion damage to copper surfaces exposed to aqueous sulphide solutions. SKBdoc 1706406, ver 1.0, Svensk Kärnbränslehantering AB.

Chen S, Wang P, Zhang D, 2014. Corrosion behaviour of copper under biofilm of sulfate-reducing bacteria. Corrosion Science 87, 407–415.

Choudhury D, Sahu J K, Sharma G D, 2011. Moisture sorption isotherms, heat of sorption and properties of sorbed water of raw bamboo (*Dendrocalamus longispathus*) shoots. Industrial Crops and Products 33, 211–216.

Cleveland C, Moghaddam S, Orazem M E, 2014. Nanometer-scale corrosion of copper in de-aerated deionized water. Journal of The Electrochemical Society 161, C107–C114.

Dong C, Mao F, Gao S, Sharifi-Asl S, Lu P, Macdonald D D, 2016. Passivity breakdown on copper: influence of temperature. Journal of The Electrochemical Society 163, C707–C717.

Dou W, Jia R, Jin P, Liu J, Chen S, Gu T, 2018. Investigation of the mechanism and characteristics of copper corrosion by sulfate reducing bacteria. Corrosion Science 144, 237–248.

Dueck A, 2004. Hydro mechanical properties of a water unsaturated sodium bentonite. Laboratory study and theoretical interpretation. PhD thesis. Department of Building and Environmental Technology, Division of Soil Mechanics and Foundation Engineering, Lund University.

Eriksen T E, Ndalamba P, Grenthe I, 1989. On the corrosion of copper in pure water. Corrosion Science 29, 1241–1250.

Eriksson P, Hedin A, 2019. Modelling of sulphide fluxes in unsaturated buffer and backfill for a KBS-3 repository. SKBdoc 1696975 ver 2.0, Svensk Kärnbränslehantering AB.

Fernández A M, Sánchez-Ledesma D M, Melón A, Robredo L M, Rey J J, Labajo M, Clavero M A, Carretero S, González A E, 2018. Thermo-hydro-geochemical behaviour of a Spanish bentonite after of the FEBEX in situ test at the Grimsel Test Site. Technical report CIEMAT/DMA/2G216/03/16. Nagra Arbeitsbericht NAB 16–25, Nagra, Switzerland.

Forsström A, Becker R, Öijerholm J, Yagodzinskyy Y, Hänninen H, Linder J, 2017. Hydrogen absorption in copper as a result of corrosion reactions in sulphide and chloride containing deoxygenated water at 90 °C in simulated spent nuclear fuel repository conditions. In Proceedings of EUROCORR 2017 – The Annual Congress of the European Federation of Corrosion, 20th International Corrosion Congress and Process Safety Congress, Prague, Czechia, 3–7 September 2017.

Ganchenkova M G, Yagodzinskyy Y N, Borodin V A, Hänninen H, 2014. Effects of hydrogen and impurities on void nucleation in copper: Simulation point of view. Philosophical Magazine 94, 3522–3548.

Giroud N, 2014. FEBEX – assessment of redox conditions in phase 2 before dismantling. Nagra Arbeitsbericht NAB 14–55, Nagra, Switzerland.

Glass R S, Van Konynenburg R A, Overturf G E, 1986. Corrosion processes of austenitic stainless steels and copper-based materials in gamma-irradiated aqueous environments. In Proceedings of Corrosion/86, Houston, TX, 17–21 March 1986. Paper 258.

Gordon A, Johansson J, Pahverk H, Börjesson E, Sjögren L, 2018. Corrosion morphology of copper in anoxic sulphide environments. SKB TR-18-14, Svensk Kärnbränslehantering AB.

Granfors M, 2017. Round-robin of hydrogen content in copper determined by melt extraction and gas analysis. SKB R-17-15, Svensk Kärnbränslehantering AB.

Grenthe I, Fuger J, Konings R J M, Lemire R J, Muller A B, Nguyen-Trung C, Wanner H, 1992. Chemical thermodynamics. Vol 1. Chemical thermodynamics of uranium. Amsterdam: North-Holland.

Guinan M W, 2001. Radiation effects in spent nuclear fuel canisters. SKB TR-01-32, Svensk Kärnbränslehantering AB.

Ha H M, Scully J R, 2013. Effects of phosphate on pit stabilization and propagation in copper in synthetic potable waters. Corrosion 69, 703−718.

Hansen T A, 1993. Carbon metabolism of sulfate-reducing bacteria. In Odom J M, Singleton R (eds). The sulfate-reducing bacteria: contemporary perspectives. New York: Springer-Verlag, 21−40.

He X, Ahn T, Gwo J-P, 2018. Corrosion of copper as a nuclear waste container material in simulated anoxic granitic groundwater. Corrosion 74, 158−168.

Hedin A, 2019. Scoping calculations of hydrogen degassing from Cu-OFP. SKBdoc 1716281 ver 1.0, Svensk Kärnbränslehantering AB.

Hedin A, Lilja C, Johansson A J, 2017. Copper corrosion in pure water – scientific and post-closure safety aspects. Proceedings of the 16th International High-Level Radioactive Waste Management Conference, Charlotte, NC, 9−13 April 2017. American Nuclear Society.

Hedin A, Johansson A J, Lilja C, Boman M, Berastegui P, Berger R, Ottosson M, 2018. Corrosion of copper in pure O_2-free water? Corrosion Science 137, 1−12.

Hernelind J, 2019a. Extended canister analyses with emphasis on tensile stresses and uneven swelling pressure. SKBdoc 1614038 ver 1.0, Svensk Kärnbränslehantering AB.

Hernelind J, 2019b. Design parameters effect on tensile stresses for the copper shell. SKBdoc 1707582 ver 2.0, Svensk Kärnbränslehantering AB.

Hultquist G, 1986. Hydrogen evolution in corrosion of copper. Corrosion Science 26, 173−176.

Hultquist G, Szakálos P, Graham M J, Sproule G I, Wikmark G, 2009. Detection of hydrogen in corrosion of copper in pure water. In Proceedings of the 17th International Corrosion Congress, Las Vegas, Nevada, 6−10 October 2008. Houston, TX: NACE International, 2378−2386.

Hultquist G, Graham M J, Szakalos P, Sproule G I, Rosengren A, Gråsjö L, 2011. Hydrogen gas production during corrosion of copper by water. Corrosion Science 53, 310−319.

Hultquist G, Graham M J, Kodra O, Moisa S, Liu R, Bexell U, Smialek J L, 2015. Corrosion of copper in distilled water without O_2 and the detection of produced hydrogen. Corrosion Science 95, 162−167.

Huotilainen C, Saario T, Toivonen A, 2018. Review of the Aaltonen-mechanism. SKB R-18-03, Svensk Kärnbränslehantering AB.

Huttunen-Saarivirta E, Ghanbari E, Mao F, Rajala P, Carpén L, Macdonald D, 2018. Kinetic properties of the passive film on copper in the presence of sulfate-reducing bacteria. Journal of The Electrochemical Society 165, C450–C460.

Håkansson R, 2000. Beräkning av nuklidinnehåll, resteffekt, aktivitet samt doshastighet för utbränt kärnbränsle. SKB R-99-74, Svensk Kärnbränslehanterng AB. (In Swedish.)

Högberg C-J, Karlsson O, Randelius M, Johansson A J, 2017. Surface morphology and elemental composition of copper canisters for disposal of spent nuclear fuel. SKB P-17-11, Svensk Kärnbränslehantering AB.

Höllmark H M, Keech P G, Vegelius J R, Werme L, Duda L-C, 2012. X-ray absorption spectroscopy of electrochemically oxidized Cu exposed to Na_2S. Corrosion Science 54, 85−89.

Ibrahim B, Zagidulin D, Behazin M, Ramamurthy S, Wren J C, Shoesmith D W, 2018. The corrosion of copper in irradiated and unirradiated humid air. Corrosion Science 141, 53−62.

Ishikawa T, McLellan R B, 1985. The diffusivity of hydrogen in copper at low temperatures. Journal of Physics and Chemistry of Solids 46, 445−447.

Jagodzinski Y, Aaltonen P, Smouk S, Tarasenko O, Hänninen H, 2000. Internal friction study of environmental effects on metals and alloys. Journal of Alloys and Compounds 310, 256−260.

Johansson A J, 2019a. Surface examination of a copper heater used for investigations of gas evolution in an unsaturated KBS-3 repository. SKBdoc 1696574 ver 1.0, Svensk Kärnbränslehantering AB.

Johansson A J, 2019b. Corrosion of copper in repository-like field tests: compilation and analysis of data. SKBdoc 1713264 ver 1.0, Svensk Kärnbränslehantering AB.

Johansson L, 2019. Exposure of copper to sulphate reducing bacteria and verification of a biofilm. Batch 2. SKBdoc 1701933 ver 1.0, Svensk Kärnbränslehantering AB.

Johansson J, Blom A, Chukharkina A, Pedersen K, 2015. Study of H_2 gas emission in sealed compartments containing copper immersed in O_2-free water. SKB TR-15-03, Svensk Kärnbränslehantering AB.

Johnson L H, LeNeveu D M, King F, Shoesmith D W, Kolar M, Oscarson D W, Sunder S, Onofrei C, Crosthwaite J L, 1996. The disposal of Canada's nuclear fuel waste: a study of post-closure safety of in-room emplacement of used CANDU fuel in copper containers in permeable plutonic rock. Volume 2: vault model. Report AECL-11494-2, COG-96-552-2, Atomic Energy of Canada.

Karnland O, Olsson S, Dueck A, Birgersson M, Nilsson U, Hernan-Hakansson T, Pedersen K, Nilsson S, Eriksen T E, Rosborg B, 2009. Long term test of buffer material at the Äspö Hard Rock Laboratory, LOT project. Final report on the A2 test parcel. SKB TR-09-29, Svensk Kärnbränslehantering AB.

King F, 1996. The potential for stress corrosion cracking of copper containers in a Canadian nuclear fuel waste disposal vault. Report AECL-11550, COG-96-94, Atomic Energy of Canada.

King F, 2004. The effect of discontinuities on the corrosion behaviour of copper canisters. SKB TR-04-05, Svensk Kärnbränslehantering AB.

King F, Lilja C, 2014. Localised corrosion of copper canisters. Corrosion Engineering, Science and Technology 49, 420–424.

King F, Litke C D, 1987. The corrosion of copper in synthetic groundwater at 150 °C. Part I. The results of short-term electrochemical tests. Technical Record TR-428, Atomic Energy of Canada.

King F, Newman R, 2010. Stress corrosion cracking of copper canisters. SKB TR-10-04, Svensk Kärnbränslehantering AB.

King F, Orazem M E, 2017. Preliminary report on the development of a kinetic model for the corrosion of copper in pure water. SKBdoc 1602591 ver 2.0, Svensk Kärnbränslehantering AB.

King F, Lilja C, Pedersen K, Pitkänen P, Vähänen M, 2010. An update of the state-of-the-art report on the corrosion of copper under expected conditions in a deep geologic repository. SKB TR-10-67, Svensk Kärnbränslehantering AB.

King F, Chen J, Martino T, Partovi-Nia R, Qin Z, Shoesmith D W, Lilja C, 2014. Sulphide mass-transport limited corrosion. SKBdoc 1422182, ver 2.0, Svensk Kärnbränslehantering AB.

King F, Chen J, Qin Z, Shoesmith D, Lilja C, 2017. Sulphide mass-transport control of the corrosion of copper canisters. Corrosion Engineering, Science and Technology 52, 210–216.

Kjeldsen K U, Joulian C, Ingvorsen K, 2004. Oxygen tolerance of sulfate-reducing bacteria in activated sludge. Environmental Science & Technology 38, 2038–2043.

Kong D, Dong C, Zhao M, Ni X, Man C, Li X, 2018. Effect of chloride concentration on passive film properties on copper. Corrosion Engineering, Science and Technology 53, 122–130.

Korzhavyi P A, Sandström R, 2014. Monovacancy in copper: Trapping efficiency for hydrogen and oxygen impurities. Computational Materials Science 84, 122–128.

Korzhavyi P A, Soroka I L, Isaev E I, Lilja C, Johansson B, 2012. Exploring monovalent copper compounds with oxygen and hydrogen. PNAS 109, 686–689.

Kristiansen P T, Massel F, Werme L, Lilja C, Duda L-C, 2015. Sulfidation of single-phase oxide on copper and as powder studied using soft x-ray spectroscopy. Journal of The Electrochemical Society 162, C785–C791.

Laaksoharju M, Smellie J, Tullborg E-L, Gimeno M, Hallbeck L, Molinero J, Waber N, 2008. Bedrock hydrogeochemistry Forsmark. Site descriptive modelling. SDM-Site Forsmark. SKB R-08-47, Svensk Kärnbränslehantering AB.

Landolt D, 2007. Corrosion and surface chemistry of metals. Lausanne, Switzerland: EPFL Press.

Leijon G, Ahlström J, Andersson-Östling H C M, 2018. In situ hydrogen charging of OFP copper during creep. SKB R-17-17, Svensk Kärnbränslehantering AB.

Li Y, Lousada C M, Soroka I I, Korzhavyi P A, 2015. Bond network topology and antiferroelectric order in cuprice CuOH. Inorganic Chemistry 54, 8969–8977.

Lousada C M, Korzhavyi P A, 2019. Hydrogen sorption capacity of crystal lattice defects and low Miller index surfaces of copper. SKBdoc 1708457 ver 1.0, Svensk Kärnbränslehantering AB.

Lousada C M, Soroka I L, Yagodzinskyy Y, Tarakina N V, Todoshchenko O, Hänninen H, Korzhavyi P A, Jonsson M, 2016. Gamma radiation induces hydrogen absorption by copper in water. Nature Scientific Reports 6, 24234. doi:10.1038/srep24234

Luterkort D, Johannesson L-E, Eriksson P, 2017. Buffer design and installation method. Installation report. SKB TR-17-06, Svensk Kärnbränslehantering AB.

Luther G W, Findlay A J, MacDonald D J, Owings S M, Hanson T E, Beinart R A, Girguis P R, 2011. Thermodynamics and kinetics of sulfide oxidation by oxygen: A look at inorganically controlled reactions and biologically mediated processes in the environment. Frontiers in Microbiology 2. doi:10.3389/fmicb.2011.00062

Lynch S P, 2012. Hydrogen embrittlement phenomena and mechanisms. Corrosion Reviews 30, 105–123.

MacDonald D D, Sharifi-Asl S, 2011. Is copper immune to corrosion when in contact with water and aqueous solutions? SSM Report 2011:09, Swedish Radiation Safety Authority.

Machel H G, 2001. Bacterial and thermochemical sulfate reduction in diagenetic settings – old and new insights. Sedimentary Geology 140, 143–175.

Madigan M T, Bender K S, Buckley D H, Sattley W M, Stahl D A, 2012. Brock biology of micro-organisms. 13th ed. Boston, MA: Pearson.

Magnusson H, Frisk K, 2017. Diffusion, permeation and solubility of hydrogen in copper. Journal of Phase Equilibria and Diffusion 38, 65–69.

Malmberg D, Åkesson M, Kristensson O, 2013. Supplementary material in addition to SR-Site modeling report TR-10-11 as requested by SSM. 2.0 The distribution of saturation times in the Forsmark repository. SKBdoc 1415879 ver 1.0, Svensk Kärnbränslehantering AB.

Mao F, Dong C, Sharifi-Asl S, Lu P, Macdonald D D, 2014. Passivity breakdown on copper: influence of chloride ion. Electrochimica Acta 144, 391–399.

Martino T, 2018. Electrochemical and corrosion examination of copper under deep geologic conditions for the application of nuclear waste containers. PhD thesis. Western University, London, Canada.

Martino T, Partovi-Nia R, Chen J, Qin Z, Shoesmith D W, 2014. Mechanisms of film growth on copper in aqueous solutions containing sulphide and chloride under voltammetric conditions. Electrochimica Acta 127, 439–447.

Martino T, Chen J, Qin Z, Shoesmith D W, 2017. The kinetics of film growth and their influence on the susceptibility to pitting of copper in aqueous sulphide solutions. Corrosion Engineering, Science and Technology 52, 61–64.

Martino T, Chen J, Guo M, Ramamurthy S, Shoesmith D W, Noël J J, 2019a. A critical review of E. Huttunen-Saarivirta et al., "Kinetic properties of the passive film on copper in the presence of sulfate-reducing bacteria", J. Electrochem. Soc. 165(9) (2018) C450-C460. Department of Chemistry and Surface Science Western, Western University, London Ontario, Canada. SKBdoc 1711670 ver 1.0, Svensk Kärnbränslehantering AB.

Martino T, Smith J, Chen J, Quin Z, Noël J J, Shoesmith D W, 2019b. The properties of electro-chemically-grown copper sulphide films. Journal of The Electrochemical Society 166, C9–C18.

Martinsson A, Sandström R, 2012. Hydrogen depth profile in phosphorus-doped, oxygen-free copper after cathodic charging. Journal of Materials Science 47, 6768–6776.

Martinsson A, Sandstrom R, Lilja C, 2013. Hydrogen in oxygen-free, phosphorus-doped copper: charging techniques, hydrogen contents and modelling of hydrogen diffusion and depth profile. SKB TR-13-09, Svensk Kärnbränslehantering AB.

Mattson E, Schückher F, 1958. An investigation of hydrogen embrittlement in copper. Journal of the Institute of Metals 87, 241–247.

Morsing Johansson J, Pedersen K, 2019. Continued measurements of stored samples from previous studies of H_2 emission in sealed compartments containing copper in O_2-free water. SKBdoc 1707895 ver 1.0, Svensk Kärnbränslehantering AB.

Motamedi M, Pedersen K, 1998. *Desulfovibrio aespoeensis* sp. nov., a mesophilic sulfate-reducing bacterium from deep groundwater at Aspö hard rock laboratory, Sweden. International Journal of Systematic Bacteriology 48, 311–315.

Motamedi M, Karnland O, Pedersen K, 1996. Survival of sulfate reducing bacteria at different water activities in compacted bentonite. FEMS Microbiology Letters 141, 83–87.

Müller A L, de Rezende J R, Hubert C R J, Kjeldsen K U, Lagkouvardos I, Berry D, Jörgensen B B, Loy A, 2014. Endospores of thermophilic bacteria as tracers of microbial dispersal by ocean currents. The ISME Journal 8, 1153–1165.

Nieh T G, Nix W D, 1981. Embrittlement of copper due to segregation of oxygen to grain boundaries. Metallurgical Transactions A 12, 893–901.

Okinaka Y, Straschil H K, 1986. Effect of inclusions on the ductility of electroless copper deposits. Journal of The Electrochemical Society 133, 2608–2615.

Ollila K, 2013. Copper corrosion experiments under anoxic conditions. SKB R-13-34, Svensk Kärnbränslehantering AB.

Ollila K, 2019. Copper corrosion experiments in pure water under anoxic conditions. Posiva Working Report 2018-19, Posiva Oy, Finland.

Olsson S, Jensen V, Johannesson L-E, Hansen E, Karnland O, Kumpulainen S, Kiviranta L, Svensson D, Hansen S, Lindén J, 2013. Prototype Repository. Hydro-mechanical, chemical and mineralogical characterization of the buffer and backfill material from the outer section of the Prototype repository. SKB TR-13-21, Svensk Kärnbränslehantering AB.

Ottosson M, Boman M, Berastegui P, Andersson Y, Hahlin M, Korvela M, Berger R, 2016. Copper in ultrapure water. SKB TR-16-01, Svensk Kärnbränslehantering AB.

Ottosson M, Boman M, Berastegui P, Andersson Y, Hahlin M, Korvela M, Rerger R, 2017. Copper in ultrapure water, a scientific issue under debate. Corrosion Science 122, 53–60.

Ottosson M, Boman M, Berastegui P, Andersson Y, Hahlin M, Korvela M, Berger R, 2018. Response to the comments by P. Szakálos, T. Åkermark and C. Leygraf on the paper "Copper in ultrapure water, a scientific issue under debate". Corrosion Science 142, 308–311.

Padovani C, Pletser D, Jurkschat K, Armstrong D, Dugdale S, Brunt D, Faulkner R, Was G, Johansson A J, 2019. Assessment of microstructural changes in copper due to gamma radiation damage. SKB TR-19-12, Svensk Kärnbränslehantering AB.

Panagopoulos C N, Zacharopoulos N, 1994. Cathodic hydrogen charging and mechanical properties of copper. Journal of Materials Science 29, 3843–3846.

Parkins R N, 2010. Environmentally assisted cracking test methods. In Cottis R A, Graham M J, Lindsay R, Lyon S B, Richardson J A, Scantlebury J D, Stott F H (eds). Shreir's corrosion. Vol. 2. 4th ed. Amsterdam: Elsevier, 1527–1546.

Pham A N, Waite T D, 2008. Oxygenation of Fe(II) in natural waters revisited: Kinetic modeling approaches, rate constant estimation and the importance of various reaction pathways. Geochimica et Cosmochimica Acta 72, 3616–3630.

Potts M, 1994. Desiccation tolerance of prokaryotes. Microbiology and Molecular Biology Reviews 58, 755–805.

Rantala J, Auerkari P, Laukkanen A, Andersson T, Saukkonen T, 2015. Material integrity of welded copper overpack: Annual report 2014. Research Report VTT-R-00773-15, Technical Research Centre of Finland.

Saetre P, 2019a. Uppdatering av fördelningskoefficienter (K$_d$) och koncentrationskvoter (CR) i kompletterande biosfärsberäkningar. SKBdoc 1712318 ver 1.0, Svensk Kärnbränslehantering AB. (In Swedish.)

Saetre P, 2019b. Uppdaterade biosfärsdata för Kärnbränsleförvarets säkerhetsanalys_Appendices. SKBdoc 1712319 ver 1.0, Svensk Kärnbränslehantering AB.

Sander R, 2015. Compilation of Henry's law constants (version 4.0) for water as solvent. Atmospheric Chemistry and Physics 15, 4399–4981.

Savolainen K, 2012. Friction stir welding of copper and microstructure and properties of the welds. PhD thesis. Aalto University, Finland.

Sellin P (ed), Åkesson M, Kristensson O, Malmberg D, Börgesson L, Birgersson M, Dueck A, Karnland O, Hernelind J, 2017. Long re-saturation phase of a final repository. Additional supplementary information. SKB TR-17-15, Svensk Kärnbränslehantering AB.

Senior N A, Newman R C, Artymowicz D, Binns W J, Keech P G, Hall D S, 2019. Communication – A method to measure extremely low corrosion rates of copper metal in anoxic aqueous media. Journal of The Electrochemical Society 166, C3015–C3017.

Sharma, 1980. Reaction of copper and copper oxide with H$_2$S. Journal of The Electrochemical Society 127, 21–26.

Sigalevich P, Cohen Y, 2000. Oxygen-dependent growth of the sulfate-reducing bacterium *Desulfovibrio oxyclinae* in coculture with *Marinobacter* sp. Strain MB in an aerated sulfate-depleted chemostat. Applied and Environmental Microbiology 66, 5019–5023.

Simpson J P, Schenk R, 1987. Hydrogen evolution from corrosion of pure copper. Corrosion Science 27, 1365–1370.

Sipilä K, Arilahti E, Lehtikuusi T, Saario T, 2014. Effect of sulphide exposure on mechanical properties of CuOFP. Corrosion Engineering, Science and Technology 49, 410–414.

SKB, 2008. Site description of Forsmark at completion of the site investigation phase. SDM-Site Forsmark. SKB TR-08-05, Svensk Kärnbränslehantering AB.

SKB, 2010a. Corrosion calculations report for the safety assessment SR-Site. SKB TR-10-66, Svensk Kärnbränslehantering AB.

SKB, 2010b. Data report for the safety assessment SR-Site. SKB TR-10-52, Svensk Kärnbränslehantering AB.

SKB, 2010c. Design, production and initial state of the buffer. SKB TR-10-15, Svensk Kärnbränslehantering AB.

SKB, 2010d. Design, production and initial state of the canister. SKB TR-10-14, Svensk Kärnbränslehantering AB.

SKB, 2010e. Fuel and canister process report for the safety assessment SR-Site. SKB TR-10-46, Svensk Kärnbränslehantering AB.

SKB, 2010f. Spent nuclear fuel for disposal in the KBS-3 repository. SKB TR-10-13, Svensk Kärnbränslehantering AB.

SKB, 2011. Long term safety for the final repository for spent nuclear fuel at Forsmark. Main report of the SR-Site project. SKB TR-11-01, Svensk Kärnbränslehantering AB.

SKB, 2014. Biosphere synthesis report for the safety assessment SR-PSU. SKB TR-14-06, Svensk Kärnbränslehantering AB.

SKB, 2015. Svar till SSM på begäran daterad 2013-02-11 om komplettering rörande radionuklid-transport och dos. SKBdoc 1418468 ver 2.0, Svensk Kärnbränslehantering AB.

Smith J M, Wren J C, Odziemkowski M, Shoesmith D W, 2007. The electrochemical response of preoxidized copper in aqueous sulfide solutions. Journal of The Electrochemical Society 154, C431–C438.

Soroka I, Jonsson M, 2019. Radiation induced corrosion of copper – an update on the mechanism. SKBdoc 1706535 ver 1.0, Svensk Kärnbränslehantering AB.

Soroka I L, Shchukarev A, Jonsson M, Tarakina N V, Korzhavyi P A, 2013. Cuprous hydroxide in a solid form: does it exist? Dalton Transactions 42, 9585–9594.

Speight J G, 2014. Handbook of offshore oil and gas operations. Elsevier Science.

SSM, 2008. Strålsäkerhetsmyndighetens föreskrifter och allmänna råd om skydd av människors hälsa och miljön vid slutligt omhändertagande av använt kärnbränsle och kärnavfall (The Swedish Radiation Safety Authority's regulations on the protection of human health and the environment in connection with the final management of spent nuclear fuel and nuclear waste) Stockholm: Swedish Radiation Safety Authority. (SSMFS 2008:37) (In Swedish.)

Stahlén J, 2019. Exposure of copper to sulphate reducing bacteria and verification of a biofilm. Batch 1. SKBdoc 1701925 ver 1.0, Svensk Kärnbränslehantering AB.

Stenlid J H, Johansson A J, Leygraf C, Brinck T, 2017. Computational analysis of the early stage of cuprous oxide sulphidation: a top-down process. Corrosion Engineering, Science and Technology 52, 50–53.

Svensson D, Lundgren C, Wikberg P, 2017. Experiments with bentonite and sulphide – results from experiments 2013–2016. SKB P-16-31, Svensk Kärnbränslehantering AB.

Svensson D, Kalinowski B E, Turner S, Dopson M, 2019. Activity of sulfate reducing bacteria in bentonite as a function of water availability. SKBdoc 1708461 ver 1.0, Svensk Kärnbränslehantering AB.

Szakálos P, Hultquist G, Wikmark G, 2007. Corrosion of copper by water, Electrochemical and Solid-State Letters 10, C63–C67.

Szakálos P, Åkermark T, Leygraf C, 2018. Comments on the paper "Copper in ultrapure water, a scientific issue under debate" by M. Ottosson, M. Boman, P. Berastegui, Y. Andersson, M. Hahlin, M. Korvela, and R. Berger. Corrosion Science 142, 305–307.

Taniguchi N, Kawasaki M, 2008. Influence of sulfide concentration on the corrosion behaviour of pure copper in synthetic seawater. Journal of Nuclear Materials 379, 154–161.

Taniguchi N, Kawasaki M, Morimasa M, 2007. Effect of sulfide on the corrosion behavior of pure copper under anaerobic condition and possibility of super long lifetime for copper overpacks. Japan Atomic Energy Agency Report, JAEA-Research 2007-022.

Taniguchi N, Kawasaki M, Morimasa M, 2008. Effect of electrode potential and material grade on the behavior of stress corrosion cracking of pure copper in synthetic seawater containing sulfide. Japan Atomic Energy Agency Report, JAEA-Research 2008-118.

Taxén C, 2013. Ytprofiler på kopparkapslar från deponeringshål 5 och 6 i försöksserien Prototyp. SKB P-13-50, Svensk Kärnbränslehantering AB. (In Swedish.)

Taxén C, Lundholm M, Persson D, Jakobsson D, Sedlakova M, Randelius M, Karlsson O, Rydgren P, 2012. Analyser av koppar från prototypkapsel 5 och 6. SKB P-12-22, Svensk Kärnbränslehantering AB. (In Swedish.)

Taxén C, Wickström L, Sparr M, 2017. Corrosion properties of cold worked or welded copper materials. SKB R-17-09, Svensk Kärnbränslehantering AB.

Taxén, C, Flyg J, Bergqvist H, 2018. Stress corrosion testing of copper in sulfide solutions. SKB TR-17-16, Svensk Kärnbränslehantering AB.

Taxén C, Flyg J, Bergqvist H, 2019. Stress corrosion testing of copper in near neutral sulfide solutions. SKB TR-19-13, Svensk Kärnbränslehantering AB.

Toijer E, 2014. Assessment of primary damage and copper precipitation in cast iron in repository conditions. Master's thesis. Royal Institute of Technology, Sweden.

Villar M V, Iglesias R J, Abós H, Martínez V, de la Rosa C, Manchón M A, 2016. FEBEX-DP onsite analyses report. Nagra Arbeitsbericht NAB 16–12, Nagra, Switzerland.

Wampler W R, Schober T, Lengeler B, 1976. Precipitation and trapping of hydrogen in copper. Philosophical Magazine 34, 129–141.

Åkesson M, Kristensson O, Börgesson L, Dueck A, Hernelind J, 2010. THM modelling of buffer, backfill and other system components. Critical processes and scenarios. SKB TR-10-11, Svensk Kärnbränslehantering AB.

Åkesson M, Börgesson L, Sandén T, Goudarzi R, 2019. Vapor transport in bentonite. Laboratory investigations and theoretical study. SKBdoc 1712120 ver 1.0, Svensk Kärnbränslehantering AB.

Yagodzinskyy Y, Malitckii E, Saukkonen T, Hänninen H, 2012. Hydrogen-enhanced creep and cracking of oxygen-free phosphorus-doped copper. Scripta Materialia 67, 931−934.

Yagodzinskyy Y, Malitckii E, Tuomisto F, Hänninen H, 2018. Hydrogen-induced strain localisation in oxygen-free copper in the initial stage of plastic deformation. Philosophical Magazine 98, 727−740.

Yang Q, Toijer E, Olsson P, 2019. Analysis of radiation damage in the KBS-3 canister materials. SKB TR-19-14, Svensk Kärnbränslehantering AB.

Yunker W H, 1990. Corrosion behavior of copper-base materials in a gamma-irradiated environment. Report WHC-EP-0188, Westinghouse Hanford Company, Richland, Washington.

Yunker W H, Glass R S, 1987. Long-term corrosion behaviour of copper-base materials in a gamma-irradiated environment. In Bates J K, Seefeldt W B (eds). Scientific basis for nuclear waste management X: symposium held in Boston, Massachusetts, USA, 1−4 December 1986. Pittsburgh, PA: Materials Research Society. (Materials Research Society Symposium Proceedings 84), 579−590.

Zhou C, Yang X, Luan G, 2006. Effect of oxide array on the fatigue property of friction stir welds. Scripta Materialia 54, 1515−1520.

SKB is responsible for managing spent nuclear fuel and radioactive waste produced by the Swedish nuclear power plants such that man and the environment are protected in the near and distant future.

skb.se